



REFERENCE ONLY

UNIVERSITY OF LONDON THESIS

Degree *PhD*

Year *2005*

Name of Author *LAMBERT, N.*

COPYRIGHT

This is a thesis accepted for a Higher Degree of the University of London. It is an unpublished typescript and the copyright is held by the author. All persons consulting the thesis must read and abide by the Copyright Declaration below.

COPYRIGHT DECLARATION

I recognise that the copyright of the above-described thesis rests with the author and that no quotation from it or information derived from it may be published without the prior written consent of the author.

LOANS

Theses may not be lent to individuals, but the Senate House Library may lend a copy to approved libraries within the United Kingdom, for consultation solely on the premises of those libraries. Application should be made to: Inter-Library Loans, Senate House Library, Senate House, Malet Street, London WC1E 7HU.

REPRODUCTION

University of London theses may not be reproduced without explicit written permission from the Senate House Library. Enquiries should be addressed to the Theses Section of the Library. Regulations concerning reproduction vary according to the date of acceptance of the thesis and are listed below as guidelines.

- A. Before 1962. Permission granted only upon the prior written consent of the author. (The Senate House Library will provide addresses where possible).
- B. 1962 - 1974. In many cases the author has agreed to permit copying upon completion of a Copyright Declaration.
- C. 1975 - 1988. Most theses may be copied upon completion of a Copyright Declaration.
- D. 1989 onwards. Most theses may be copied.

This thesis comes within category D.

This copy has been deposited in the Library of *UCL*

This copy has been deposited in the Senate House Library, Senate House, Malet Street, London WC1E 7HU.

Theoretical and Experimental Studies
of the Structure and Reactivity of
Doubly-Charged Ions in the
Gas Phase.

SUBMITTED BY
Natalie Lambert

FOR THE DEGREE OF
Doctor of Philosophy

SUPERVISED BY
Prof. Stephen D. Price
Dr. Nikolas Kaltsoyannis



University College London, 2005

UMI Number: U592226

All rights reserved

INFORMATION TO ALL USERS

The quality of this reproduction is dependent upon the quality of the copy submitted.

In the unlikely event that the author did not send a complete manuscript and there are missing pages, these will be noted. Also, if material had to be removed, a note will indicate the deletion.



UMI U592226

Published by ProQuest LLC 2013. Copyright in the Dissertation held by the Author.
Microform Edition © ProQuest LLC.

All rights reserved. This work is protected against
unauthorized copying under Title 17, United States Code.



ProQuest LLC
789 East Eisenhower Parkway
P.O. Box 1346
Ann Arbor, MI 48106-1346

Abstract

The purpose of the research described in this thesis is to investigate certain aspects of the reactivity of doubly-charged cations (dications) with neutral molecules in the gas phase, specifically, the mechanisms governing the bond-forming reactivity of dications with neutrals as well as the degree of state-selectivity involved in their electron transfer reactivity.

Computational investigations of the mechanisms governing the bond-forming reactivity in the following systems have been performed: $\text{CF}_2^{2+} + \text{H}_2\text{O}$; $\text{Ar}^{2+} + \text{NH}_3$ and $\text{CF}_3^{2+} + \text{H}_2$. All of these systems are found to possess a well in their potential energy surfaces corresponding to an associated complex between the dication and the neutral. For the systems involving molecular dications (CF_2^{2+} and CF_3^{2+}), the mechanisms that emerge from the quantum chemical calculations indicate a pattern of reactivity that is in support of computational and experimental studies previous to and concurrent with the work presented in this thesis. This mechanistic pattern involves three main steps: bond formation, rearrangement and fragmentation, indicating a degree of complexity in bond-forming dication-molecule reactions that had not been previously expected. The mechanisms calculated quantum chemically were compared with experimental studies on the same system, either performed previously by others or as part of the work for this thesis, and found to be in good agreement.

Crossed-beam collision experiments employing time-of-flight mass spectrometric analysis of the products were performed on two dication-neutral systems: $\text{CF}_2^{2+} + \text{D}_2\text{O}$ and $\text{SF}_2^{2+} + \text{H}_2\text{O}$. The results of experiments on

$\text{CF}_2^{2+} + \text{D}_2\text{O}$ were compared with previous experimental studies on $\text{CF}_2^{2+} + \text{H}_2\text{O}$ in order to determine the possible existence of an intermolecular isotope effect. No isotope effect was observed within the experimental error, in agreement with our predictions from theoretical rate constant calculations.

Experiments on the $\text{SF}^{2+} + \text{H}_2\text{O}$ system were carried out in order to determine the relative degree of dissociative and non-dissociative electron transfer. The ratio of the product ions corresponding to these two processes, S^+/SF^+ , was then compared with a ratio determined from theoretical calculations. These calculations involved the determination of Landau-Zener probabilities for forming products in a given electronic and vibrational state, as well as Franck-Condon factors for the electron capture of SF^{2+} , in order to determine the degree of state-selectivity in the formation of electron transfer products. Good agreement was found between the experimental and theoretical S^+/SF^+ ratios and it was also found that only excited states contributed to the formation of electron transfer products.

Contents

1	Introduction	8
1.1	Thermodynamic Properties of Dications	11
1.2	Reactivity of Dications	13
1.2.1	Previous Experimental Studies of Dication Reactivity .	13
1.2.2	Previous Computational Studies of Dication Reactivity	19
1.3	Theoretical Background	22
1.3.1	Electronic Structure Calculations	22
1.3.2	Rate Constants and RRKM/Quasi-equilibrium Theory	44
1.3.3	Landau-Zener Theory	49
1.3.4	Calculation of Franck-Condon Factors	53
1.4	Experimental Background	61
1.4.1	Methods of Dication Generation	61
1.4.2	Apparatus Used to Study Dication-Neutral Reactions .	63
1.4.3	Data Analysis	67
2	The bond-forming reaction between CF_2^{2+} and $\text{H}_2\text{O}/\text{D}_2\text{O}$.	71
2.1	Introduction	71
2.2	Computational Details	73
2.3	Experimental Details	74
2.4	Results and Discussion	76
2.4.1	Computational Results: Reaction Mechanism	76
2.4.2	Computational Results: Rate Constants	82
2.4.3	Experimental Results	82
2.4.4	Discussion	86
2.5	Conclusions	87
3	The bond-forming reaction between Ar^{2+} and NH_3.	89
3.1	Introduction	89
3.2	Computational Details	90
3.3	Results and Discussion	92
3.3.1	Single-reference methods	92

3.3.2	Multireference methods	92
3.4	Conclusions	102
4	A computational study of the mechanism for the formation of HCF_2^+ from CF_3^{2+} and H_2	104
4.1	Introduction	104
4.2	Computational Details	107
4.3	Results and Discussion	108
4.3.1	Computational Results	108
4.3.2	Comparison With Prague Experimental Results	123
4.4	Conclusions	128
5	Experimental cross sections and theoretical state-to-state probabilities for electron transfer between SF^{2+} and H_2O	130
5.1	Introduction	130
5.2	Details of the Experiment	132
5.3	Details of Calculations	136
5.4	Results and Discussion	137
5.4.1	Experimental Results	137
5.4.2	Results of Calculations	140
5.4.3	Discussion	156
5.5	Conclusions	159
A	FORTTRAN90 source code for a program written to calculate unimolecular dissociation rate constants using the RRKM/QET equation	161
B	FORTTRAN90 source code for a program written to calculate Franck-Condon factors from the vibrational wavefunctions of the initial and final states.	165
C	Calculated Franck-Condon factors	168
D	Colour maps of Franck-Condon factors for transitions from $X^2\Pi \text{SF}^{2+}$ to $C^3\Sigma^- \text{SF}^+$, $a^1\Delta \text{SF}^+$, $b^1\Sigma^+ \text{SF}^+$, $c^1\Sigma^- \text{SF}^+$ and $e^1\Delta \text{SF}^+$.	198
E	Calculated term energies for some product states of the reaction of SF^{2+} with H_2O, relative to the $X^3\Sigma^- \text{SF}^+ + \widetilde{X}^2B_1 \text{H}_2\text{O}^+$ state.	204

F	Landau-Zener cross sections for some product states of the reaction of SF^{2+} with H_2O, relative to the $X^3\Sigma^- \text{SF}^+ + \tilde{X}^2B_1 \text{H}_2\text{O}^+$ state.	208
----------	---	------------

Acknowledgements

There are many people that have helped me in so many different ways during the course of my 3.5 years at UCL, who deserve all of my gratitude and thanks. They are:

My supervisors, Steve and Nik, for sharing so much of their knowledge and time. I could not have asked for more dedicated, supportive and knowledgeable supervisors. You have my greatest respect and gratitude.

Mom, Dad and Sophie, for their unconditional love and support, I cannot express how lucky I am to have such a wonderful family. Angie, for always being there, always knowing what to say, and frankly, being awesome. Gaby, Louise, Deb and Yehuda, for making first London and then my whole life so much more beautiful, fun and full. I love you all immensely.

Emma, Natalie, Simon, Kate and Aileen, for providing me with a million different kinds of support, for which I am so grateful. Andrea, Kieran, Luke, Giusy, and the past and present members of G25, G19 and the Physical Chemistry group, for all of their help over the years and for making UCL Chemistry such a fun place to work.

Julia W. and Julia B., for having the unlucky task of living with my ups and downs and for making home really feel like home.

Marc V., Marc T., Atanga, Thalie, Sholem and Mike, for your support, advice, jokes and love in pen and in person.

Prof. Jan Hrušák, Dr. Jeremy Harvey and the members of the MCI Network, for many very helpful discussions. Lizzy Boleat, for all of her help with using LEVEL and calculating FCFs. Dominic Kearney, for his help with the experiments.

Dr. Krzysztof Borowiec, for being the best teacher for all things and for encouraging me to do a Ph.D. Mike Scamell, for introducing me to Chemistry and lighting the spark.

Pierre Elliott Trudeau, for inspiration.

I am also very grateful to the European Union Research Training Network 1-1999-00254 (MCI-net) for funding.

Chapter 1

Introduction

Doubly charged cations (dications) are commonly discussed in the context of salts and complexes, stabilised either by a solvation shell in solution, their anionic partners in a crystalline salt or the ligands in a complex. The dications in a pure metal are stabilised by a sea of delocalised electrons. In the gas phase, dications have no such stabilising forces. The Coulombic repulsion between the two like charges in such close proximity causes gas phase dications to be quite high in internal energy.

The storage of large amounts of internal energy in an atom or small molecule is precisely what makes dications interesting and unique. A typical kinetic energy release for the separation of a molecular dication into two singly charged fragments is of the order of 6 eV. Despite this, in the last two decades it has been shown that many dications possess one or more long-lived ($\tau \geq \mu s$) metastable electronic states [1, 2]. In addition, the double ionization cross sections of many dication precursors have been shown to be largely

underestimated by most early experiments due to the inefficient detection of the highly energetic products of double ionization [3–9]. In light of these discoveries, interest in small gas-phase dications has been growing steadily since the 1980's. These efforts have revealed a rich and varied dication reactivity, showing dications to be important in the chemistry of the atmosphere and of the interstellar medium, as well as in plasma etching processes used in the production of electronics.

The purpose of this thesis is to elucidate some previously unexplored aspects of the reactivity of dications with neutral molecules. Four different systems have been investigated: $\text{CF}_2^{2+} + \text{H}_2\text{O}/\text{D}_2\text{O}$ (Chapter 2); $\text{Ar}^{2+} + \text{NH}_3$ (Chapter 3); $\text{CF}_3^{2+} + \text{H}_2$ (Chapter 4) and $\text{SF}^{2+} + \text{H}_2\text{O}$ (Chapter 5). Chapters 2, 3 and 4 present the results of computational studies of the mechanisms of the bond-forming reactions between the dication and neutral in question. These calculated mechanisms are then used to rationalise the results of time-of-flight mass spectrometric (TOFMS) collision experiments, which have either been carried out previously by others (Chapters 3 and 4) or as part of the work presented for this thesis (Chapters 2 and 5). The mechanisms that arise from these calculations reveal a pattern of dication-neutral reactivity that is more complicated than one might expect. In all cases we predict the formation of a doubly charged collision complex between the dication and the neutral that exists in a potential well with a barrier to fragmentation or rearrangement. In two cases (Chapters 2 and 4), intramolecular rearrangements also form part of the reaction mechanism, a result that is in agreement with previous findings for other systems.

Chapter 5 presents the results of an investigation into the degree of state-selectivity of the electron transfer reaction between a dication and a neutral molecule. Crossed-beam collision experiments were performed between SF^{2+} and H_2O and the ratio of the cross sections for forming the electron transfer products S^+ and SF^+ determined by TOFMS. Theoretical calculations were carried out in order to determine which electronic and vibrational states of SF^+ (and to some extent H_2O^+) are populated following electron transfer at a given collision energy. Interestingly, it is shown that some relatively highly excited states of SF^+ and H_2O^+ have the greatest contribution to the final S^+/SF^+ product intensity ratio. Specifically, the ground state product asymptote does not contribute at all. The theoretical S^+/SF^+ ratio is compared with that obtained from the experimental data and is found to be in good agreement.

Overall, the results of these four studies have shown that only very specific routes through the potential energy surface for the reaction of a dication with a neutral are likely to be followed, both for bond-forming and electron transfer processes. This indicates a degree of specificity in the reactions of dications with neutrals that had not previously been predicted.

This Chapter begins with a discussion of the properties of dications and their reactivity, particularly of the bond-forming and electron transfer kind. Following this, a survey of the theoretical and experimental techniques employed for the studies described in this thesis is presented. The original work of thesis is then presented in Chapters 2 to 5 as described above.

1.1 Thermodynamic Properties of Dications

The lifetime and stability of a dication in the gas phase depends on a number of factors. The presence of a thermodynamic barrier to charge separation can increase a dication's lifetime. The relative energy of the charge separated products to the dication is also important. Both of these effects can be best illustrated by examining the potential energy curves of two dissociation pathways: one that corresponds to the mutual Coulombic repulsion of two monocationic fragments and an associative pathway which assumes localisation of the double charge on one fragment. Figure 1.1 illustrates the importance of the way in which these two curves cross. If one assumes that the dissociation of the dication occurs on the adiabatic pathway (illustrated by the arrows), in Figure 1.1a not only is the dication lower in energy than the separated singly charged ions, there is also a relatively large barrier to this dissociation. In such a situation the dication is stable. In Figure 1.1b the charge separated ions are lower in energy than the dication, however there is still a large activation to charge separation. Such a dication is termed metastable. When the charge separated products are lower in energy than the dication and there is little or no activation barrier, as in Figure 1.1c, the dication is unstable. Most small non-metal dications of the kind discussed in this thesis possess at least one accessible metastable state.

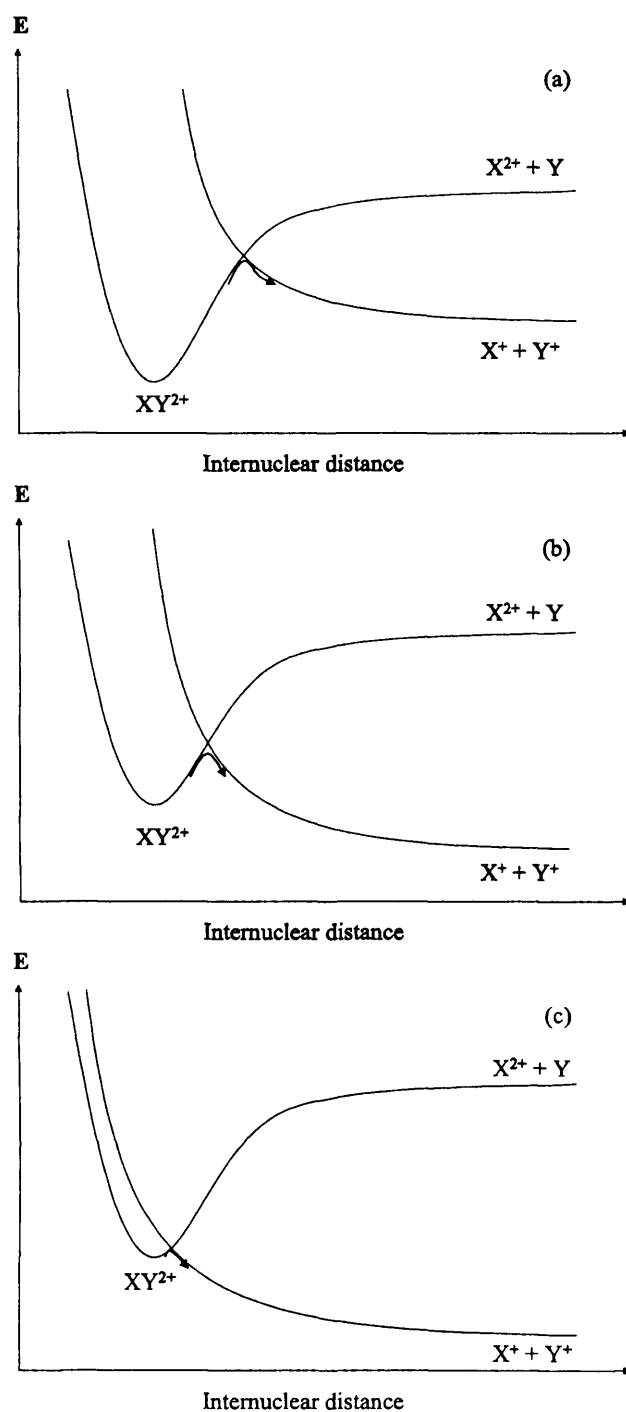
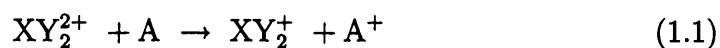


Figure 1.1: Schematic representation of the potential energy of a dication XY^{2+} as a function of the interatomic distance of two fragments. The position of the curve for charge separation relative to the potential well of the dication can affect the dication's stability.

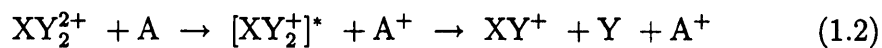
1.2 Reactivity of Dications

1.2.1 Previous Experimental Studies of Dication Reactivity

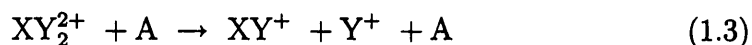
In general, a metastable dication always seeks to separate its two like charges. Upon collision with a neutral, it will most commonly redistribute part of its charge onto the neutral *via* electron transfer, either non-dissociative:



or dissociative:



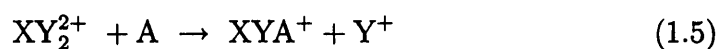
Some other possible outcomes of an interaction between a dication and a neutral are collision-induced charge separation:



collision-induced neutral loss:



and bond-forming reactivity:



In the case of dissociative electron transfer, the transfer of an electron from the neutral to the dication produces a dissociative monocation state. Loss of a neutral fragment then stabilises the monocation. Collision-induced charge separation and collision-induced neutral loss processes result in the neutral collision partner accepting no charge. In the former case, the collision provides enough energy for the dication to overcome the barrier to charge separation. In the latter case, the collision energy is used to overcome the activation barrier to loss of a neutral fragment from the dication, resulting in a more stable dication state. Bond-forming reactions involve the formation of a product ion that is composed of atoms from both the dication and the neutral. Compared with the electron transfer processes shown in equations 1.1 and 1.2, the cross sections for products from a bond-forming reaction are generally quite small.

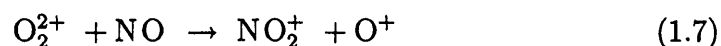
The kinds of dication-molecule reactions that will be investigated in this thesis are non-dissociative and dissociative electron transfer (equations 1.1 and 1.2) and bond-forming (resulting in two monocation products, as in equation 1.5). Studies of dication reactivity in the literature have thus far been dominated by investigations of electron transfer processes, due to the large experimental cross sections for generating electron transfer products fol-

lowing dication-neutral collisions. Early studies of dication-neutral electron transfer processes were prompted by the observation by Friedlander *et al.* in 1932 [10] that the spontaneous decomposition of CO^{2+} to $\text{C}^+ + \text{O}^+$ results in a much greater yield of O^+ relative to C^+ , indicating that dissociative electron transfer may be occurring as well as unimolecular dissociation. Melton and Wells performed the first mass spectrometric study of collisions of CO^{2+} with the rare gases (Rg) in order to determine the extent of dissociative electron transfer [11]. A series of studies examining the electron transfer reactivity of CO^{2+} with H_2 , N_2 and the rare gases then followed [12–16]. All of these CO^{2+} studies took place at high collision energies, in the range of keV, and until the early 1990s most other studies of dication-neutral reactions were also carried out either at these high collision energies, or occasionally at thermal energies in drift tube experiments. The dications investigated in these high collision energy studies were $\text{C}_6\text{H}_6^{2+}$, CS_2^{2+} , NO^{2+} and CO_2^{2+} [17–22]. Thermal energy experiments involved the dications C^{2+} , N^{2+} , O^{2+} and Rg^{2+} interacting with rare gas and small molecular neutrals such as H_2 , N_2 , O_2 , CO_2 , CH_4 and C_2H_2 [23–28].

Although some low collision energy studies (in the range of eV) of electron transfer reactions between dications and neutrals were performed earlier (Friedrich *et al.* [29] studied electron transfer between Ar^{2+} and He and Pedersen *et al.* [30] studied the $\text{CO}^{2+} + \text{He}$ system), it was only in the 1990's that such low energy studies became more common due to the emergence of custom-built apparatus. A host of new dication systems could then be investigated, involving such dications as CF_n^{2+} , SF_n^{2+} , CO_2^{2+} , OCS^{2+} ,

SiF_n^{2+} , N_2^{2+} , He^{2+} and CHCl^{2+} in collisions with the rare gases and small molecules [31–36].

As a result of some of these low collision energy studies of dication reactivity, some chemical reactions in which new bonds are formed were noticed. The first report of a bond-forming reaction between a dication and a neutral was by Chatterjee *et al.* for the $\text{O}_2^{2+} + \text{NO}$ system [37]:



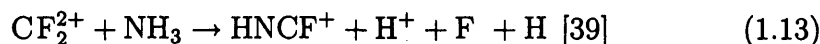
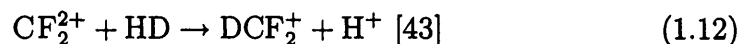
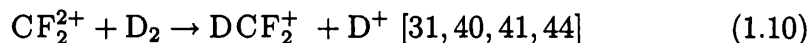
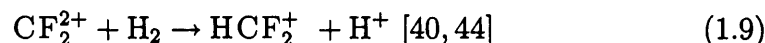
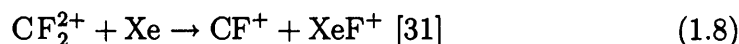
However, the extent of this special kind of dication-neutral reactivity was revealed in a study five years later by Price *et al.* on a series of eight different dications and six different neutral collision partners [31]. Since then, a number of bond-forming dicationic systems have been studied [31, 35, 36, 38–44]. The most common dications used in these reactions were SF_n^{2+} ($n = 2 - 4$), CF_n^{2+} ($n = 1 - 3$), and CO_2^{2+} . Studies of bond-forming dication reactions have also been carried out for OCS^{2+} [31], Ar^{2+} [45] and CHCl^{2+} [36]. In order for such experiments to be successful in producing bond-forming products in measurable amounts, the dication under study must be stable enough to avoid fragmentation upon impact with the neutral collision partner. In addition, the neutral should be relatively small and electron-donating. Some common neutral collision partners are Xe, Ar, H_2 , D_2 , O_2 , H_2O , NH_3 and CO. A list of dication-neutral collision systems whose bond-forming reactivities have been studied is given in Table 1.1.

The most extensively studied dication in the context of bond-forming reactions is CF_2^{2+} . Six chemical products have thus far been observed following

dication	collision partner(s)	observed bond-forming product(s)	reference
O_2^{2+}	NO	NO_2^+	[37]
CF_n ($n=1-3$)	Xe, D ₂ , O ₂ , H ₂ O, H ₂ S	XeF^+ , DCF_2^+ , DCF^+ , CO^+ , OCF^+ , OSF^+	[31, 39–44, 46, 47]
SF_n ($n=2-4$)	Xe, CO	XeF^+ , OCF^+	[31]
CO_2^{2+}	Xe, D ₂ , CO ₂ , CO	XeO^+ , DCO^+ , DCO_2^+ , OD^+	[31, 35]
OCS^+	D ₂	DS^+	[31]
$CHCl^{2+}$	D ₂	$CHDCl^+$, HD_2^+	[48]
Ar^{2+}	N ₂ , O ₂ , CO, CO ₂ , NH ₃	ArN^{2+} , ArC^{2+} , ArO^{2+} , ArO^+ , $ArNH^+$, ArN^+	[45, 49, 50]

Table 1.1: Previous experimental studies of bond-forming reactions between dications and neutral atoms and molecules and the bond-forming products observed.

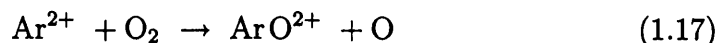
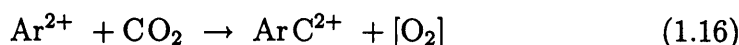
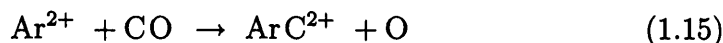
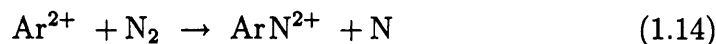
collision experiments with CF_2^{2+} :



Reaction 1.8 is interesting in that it is the only chemical reaction with CF_2^{2+} in which the C atom is not involved in the bond formation. Instead, the ionic fragment F^+ is transferred from the dication to the Xe. For the reactions in equation 1.9 and 1.10, no isotope effect was observed and experimental results suggested a barrier-less process, indicative of a direct mechanism. The two possible outcomes of the bond-forming reaction between CF_2^{2+} and HD

are given in equations 1.11 and 1.12. About twice the yield of DCF_2^+ was observed relative to HCF_2^+ . Collision experiments performed on the $\text{CF}_2^{2+} + \text{NH}_3$ system (reaction 1.13) showed that the formation of the product ion HNCF^+ exhibits a marked collision energy dependence. This suggests that there exists a barrier on the reaction path, which would imply a mechanism involving at least one collision complex. A discussion of the mechanisms for some of the above reactions as determined by previous quantum chemical calculations will be given in Section 1.2.2.

Interestingly, as can be seen in Table 1.1, the Ar^{2+} dication has been observed to exhibit a strong propensity for bond-forming reactivity in which the double charge is retained:



Although reactions such as these, in which the double charge is conserved in the product following bond-formation, have been previously observed for some transition metal dications, Ar^{2+} is the first non-metal dication to have been observed to participate in such reactions.

It is important to mention that the reactivity of “heavy” dications, such as metal-bearing dications or cluster dications (that may also contain metals),

is often quite different from that of small non-metal dications. For example, instances of bond-forming reactions are more common and the cross sections for forming products with new bonds are higher relative to bond-forming reactions involving small dications. Cross sections for forming electron transfer products are smaller and sometimes non-existent. This is due to the larger size of these dications and lower ionization potentials of their precursors. However, the reactivity of “heavy” dications is outside of the scope of this thesis, and hence will not be examined further. A good discussion of metal dication reactivity can be found in a review by Schröder and Schwarz [51].

1.2.2 Previous Computational Studies of Dication Reactivity

A number of computational studies exist on the structures and thermodynamic properties of the ground and excited states of molecular dications. Computational investigations of *reactions* of dications with neutral molecules are, however, scarce. This is due to the inherent difficulty of modelling the interaction of a dication with a neutral computationally. Since the repulsive state involving two monocations is almost always lower in energy, it is often difficult if not impossible to effectively model the interaction of a dication with a neutral without inadvertently falling to the lower energy repulsive state.

Due to the direct nature of electron transfer mechanisms, there has been no need for quantum chemical calculations to elucidate the mechanisms for these reactions. However, the relative energetics of the product and reactant

The third study by Roithová *et al.*[48] characterised the stationary points on the potential energy surfaces leading to the formation of the bond-forming product ion CHDCl^+ from collisions of the CHCl^{2+} dication with D_2 . They observe a number of different pathways, all of which appear to proceed *via* a similar mechanism to that originally suggested by Mrázek *et al.*, in which a collision complex is formed between the dication and the neutral, followed by internal H atom rearrangement and finally fragmentation of the complex to products. The mechanisms that we calculate for the $\text{CF}_2^{2+} + \text{H}_2\text{O}$ and $\text{CF}_3^{2+} + \text{H}_2$ systems that are discussed in Chapters 2 and 4, respectively, both agree with this general pattern of dication-neutral reactivity observed by Mrázek *et al.* and Roithová *et al.*.

In the fourth and most recent study, Ascenzi *et al.* provide the energetics of the entrance and exit channels for the bond-forming reaction pathways that result from collisions of Ar^{2+} with O_2 , showing that the formation of the ArO^+ and ArO^{2+} product ions in their ground and some excited states is exothermic [50].

1.3 Theoretical Background

1.3.1 Electronic Structure Calculations

Ab Initio Methods

Most physical processes on a human scale can be well described by classical mechanics and electromagnetism. These do not, however, take into account the wave-particle duality of all matter as suggested by the *de Broglie* relation:

$$\lambda = \frac{h}{p} \quad (1.18)$$

The wave-like nature of matter is described by its wavelength λ and the particle-like nature by its momentum p , where h is Planck's constant. At the atomic scale this wave-particle duality becomes very important due to the very small masses of the particles. As a result, the properties of a particle such as an electron must be described by a wavefunction ψ . The time-independent Schrödinger equation (SE) allows the energy E of a system described by the wavefunction to be determined *via* an eigenvalue equation:

$$\mathbf{H}\psi = E\psi \quad (1.19)$$

\mathbf{H} is the Hamiltonian operator, which consists of two parts: the kinetic and potential energy operators for the system:

$$\mathbf{H} = \mathbf{T} + \mathbf{V} \quad (1.20)$$

Although the time-independent SE neglects relativistic effects, these are significant only for atoms heavier than the period 3 elements, and have therefore not been taken into account in this study.

The Born-Oppenheimer Approximation The SE can only be solved exactly for hydrogenic (one-electron) systems. For it to be of use for more complex systems with more than one electron, some approximations must be made. The first of these is the *Born-Oppenheimer* approximation (BO), which assumes that the position of the nucleus of an atom is fixed. This assumption is generally valid due to the much greater mass of the nucleus relative to the electron. As such, any movement of the nucleus is accompanied by an instantaneous response by its electrons. This approximation requires that the SE be solved only for the electrons of the system, rather than for the electrons *and* the nuclei. The Hamiltonian operator therefore becomes the *electronic Hamiltonian*:

$$\begin{aligned} \mathbf{H}_e &= \mathbf{T}_e + \mathbf{V}_{ne} + \mathbf{V}_{ee} \\ &= -\sum_i^N \frac{1}{2} \nabla_i^2 - \sum_i^N \sum_a^N \frac{Z_a}{|\mathbf{R}_a - \mathbf{r}_i|} + \sum_i^N \sum_{j>i}^N \frac{1}{|\mathbf{r}_i - \mathbf{r}_j|} \end{aligned} \quad (1.21)$$

since the kinetic energy of the nucleus, \mathbf{T}_n , is assumed to be zero and the internuclear repulsion, \mathbf{V}_{nn} , is assumed to be constant. As can be seen in equation 1.21, \mathbf{H}_e includes electronic positions and momenta (\mathbf{r} and ∇_i^2) as variables, but includes only nuclear positions (\mathbf{R}) as constants.

The Hartree-Fock Self-Consistent Field Method Once the Born-Oppenheimer approximation has been made, the most commonly used method for finding an approximate solution to the SE (that now makes use of the electronic Hamiltonian) for systems with more than one electron is the *Hartree-Fock* (HF) *Self-Consistent Field* (SCF) method. The total wave function ψ is taken to be an antisymmetrized product of individual one-electron wave functions ϕ (or *spin-orbitals*) in the form of the *Slater determinant* (SD). Spin-orbitals are a product of a spatial atomic or molecular orbital function and a spin function. Writing the wavefunction as an SD takes into account the Pauli principle, which states that the total wavefunction must be antisymmetric with respect to the interchange of two electrons. The SD is then:

$$\psi(\mathbf{x}_i, \mathbf{R}) = \Phi = \frac{1}{\sqrt{N!}} \begin{vmatrix} \phi_1(1) & \phi_2(1) & \dots & \phi_N(1) \\ \phi_1(2) & \phi_2(2) & \dots & \phi_N(2) \\ \vdots & \vdots & \ddots & \vdots \\ \phi_1(N) & \phi_2(N) & \dots & \phi_N(N) \end{vmatrix} \quad (1.22)$$

where \mathbf{x}_i are the spin and space co-ordinates for an electron i and N is the number of electrons in the system. The columns in the SD are for a given molecular spin-orbital and the rows are for a given electron. The formation of a total wave function from one SD implies that the coordinates of a given electron are independent of those of the other electrons. As a result, the interaction between electrons or *electron correlation* is neglected. One way that this assumption can be improved upon is by adding more SD's to the total wavefunction in a linear combination. This will be discussed in more

detail in the next Section.

The quality of the spin-orbitals in the SD (and hence the quality of ψ) can be evaluated using the *variation theorem*. This states that the value of the *Rayleigh ratio* \mathcal{E} , will always be greater than or equal to the true ground state energy of the system:

$$\mathcal{E} \geq E_0 \quad (1.23)$$

$$\mathcal{E} = \frac{\langle \psi_{\text{trial}} | \mathbf{H} | \psi_{\text{trial}} \rangle}{\langle \psi_{\text{trial}} | \psi_{\text{trial}} \rangle} \quad (1.24)$$

where ψ_{trial} is any trial wavefunction. The problem is then reduced to finding a trial function that minimizes \mathcal{E} . Doing so results in a set of *Hartree-Fock equations*:

$$\mathbf{F}_i \phi_i = \epsilon_i \phi_i \quad (1.25)$$

where \mathbf{F}_i is the *Fock operator* and ϵ_i are the spin-orbital energies. \mathbf{F}_i contains three important operators: the *core Hamiltonian* \mathbf{h}_i , the *Coulomb operator* \mathbf{J}_i and the *Exchange operator* \mathbf{K}_i :

$$\mathbf{F}_i = \mathbf{h}_i + \sum_j^N (\mathbf{J}_j - \mathbf{K}_j) \quad (1.26)$$

$$\mathbf{h}_i = -\frac{1}{2} \nabla_i^2 - \sum_a \frac{Z_a}{|\mathbf{R}_a - \mathbf{r}_i|} \quad (1.27)$$

$$\mathbf{J}_i |\phi_j \rangle = \langle \phi_i | \frac{1}{|\mathbf{r}_i - \mathbf{r}_j|} | \phi_i \rangle | \phi_j \rangle \quad (1.28)$$

$$\mathbf{K}_i |\phi_j \rangle = \langle \phi_i | \frac{1}{|\mathbf{r}_i - \mathbf{r}_j|} | \phi_j \rangle | \phi_i \rangle \quad (1.29)$$

The core Hamiltonian describes the kinetic energy of the electron i and its

interaction with the fields of all nuclei a , assuming that there are no other electrons. The Coulomb and Exchange operators take into account electron-electron repulsion. J_i describes the Coulombic repulsion between electrons, and K_i represents the change in energy resulting from the exchange of two electrons of like spin. J_i is a local operator, whereas K_i is a nonlocal operator and has no classical analogue. This means that although one can obtain the Coulomb potential at \mathbf{x}_i using the local J_i operator, the exchange potential is not defined for just one given \mathbf{x}_i , since the value of the exchange potential depends on ϕ_j over all space. For this reason it is also sometimes called an *integral operator*.

As can be seen in equation 1.26, the operation of F_i on spin-orbital ϕ_i is dependent on J_j and K_j , both of which operate on the spin-orbital ϕ_j . As a result, the Fock equations must be solved iteratively. Once a Fock operator is obtained, this generates the new spin-orbitals that are used to build the SD. The process is repeated until the product spin-orbitals do not differ significantly from the spin-orbitals of the previous cycle, according to a given convergence criterion. The equations are then said to be *self-consistent*.

HF equations based on pure spin-orbitals are only practical for atomic and diatomic systems. For more complex systems, spin-orbitals are approximated using a *linear combination of atomic orbitals (LCAO)* as *molecular orbitals (MO)* in the form of a *basis set*. The larger the basis set, the better the approximation. Basis sets will be discussed in more detail in Section 1.3.1.

If each electron is described by its own spatial and spin function in the overall wavefunction, this is termed *Unrestricted Hartree-Fock (UHF)*, and

is generally applied to open shell systems. For closed shell systems, the restriction can be made that two electrons are assigned to each spatial orbital, one with spin up (α) and one with spin down (β). This is called *Restricted Hartree-Fock* (RHF) and is practical for closed shell systems as it reduces the total number of orbitals in the overall wavefunction, minimizing computational cost. For this reason, the *Restricted Open Shell Hartree-Fock* (ROHF) method is often used for open shell systems, whereby all paired electrons are expressed in the RHF manner, and only the unpaired electrons have their own spatial and spin orbitals.

It should be noted that HF methods, particularly RHF, only treat the repulsion between one electron and the field of all other electrons in the system. Electron-electron interactions are dealt with only in an average way, which fails particularly when electrons come into close proximity of one another. Hence, electron correlation is often defined as the difference between the true energy of the system and the HF energy. As the size of a molecule increases and the number of electrons increase, the electron correlation becomes greater.

Due to the greater flexibility of the UHF method, a greater number of states are included in the wavefunction. This, in effect, accounts for some electron correlation, lowering the overall energy of the system relative to a pure R(O)HF treatment. However, this also introduces the problem of spin contamination, or the contribution of higher spin states to the overall wavefunction (i.e. singlet states can be contaminated by triplet and quintet states, doublet states are contaminated by quartet states, etc.). Moreover,

the inclusion of some electron correlation in the UHF method is more of a fortuitous result rather than a systematic treatment. For molecules with greater numbers of electrons, electron correlation becomes so important that HF methods no longer give meaningful results. For this reason, post-Hartree-Fock electron correlation methods were developed.

Single Reference Electron Correlation Methods Although there are many important differences between the various *ab initio* post-HF methods, in one way or another their treatment of electron correlation always involves the construction of a trial wave function that is a sum of many SD's rather than just one. The wave function can then be written as:

$$\Psi = a_0\Phi_0 + \sum_{i=1} a_i\Phi_i \quad (1.30)$$

where Φ_0 is the HF determinant in which all spin-orbitals form the reference configuration. The additional determinants take into account excitations by replacing one or more of the occupied reference spin-orbitals with an unoccupied spin-orbital belonging to an excited state. *Singly, doubly, triply, etc.* excited SD's have each had one, two, three, etc. reference MOs replaced by a corresponding number of excited state MO's. They are referred to as *Singles* (S), *Doubles* (D), *Triples* (T), etc. The greater the number of excitations represented, the higher the quality of the wave function. It is therefore clear that the size of the basis set is also important in the determination of an accurate solution. The larger the basis set, the greater the number excitations possible. This is illustrated in Figure 1.3, where full correlation implies all

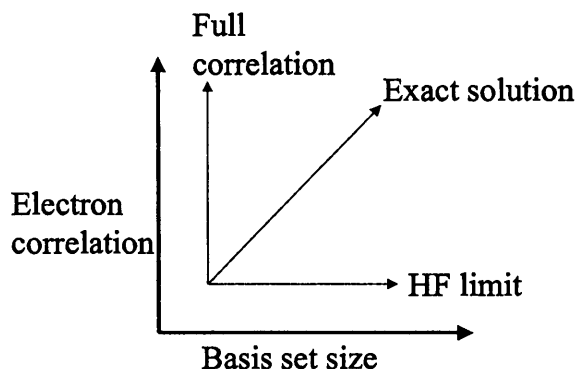


Figure 1.3: The quality of the solution of the Schrödinger equation depends on both the method and the basis set.

possible excitations from the reference configuration. It should be noted that only excitations of the same symmetry as the reference state can contribute to its energy. One of the ways in which electron correlation methods differ is in the manner in which they select which additional determinants should contribute to the total wavefunction.

The problem of electron correlation can be divided into two different categories: *dynamic* correlation, which is used to describe the effect of the presence of an electron in the field of one or more other electrons; and *non-dynamic* or *static* correlation, which addresses the fact that for certain systems, a number of different electronic configurations can contribute to the overall wavefunction of the system at a given geometry. The inclusion of static correlation usually implies the expression of the total wavefunction as a linear combination of many reference wavefunctions, giving rise to the term *multireference methods*. These methods will be described in more detail in the next section. This section will examine some of the more common *sin-*

gle reference post-Hartree-Fock methods that were devised to account for dynamic electron correlation. These methods involve the inclusion of extra SDs in the total wavefunction that correspond to excitations from a single reference wavefunction. It should be noted that although there is a distinction made between static and dynamic correlation in the way in which they are treated in multi- and single-reference methods, respectively, in practice this distinction is not so clear. The construction of the total wavefunction in single-reference methods will inadvertently include corrections for some static correlation, and vice versa.

There are three primary single reference electron correlation methods. These are *Many Body* (or *Møller-Plesset*) *Perturbation Theory* (MPPT), *Configuration Interaction* (CI), and *Coupled Cluster* (CC). MP and CI methods include all possible excitations but to a restricted level (2nd order, 3rd order, etc.) CC on the other hand, includes corrections to a restricted extent, but to infinite order. Of these three methods, the CC method was the most extensively applied method in the studies presented in this thesis. Accordingly, a brief description of MP_n and CI methods will be given, followed by a more detailed description of the CC method.

Many body perturbation theory was first developed by Rayleigh and Schrödinger and assumes that the correlation corrected Hamiltonian is the sum of the Hamiltonian for a known problem (H_0) and a small perturbation Hamiltonian H' :

$$\mathbf{H} = \mathbf{H}_0 + \lambda\mathbf{H}' \quad (1.31)$$

where λ determines the extent of the perturbation.

Møller-Plesset perturbation theory takes \mathbf{H}_0 to be the sum of the one-electron Fock operators [56]. Since this counts the average electron-electron repulsion energy twice, the perturbation is therefore the exact electron-electron repulsion minus twice the average repulsion:

$$\mathbf{H}' = \mathbf{H} - \mathbf{H}_0 = \mathbf{V}_{ee} - 2 \langle \mathbf{V}_{ee} \rangle \quad (1.32)$$

where \mathbf{V}_{ee} is known from equation 1.21.

By expanding the eigenfunctions Ψ_0 and energy eigenvalues a_0 as a Taylor series and equating terms in equal powers of λ , expressions for the zeroth ($a_0^{(0)}$), first ($a_0^{(1)}$), second ($a_0^{(2)}$), etc. order energy corrections can be obtained. The sum of the zeroth and first order corrections is simply the Hartree-Fock energy E_{HF} . Corrections due to electron correlation are introduced as of the second order correction term. MPPT methods that include corrections up to the n -th order are termed MP_n methods. It has been shown that improvements in recovering electron correlation are most significant in steps of $2n + 2$. This is because electrons most commonly interact in pairs. Hence, the improvement gained in including fourth order terms is much greater than that of including third order terms.

It is important to note that MP_n methods are only reliable for systems where the correction for electron correlation is small, since the assumption in using a Taylor series expansion for Ψ_0 and a_0 is that the perturbation is small. For systems where electron correlation is expected to have a strong contribution to the total energy, it may be preferable to use CI-based methods. This

involves constructing the total wavefunction as a sum of the HF determinant plus additional determinants corresponding to N -electron excitations of the reference configuration:

$$\Psi = a_0\Psi_{\text{HF}} + \sum_S a_S\Phi_S + \sum_D a_D\Phi_D + \sum_T a_T\Phi_T + \cdots = \sum_i^N a_i\Phi_i \quad (1.33)$$

For single-reference CI, it is assumed that the reference orbitals are a good description of the system and therefore are not re-optimized.

CI is a variational method. Therefore, using the CI wavefunction, the energy is minimized by the variational method described above in equation 1.24. This results in a set of CI *secular equations* of the form $\mathbf{H}_{ij} = \langle\phi_i|\mathbf{H}|\phi_j\rangle$. If all excitations of all N electrons are represented in the CI matrix, this is called *full CI*. However, since the largest contributions to the overall CI wavefunction are the Φ_D terms, a common simplification involves including only the singles and doubles terms, or CISD. This truncation of the CI wavefunction results in CISD *not being size consistent*, which means that the sum of the energies of two fragments calculated separately will be lower than the energy of one system consisting of the same two fragments at large separation. MP_n and CC methods, by comparison, are size consistent. A number of methods have been developed that provide corrections to the CISD method in order to make it size consistent. Such methods are Quadratic CISD (QCISD), Averaged Coupled-Pair Functional (ACPF) and Averaged Quadratic Coupled Cluster (AQCC), and they all involve the inclusion of higher order terms in different ways and to varying extents. The QCISD method has been shown

to be essentially mathematically equivalent to CCSD.

The CC wavefunction is written as:

$$\Psi_{\text{CC}} = e^{\mathbf{T}} \Phi_0 \quad (1.34)$$

where \mathbf{T} is the *cluster operator* ($\mathbf{T} = \mathbf{T}_1 + \mathbf{T}_2 + \mathbf{T}_3 + \dots + \mathbf{T}_N$) and $e^{\mathbf{T}}$ can be expanded by a Taylor series:

$$e^{\mathbf{T}} = 1 + \mathbf{T} + \frac{1}{2}\mathbf{T}^2 + \frac{1}{6}\mathbf{T}^3 + \dots \quad (1.35)$$

This can be re-written as:

$$e^{\mathbf{T}} = 1 + \mathbf{T}_1 + (\mathbf{T}_2 + \frac{1}{2}\mathbf{T}_1^2) + (\mathbf{T}_3 + \mathbf{T}_2\mathbf{T}_1 + \frac{1}{6}\mathbf{T}_1^3) + \dots \quad (1.36)$$

The first term generates the reference HF SD, the second all the singly excited determinants, the third all the doubly excited determinants, and so on. “Pure” terms such as \mathbf{T}_2 are referred to as *connected*, because the electrons they describe act together. *Disconnected* terms such as \mathbf{T}_1^2 describe electrons that act independently. For example, the disconnected operator $\mathbf{T}_2\mathbf{T}_1$ corresponds to the excitation of a pair of interacting electrons independently of the excitation of another single electron.

The cluster operator \mathbf{T} operates on the reference HF wave function in the following way:

$$\mathbf{T}_1 \Phi_0 = \sum_i^{\text{occ}} \sum_a^{\text{vir}} t_i^a \phi_i^a \quad (1.37)$$

$$\mathbf{T}_2\Phi_0 = \sum_{i < j}^{\text{occ}} \sum_{a < b}^{\text{vir}} t_{ij}^{ab} \phi_{ij}^{ab} \quad (1.38)$$

$$\vdots$$

The t coefficients are called *amplitudes*. As can be seen, excitations to infinite order are included.

In the case of CCSD [57], only the singles and doubles terms of the cluster operator are used (i.e. \mathbf{T}_1 and \mathbf{T}_2). The exponential operator can then be written as

$$e^{\mathbf{T}} = 1 + \mathbf{T}_1 + (\mathbf{T}_2 + \frac{1}{2}\mathbf{T}_1^2) + (\mathbf{T}_2\mathbf{T}_1 + \frac{1}{6}\mathbf{T}_1^3) + \dots \quad (1.39)$$

Using only singles and doubles operators, all excitations can be represented. It should be noted, however, that excitations greater than 2 are only represented in an approximate way since any connected or disconnected terms involving \mathbf{T}_n ($n > 2$) are not included. This approximation is generally valid, since the doubles amplitudes tend to carry the most weight (and correspondingly, disconnected terms involving \mathbf{T}_2 carry more weight than those that do not). In addition, as n increases, \mathbf{T}_n becomes less important, since it is rare to have such a large number of interacting electrons.

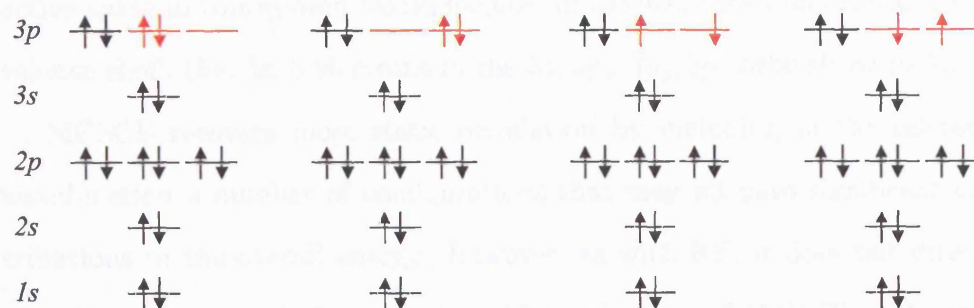
The CCSD method can be improved by including triples. A pure CCSDT method is very computationally expensive, however, so to compensate the triples can be evaluated using MPPT and their amplitudes added to the CCSD result, giving CCSD(T). Triples can be added perturbatively to the QCISD method in the same manner, giving QCISD(T).

It should be noted that CC methods work well only for “true” ground state systems, where the HOMO-LUMO gap is large. This is because CC methods rely on the approximation that the T_2 term contributes the most to the correlation energy. A system which has a mixing of states would have a much greater weighting to the T_1 term (single excitations), yielding unreliable results. Within a CC calculation, the T_1 -*diagnostic* can give an indication as to the degree of multireference character of a given system [58]. It is defined as:

$$T_1 = \frac{|\mathbf{t}_1|}{\sqrt{N}} \quad (1.40)$$

where \mathbf{t}_1 is the singles amplitude vector and N is the number of electrons. The Q_1 -diagnostic is defined in a similar way for QCISD(T). In cases where the T_1 -diagnostic is large (usually taken as $T_1 > 0.02$ for closed shell systems), multireference methods must be used.

Multireference Electron Correlation Methods Hartree-Fock methods assume that only occupied orbitals contribute to the total energy of a system. Multireference methods will optimize both occupied *and* virtual orbitals in a given *active space* specified by the user, allowing the energies of both occupied and virtual orbitals to contribute to the total electronic energy. This is illustrated in Figure 1.4, where the singlet Ar^{2+} dication is given as an example. An active space comprising two electrons and two $3p$ orbitals has been chosen for simplicity. This generates four determinants but only three different configurations. Since a configuration refers only to the overall multiplicity of the molecule and the occupation of each orbital, not



Determinant 1 Determinant 2 Determinant 3 Determinant 4
 (Configuration 1) (Configuration 2) (Configuration 3) (Configuration 3)

Figure 1.4: A 2-electron, 2-orbital active space for singlet Ar^{2+} .

the spin of each electron, one configuration such as configuration 3 in Figure 1.4 can be made up of more than one determinant. Therefore methods like ROHF are multi-determinantal, but not multiconfigurational. Methods such as Multiconfigurational SCF (MCSCF) are both multi-determinantal and multiconfigurational. The MCSCF method simply involves carrying out the HF-SCF procedure using a multiconfigurational reference wavefunction. This wavefunction is constructed as the sum of all allowed configurations that can be generated within a given active space. If all possible arrangements of electrons are allowed in a given active space, this is called Complete Active Space MCSCF (CASSCF).

It is important to note that although a (2,2) active space for singlet Ar^{2+} was chosen for simplicity as an example in Figure 1.4, in practice, since the three 3p orbitals are degenerate, it would be unwise to exclude the third p orbital and the extra electron pair from the active space. In fact, a sensible

active space in this system would include all the electrons and orbitals in the valence shell, that is, 6 electrons in the $3s, 3p_x, 3p_y, 3p_z$ orbitals or (6,4).

MCSCF recovers most static correlation by including in the reference wavefunction a number of configurations that may all have significant contributions to the overall energy. However, as with HF, it does not directly recover much dynamical correlation. Multireference CI (MRCI) is the most commonly used method to include dynamical correlation as well as static correlation. MRCI simply involves carrying out the CISD procedure using the MCSCF wavefunction as the reference. As with single-reference CISD, MRCI is also not size extensive. Therefore, multireference extensions of methods that correct the size-inconsistency of CISD, such as AQCC discussed above, have been developed (i.e. MR-AQCC).

Excited States and State-Averaging It is clear that the treatment of systems of electronically excited states requires the use of post-HF methods, ideally multireference methods. CASSCF and MRCI (or MR-AQCC) are commonly used for the modelling of excited states. However, in systems that possess curve crossings or conical intersections, variationally optimizing the wavefunction to the energy of an excited state can become problematic in the region of the crossing as the energy of an excited state can actually fall below that of the “ground” state after the crossing. In such a case the orbitals will then be optimized to the energy of the incorrect state.

For this reason, calculations of potential energy surfaces of excited states are often performed using *state-averaged* (SA) techniques such as SA-CASSCF

or SA-MRCI. These methods optimize the orbitals to the average energy of the multiple states in question. In this manner, the stability of the solutions can be maintained. However, this comes at the expense of the accuracy of the final solutions, since the use of an average energy as the variational target for multiple states causes a raising of the energies of the lower states and a lowering of the energies of the higher states.

Density Functional Theory

In 1964 it was shown by Hohenburg and Kohn that the ground state energy of a system is a direct function of the electron density [59]. Whereas the wavefunction is governed by the coordinates of each electron in the system, the electron density is dependent only on its own three coordinates, which is independent of the number of electrons. The exact electron density matrix ($\rho(\mathbf{r})$) can be approximated as a sum of one-electron densities, known as *Kohn-Sham* (KS) orbitals $\phi(\mathbf{r})$ [60]:

$$\rho(\mathbf{r}) = \sum_i^N |\phi_i(\mathbf{r})|^2 \quad (1.41)$$

Although the use of an orbital representation re-introduces the need for electronic coordinates, it will be seen that the use of density functionals greatly simplifies the calculation of electron correlation. This provides results that often rival *ab initio* CI accuracy, but with HF effort.

As with HF theory, the total energy functional with respect to $\rho(\mathbf{r})$ can be divided into kinetic energy, nuclear-electronic attraction and electron-

electron repulsion functionals, $T_S[\rho]$, $E_{ne}[\rho]$ and $E_{ee}[\rho]$ respectively. As before, the electron-electron repulsion is divided into Coulomb ($J[\rho]$) and Exchange ($K[\rho]$) parts. The relationship between the total ground state energy and the electron density can then be written as:

$$E_{DFT}[\rho] = T_S[\rho] + E_{ne}[\rho] + J[\rho] + E_{XC}[\rho] \quad (1.42)$$

$$= \sum_i^N \left\langle \phi_i \left| -\frac{1}{2} \nabla^2 \right| \phi_i \right\rangle + \sum_a \int \frac{Z_a \rho(\mathbf{r})}{|\mathbf{R}_a - \mathbf{r}|} d\mathbf{r} + \frac{1}{2} \int \int \frac{\rho(\mathbf{r}) \rho(\mathbf{r}')}{|\mathbf{r} - \mathbf{r}'|} d\mathbf{r} d\mathbf{r}' + E_{XC}[\rho]$$

In this case T_S is only an approximation to the exact kinetic energy based on the assumption of non-interacting electrons. E_{XC} is the *exchange-correlation* energy. It incorporates the exchange energy functional K , corrections to the kinetic energy and the non-Coulombic electron-electron repulsion.

The exact form of E_{XC} is not known. A first approximation separates the exchange and correlation parts:

$$E_{XC} = E_X + E_C \quad (1.43)$$

The *Local Spin Density Approximation* (LSDA) assumes that the electron density can be described as a uniform electron gas, with electrons of opposite spin (α and β) treated independently:

$$E_X^{LSDA} = -\frac{3}{4} \left(\frac{3}{\pi} \right)^{\frac{1}{3}} \int (\rho_\alpha + \rho_\beta)^{\frac{4}{3}} d\mathbf{r} \quad (1.44)$$

The correlation energy is assumed to be negligible. Although some LSDA functionals have been proposed to take into account electron correlation

(Vosko, Wilk and Nusair (VWN)[61]; Perdew and Wang (PW91)[62]), most LSDA methods underestimate the exchange energy and overestimate the correlation. This is a result of the assumption of a uniform electron gas. LSDA methods can be improved upon using the *Generalized-Gradient Approximation* (GGA). This takes the non-uniformity of the electron gas into account by including the gradients of the density. A number of functionals have been proposed as corrections to the LSDA exchange energy (PW86 [63], B88 [64]), as well as functionals that describe the correlation energy (P86 [65,66], LYP [67]). All of these functionals make use of parameters which are fitted to accurate experimental data. It is for this reason that DFT is often referred to as a *semi-empirical* method, although in principle it is theoretically exact.

Greater accuracy has been achieved through the development of *hybrid* methods. These incorporate an exchange energy term that is evaluated using HF methods, using KS orbitals instead of Fock orbitals. Of relevance to this work is the B3LYP hybrid, which makes use of *Becke's 3-parameter functional* (E_{XC}^{B3}) and the *Lee-Yang-Parr* GGA correction to the correlation energy (ΔE_C^{LYP}):

$$E_{XC}^{B3} = E_X^{LSDA} + E_C^{LSDA} + a_0 (E_X^{HF} - E_X^{LSDA}) + a_X \Delta E_X^{B88} + a_C \Delta E_C^{LYP} \quad (1.45)$$

where a_0 , a_X and a_C are empirical parameters.

Basis Sets

A complete basis set of an infinite LCAO is an exact representation of the electronic structure of a system. Hence, in general, the larger the basis set, the more accurate the representation. There exist in general two kinds of basis function: *Slater-Type Orbitals* (STO):

$$\chi_{\zeta,n,l,m}(r, \theta, \phi) = NY_{l,m}(\theta, \phi) r^{n-1} e^{-\zeta r} \quad (1.46)$$

and *Gaussian-Type Orbitals* (GTO):

$$\chi_{\zeta,n,l,m}(r, \theta, \phi) = NY_{l,m}(\theta, \phi) r^{2n-2-l} e^{-\alpha r^2} \quad (1.47)$$

where $Y_{l,m}(\theta, \phi)$ are the spherical harmonics. The important difference between STOs and GTOs is the r^2 dependence in the exponential term in GTOs. Although STOs are more accurate (they are exactly the radial dependence of hydrogenic atomic orbitals), up to the same accuracy can be achieved by simply using linear combinations of more GTOs, whose integrals are much easier to compute. For this reason, GTOs are commonly used in computational codes that employ analytical integration schemes (when numerical integration schemes are used there is no computational advantage in using GTOs).

Further computational efficiency can be achieved by using *Contracted Gaussian-Type Orbitals* (CGTOs). A CGTO comprises of a contraction of typically 3-6 GTOs or *Primitive Gaussian-Type Orbitals* (PGTOs). The

result is a fixed, non-dynamic LCAO that is sufficient for the description of electrons that are not as chemically important (usually the core electrons). Therefore most basis sets are *split-valence* in one way or another, indicating that the set consists of a mixture of CGTOs and PGTOs.

A *minimum basis set* contains only one basis function per occupied orbital in the system. The electron distribution can only be accounted for in an average way, and therefore more functions are necessary to describe variations in electron density. Orbitals which are *tight* or *diffuse* to varying degrees (the more diffuse a basis function, the smaller its exponent) can be included using nZ methods, where each basis function of the same type (s, p, d etc.) in the minimum basis is augmented by a factor of n . DZ is double-zeta, TZ is triple-zeta, etc.

The polarising effect that the orbitals in one atom can have on another is accommodated by adding *polarization* functions. For example, some p -character can be added to an s -orbital by the addition of a polarisation function.

Different families of basis sets exist, their differences lying mostly in the contraction schemes of the PGTOs. Atomic Natural Orbitals (ANO) basis sets were developed by carrying out atomic electronic structure calculations using electron correlation methods in order to determine the ideal functional coefficients and exponents for the contraction of a large number of PGTOs. Correlation-consistent (cc) (also known as Dunning) basis sets are constructed in a similar fashion, except that fewer original PGTOs are used. This is justified by making the assumption that the electron correlation need

be considered only for the valence electrons. Dunning basis sets are labelled in the form cc-pVnZ, i.e. correlation-consistent polarisation valence n -zeta. The addition of the “aug” prefix indicates the inclusion of diffuse functions. A number of different Dunning basis sets were used for the calculations presented in Chapters 3, 4 and 5 of this thesis.

Pople-style basis sets are also split-valence basis sets comprising a combination of CGTOs, PGTOs, diffuse functions and polarization functions. For example, the 6-311++G(2df,2pd) basis set was used for the calculations described in Chapter 2. The Pople basis set labelling in this case indicates that the set consists of one CGTO built from 6 PGTOs for the core electrons; three CGTOs consisting of three, one and one PGTOs to describe the valence electrons near the nucleus, middle and outer regions of the atom respectively; diffuse s - and p -functions for non-hydrogen atoms; diffuse s -functions for hydrogens (these are denoted by the + symbols); two d and one f polarization functions on non-hydrogen atoms and two p and one d polarization functions on hydrogens.

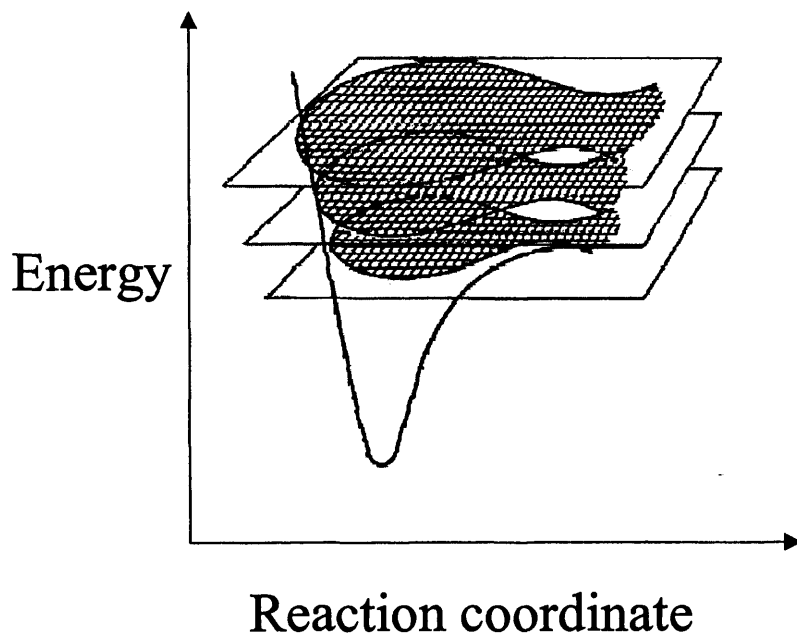


Figure 1.5: A schematic dissociation potential energy surface, with associated phase space [68].

1.3.2 Rate Constants and RRKM/Quasi-equilibrium Theory

While a PES can provide “rules” for which processes are possible at a given energy, it provides no information, however, as to their *likelihoods*. A certain process may be thermodynamically possible, however the rates may be so slow that common interaction times are not sufficient to yield products in measurable amounts. For this reason, the calculation of rate constants can provide useful additional information to a computational study that seeks to explain experimental behaviour.

Figure 1.5 shows a schematic PES for a unimolecular dissociation with a

large barrier to dissociation. Superimposed upon it are cross sections of the phase space volume which this PES occupies. The “width” of this volume at any given point represents the number of configurations available to the system at that point. That is, at a given geometry and a given energy, there is a finite number of ways that the system can distribute its internal energy. As the energy increases for a given geometry, the number of configurations increases. A system at constant energy is restricted to one phase space surface, and the transition state is defined as the narrowest region of the surface. The shape of the phase space volume, as with the PES, is characteristic of the system. The *critical surface* is located at the energy of the saddle point and has all dimensions orthogonal to the reaction co-ordinate. The rate of the dissociation is then the flux of molecules through the critical surface:

$$\text{rate} = \phi = \frac{d\aleph(q^\ddagger, p^\ddagger)}{dt} \quad (1.48)$$

where q^\ddagger and p^\ddagger are the position and momentum vectors, respectively, at the transition state (\ddagger). The flux can also be expressed as the number of molecules \aleph times the ratio of the phase space area of the critical surface to the phase space area at the total energy of the system.

$$\phi = \frac{d\aleph(q^\ddagger, p^\ddagger)}{dt} = \frac{\aleph dq^\ddagger dp^\ddagger \int_{H=E-E_0-\epsilon} \cdots \int dq_1^\ddagger \cdots dq_{n-1}^\ddagger dp_1^\ddagger \cdots dp_{n-1}^\ddagger}{\int_{H=E} \cdots \int dq_1 \cdots dq_n dp_1 \cdots dp_n} \quad (1.49)$$

where $q_n^\ddagger, p_n^\ddagger$ are the position and momentum vectors for each coordinate n in the system (except for the critical mode, whose position and momentum vectors are q^\ddagger and p^\ddagger as mentioned above). E is the total energy of the

system, E_0 is the activation energy and ϵ^\ddagger is the translational energy at the transition state, that is, the energy that is not available for distribution through vibrational modes. This is illustrated in Figure 1.6. Note that all energies take into account zero-point energies. Also, the critical phase space area is determined over one fewer dimension ($n - 1$) than the phase space area at the total energy of the system, since it does not include the reaction co-ordinate.

Since the rate is related to the flux through the critical surface, the time dependence applies only to q^\ddagger, p^\ddagger . Since we know that $dq^\ddagger/dt = p^\ddagger/\mu$, we can let $dq^\ddagger dp^\ddagger = p^\ddagger dp^\ddagger/\mu$. But this is also the derivative of the translational energy $\epsilon = p^{\ddagger 2}/2\mu$. Thus, we can rewrite Equation 1.49 as:

$$\phi = \frac{\aleph d\epsilon^\ddagger \int_{H=E-E_0-\epsilon} \cdots \int dq_1^\ddagger \cdots dq_{n-1}^\ddagger dp_1^\ddagger \cdots dp_{n-1}^\ddagger}{\int_{H=E} \cdots \int dq_1 \cdots dq_n dp_1 \cdots dp_n} \quad (1.50)$$

The classical concept of a phase space area can be “quantized” by dividing it by a factor of h^n to give a quantum density of states. Hence, ϕ can be expressed as a ratio of densities of states (ρ):

$$\phi = \aleph d\epsilon^\ddagger \frac{h^{n-1} \rho(E - E_0 - \epsilon)}{h^n \rho(E)} \quad (1.51)$$

It is important to note that equation 1.51 takes into account only one possible distribution of energy, or only one value of ϵ . To include all configurations, the transition state density of states must be integrated over all possible translational energies. Since the rate constant $k(E) = \phi/\aleph$, the final

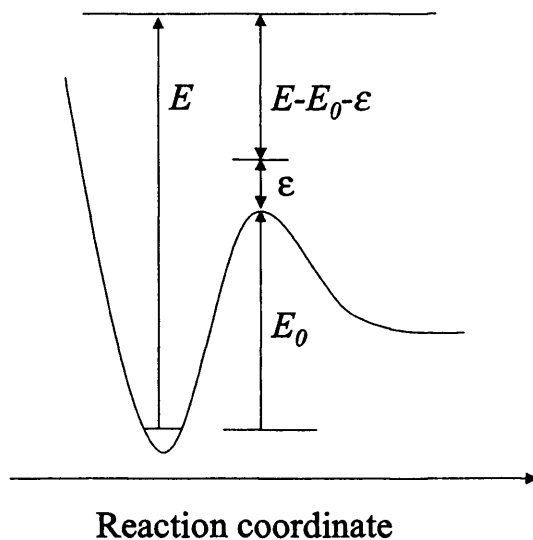


Figure 1.6: The energy distribution of a unimolecular dissociation [69]. The energy at the transition state, $E - E_0$, is distributed between the translational energy ϵ and the vibrational modes $E - E_0 - \epsilon$.

form of the equation for the rate constant is then:

$$k(E) = \frac{\sigma N^\ddagger(E - E_0)}{h\rho(E)} \quad (1.52)$$

where σ is the reaction degeneracy. A molecule with higher symmetry will have a greater flux of molecules through the critical phase space.

Equation 1.52 is a part of two analogous statistical rate theories that were developed in parallel: Rice-Ramsperger-Kassel-Marcus (RRKM) theory for reactions of neutral molecules, and quasi-equilibrium theory (QET) for ionic species, with particular application to mass spectrometry [69]. It should be noted that these are simplified statistical rate models that do not take into account the effects of rotational excitation, anharmonicity of the vibrational

oscillators and the possibility of tunneling. More sophisticated models that take such effects into account are described by Baer and Hase [68]. However, in most cases the errors in obtaining accurate barrier heights are greater than those of omitting rotational, anharmonicity and tunneling effects. Moreover, when rate constants are expressed as ratios, as is the case for the studies that make use of the RRKM equation in this thesis, most of the errors due to these effects would partially cancel.

1.3.3 Landau-Zener Theory

The simplest interaction of a dication with a neutral is electron transfer. This interaction can be understood as an adiabatic crossing from the association potential of the dication + neutral to the Coulombic repulsion potential of the corresponding monocation + monocation, such as was shown in Figure 1.1. However, the probability of a charge transfer reaction actually taking place, or the size of the reaction cross section, depends on how and where these two curves intersect. If the crossing occurs at a large interspecies separation r , then the electron will have difficulty tunneling from the neutral to the dication and the charge transfer probability will be small. If the crossing occurs at a small r , the electronic coupling between the two states will be very strong, resulting in curve hopping both on approach and on separation of the two fragments, resulting in no net electron transfer. Therefore, there exists an ideal range of r , or a “reaction window”, in which the electronic coupling between the two states is high enough to promote the transfer of an electron from the neutral to the dication, but low enough to ensure that the electron will not transfer back to the neutral precursor, resulting in a favourable electron transfer probability. According to the Landau-Zener reaction window theory, this ideal range is between 2-6 Å [70–72]. See Figure 1.7 for an illustration of the reaction window concept.

In order to determine the location of the curve crossing for a given system, it is possible to model the reactant and product state potential curves. The

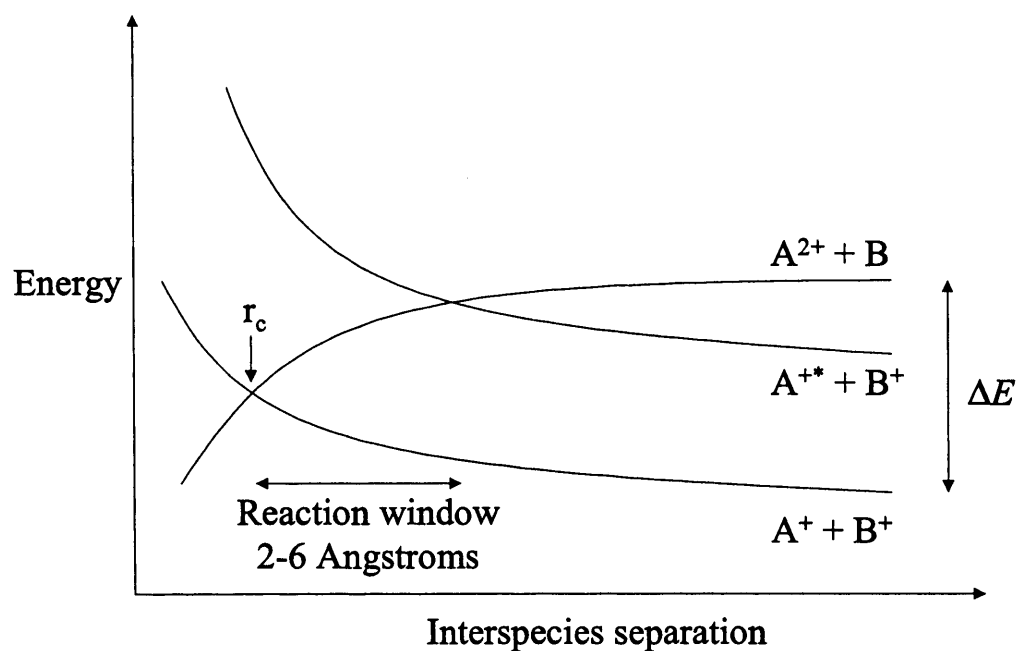


Figure 1.7: Schematic diagram to illustrate the reaction window concept. The likelihood of an electron transfer reaction occurring successfully depends on where the reactant and product potentials cross (r_c) and the reaction exothermicity (ΔE).

polarization attraction between the dication and the neutral is given by:

$$V_1 = \frac{-Z^2 e^2 \alpha}{2r^4} + \Delta E \quad (1.53)$$

where Z is the charge of the dication and ΔE is the reaction exothermicity, or the difference in energy between the reactant and product state asymptotes.

The Coulombic repulsion is simply given by:

$$V_2 = \frac{e^2}{r} \quad (1.54)$$

where $V = 0$ at the infinite separation of the two monocations. These two equations can then be solved for r to determine the curve crossing radius r_c .

The curve crossing radius can give an indication as to whether electron transfer will be favoured or not, but in order to obtain cross sections for the formation of given electron transfer products, the Landau-Zener model can be applied. This states that the probability for a crossing from a reactant to a product state is given by:

$$P = 2\delta(1 - \delta) \quad (1.55)$$

$$\delta = \exp\left(\frac{-\pi |H_{12}|^2}{2\hbar |V'_1 - V'_2| v}\right) \quad (1.56)$$

where H_{12} is the electronic coupling matrix between the two states, V'_i are the slopes of the two potentials at the crossing radius r_c and v is the relative radial velocity of the two reactants. H_{12} can be determined with greater accuracy if the electronic wavefunctions of the products and reactants are

known at r_c , or it can be approximated empirically. The empirical formalism for H_{12} that is implemented in a program written by S. D. Price that we use in Chapter 5 in order to estimate cross sections for the electron transfer reactions of SF^{2+} with H_2O is given below, as proposed by Olson *et al.* [73]:

$$|H_{12}| = 1.0(I_A I_B) r_c^{*2} e^{-1.72 r_c^*} \quad (1.57)$$

$$r_c^* = \left(\frac{I_A^{1/2} + I_B^{1/2}}{\sqrt{2}} \right) r_c \quad (1.58)$$

where I_i is the ionization potential of fragment i .

The probability given in equation 1.55 can then be integrated over the range of viable impact parameters b to obtain the reaction cross section σ :

$$\sigma = \int_0^{b_{\max}} 2\pi b P db \quad (1.59)$$

1.3.4 Calculation of Franck-Condon Factors

The Harmonic Oscillator

To a first approximation, the vibrations of a diatomic molecule can be modelled as a simple harmonic oscillator where the interatomic distance x is governed by the force of the bond F :

$$F = -kx \quad (1.60)$$

and k is the force constant of the bond. Since the force is the derivative of the potential with respect to x , the potential V can be expressed as:

$$V = \frac{1}{2}kx^2 \quad (1.61)$$

The vibrational wavefunction for the system can then be determined by solving the Schrödinger equation (given in Section 1.3.1 by Equation 1.20) where the Hamiltonian consists of $\mathbf{T} = -\frac{\hbar}{2m} \frac{d^2}{dx^2}$ (m is the reduced mass of the diatomic) and $\mathbf{V} = \frac{1}{2}kx^2$:

$$-\frac{\hbar}{2m} \frac{d^2\psi}{dx^2} + \frac{1}{2}kx^2\psi = E\psi \quad (1.62)$$

The solution to this differential equation requires the introduction of a quantum number v . This results in wavefunctions of the form:

$$\psi_v = N_v H_v e^{-\frac{\sqrt{mk}}{2\hbar} x} \quad (1.63)$$

where H_v is the Hermite polynomial for a given value of v and N_v is the normalisation constant. The energy eigenvalue is then:

$$E = \left(v + \frac{1}{2}\right)h\nu \quad (1.64)$$

where ν is the vibrational frequency. Thus, the energy of the harmonic oscillator is quantised and all of its energy levels are equally spaced by $h\nu$.

However, a diatomic molecule is not a true harmonic oscillator. Although the parabolic harmonic oscillator potential can model a diatomic quite well at internuclear distances near the equilibrium, at long interatomic distances a finite potential is required that approaches the dissociation limit asymptotically. In practice, the potential energy curves for the dissociation of a diatomic molecule are unique to the molecule and electronic state in question. Although the Schrödinger equation can be solved exactly for the harmonic oscillator, the potentials required to accurately model real diatomic molecules often generate a form of the Schrödinger equation that cannot be solved analytically. In such cases, numerical methods must be used.

The Numerov Method

In order to perform a numerical solution to the Schrödinger equation, we can evaluate it over a series of short intervals s of the potential (See Figure 1.8). We begin by noting that any function $f(x)$ can be expressed in the form of a Taylor series:

$$f(x) = f(x_n) + \frac{f'(x_n)(x - x_n)^1}{1!} + \frac{f''(x)(x - x_n)^2}{2!} + \dots \quad (1.65)$$

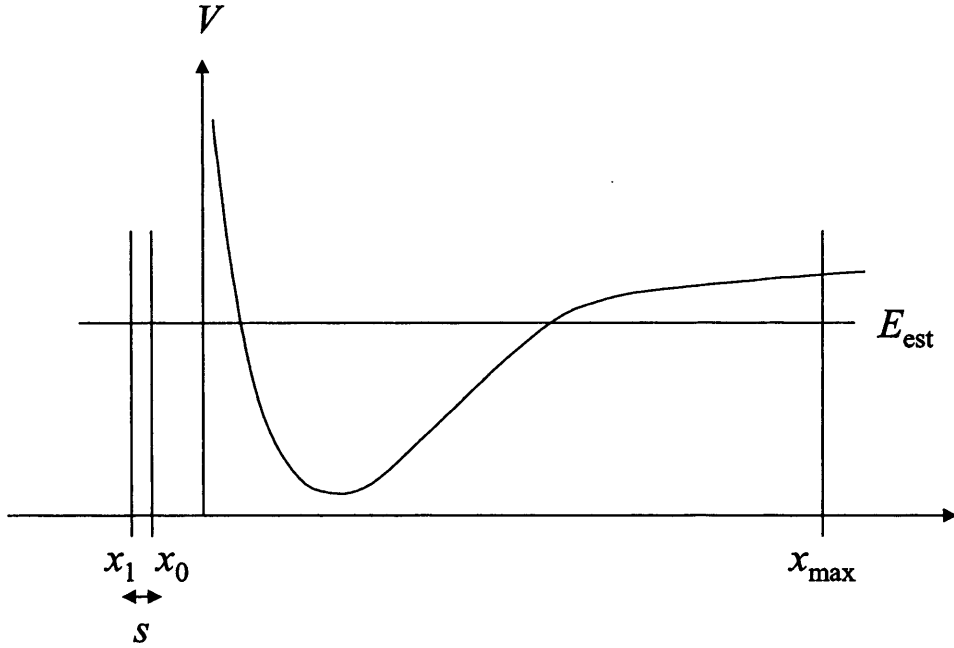


Figure 1.8: Potential energy curve for a diatomic molecule.

By setting $s = x - x_n$, we obtain expressions for the endpoints of the two intervals adjacent to x_n :

$$f(x_n+s) \approx f(x_n) + f'(x_n)s + \frac{1}{2}f''(x_n)s^2 + \frac{1}{6}f'''(x_n)s^3 + \frac{1}{24}f^{(iv)}(x_n)s^4 + \frac{1}{120}f^{(v)}(x_n)s^5 \quad (1.66)$$

$$f(x_n-s) \approx f(x_n) - f'(x_n)s + \frac{1}{2}f''(x_n)s^2 - \frac{1}{6}f'''(x_n)s^3 + \frac{1}{24}f^{(iv)}(x_n)s^4 - \frac{1}{120}f^{(v)}(x_n)s^5 \quad (1.67)$$

For small s , we can ignore the terms in s^6 and higher because they will have a negligible contribution. By adding equations 1.66 and 1.67 to obtain one expression we get:

$$f(x_n+s) + f(x_n-s) \approx 2f(x_n) + f''(x_n)s^2 + \frac{1}{12}f^{(iv)}(x_n)s^4 \quad (1.68)$$

We can use this expression to evaluate the wavefunction ψ , but the last two terms require that we evaluate ψ'' and $\psi^{(iv)}$. By rearranging the Schrödinger equation given above in equation 1.62, we have $\psi'' = m/\sqrt{2}[2V(x) - 2E]\psi$. To obtain an expression for $\psi^{(iv)}$, we replace ψ'' in equation 1.68 and let $x_n + s = n + 1$, $x_n - s = n - 1$:

$$\psi''_{n+1} \approx -\psi''_{n-1} + 2\psi''_n + \psi_n^{(iv)}s^2 + \frac{1}{12}\psi_n^{(vi)}s^4 \quad (1.69)$$

By multiplying the above equation by s^2 and rearranging, we obtain an expression for the $\psi^{(iv)}s^4$ term in equation 1.68:

$$\psi^{(iv)}s^4 \approx \psi''_{n+1}s^2 + \psi''_{n-1}s^2 - 2\psi''_ns^2 - \frac{1}{12}\psi^{(vi)}s^6 \quad (1.70)$$

Neglecting as before the term in s^6 , letting $\psi'' = m/\sqrt{2}[2V(x) - 2E]\psi = G\psi$ and substituting this into the above this gives:

$$\psi^{(iv)}s^4 \approx G_{n+1}\psi_{n+1}s^2 + G_{n-1}\psi_{n-1}s^2 + 2G_n\psi_n s^2 \quad (1.71)$$

We now have expressions for ψ'' and $\psi^{(iv)}s^4$ that we can replace into equation 1.68 and solve for ψ_{n+1} :

$$\psi_{n+1} \approx \frac{2\psi_n - \psi_{n-1} + \frac{5}{6}G_n\psi_n s^2 + \frac{1}{12}G_{n-1}\psi_{n-1}s^2}{1 - \frac{1}{12}G_{n+1}s^2} \quad (1.72)$$

Hence, we can obtain the solution to the Schrödinger equation at ψ_{n+1} if we know the solution at ψ_n and ψ_{n-1} . For the first iteration when $n = 1$, we

make an estimate of the energy eigenvalue E_{est} and choose the first two points x_0 and x_1 outside the potential at E_{est} (see Figure 1.8) where we expect the wavefunction to be zero. We assume that $\psi_{n-1} = 0$ and ψ_n is very small and then solve equation 1.72 for ψ_{n+1} . This is repeated for $n = 2, n = 3$ and so on until a maximum value x_{max} is reached (x_{max} is taken at a point far outside the potential near the asymptotic limit). If E_{est} is a true eigenvalue, then $\psi(x_{\text{max}}) = 0$. However, if $\psi(x_{\text{max}}) \neq 0$, then the whole iteration is restarted with a new estimate of E_{est} .

The number of nodes in the wavefunction calculated after one full iteration can give an indication as to the “location” of E_{est} . If there are no nodes in the wavefunction, then E_{est} is less than E_0 . If there is one node, then E_{est} is between E_1 and E_2 , and so on. Therefore the number of nodes in the wavefunction can be used to determine whether E_{est} needs to be increased or decreased to approach the desired eigenvalue. Once an exact eigenvalue is found (where $\psi(x_{\text{max}}) = 0$), the wavefunction can be normalised and the process repeated to determine a new eigenvalue.

This method of numerical integration involving a three-term recursion relation such as that given in equation 1.72 was first developed by Numerov in 1933 [74]. Since then, numerous different variations of this method have been suggested for improved efficiency in different applications. Using this method, the energies of the vibrational levels of a diatomic and the corresponding wavefunctions can be calculated regardless of the analytical form of the potential.

The Franck-Condon Principle

When a molecule absorbs radiation, the extra energy can cause an electronic rearrangement such that the molecule moves to a more excited state or an ionic state. Due to the large difference in mass between atomic nuclei and electrons, when an electronic transition occurs, the response of the nuclei is not instantaneous. Therefore, at the moment of the electronic transition, the molecule retains its original geometry from its initial state. If the geometries of the two states are not exactly the same, this will result in the final state being populated with a certain degree of vibrational excitation. The Franck-Condon principle states that the most likely transition between two electronic or charge states of a molecule will take place at the geometry that corresponds to the maximum in the vibrational wavefunction for the initial state of the molecule to the vibrational level in the final state that has a corresponding maximum at the same geometry. This is illustrated in Figure 1.9.

Given the Born-Oppenheimer approximation, the nuclear and electronic parts of the transition dipole moment for the electronic transition can be evaluated separately. The transition dipole moment is given by

$$\mu_{fi} = \langle \epsilon_f v_f | -e \sum_i \mathbf{r}_i + e \sum_l Z_l \mathbf{R}_l | \epsilon_i v_i \rangle = \langle \psi_f | \boldsymbol{\mu}_e + \boldsymbol{\mu}_n | \psi_i \rangle \quad (1.73)$$

where ϵ and v are the electronic and vibrational parts, respectively, of the wavefunction ψ . e and Z are the electronic and nuclear charges and \mathbf{r} and \mathbf{R} are the electronic and nuclear position vectors, respectively, relative to the centre of charge of the molecule. The i and f indices refer to the initial and

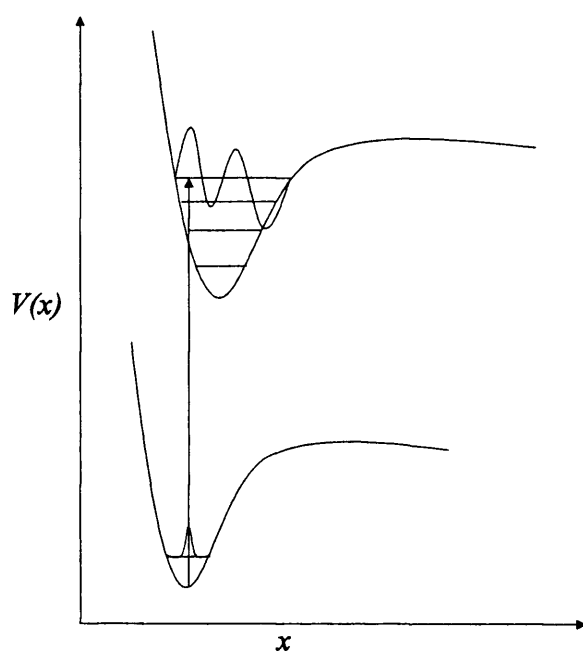


Figure 1.9: Schematic diagram illustrating the Franck-Condon principle. If the geometries of the initial and final states in an electronic transition are different, the transition will take place at the equilibrium geometry of the initial state, resulting in vibrational excitation in the final state.

final states, respectively. Since $\langle \varepsilon_f | \varepsilon_i \rangle = 0$, because two different electronic states are orthogonal, the only term that survives is:

$$\mu_{fi} = \langle \varepsilon_f | \mu_e | \varepsilon_i \rangle \langle v_f | v_i \rangle = \mu_{\varepsilon_f, \varepsilon_i} S(v_f, v_i) \quad (1.74)$$

$S(v_f, v_i)$ is the overlap integral of the vibrational wavefunctions of the two states. Since we can assume a constant average value of $\mu_{\varepsilon_f, \varepsilon_i}$ thanks to the Born-Oppenheimer approximation, the intensity of the electronic transition is proportional to the square modulus of the overlap integral $|S(v_f, v_i)|^2$, which is also known as the Franck-Condon factor (FCF). A FCF is a value between 0 and 1 and corresponds to the probability of the transition.

Therefore, given the potentials for two different electronic or charge states of a diatomic molecule, we can calculate the number of vibrational levels in the well of each potential, in addition to the energies and vibrational wavefunctions for each level, using the Numerov method. Using the vibrational wavefunctions for the initial and final states of the molecule for a given electronic transition, we can calculate the square modulus of their overlap integral and this provides the Franck-Condon factor or probability for that transition.

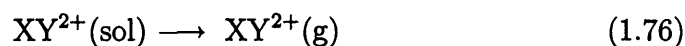
1.4 Experimental Background

1.4.1 Methods of Dication Generation

A number of methods exist for the formation of a dication: electron ionization (EI),



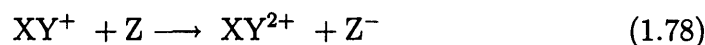
electrospray ionization (ESI),



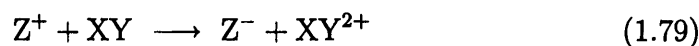
photoionization (PI),



charge stripping (CS)



and double-charge transfer (DCT).



EI involves the ejection of electrons from a neutral precursor gas by bombardment with high energy electrons. The dication can be formed by immediate ejection of two electrons, or *via* a monocation intermediate. A filament is often used as the source of electrons. ESI requires that the dication or its

precursor be in solution, which is then nebulised into the source in a very fine spray. The drawback of such a method is the possible reaction of the dication (or the collision gas) with the solvent. PI makes use of high energy photons, usually in the form of ultraviolet light, to promote the ejection of two electrons from a neutral precursor. This technique has a tendency to stimulate the formation of unstable highly excited states which promptly dissociate, resulting in low yields of the required dication. The CS method involves the collision of a mass-selected beam of monocations of high kinetic energy (keV) with a neutral gas. The high kinetic energy of the monocations is used to promote the stripping of an extra electron by the neutral in a high energy collision. DCT works in a similar way to CS, however the dication is formed from a slow neutral instead of a monocation. The high energy collision in this case results in the transfer of two electrons from the neutral to the high kinetic energy cation. Analysis of the kinetic energy of the resulting monoanion can provide information as to the energetics of the dication formed.

EI, CS and DCT are the most commonly used methods of dication generation as they are practical, give relatively high yields and can provide important information on the energetics of the formation of the dication. EI, however, has so far been the only method used in the investigations of bond-forming reactions with dications. This is because the introduction of an additional species into the system is not required, an important simplification. In addition, the apparatus for the EI method is simple and robust.

1.4.2 Apparatus Used to Study Dication-Neutral Reactions

The specificity of the study of dication-neutral reactions calls for novel mass spectrometric techniques. In general, this consists of an EI source, a MS for selection of the dication, a reaction chamber, a second MS for mass analysis of the products and a detector. There are two groups, in addition to Steve Price's group at UCL, that have been the most involved in the investigations of the electron transfer and bond-forming reactions of dications with neutral atoms and molecules: Davide Bassi's group at the University of Trento in Trento, Italy and Zdenek Herman's group at the J. Heyrovský Institute of Physical Chemistry in Prague, Czech Republic. The experimental setups of each of these groups will be briefly described below, followed by a more detailed description of the apparatus used for the experiments described in this thesis as part of Steve Price's group at UCL.

The instrument used in Bassi's group [75] in Trento, Italy works in the following way. The neutral precursor gas is ionized in the EI source with a small electron current and electron energy, typically 0.1 mA and 18-65 eV respectively, in order to prevent the formation of excited electronic states. The dication beam is selected by a magnetic sector MS and focused by an Einzel lens. It then enters a scattering cell fitted with an octopole ion guide. The neutral collision gas is introduced at low pressures ($< 10^{-4}$ mbar), and the ion beam energy is varied by changing the dc voltage applied to the octopole rods. The ions are then focused through another Einzel lens into a

quadrupole MS, which performs the final mass analysis, and onto an electron multiplier detector. Saturation of the detector is prevented by focusing the primary beam to the isotope of lowest abundance. The advantage of this instrument is the use of an octopole in the scattering cell as an ion guide. The final mass resolution is then quite high since the original energy spread is small.

A similar setup is used in Prague, Czech Republic, by Herman's group [2]. The EI source uses 120-150 eV electrons to produce the dications, which are selected, as with Bassi's instrument, by a magnetic sector. A series of lenses then focuses the beam and decelerates it to the desired collision energy. The primary ion beam then encounters a perpendicular neutral collision gas beam, and the products are passed through a stopping-potential energy analyser which analyses the energy of the beam. The ions go on to be mass analysed by another magnetic sector MS and then to an electron multiplier detector. Although this experiment doesn't benefit from the resolution imparted by the octopole ion guide in Bassi's experiment, it has the advantage of providing angular distributions of the products by simply rotating the collision gas beam with respect to the primary ion beam. This can provide extra information as to the dynamics of the reaction under study.

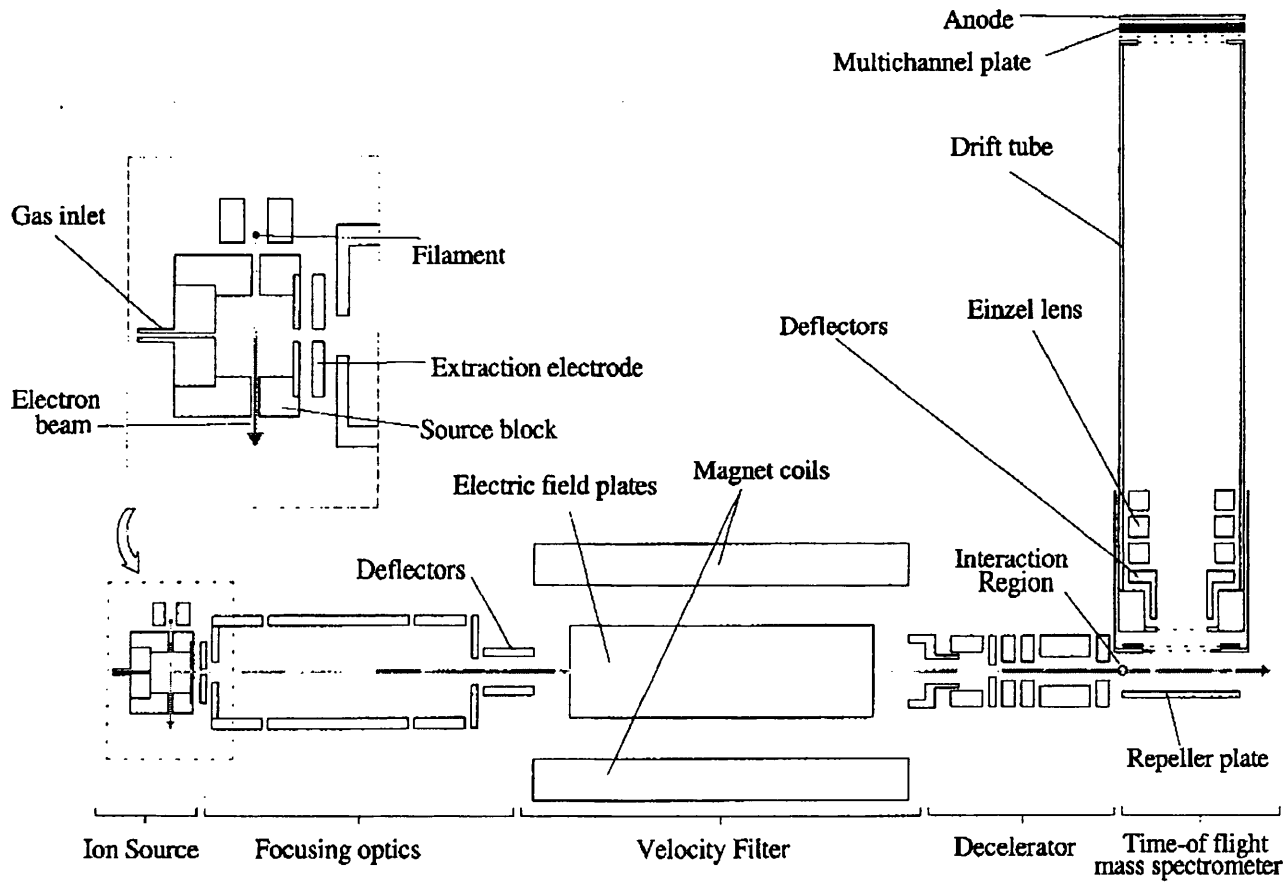
The apparatus used for the experiments described in this thesis is shown in Figure 1.10. A $10\mu\text{A}$ electron current is produced in the EI source by passing 3.7 A through a tungsten filament. The electrons are focused to a 150 eV beam which is used to ionise the precursor gas. The pressure in the EI source is kept low ($\sim 10^{-6}$ Torr) to prevent collisions between the

product dication and the precursor gas (or other product ions), which would reduce the dication yield. The ions produced are guided into a series of focusing optics *via* an extraction electrode. These optics focus the ions into a narrow beam and guide them into a Wien velocity filter. This consists of a set of two parallel electric field plates perpendicular to two magnetic coils. The magnetic and electric fields can be varied so that only ions with a certain velocity maintain a straight trajectory through the filter and avoid colliding with the walls. Since in principle all the ions leave the source with the same energy, their velocities are therefore a direct function of their mass ($E = \frac{1}{2}mv^2$). In this way a “pure” beam of the desired dication is obtained.

The dications are then decelerated to the required collision energy before entering the interaction region in the source of the TOFMS where the neutral collision gas is introduced. The pressure in the interaction region is maintained at $\sim 10^{-6}$ mbar in order to promote the conservation and formation of bonds. A repeller plate behind the source of the TOFMS pulses all product ions down a field-free drift tube with equal energies, therefore separating the ions out as a function of their masses. They hit a multichannel plate detector which times the duration of each ion’s journey from the instant of the repeller plate pulse. The time it take for an ion to travel down the drift tube is related to its velocity, which as before is a function of its mass.

When an ion hits the multichannel plate (MCP) detector, an electron is ejected from the surface of the channel. This electron then collides with the surface of the channel, releasing more electrons, which continue in the same way. This electron multiplication results in a measurable pulse of charge at

Figure 1.10: Crossed-beam apparatus used for the experiments.



the end of the channel. In this way, the single event of an ion hitting an anode surface can be multiplied into a measurable signal. A discriminator behind the MCP sets a threshold charge below which the signal is not transmitted as an ion count. Each “real” ion count is collected in a memory module which stores a fixed number of counts, or a *cycle* (corresponding to 512k of memory) before downloading the data to the computer.

All of the collision reactions carried out experimentally for the work presented in this thesis were performed at low collision energies, usually between 3-12 eV in the laboratory frame (LAB). If the LAB velocity of the dication is much greater than that of the neutral, and there are no external forces acting on the system (as is the case in the interaction region prior to the repeller plate pulse), these LAB energies can be converted to center of mass (COM) energies in the following way:

$$E_{\text{coll}}^{\text{LAB}} = \frac{\mu}{m} E_{\text{coll}}^{\text{COM}} \quad (1.80)$$

where μ is the reduced mass of the dication and the neutral and m is the mass of the dication.

1.4.3 Data Analysis

Before any reliable conclusions can be drawn from the results of the experiments, the data must first be corrected for some known effects of the apparatus. Peak intensities in the mass spectrum can be artificially affected in a number of ways: first, there always exists in the instrument a certain

number of stray ions. These produce a fairly constant level of background noise in the spectrum. Second, fragmentation processes not related to collisions with the reactant neutral are inevitable, and these can contribute to the intensities of some product ion peaks. Third, due to a 32 ns deadtime in the discriminator, some dication counts can be missed, artificially decreasing the peak intensity. Systematic errors are eliminated by expressing product peak intensities (I) as ratios (R) to the much more abundant and therefore effectively constant dication peak.

Corrections for Stray Ions and Unimolecular Events

Background noise can be easily corrected by taking the average intensity of the spectrum over a peakless region and subtracting this from the peaks of interest.

$$I_{\text{obs}} = I_{\text{raw}} - N_2 \frac{I_{\text{noise}}}{N_1} \quad (1.81)$$

I_{obs} is the true peak intensity, I_{raw} is the raw data peak intensity, I_{noise} is the average noise intensity over the chosen range, N_1 is the number of channels in that range and N_2 is the number of channels that make up the peak being corrected.

At each collision energy, three runs were performed with the collision gas on, and two with the collision gas off. This is to monitor the ions being generated from processes not related to collisions with the neutral. They can then be subtracted from the ion intensities from runs with the gas on in the following way:

$$R'_{\text{obs}} = \frac{\sum R_{\text{obs}}^{\text{gas on}}}{3} - \frac{\sum R_{\text{obs}}^{\text{gas off}}}{2} \quad (1.82)$$

where R indicates that the peak intensity is given relative to the dication peak ($R_{\text{obs}} = I_{\text{obs}}^{\text{product}} / I_{\text{obs}}^{\text{dication}}$). $\sum R_{\text{obs}}^{\text{gas on}}$ is the peak intensity ratio averaged over the three runs with collision gas on and $\sum R_{\text{obs}}^{\text{gas off}}$ is the average peak intensity ratio over the two gas off runs. Notice that the noise-corrected I_{obs} intensities are used in all cases.

Corrections for Discriminator Saturation For a dicationic chemical reaction, the dication is always the most abundant peak in the mass spectrum by about three orders of magnitude. As a result, saturation of the discriminator is only an important problem for the detection of the dication. That is, if two dications arrive at the detector at the same time, the second ion will not be counted because of a 32 ns deadtime in the discriminator between counts.

In order to determine the extent of the effect of missed dication counts, Kearney *et al.* [47] measured R'_{obs} over a series of dication count rates. They obtained an exponential distribution that converges to a minimum value of R_{obs} at low count rates (or large acquisition times). Since the error in the true ion intensity ratio R_{real} will be minimised with longer acquisition times t (lower dication currents) due to the lower number coincident dication arrivals, the minimum R'_{obs} value in the distribution at large t corresponds to the true ion intensity ratio R_{real} . By plotting $R'_{\text{obs}}/R_{\text{real}}$ as a function of t , they obtained following expression:

$$\frac{R'_{\text{obs}}}{R_{\text{real}}} = \frac{a}{t^n} + 1 \quad (1.83)$$

where the fitting parameters a and n are 1.40715×10^{13} and 5.9353 respec-

tively. Kearney *et al.* found that this calibration curve and its a and n parameters can be applied to a variety of different small dication-molecule collision systems.

Chapter 2

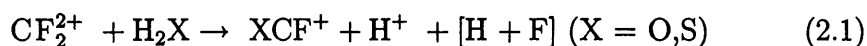
The bond-forming reaction between CF_2^{2+} and $\text{H}_2\text{O}/\text{D}_2\text{O}$.

The work presented in this Chapter has been published as:

N. Lambert, N. Kaltsoyannis and S. D. Price; “The bond-forming reaction between CF_2^{2+} and $\text{H}_2\text{O}/\text{D}_2\text{O}$: a computational and experimental study”; *J. Chem. Phys.*; 119 (2003) 1421.

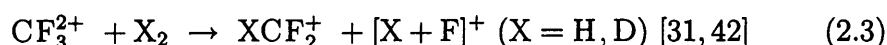
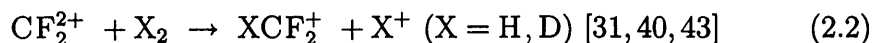
2.1 Introduction

In 2001, the group of Kearney and Price performed a series of crossed-beam collision experiments between CF_2^{2+} and H_2X ($\text{X} = \text{O}, \text{S}$) [47]. The results of these experiments indicated that the bond-forming product ion XCF^+ had been produced in small quantities:



The possibility of an H/D isotope effect in reaction 2.1 is of particular interest. Previous studies of isotope effects in bond-forming dicationic reac-

tions have involved the reaction of CF_2^{2+} , CF_3^{2+} , and CO_2^{2+} with H_2 , D_2 , and HD:



In all three cases, collisions with HD favour the formation of the deuterated products: DCF_2^+ (reactions 2.2 and 2.3) or DCO^+ (reaction 2.4). However, slightly greater yields of HCO^+ relative to DCO^+ are obtained from reactions of CO_2^{2+} with H_2 or D_2 . In addition, for reactions of CF_2^{2+} with H_2 or D_2 , HCF_2^+ formation has twice the relative cross section of DCF_2^+ .

Also of interest in reaction 2.1 is the possibility of forming molecular $[\text{H} + \text{F}]$ as a neutral product. No confirmed account of a neutral molecular product from a reaction between a dication and a neutral currently exists. Of course, traditional crossed-beam experimental techniques cannot determine whether the neutral products from such a reaction are in fact molecular or atomic, and the computational studies of dication reactions available in the literature have not dealt with reactions that yield more than a single atomic neutral product.

This Chapter consists of a three-pronged study of the bond-forming pathway between CF_2^{2+} and $\text{H}_2\text{O}/\text{D}_2\text{O}$. First, a computational investigation of the reaction mechanism is presented, including a comparison of the activation

energies for the H₂O and the D₂O pathways. Second, a comparative rate constant analysis is given for the activation steps of the reaction of CF₂²⁺ with H₂O and with D₂O. Finally, the ion yields of a series of crossed-beam experiments between CF₂²⁺ and D₂O are compared with those from previous collision experiments between CF₂²⁺ and H₂O [47]. Given the results of these studies, the ground state potential energy surface for reaction 2.1 is presented. The neutral product of this reaction is confirmed as molecular HF, formed in its ground electronic state together with OCF⁺ and H⁺. It is also shown that an intermolecular isotope effect is not experimentally observed between the H₂O and the D₂O pathways due to kinetic factors.

2.2 Computational Details

All quantum chemical calculations were performed using the *Gaussian98* program [76]. Geometries were optimized using the B3LYP hybrid DFT method [67, 77]. Single point calculations were then performed at these optimized geometries at the CCSD(T) level [57, 78]. The 6-311++G(2df,2pd) basis set was used for all calculations.

Transition state searches were performed both by direct optimizations to saddle points and by Synchronous Transit-Guided Quasi-Newton (STQN) methods. To ensure that all minima and saddle points were on the same reaction path, Intrinsic Reaction Coordinate (IRC) calculations were performed at each transition state. All minima and transition states were characterised by harmonic vibrational frequency analysis at the B3LYP level. Zero-point

energy corrections were taken from these frequency calculations.

Rate constants for the first and second activation steps in the reaction mechanism were determined using the Rice-Ramsperger-Kassel-Marcus/Quasi-Equilibrium Theory (RRKM/QET) rate constant equation for a unimolecular dissociation [69], as discussed in Section 1.3.2:

$$k(E) = \frac{\sigma N^\ddagger(E - E_0)}{h\rho(E)} \quad (2.5)$$

where E is the total energy of the system, E_0 is the activation energy, $N^\ddagger(E - E_0)$ is the sum of available vibrational states at the transition state, $\rho(E)$ is the density of states of the parent ion, and σ is the reaction degeneracy. A FORTRAN90 program was written to calculate the sums and densities of states, using algorithms written by Beyer and Swinehart [79]. These calculations employed the zero-point corrected energies and harmonic frequencies from the quantum chemical calculations. The source code for the FORTRAN90 program is given in Appendix A.

2.3 Experimental Details

A detailed description of the experimental setup used for the collision experiments, and the subsequent data analysis procedures, was given in Sections 1.4.2 and 1.4.3. The experiments discussed in this chapter were performed using CF_4 as the precursor gas, ionised by 150 eV electrons, and D_2O as the neutral collision partner. The pressures in the source and interaction region were maintained at 4×10^{-6} Torr and 3×10^{-6} Torr, respectively.

Collision energies ranged from 3.0-12.0 eV in the laboratory frame, in 1.0 eV intervals.

Improved Noise and Background Corrections For Small, Difficult to Resolve Peaks For the case of the reaction of $\text{CF}_2^{2+} + \text{H}_2\text{O}/\text{D}_2\text{O}$, the OCF^+ product ion signal at mass 47 is very small relative to its CF_2^+ neighbour at mass 50. Also, due to its very low intensity, small errors in noise subtraction can produce large errors in the final OCF^+ peak intensity. For these reasons, generalised formulae for noise and background corrections as explained above are not sufficient to give accurate results. To get accurate peak intensities for both the OCF^+ and the CF_2^+ peaks, the use of Gaussian fitting methods are necessary.

The region of the OCF^+ and CF_2^+ peaks can be accurately fitted by three Gaussian functions $P(x)$:

$$P(x) = \frac{1}{\sigma\sqrt{2\pi}} e^{-(x-\mu)^2/(2\sigma^2)} \quad (2.6)$$

where μ is the mean value and σ is the standard deviation. Varying μ moves the centre of the curve and σ governs the width of the peak. Finally, two linear background curves are included to correct for noise. These extra curves are necessary because the background noise profile is not constant in the region of the peaks being analysed. The μ and σ parameters for each Gaussian and the slopes of the two background curves can then be modified in order to obtain the ideal fit for each individual spectrum. The sum of two Gaussians and the background curves is used to fit the CF_2^+ peak and

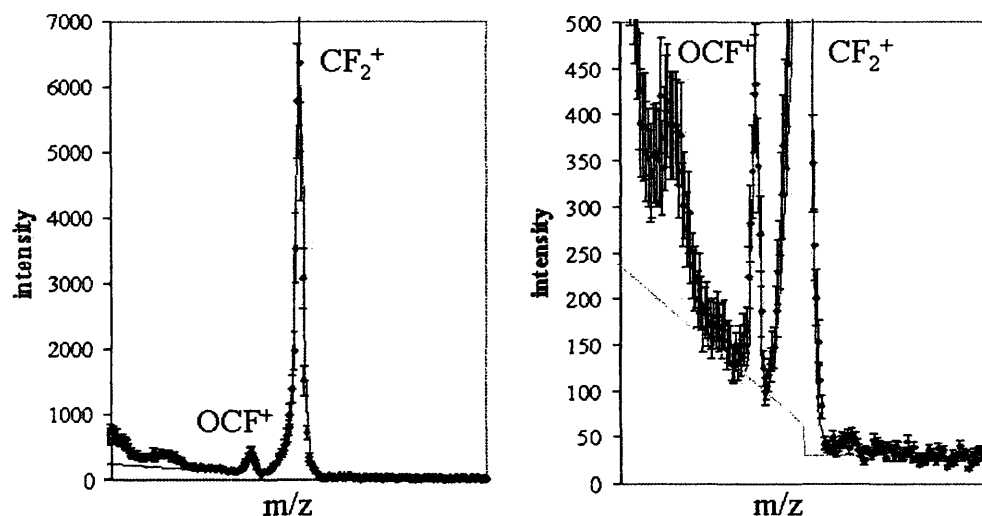


Figure 2.1: Both plots show the same region of the mass spectrum but on different scales. One Gaussian function is used to fit the OCF^+ peak. Two Gaussian functions are used to fit the CF_2^+ peak (one for the main peak, another to fit the shoulder at low m/z). Two linear curves are used to fit the background.

the sum of one Gaussian and the background curves fits the OCF^+ peak. A sample fit is shown in Figure 2.1.

2.4 Results and Discussion

2.4.1 Computational Results: Reaction Mechanism

Figure 2.2 shows the calculated mechanism for reaction 2.1, which shares some similarities with that of Mrázek *et al.* for $\text{CO}_2^{2+} + \text{H}_2/\text{D}_2$ [35], most notably the hydrogen rearrangement, and subsequent proton loss, as activation steps. Unlike Mrázek *et al.*'s mechanism, however, following the first

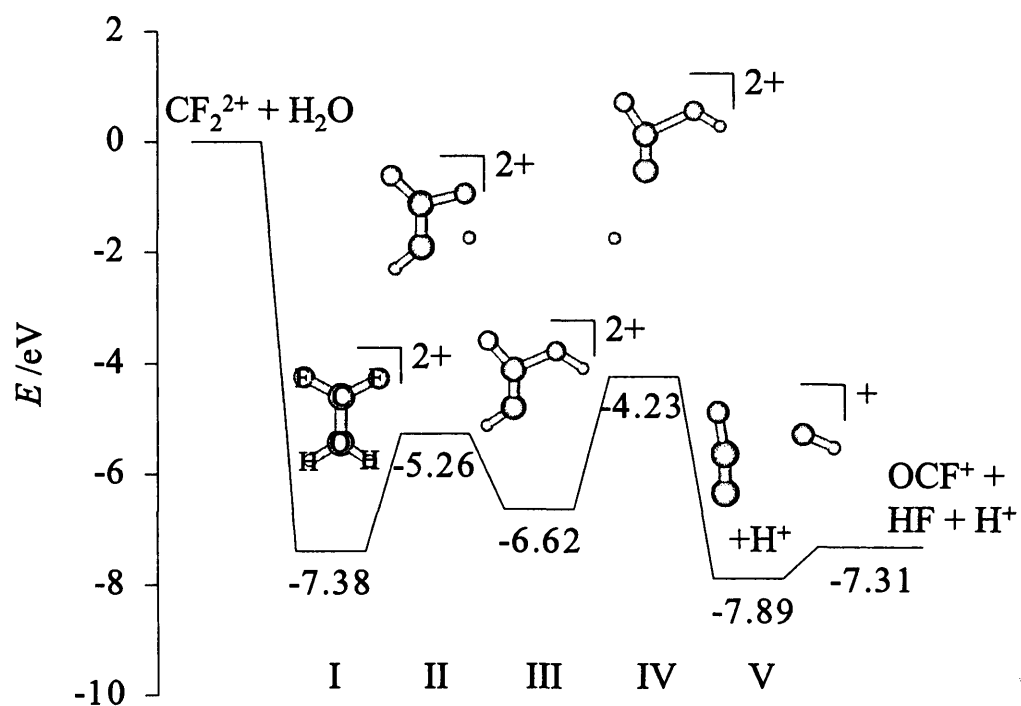


Figure 2.2: A schematic representation of the stationary points on the potential energy surface for the reaction $\text{CF}_2^{2+} + \text{H}_2\text{O} \rightarrow \text{OCF}^+ + \text{H}^+ + \text{HF}$

association of the dication with the neutral (to form I), the entire reaction takes place in C_s symmetry.

The first step in the reaction is the formation of the C-O bond to give the C_{2v} intermediate I. To verify that this first step does not require activation, a series of constrained geometry optimizations were performed in which the distance between the C and O atoms of the reactants was fixed and all other geometric variables optimized. The C-O distance was then varied from 1.0 Å to 4.0 Å in increments of 0.1 Å and, as expected, no transition state was found between the reactants and minimum I in this region of the surface. Restricted geometry optimizations in which the C-O distance was greater than 4.0 Å became problematic due to incorrect charge distributions. However it is reasonable to assume that no transition state would exist at C-O distances greater than 4.0 Å.

The first activation step (*via* transition state II) involves hydrogen transfer from the oxygen to one of the fluorine atoms to form intermediate III. Subsequently, a proton is lost and during this process the C-HF bond lengthens from 1.457 Å in intermediate III to 1.753 Å in transition state IV and to 2.252 Å in intermediate V. Finally, intermediate V fragments to give two molecular products: OCF^+ and HF. In order to verify that the HF molecule is formed in its ground state, a series of restricted geometry optimizations were performed in which all parameters were held fixed except for the O-C, C-F_a and F_b-H bond distances (see Figure 2.3). The energy for each optimization is plotted as a function of the C-F_b bond distance, which was fixed at a series of values between 2.25 Å and 62.25 Å. All energies are given

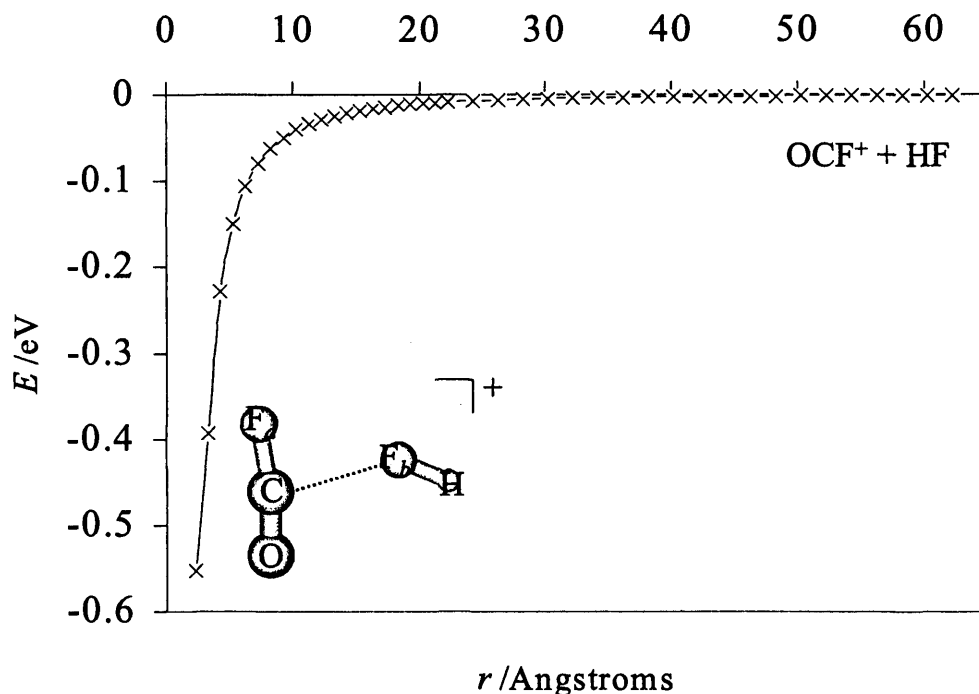


Figure 2.3: The results of a series of restricted geometry optimizations tracing the reaction path corresponding to the dissociation of intermediate V to OCF⁺ and HF (see Figure 2.2). All geometric parameters were fixed during the optimizations except for the O-C, C-F_a and F_b-H bond distances. The "r" parameter is the C-F_b bond distance. All energies are given relative to the sum of the energies of fully optimized OCF⁺ and HF in their ground states.

relative to the sum of the ground state energies of fully optimized OCF⁺ and HF, calculated separately. The size-consistent B3LYP method was used with the 6-311++G(2df,2pd) basis set for all calculations shown on Figure 2.3. As can be seen, the dissociation of intermediate V to OCF⁺ and HF does not proceed *via* a transition state. As the C-F_b distance lengthens, the energy of the system approaches the asymptote at 0 eV, indicating that the neutral HF product is indeed formed in its non-dissociative ground state.

It is pleasing to note that this calculated mechanism was later experimentally verified by the Price group [80]. They used a position-sensitive coincidence mass spectrometer (PSCO) to carry out collision experiments between CF_2^{2+} and H_2O . For a three-body reaction such as the one discussed in this Chapter (equation 2.1), the PSCO can determine the initial velocity vectors for all three products on a per-event basis. The results indicated that proton loss occurs in a step that is temporally distinct from the fragmentation of OCF_2H^+ to OCF^+ and HF , which is in agreement with our calculated mechanism.

IRC calculations were performed from both saddle points II and IV in both directions to ensure that all of the calculated stationary points were indeed on the same reaction path. In addition, a CCSD(T) T_1 -diagnostic was calculated at each saddle point to check the weight of the CC singles operator for each of the transition states. For a closed-shell system, a value of 2.0% is generally considered to be a conservative threshold for the T_1 -diagnostic, i.e. above this value a system may well possess significant multireference character [58]. Values of 1.71% and 1.67% were obtained for the first (II) and second (IV) transition states respectively, indicating an acceptably low degree of multireference character of the wavefunction at these points. Saddle points tend to be the most highly multiconfigurational regions of a PES, therefore an extension of the calculation to multireference methods was deemed unnecessary.

The geometries of all optimized structures are presented in Table 2.1. Dihedral angles are not given as all structures are either linear or planar.

structure	C-O	C-F	O-H	F-H	F-C-F	O-C-F	H-O-C
CF ₂ ²⁺ (¹ A)		1.148			180.0°		
H ₂ O (¹ A)			0.961				105.1° (H-O-H)
I (¹ A)	1.356	1.216	1.014		125.5°	117.3°	121.5°
II (¹ A)	1.269	1.202, 1.329	1.018, 1.431	1.318	123.0°	102.1°	129.4°
III (¹ A)	1.203	1.210, 1.457	1.013	0.999	107.6°	114.1°	124.6°
IV (¹ A)	1.144	1.214, 1.753	2.271	0.956	95.71°	114.9°	158.2°
V (¹ A)	1.116	1.203, 2.252		0.933	84.71°	104.2°	
OCF ⁺ (¹ A)	1.114	1.200				180.0°	
HF (¹ A)				0.923			

Table 2.1: Geometric parameters of optimized structures on the potential energy surface for CF₂²⁺ + H₂O → OCF⁺ + HF + H⁺. All bond distances are in angstroms (Å). Structures labelled I-V are shown in Figure 2.2. All calculations were performed with no symmetry constraints.

	first activation (eV)	second activation (eV)
CF ₂ ²⁺ + H ₂ O	2.113	2.392
CF ₂ ²⁺ + D ₂ O	2.157	2.461
difference (H - D)	-0.044	-0.069

Table 2.2: Comparison of activation energies in the CF₂²⁺ + H₂O and CF₂²⁺ + D₂O pathways.

The geometry of the ¹Σ_g⁺ ground state of CF₂²⁺, with a C-F bond length of 1.148 Å, agrees well with previous calculations by Hrušák *et al.*, which found values of 1.150 Å and 1.153 Å using B3LYP and CCSD(T), respectively [81]. A more recent MR-AQCC/ANO study, also by Hrušák, found a C-F bond length of 1.154 Å [82].

Zero-point energies for each of the stationary points were calculated from frequency calculations at the B3LYP level in order to allow comparison of the activation energies for the H₂O and D₂O pathways. These are shown in Table 2.2. The H₂O pathway is only slightly favoured, in the first case by 0.04 eV and in the second by 0.07 eV.

2.4.2 Computational Results: Rate Constants

The rate constants for both activation steps (I \rightarrow II and III \rightarrow IV) for the $\text{CF}_2^{2+} + \text{H}_2\text{O}$ and $\text{CF}_2^{2+} + \text{D}_2\text{O}$ reactions were calculated using RRKM/QET theory. This method has previously been used with success in a similar context [42]. Figure 2.4 plots the relative rate constants of the D_2O and H_2O reactions through transition states II and IV as a function of the center-of-mass collision energy.

Despite the rates for both activations being greater by 40%-65% for the H_2O pathway, all of the rate constants are very large, of the order of $10^{12}\text{s}^{-1} - 10^{14}\text{s}^{-1}$ (see Tables 2.3 to 2.6). It is therefore not expected that this kinetic isotope effect would be detectable in our collision experiment. To observe such an intermolecular isotope effect between two separate reactions, the metastable complexes involved must survive for at least several nanoseconds to give metastable signals, allowing the intensity ratio of the signal of the OCF^+ ion to that of the complex to be monitored. Such lifetimes are significantly longer than those we calculate for the intermediate complexes in the present system.

2.4.3 Experimental Results

Figure 2.5 shows a typical raw mass spectrum following the collision of CF_2^{2+} with D_2O . The chemical product ion OCF^+ is clearly visible at mass 47. Due to the single collision conditions maintained in this experiment, ion peak intensities I_j follow the order: $\text{CF}_2^{2+} > \text{CF}^+ > \text{D}_2\text{O}^+ > \text{CF}_2^+ > \text{OCF}^+$.

Figure 2.6 shows $R_{\text{real}}^{\text{OCF}^+}$ as a function of the centre-of-mass (COM) col-

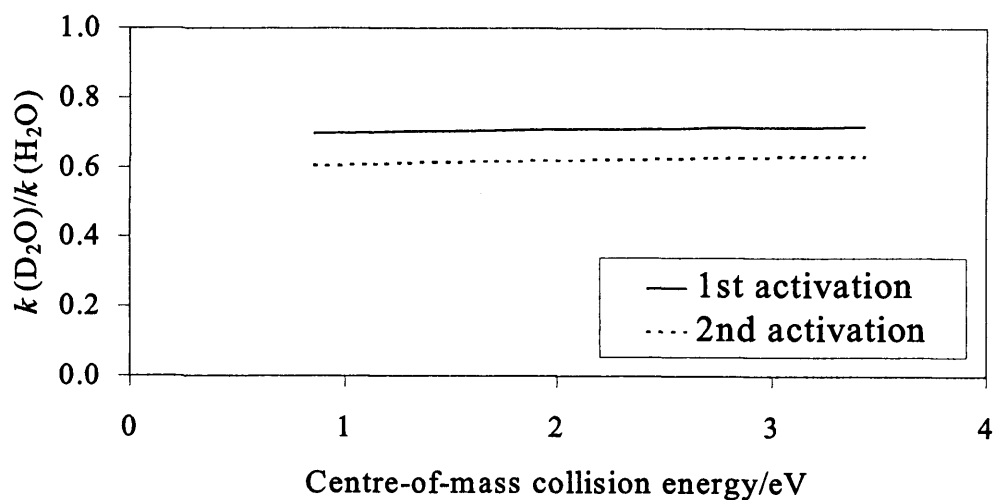


Figure 2.4: A plot comparing dissociation rate constants for the H_2O and D_2O pathways calculated as a function of centre-of-mass collision energy.

COM collision E (eV)	k	$N^\ddagger(E - E_0)$	$\rho(E)$
0.857143	1.776×10^{12}	2.404×10^{11}	4.058×10^9
1.14286	1.980×10^{12}	3.754×10^{11}	5.683×10^9
1.42857	2.191×10^{12}	5.757×10^{11}	7.879×10^9
1.71429	2.408×10^{12}	8.690×10^{11}	1.082×10^{10}
2.00000	2.630×10^{12}	1.292×10^{12}	1.473×10^{10}
2.28571	2.858×10^{12}	1.895×10^{12}	1.988×10^{10}
2.57143	3.090×10^{12}	2.744×10^{12}	2.662×10^{10}
2.85714	3.326×10^{12}	3.925×10^{12}	3.537×10^{10}
3.14286	3.565×10^{12}	5.550×10^{12}	4.667×10^{10}
3.42857	3.807×10^{12}	7.766×10^{12}	6.115×10^{10}

Table 2.3: Rate constants for the first dissociation on the bond-forming pathway between CF_2^{2+} and H_2O .

COM collision E (eV)	k	$N^\ddagger(E - E_0)$	$\rho(E)$
0.857143	1.008×10^{14}	2.052×10^{13}	6.105×10^9
1.14286	1.194×10^{14}	3.521×10^{13}	8.838×10^9
1.42857	1.396×10^{14}	5.888×10^{13}	1.264×10^{10}
1.71429	1.614×10^{14}	9.623×10^{13}	1.787×10^{10}
2.00000	1.845×10^{14}	1.540×10^{14}	2.501×10^{10}
2.28571	2.091×10^{14}	2.416×10^{14}	3.465×10^{10}
2.57143	2.349×10^{14}	3.725×10^{14}	4.754×10^{10}
2.85714	2.619×10^{14}	5.648×10^{14}	6.466×10^{10}
3.14286	2.899×10^{14}	8.435×10^{14}	8.723×10^{10}
3.42857	3.191×10^{14}	1.242×10^{15}	1.167×10^{10}

Table 2.4: Rate constants for the second dissociation on the bond-forming pathway between CF_2^{2+} and H_2O .

COM collision E (eV)	k	$N^\ddagger(E - E_0)$	$\rho(E)$
0.857143	1.240×10^{12}	9.495×10^{11}	2.295×10^{10}
1.14286	1.388×10^{12}	1.496×10^{12}	3.231×10^{10}
1.42857	1.541×10^{12}	2.315×10^{12}	4.503×10^{10}
1.71429	1.700×10^{12}	3.522×10^{12}	6.212×10^{10}
2.00000	1.863×10^{12}	5.277×10^{12}	8.493×10^{10}
2.28571	2.030×10^{12}	7.795×10^{12}	1.151×10^{11}
2.57143	2.201×10^{12}	1.136×10^{13}	1.548×10^{11}
2.85714	2.374×10^{12}	1.635×10^{13}	2.064×10^{11}
3.14286	2.550×10^{12}	2.325×10^{13}	2.734×10^{11}
3.42857	2.729×10^{12}	3.271×10^{13}	3.594×10^{11}

Table 2.5: Rate constants for the first dissociation on the bond-forming pathway between CF_2^{2+} and D_2O .

COM collision E (eV)	k	$N^\ddagger(E - E_0)$	$\rho(E)$
0.857143	6.087×10^{13}	6.818×10^{13}	3.358×10^{10}
1.14286	7.268×10^{13}	1.186×10^{14}	4.892×10^{10}
1.42857	8.555×10^{13}	2.008×10^{14}	7.038×10^{10}
1.71429	9.944×10^{13}	3.320×10^{14}	1.001×10^{11}
2.00000	1.143×10^{14}	5.368×10^{14}	1.408×10^{11}
2.28571	1.301×10^{14}	8.506×10^{14}	1.960×10^{11}
2.57143	1.468×10^{14}	1.323×10^{15}	2.702×10^{11}
2.85714	1.643×10^{14}	2.023×10^{15}	3.692×10^{11}
3.14286	1.826×10^{14}	3.045×10^{15}	5.001×10^{11}
3.42857	2.015×10^{14}	4.516×10^{15}	6.718×10^{11}

Table 2.6: Rate constants for the second dissociation on the bond-forming pathway between CF_2^{2+} and D_2O .

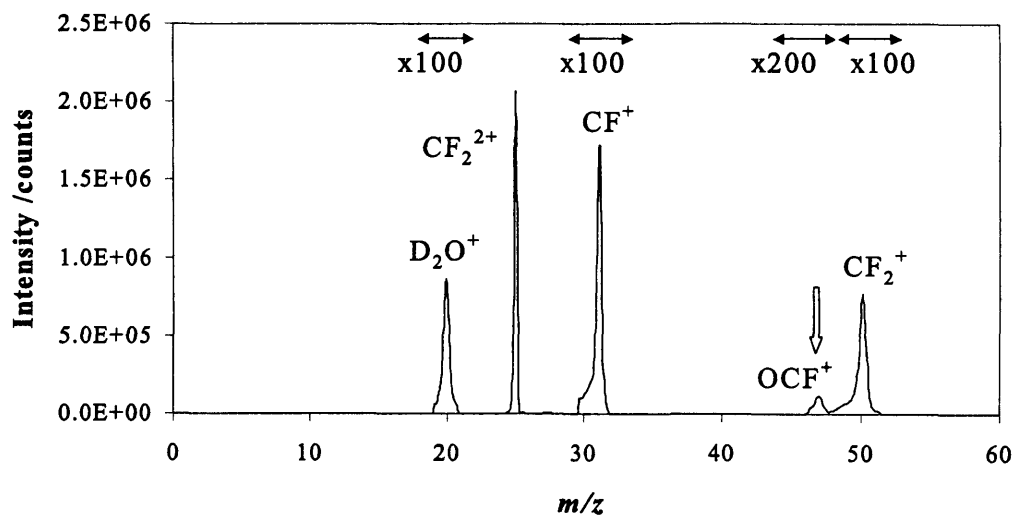


Figure 2.5: A typical raw mass spectrum recorded following collisions of CF_2^{2+} with D_2O .

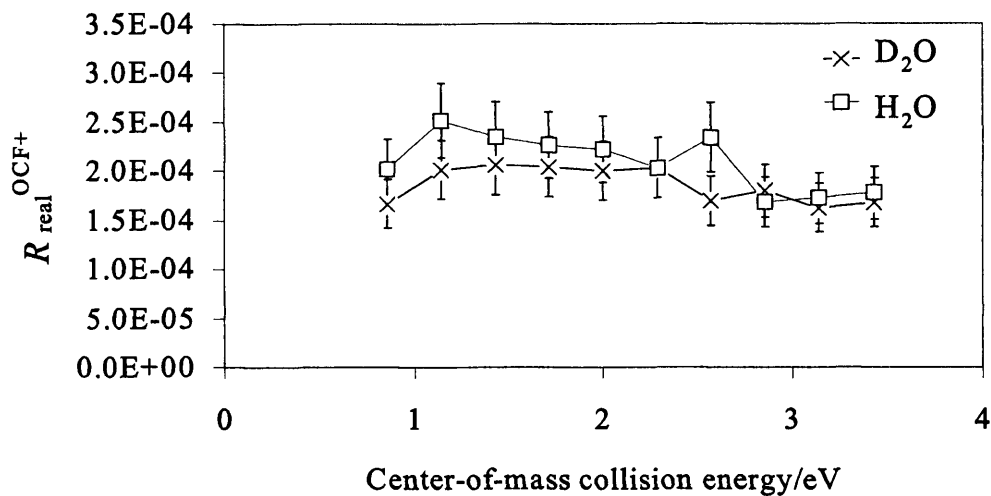


Figure 2.6: A plot of $R_{\text{real}}^{\text{OCF}^+}$ as a function of centre-of-mass collision energy (see text for details).

lision energy for both the D₂O and the earlier [47] H₂O experiments. As can be seen, no isotope effect is observed within the experimental error limits. $R_{\text{real}}^{\text{OCF}^+}$ also appears to remain approximately constant with changes in collision energy.

2.4.4 Discussion

The lack of an experimentally observable intermolecular isotope effect, despite the formation of OCF⁺ from collisions of CF₂²⁺ with H₂O being favoured relative to collisions with D₂O by both activation energies and rate constants, can be explained as following. In order to distinguish between the rates of the two reactions in different collision systems (with H₂O and D₂O), we must be able to detect the metastable complex ion (Structure I on Fig-

ure 2.2). By comparing the relative magnitudes of the signals for the complex and OCF^+ for both the H_2O and the D_2O collision systems, we could obtain an indication of the relative rates of formation of OCF^+ . However, in order to observe its ion signals, the transient complex must have a lifetime of at least several nanoseconds. It is not surprising, then, that we do not detect such metastable complexes as we have calculated their lifetimes to be of the order of picoseconds. Any complexes formed decay rapidly to products, thus our measurement of R_{real} only probes the reactive *flux* through the initial complex to the channel of interest. Since complex formation is equally facile with either H_2O or D_2O , this flux (and hence R_{real}) will be the same for both the H_2O and D_2O experiments even though the complex decomposes more rapidly for H_2O .

2.5 Conclusions

The ground state stationary points on the potential energy surface of the reaction of CF_2^{2+} with $\text{H}_2\text{O}/\text{D}_2\text{O}$ to give the bond-forming molecular product OCF^+ have been calculated quantum chemically. The mechanism calculated for this reaction involves an initial complexation, internal hydrogen migration *via* a first transition state followed by proton loss *via* a second transition state. In the final step of the reaction, the complex fragments to give two molecular products in their ground states, OCF^+ and HF .

Crossed-beam collision experiments were performed between CF_2^{2+} and D_2O and when the OCF^+ product ion intensities were compared with those

obtained from previous experiment performed using H₂O as the collision gas, it was found that no intermolecular isotope effect was present. In addition, the OCF⁺ ion intensity was found to stay constant with respect to collision energy.

Rate constants have been calculated for the activation steps in both the H₂O and D₂O pathways. Despite both activation energies and rates slightly favouring the H₂O pathway, the rate constants are so large in all cases that no measurable intermolecular isotope effect is observable on comparison of independent H₂O/D₂O collision experiments. This is in agreement with the observed experimental results.

Chapter 3

The bond-forming reaction between Ar^{2+} and NH_3 .

Both the experimental work performed by D. Kearney and the work presented in this Chapter have been published collaboratively as:

N. Lambert, D. Kearney, N. Kaltsoyannis and S. D. Price; "The bond-forming reactions of atomic dications with neutral molecules: Formation of ArNH^+ and ArN^+ from collisions of Ar^{2+} with NH_3 ."; *J. Am. Chem. Soc.*; 126 (2004) 3658.

3.1 Introduction

In 2004, Dominic Kearney in the Price group at UCL performed a series of crossed-beam collision experiments between Ar^{2+} and NH_3 over a range of collision energies (1-14 eV in the laboratory frame), using the same apparatus and data analysis procedure as described in Sections 1.4.2 and 1.4.3. As well as the usual products of dissociative and non-dissociative electron transfer, Ar^+ , NH_3^+ , NH_2^+ , NH^+ , N^+ and H^+ , he also observed two bond-forming product ions: ArNH^+ and ArN^+ . Even more interestingly, he found

that the yield of ArNH^+ would decrease as a function of increasing collision energy, whereas the yield of ArN^+ would increase correspondingly [83]. Such a relationship indicates that the formation of ArNH^+ and of ArN^+ are governed by the same mechanism, and possibly that ArN^+ is formed by the fragmentation of ArNH^+ .

In this Chapter, in order to provide rationalisation for the experimental results and to verify the hypothesis of a single mechanism for the formation of ArNH^+ and ArN^+ , a quantum chemical investigation of the key features of the calculated PES for the bond-forming reaction $\text{Ar}^{2+} + \text{NH}_3 \longrightarrow \text{ArN}^+ + \text{H}^+ + 2\text{H}$ is presented, which reveals a reaction pathway that is consistent with the experimental data. Significantly, it is found that the bond-forming pathway lies on a singlet potential energy surface and is not accessible for Ar^{2+} in its ground (^3P) state.

3.2 Computational Details

Geometry optimizations of the ground state stationary points on the potential energy surface for the reaction $\text{Ar}^{2+} + \text{NH}_3 \longrightarrow \text{ArN}^+ + \text{H}^+ + 2\text{H}$ were initially performed using the DFT hybrid method B3LYP in conjunction with the large Pople basis set 6-311++G(2df,2pd). However, single point CCSD(T) calculations performed on the optimized geometries were problematic. T_1 -diagnostic calculations, as described in Section 1.3.1, were attempted on all stationary points. A T_1 value of 2.0% is a generally accepted threshold for closed-shell systems above which multireference methods should be used.

The T_1 -diagnostic values obtained for the first three stationary points on the surface were large, up to 2.6%. CCSD(T) calculations on the remaining stationary points on the surface did not converge at all, due to difficulties in minimizing the singles vector. This may be due to many of these remaining stationary points being open shell. Hence, it was clear that the use of multireference methods would be necessary for this system.

Therefore, geometry optimizations were performed using the multiconfigurational CASSCF method and the aug-cc-pvtz basis set. A full valence active space was used, where the N 1s and the Ar 1s, 2s and 2p atomic orbitals were kept inactive but allowed to relax during the geometry optimizations. The resulting wave functions consisted of up to 32,000 configuration state functions (CSF). No symmetry constraints were imposed during the geometry optimizations. Vibrational frequency analyses were used to obtain zero-point energies and to characterize the transition states and IRC calculations were performed on all transition states in order to verify that they are indeed on the same reaction path as their adjacent minima.

Single-point energy calculations were then performed on the CASSCF optimized geometries using the MRCI method with the same basis set. The same full valence active space as that employed for the geometry optimizations was used. To minimize computational costs, only those reference configurations with a weighting greater than 0.01 were selected. For each calculation, the square of the normalization coefficient for the wavefunction made up from these selected configurations was always greater than 0.997.

Single-reference B3LYP and CCSD(T) calculations were carried out us-

ing *Gaussian 98*, revision A.9 [76]. The multireference CASSCF[84, 85] and MRCI[86, 87] calculations were carried out using MOLPRO v.2002.3[88].

3.3 Results and Discussion

3.3.1 Single-reference methods

The stationary points on the PES of the bond-forming reaction between Ar^{2+} and NH_3 as calculated using B3LYP are shown in Figure 3.1. The mechanism first involves the formation of the Ar-N bond to give ArNH_3^{2+} , the global minimum for the pathway. This is followed by loss of a proton from the complex *via* a transition state with an activation energy of 3.44 eV to give $\text{ArNH}_2^+ + \text{H}^+$. An H atom then dissociates from ArNH_2^+ *via* an activation barrier of 5.86 eV to leave $\text{ArNH}^+ + \text{H}$. The last remaining H atom can also dissociate from ArNH^+ with an activation energy of 3.49 eV, leaving ArN^+ and an H atom in their ground states. The final products are hence $\text{ArN}^+ + \text{H}^+ + 2\text{H}$. For each stationary point, geometric parameters are given in Table 3.1, and the total energies and zero-point energy corrections are given in Table 3.2.

3.3.2 Multireference methods

Figure 3.2 shows the stationary points along the PES of the reaction of Ar^{2+} with NH_3 to produce ArNH^+ and ArN^+ , calculated using CASSCF and MRCI methods. As with the mechanism calculated using B3LYP, the first step forms the Ar-N bond to give ArNH_3^{2+} , followed by charge separation

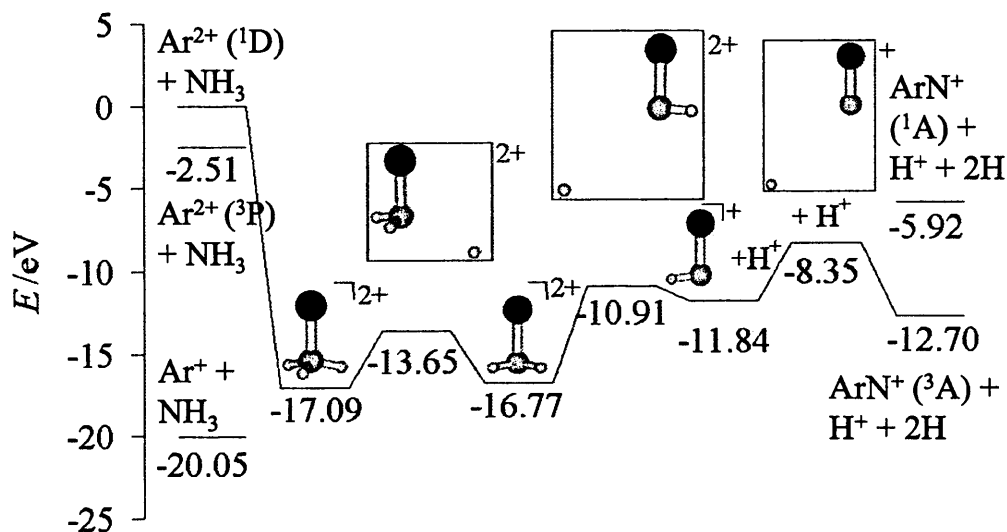


Figure 3.1: The calculated stationary points on the potential energy surface for the reaction $\text{Ar}^{2+} + \text{NH}_3 \rightarrow \text{ArN}^+ + \text{H}^+ + 2\text{H}$, calculated using the B3LYP method. No symmetry constraints were imposed during the calculations.

Structure	Ar-N	N-H	Ar-N-H	H-N-H
NH_3 (^1A)		1.013 [3]		107.5° [3]
ArNH_3^{2+} (^1A)	1.811	1.050 [3]	104.8° [3]	113.7° [3]
transition state 1 (^1A)	1.850	1.037 [2], 2.915	99.69° [2], 119.9°	113.1° [2], 109.8°
ArNH_2^+ (^1A)	1.907	1.034 [2]	97.40° [2]	106.6°
transition state 2 (^1A)	1.923	1.040, 4.757	94.85°, 130.1°	122.0°
ArNH^+ (^2A)	2.099	1.081	118.3°	
transition state 3 (^2A)	1.863	4.304	134.9°	
ArN^+ (^3A)	1.886			
ArN^+ (^1A)	1.846			

Table 3.1: Geometric parameters of B3LYP optimized structures on the singlet potential energy surface for $\text{Ar}^{2+} + \text{NH}_3 \rightarrow {}^3\text{ArN}^+ + \text{H}^+ + 2\text{H}$ (see Figure 3.1). All bond distances are in angstroms (\AA). The number of degenerate bond lengths and angles are given in square brackets. No symmetry constraints were imposed during the calculations.

Structure	Total energy/ Hartrees	Zero-point energy correction/Hartrees
NH ₃ (¹ A)	-56.46732203	0.034252
ArNH ₃ ²⁺ (¹ A)	-583.0809804	0.038246
transition state 1 (¹ A)	-582.9431386	0.026571
ArNH ₂ ⁺ (¹ A)	-583.0560856	0.025106
transition state 2 (¹ A)	-582.8274284	0.011705
ArNH ⁺ (² A)	-582.3566165	0.009005
transition state 3 (² A)	-582.2204909	0.001229
ArN ⁺ (³ A)	-581.7128346	0.001180
ArN ⁺ (¹ A)	-581.6290209	0.001289
Ar ²⁺ (³ A)	-525.9542408	-
Ar ²⁺ (¹ A)	-525.8618208	-
H (² S)	-0.502257	-

Table 3.2: B3LYP total energies and zero-point energy corrections for optimized structures on the singlet potential energy surface for $\text{Ar}^{2+} + \text{NH}_3 \rightarrow \text{ArN}^+ + \text{H}^+ + 2\text{H}$ (see Figure 3.1).

via transition state 1 on Figure 3.2. Also in agreement with the B3LYP mechanism, ArNH_3^{2+} is the global minimum for the pathway, and the final products are ${}^3\text{ArN}^+ + \text{H}^+ + 2\text{H}$. However, the activation energy for the charge separation is much larger, 5.74 eV relative to the 3.44 eV calculated using B3LYP. Then, following the charge separation, the final two steps of the mechanism in which the last remaining H atoms dissociate from the Ar-N complex are barrierless when calculated using multireference methods. This is in stark contrast with the mechanism calculated by B3LYP, which predicts two more transition structures corresponding to each H atom loss.

In order to verify that the last two steps of the reaction mechanism are indeed activation-less, a series of restricted geometry optimizations were performed to map the potential energy surface for H atom loss from ArNH_2^+

and from ArNH^+ . In both cases, all geometric parameters were optimized except for the N-H bond distance corresponding to the reaction co-ordinate r , which was held fixed over a range of values between 1.0 Å and 6.3 Å for the dissociation of ArNH_2^+ and between 1.0 Å and 11.8 Å for the dissociation of ArNH^+ . Due to a nearby curve crossing with the $\text{ArNH} + \text{H}^+$ pathway, restricted geometry optimizations for the dissociation of ArNH_2^+ were not continued past $r = 6.3$ Å. These calculations were performed using the CASSCF method and aug-cc-pVTZ basis set as described above. It should be noted that in order to successfully plot the surface for the dissociation of ArNH_2^+ to $\text{ArNH}^+ + \text{H}$, a slightly larger active space than that used for the ArNH_2^+ stationary point was needed. Although this larger active space may result in a lowering of the relative energies, the shape of the surface is not expected to change.

The results of the restricted geometry optimizations are shown in Figure 3.3. All energies are given relative to the sum of the energies of the products, calculated individually. These plots clearly show the lack of an activation barrier for the loss of an H atom from either ArNH_2^+ or ArNH^+ . Such a result is not surprising, as the reverse processes correspond to attractive cation-neutral associations. Figure 3.3b also shows that the energy of the dissociation limit corresponds to that of the $^3\text{ArN}^+ + \text{H}$ product asymptote, confirming that ArN^+ is formed in its ground triplet state. For each stationary point on the PES shown in Figure 3.2, geometric parameters are given in Table 3.3, and the total energies and zero-point energy corrections are given in Table 3.4.

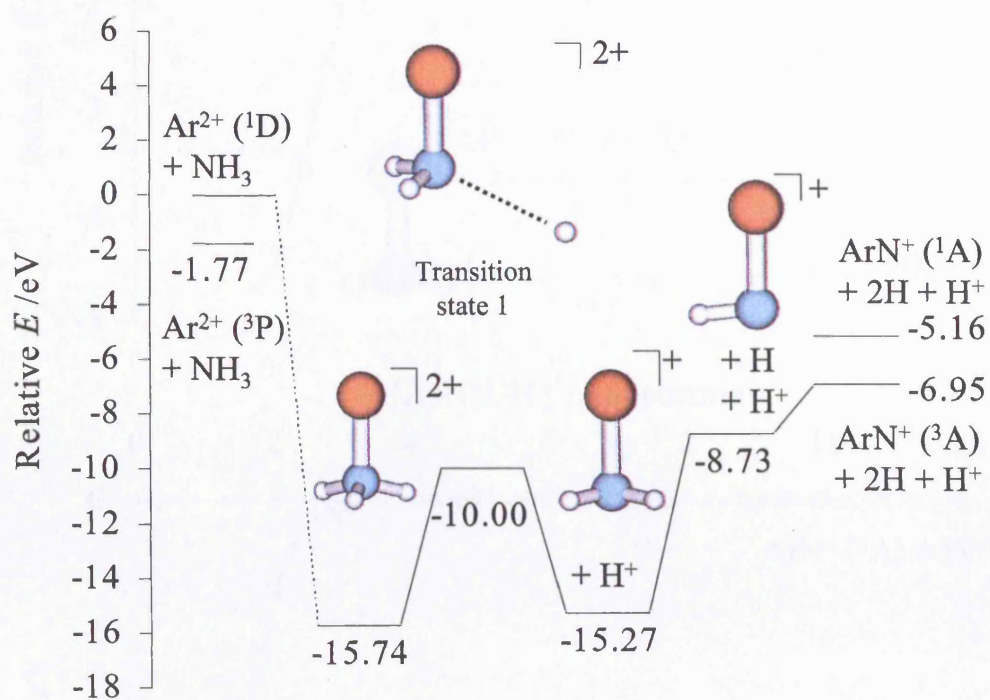


Figure 3.2: The calculated stationary points on the potential energy surface for the reaction ${}^1\text{Ar}^{2+} + \text{NH}_3 \rightarrow \text{ArN}^+ + \text{H}^+ + 2\text{H}$. Geometries were optimized using the CASSCF method, and energies at each stationary point refined using the MRCI method.

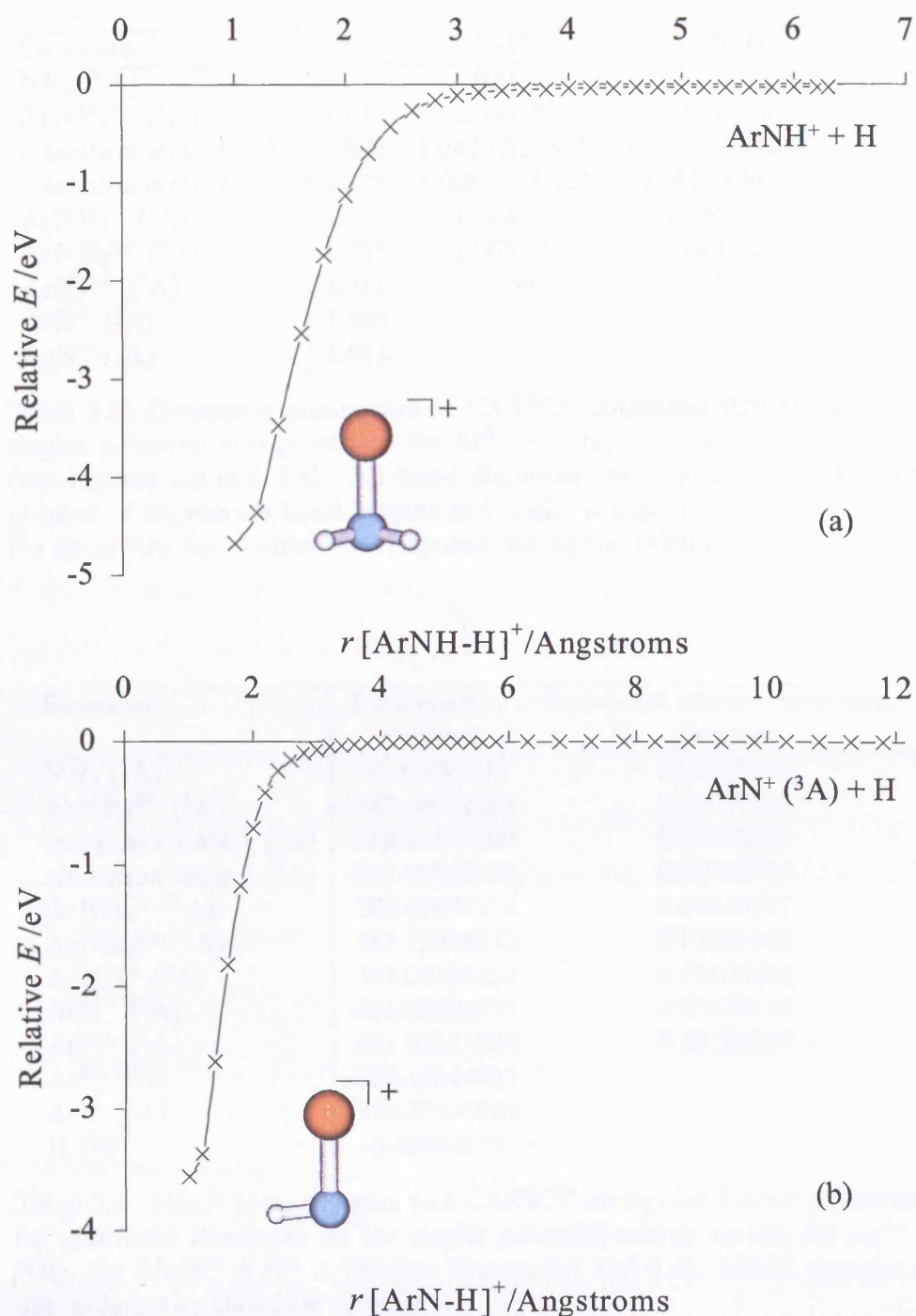


Figure 3.3: The results of a series of restricted geometry optimizations tracing the final two stages of the reaction mechanism shown in Figure 3.2: (a) the dissociation of ArNH_2^+ to $\text{ArNH}^+ + \text{H}$; (b) the dissociation of ArNH^+ to ${}^3\text{ArN}^+ + \text{H}$. In both cases, all geometric parameters were allowed to optimize at each point except for one N-H bond distance r , which is plotted on the x -axis. Energies are given relative to the sum of the energies of the fully optimized ground state geometries of the products.

Structure	Ar-N	N-H	Ar-N-H	H-N-H
NH ₃ (¹ A)		1.022 [3]		105.1° [3]
ArNH ₃ ²⁺ (¹ A)	1.817	1.056 [3]	105.0° [3]	113.6° [3]
transition state 1 (¹ A)	1.863	1.042 [2], 2.811	98.61° [2], 118.9°	115.3° [2], 107.6°
transition state 2 (¹ A)	1.825	1.056 [2], 2.522	99.87°, 126.1°	134.1°
ArNH ₂ ⁺ (¹ A)	1.951	1.044 [2]	95.80° [2]	104.6°
ArNH ₂ ²⁺ (² A)	1.737	1.065 [2]	114.1° [2]	132.0°
ArNH ⁺ (² A)	1.911	1.059	96.05°	
ArN ⁺ (³ A)	1.886			
ArN ⁺ (¹ A)	1.841			

Table 3.3: Geometric parameters of CASSCF optimized structures on the singlet potential energy surface for $\text{Ar}^{2+} + \text{NH}_3 \rightarrow {}^3\text{ArN}^+ + \text{H}^+ + 2\text{H}$ (see Figures 3.2 and 3.4). All bond distances are in angstroms (Å). The number of degenerate bond lengths and angles are given in square brackets. No symmetry constraints were imposed during the calculations.

Structure	Total energy/ Hartrees	Zero-point energy correction/ Hartrees
NH ₃ (¹ A)	-56.46732203	0.03385888
ArNH ₃ ²⁺ (¹ A)	-582.44642014	0.03827394
transition state 1 (¹ A)	-582.22404000	0.02695533
transition state 2 (¹ A)	-581.60535030	0.01298255
ArNH ₂ ⁺ (¹ A)	-582.41605214	0.02516017
ArNH ₂ ²⁺ (² A)	-581.72068632	0.02205933
ArNH ⁺ (² A)	-581.66198209	0.01108234
ArN ⁺ (³ A)	-581.08684331	0.00122156
ArN ⁺ (¹ A)	-581.02111624	0.00126389
Ar ²⁺ (³ A)	-525.46144255	-
Ar ²⁺ (¹ A)	-525.39628688	-
H (² S)	-0.49982118	-

Table 3.4: MRCI total energies and CASSCF zero-point energy corrections for optimized structures on the singlet potential energy surface for $\text{Ar}^{2+} + \text{NH}_3 \rightarrow {}^3\text{ArN}^+ + \text{H}^+ + 2\text{H}$ (see Figures 3.2 and 3.4). MRCI energies do not include the Davidson correction.

The calculated mechanism shown in Figure 3.2 confirms that ArNH^+ and ArN^+ are formed from the same reactive channel, as indicated by the experimental results. It is interesting to note that the bond-forming dication complex ArNH_3^{2+} is found to be stable with respect to dissociation to $\text{Ar}^+ + \text{NH}_3^+$ only when formed in the singlet state; attempts to converge a geometry optimization to a stable triplet structure were unsuccessful. Such an effect is not surprising when one considers that the initial formation of the Ar-N bond will involve the donation of a lone pair from the nitrogen into a vacant argon p -orbital, which only exists for $^1\text{Ar}^{2+}$. The lowest energy electronic configuration of the triplet ArNH_3^{2+} complex involves the promotion of an electron from a bonding to an anti-bonding orbital, lowering the Ar-N bond order and increasing the total energy of the complex. Therefore it appears that only singlet states of Ar^{2+} , not the ground triplet state, contribute to bond-forming reactivity in this system. This prediction is not in disagreement with the experimental results, since it has been shown that EI ionization of Ar at around 0.1 keV electron energies yields a statistical distribution of the 3P , 1D and 1S states of Ar^{2+} [89].

The calculated mechanism also provides rationalisation for the observation of opposite collision energy dependencies for the formation of the product ions ArNH^+ and ArN^+ . As can be seen on Figure 3.2, breaking an N-H bond in the ArNH_2^+ ion requires an excitation of 6.54 eV, and breaking the N-H bond in the ArNH^+ complex requires an additional 1.78 eV. The reactants lie at an energy of 15.27 eV above the $\text{ArNH}_2^+ + \text{H}^+$ asymptote, therefore every reactive event in principle begins with enough energy to reach

completion and form ArN^+ . However, such an analysis neglects the energy removed from the system, in the form of kinetic energy, during the charge separating dissociation of ArNH_3^{2+} to form ArNH_2^+ and H^+ . The measured kinetic energy release distributions for such processes are typically centered around 6-8 eV, with a width of several eV [35, 41, 44]. The loss of such large amounts of energy significantly reduces the internal energy content of the ArNH_2^+ ion. Specifically, for collisions at a center-of-mass energy of 0 eV, the charge-separating dissociation will reduce the internal energy contents of the ArNH_2^+ ions to a range of values between about -6 to -8 eV on Figure 3.2. Only those ArNH_2^+ ions that are formed with an internal energy of -6.95 eV or greater will proceed to the product asymptote ${}^3\text{ArN}^+ + \text{H}^+ + 2\text{H}$, while those ArNH_2^+ ions formed with less than -6.95 eV will only go as far as the $\text{ArNH}^+ + \text{H}^+ + \text{H}$ asymptote. With increasing collision energy, the residual internal energy of ArNH_2^+ will be higher, increasing the probability of complete dissociation to ArN^+ . Thus, increasing the collision energy increases the yield of ArN^+ and correspondingly decreases the yield of ArNH^+ , reproducing the behaviour observed experimentally. Such sequential dissociations have been observed before for similar endothermic fragmentation steps in the bond-forming reactions between rare gas ions and molecules[90–92].

It is also of interest to consider an alternative pathway to the formation of ArNH_2^+ and ArNH^+ that involves initial neutral loss in the dissociation of ArNH_3^{2+} rather than charge separation. The stationary points along this alternative pathway were calculated in the same way as for the first pathway

shown in Figure 3.2, and the results are shown in Figure 3.4. The geometric parameters of ArNH_2^{2+} and transition state 2 are given in Table 3.3. As can be seen in Figure 3.4, the neutral loss pathway is also consistent with the observed experimental collision energy dependencies of the formation of the ArNH^+ and ArN^+ ions. Assuming again 0 eV collision energy, the reactants will always have sufficient energy to form ArNH^+ , since the amount of internal energy of the ArNH_2^{2+} ion lost to the H atom in the neutral loss step should be small, less than 1 eV. However, the kinetic energy release of the charge separation of ArNH_2^{2+} to ArNH^+ and H^+ will reduce the internal energy of ArNH^+ to approximately -6 to -8 eV on Figure 3.4. As described above, in this situation again the probability of the ArNH^+ ion having enough internal energy to fragment to ArN^+ and H will increase with increasing collision energy. This would also result in the experimentally observed increase in the ArN^+ ion yield with a corresponding decrease in the ArNH^+ ion yield with increasing collision energy.

In trying to decide which pathway is operating to form ArNH^+ , it is expected that the pathway in which charge separation occurs first will be kinetically favoured, as its rate-limiting transition state lies 2.86 eV lower in energy than that of the neutral loss pathway. In addition, we would expect a small dication such as ArNH_3^{2+} to favour decay *via* initial charge separation in order to achieve the 5.24 eV stabilization of the $\text{ArNH}_2^+ + \text{H}^+$ state relative to the $\text{ArNH}_2^{2+} + \text{H}$ state. Indeed, the vast majority of dications derived from small molecules predominantly decay *via* charge separation rather than neutral loss [35, 44, 93, 94]. Pathways such as the one

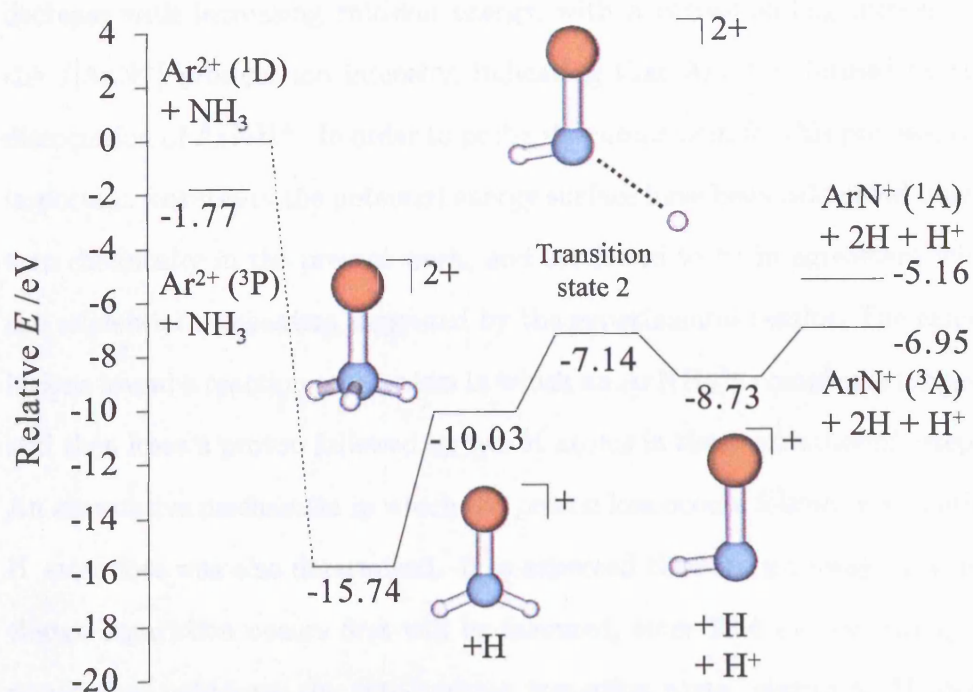


Figure 3.4: A schematic representation of the stationary points on the potential energy surface of an alternate pathway for the reaction ${}^1\text{Ar}^{2+} + \text{NH}_3 \rightarrow {}^3\text{ArN}^+ + \text{H}^+ + 2\text{H}$, in which the adduct dication decomposes *via* initial neutral loss, as opposed to initial charge separation (see Figure 3.2.)

shown in Figure 3.4 in which neutral loss occurs in the first step may be of importance in larger systems where there is greater stabilization of the dipositive charge.

3.4 Conclusions

Previous crossed-beam collision experiments between Ar^{2+} and NH_3 revealed a bond-forming reaction channel that leads to the formation of the molecular ions ArNH^+ and ArN^+ . The product ion intensity $I[\text{ArNH}^+]$ was found to

decrease with increasing collision energy, with a corresponding increase in the $I[\text{ArN}^+]$ product ion intensity, indicating that ArN^+ is formed by the dissociation of ArNH^+ . In order to probe the mechanism for this process, the important features of the potential energy surface have been calculated quantum chemically in the present work, and are found to be in agreement with the sequential mechanism suggested by the experimental results. The calculations reveal a reaction mechanism in which an ArNH_3^{2+} complex is formed, and then loses a proton followed by two H atoms in three endothermic steps. An alternative mechanism in which the proton loss occurs following an initial H atom loss was also determined. It is expected that the pathway in which charge separation occurs first will be favoured, since 2.86 eV less energy is required to overcome the rate-limiting transition state relative to H atom loss.

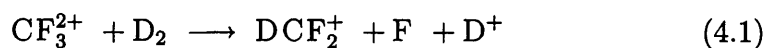
The work presented in this Chapter has also shown the important differences that can arise from the calculation of a reaction PES using single- or multireference methods. Calculation of the mechanism for the bond-forming reaction between Ar^{2+} and NH_3 using single-reference methods indicated that two H-atom loss steps proceeded *via* transition states. Calculation of the same mechanism using multireference methods showed that these two steps were barrier-less. The latter result is more sensible when one considers the reverse process, the association of an H-atom with a small monocation. One would not expect a barrier to such a process.

Chapter 4

A computational study of the mechanism for the formation of HCF_2^+ from CF_3^{2+} and H_2

4.1 Introduction

In the context of bond-forming reactions between dications and neutrals, one collision system that has received particular attention is $\text{CF}_3^{2+} + \text{X}_2$ ($\text{X} = \text{H}, \text{D}$). The bond-forming product ion DCF_2^+ was first observed by Price *et al.* in 1994 [31] in an experimental study of collisions of CF_3^{2+} with D_2 . No F^+ or DF^+ ions were reported in this study, so the following reaction mechanism was proposed for the formation of DCF_2^+ :



Price *et al.* suggested that the mechanism for the formation of DCF_2^+ from CF_3^{2+} and D_2 involved D^- transfer from the neutral to the dication. A later study by Tafadar *et al.* [42] of collisions between CF_3^{2+} and HD

demonstrated an intramolecular isotope effect in the formation of HCF_2^+ and DCF_2^+ . This isotope effect was explained in terms of a preferential orientation of the reactants preceding the chemical reaction. However, Tafadar *et al.* also reported the observation of the HF^+/DF^+ bond-forming products, whose formation did not exhibit an intramolecular isotope effect. This indicated that the orientational mechanism may not be the dominant effect in the dynamics. If such a mechanism were operating, one would expect *all* products of the bond-forming reaction to demonstrate an intramolecular isotope effect. In a more recent study by Tafadar *et al.* [46] on the reactions of CF_3^{2+} with H_2 and D_2 it was also noted that the cross sections for the formation of the XCF_2^+ and XF^+ ions had significantly different collision energy dependencies, suggesting that XCF_2^+ and XF^+ are formed *via* two different mechanisms.

As the existing experimental data could not provide any additional clues as to the mechanisms for the reactions of CF_3^{2+} with X_2 to give XCF_2^+ and XF^+ , it became necessary to look to previous computational studies of the potential energy surfaces of bond-forming dication-molecule reactions for further insight. On the basis of the results of the quantum chemical studies by Mrázek *et al.* [35] on the reaction of CO_2^{2+} with H_2 and by Hrušák [55] on $\text{CF}_2^{2+} + \text{H}_2$ (as discussed in Section 1.2.2), Tafadar *et al.* [46] suggested that the reaction of CF_3^{2+} with X_2 may be occurring *via* a similar mechanism to those suggested in the previous two quantum chemical studies. The first step would involve the formation of an $[\text{X}_2\text{-CF}_3]^{2+}$ collision complex, followed by X-atom migration from the C to an F atom. Formation of the

products $\text{XCF}_2^+ + \text{X}^+ + \text{F}$ could then occur by subsequent cleavage of an F-X bond and a C-F bond in two steps, while the formation of $\text{XCF}_2^+ + \text{XF}^+$ could occur by a simple C-F bond cleavage. Crucially, the reaction co-ordinate which defines the pathway for formation of X^+ is the F-X bond cleavage. RRKM calculations performed by Tafadar *et al.* [46] on the $\text{CO}_2^{2+} + \text{HD}$ system showed that the rate for the O-D cleavage is 66% slower than for O-H cleavage, due to a greater number of accessible vibrational states at the transition state leading to H^+ loss rather than D^+ loss. The same argument could be applied for the formation of X^+ by F-X bond cleavage in the $\text{CF}_3^{2+} + \text{X}_2$ system. Of course, there would be no kinetic competition for the formation of XF^+ , as the reaction co-ordinate of interest (C-F bond breaking) does not involve an X atom. This statistical argument was used to explain why an isotope effect is noticed in the formation of XCF_2^+ but not XF^+ in the reaction of CF_3^{2+} with HD [46].

In this Chapter, the results of a series of *ab initio* calculations on the important features of the potential energy surface for the reaction between CF_3^{2+} and H_2 are presented. These calculations reveal four primary pathways to the formation of the experimentally observed products. We find that these mechanisms support the explanation suggested by Tafadar *et al.* [42] for the observed isotopic effects. The energetics of these calculated mechanisms are compared with the results of a series of crossed-beam scattering experiments between CF_3^{2+} and D_2 performed by Žabka and Herman [95] and are found to correspond well.

4.2 Computational Details

Although other approaches were attempted (as discussed in the main text), the *ab initio* QCISD method was selected for the full characterization of the stationary points along the potential energy surfaces for the bond-forming reactions of CF_3^{2+} and H_2 to give either $\text{HCF}_2^+ + \text{H}^+ + \text{F}$ or $\text{HCF}_2^+ + \text{HF}^+$. The 6-311G(d,p) basis set was used for all production calculations. Geometry optimizations were performed at the QCISD level, followed by frequency calculations in order to characterise each stationary point and to obtain the zero-point energy. Single-point calculations were then performed on each of the optimized geometries at the QCISD(T) level in order to refine the energies of each structure.

IRC calculations using QCISD were performed along the reactive mode corresponding to the imaginary frequency of each transition state to verify the connectivity of all minima and saddle points. Where necessary, restricted geometry optimizations were performed in order to map out certain problematic regions of a surface. The *Gaussian03* program was used for all calculations [96].

4.3 Results and Discussion

4.3.1 Computational Results

Ab initio versus DFT methods and the T_1 -diagnostic

The stationary points along a number of pathways on the PES for the bond-forming reaction of CF_3^{2+} with H_2 were first optimized using the B3LYP hybrid DFT method with the 6-311G(d,p) Pople style basis set. Four distinct pathways were found leading to the formation of the bond-forming product ion, HCF_2^+ . Three key barrier heights for the dominant reactive pathway were recalculated at the B3LYP level using the larger 6-311++G(2df,2pd) basis set. Differences in these three barrier heights between those calculated at the B3LYP/6-311G(d,p) level and those calculated at the B3LYP/6-311++G(2df,2pd) level were all less than 0.06 eV. Therefore the extra diffuse and polarization functions were omitted from subsequent calculations in order to save computational time. It is unsurprising that diffuse functions are not required to satisfactorily model systems with one or more positive charges.

Single-point energy calculations were then performed on the B3LYP-optimized geometries using the CCSD(T) method and the 6-311G(d,p) basis set. The T_1 -diagnostic was also evaluated for each point using CCSD(T). As discussed in Section 1.3.1, the T_1 -diagnostic of Lee and Taylor [58] is a measure of the weighting of the single excitations in the cluster operator:

$$T_1 = \sqrt{\frac{\sum_i^{\text{occ}} \sum_a^{\text{vir}} (t_i^a)^2}{n}} \quad (4.2)$$

where t_i^a is the amplitude of single excitations from occupied orbital i to virtual orbital a , and n is the number of electrons. The T_1 -diagnostic is often used as a qualitative estimate of the degree of multireference character of a system. A value of 0.02 for the T_1 -diagnostic was suggested by Lee and Taylor as a threshold above which the reliability of single reference methods would become questionable [58]. However, they also noted that the threshold may well be higher for open-shell systems. Since then, a number of studies have shown that T_1 -diagnostic values of up to 0.045 may be acceptable in open-shell systems [58, 97–99]. The T_1 -diagnostic values calculated for the stationary points in our system lay between 0.018 and 0.027. Although these fall below the open-shell threshold of 0.045, we felt it would be useful to compare our B3LYP-optimized PES's with those calculated by a different method, ideally one which recovers more dynamic electron correlation.

The obvious method to use in order to include possible multireference effects is the MRCI method. We first attempted to perform geometry optimizations at the CASSCF level using a full valence active space and the cc-pvtz basis set using the Molpro v.2002.3 code [88]. For our largest structures, a full valence active space consisted of 15 electrons in 13 orbitals. However, it soon became clear that such active spaces would not be sufficient for a meaningful investigation of the potential energy surface as there existed many energetically near-degenerate orbitals of similar character at the active space limit. Since we were investigating a reaction pathway which involves many different reactive coordinates, it would have been necessary to include orbitals relevant to all of these coordinates. Unfortunately, such an

enlargement of the active space was not computationally feasible.

We subsequently decided to make use of the QCISD method in order to investigate the PES. Although a single reference method, QCISD is a high level *ab initio* approach that recovers much dynamic correlation and a good deal of nondynamic correlation as well. QCISD is size-consistent, and has a reasonably efficient implementation of analytic gradients and numerical frequencies in the *Gaussian03* program [96]. Stationary point geometries, zero-point energies, vibrational frequencies and IRC calculations were all performed using QCISD and the 6-311G(d,p) basis set. QCISD(T)/6-311G(d,p) single-point energies and Q_1 -diagnostics were then evaluated on the optimized geometries. The Q_1 -diagnostic is the QCISD equivalent [100] of the coupled cluster T_1 -diagnostic, and the same thresholds for the suitability of single reference methods apply (i.e. 0.020 for closed shell and 0.045 for open shell systems).

The same four pathways as evaluated at the B3LYP level were found and are shown in Figures 4.1, 4.2, 4.3 and 4.4. The general shapes of the surfaces calculated at the QCISD(T)//QCISD level are not significantly different to those calculated at the B3LYP level. As can be seen from the relative barrier heights given in Table 4.1, the largest difference in activation energies between the two methods is 0.49 eV. Most of the geometries of the stationary points remained very similar as well. The geometric parameters for each stationary point calculated at the QCISD level are given in Tables 4.2 and 4.3. The total energies, zero-point energies and Q_1 -diagnostics for each stationary point are given in Table 4.4.

Although most of the geometries of the stationary points calculated at the

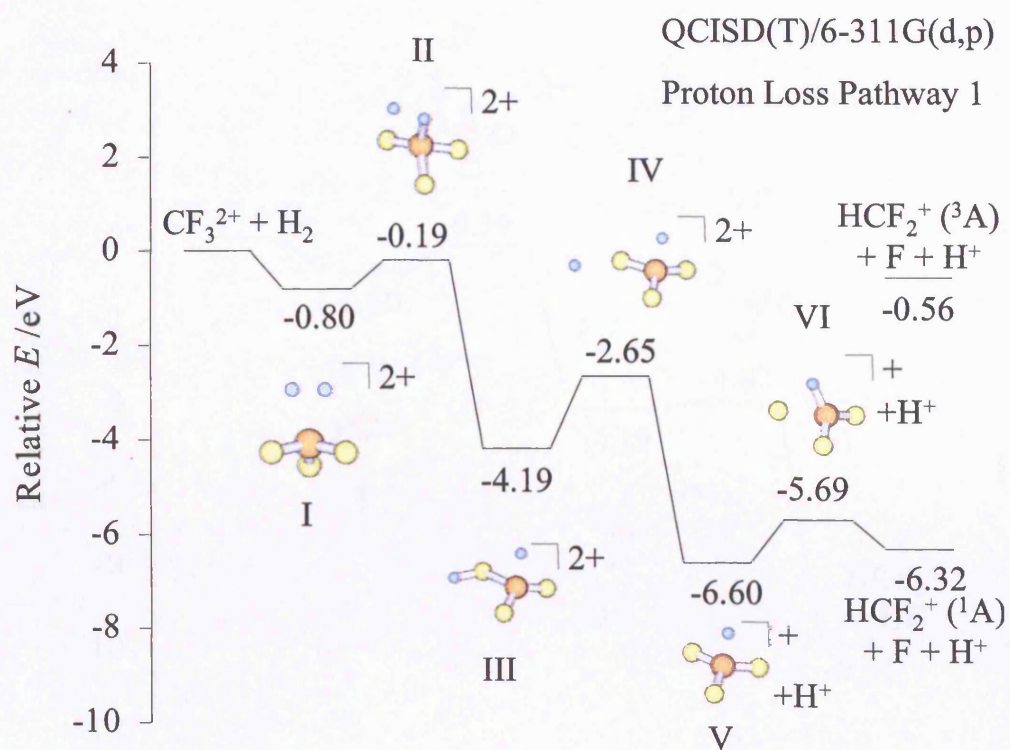


Figure 4.1: Calculated stationary points on one pathway on the potential energy surface for the reaction $\text{CF}_3^{2+} + \text{H}_2 \rightarrow \text{HCF}_2^+ + \text{H}^+ + \text{F}$. This pathway involves proton loss following complexation and is referred to in the text as PL1 (Proton Loss 1).

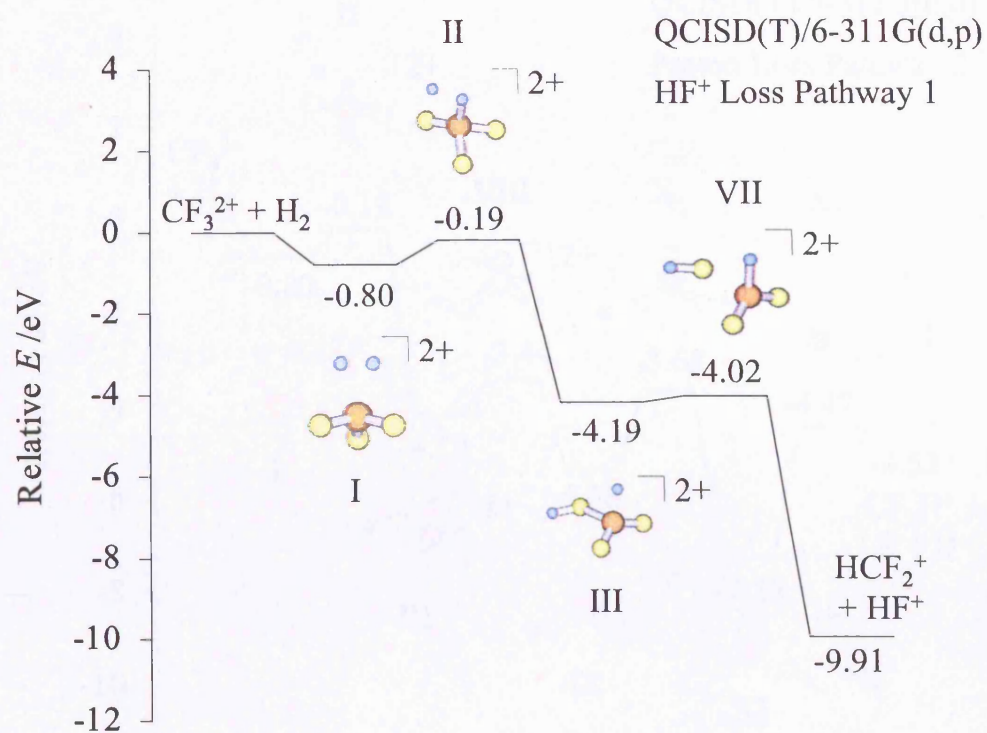


Figure 4.2: Calculated stationary points on one pathway on the potential energy surface for the reaction $\text{CF}_3^{2+} + \text{H}_2 \rightarrow \text{HCF}_2^+ + \text{HF}^+$. This pathway involves loss of HF^+ following complexation and is referred to in the text as HFL1 (HF^+ Loss 1).

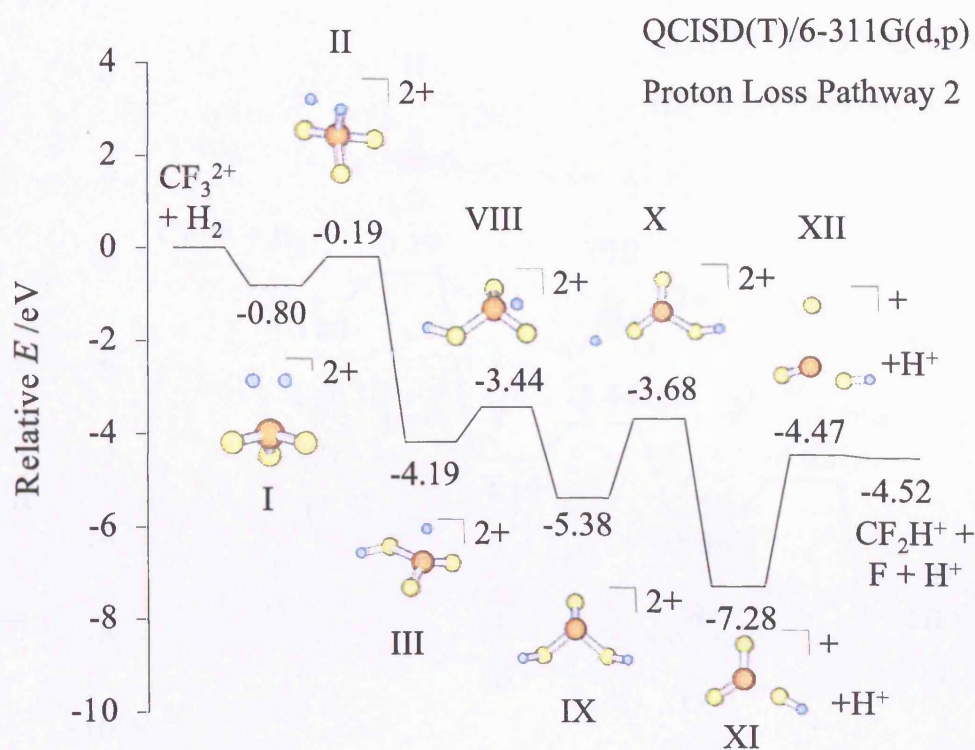


Figure 4.3: Calculated stationary points on one pathway on the potential energy surface for the reaction $\text{CF}_3^{2+} + \text{H}_2 \rightarrow \text{HCF}_2^+ + \text{H}^+ + \text{F}$. Like the PL1 pathway, this pathway also involves proton loss following complexation. However, an extra rearrangement step takes place before the fragmentation. This pathway is referred to in the text as PL2 (Proton Loss 2).

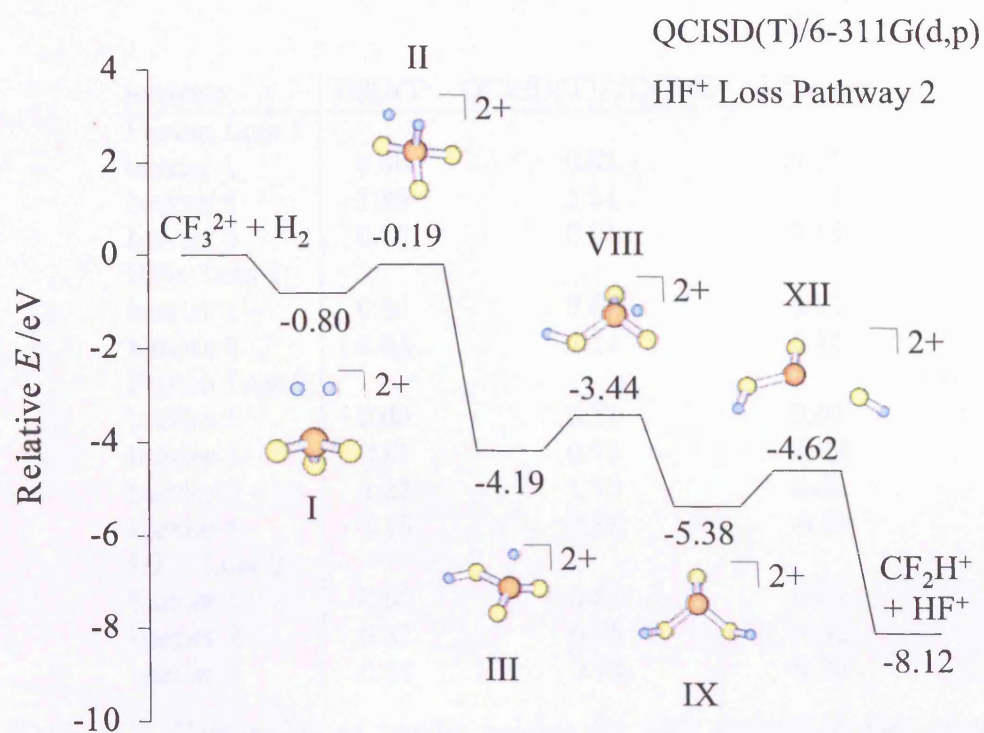


Figure 4.4: Calculated stationary points on one pathway on the potential energy surface for the reaction $\text{CF}_3^{2+} + \text{H}_2 \rightarrow \text{HCF}_2^+ + \text{HF}^+$. Like the HFL1 pathway, this pathway involves loss of HF^+ following complexation. However, an extra rearrangement step takes place before the fragmentation. This pathway is referred to in the text as HFL2 (HF^+ Loss 2).

pathway	B3LYP	QCISD(T)//QCISD	difference
Proton Loss 1			
barrier 1	0.60	0.61	0.01
barrier 2	1.40	1.54	0.14
barrier 3	0.76	0.91	0.15
HF+ Loss 1			
barrier 1	0.60	0.61	0.01
barrier 2	0.04	0.17	0.13
Proton Loss 2			
barrier 1	0.60	0.61	0.01
barrier 2	0.87	0.75	-0.12
barrier 3	1.22	1.70	0.49
barrier 4	3.15	2.81	-0.32
HF+ Loss 2			
barrier 1	0.60	0.61	0.01
barrier 2	0.87	0.75	-0.12
barrier 3	0.54	0.76	0.22

Table 4.1: Comparison of barrier heights for each activation step in all four calculated pathways, as determined by B3LYP and QCISD(T)//QCISD methods. Barrier heights and differences are given in eV. Barrier numbers are given in the order in which they are encountered in the reaction mechanism.

symbol	structure	H-C/Å	H-F/Å	C-F/Å
I	H ₂ CF ₃ ²⁺ (² A)	1.47[2]		1.36[2],1.22
II	H ₂ CF ₃ ²⁺ TS (² A)	1.22	1.48	1.35[2],1.30
III	HC(FH)F ₂ ²⁺ (² A)	1.42	1.86	1.23[2],1.51
IV	HC(FH)F ₂ ²⁺ TS (² A)	1.43	1.91	1.25[2],1.34
V	HCF ₃ ⁺ (² A)	2.74		1.23[3]
VI	HCF ₃ ⁺ TS (² A)	1.14		1.25[2],1.60
VII	HCF ₂ FH ²⁺ TS (² A)	1.33	0.97	1.21[2],1.79
VIII	HC(FH)F ₂ ²⁺ TSb (² A)	1.43	0.99	1.22,1.35,1.48
IX	C(FH) ₂ F ²⁺ (² A)		0.98[2]	1.50[2],1.21
X	C(FH) ₂ F ²⁺ TS (² A)		1.95,0.95	1.23,1.64,1.31
XI	CF ₃ H ⁺ (² A)		0.94	1.24[2],1.89
XII	CF ₃ H ⁺ TS (² A)		0.92	1.17,2.17,1.96
XIII	CF ₂ HFH ²⁺ (² A)		0.96,0.98	1.17,1.57,1.86
	CF ₃ ²⁺ (² A)			1.18[2], 1.55
	H ₂ (¹ A)	0.74 (H-H)		
	HCF ₂ ⁺ (¹ A)	1.09		1.23[2]
	HCF ₂ ⁺ (³ A)	2.88		1.22[2]
	HF ⁺ (² A)		0.99	
	F (² P)			
	CF ₂ H ⁺ TS (¹ A)	1.33		1.45,1.21
	CF ₂ H ⁺ (¹ A)		0.92	1.17,2.19

Table 4.2: Bond lengths for all calculated (QCISD) structures. The symbols in the first column refer to labels used in Figures 4.1, 4.2, 4.3 and 4.4. Numbers in square brackets indicate the number of degenerate bond lengths. No symmetry constraints were imposed during any of the geometry optimizations.

symbol	structure	H-C-F	F-C-F	H-F-C
I	$\text{H}_2\text{CF}_3^{2+}$ (^2A)	93.6[2],108.4	120.7[2],91.1	
II	$\text{H}_2\text{CF}_3^{2+}$ TS (^2A)	112.6[2],108.7	116.5[2],92.0	
III	$\text{HC}(\text{FH})\text{F}_2^{2+}$ (^2A)	102.1,104.8,98.0	127.5,112.3,107.5	124.4
IV	$\text{HC}(\text{FH})\text{F}_2^{2+}$ TS (^2A)	99.7[2],100.7	115.0[2],121.2	161.3
V	HCF_3^+ (^2A)	90.4[3]	120.0[3]	
VI	HCF_3^+ TS (^2A)	117.2[2],78.1	109.2,117.9	
VII	$\text{HCF}_2\text{FH}^{2+}$ TS (^2A)	113.6,71.7,111.3	129.9,111.0,103.3	127.7
VIII	$\text{HC}(\text{FH})\text{F}_2^{2+}$ TSb (^2A)	57.0,131.3,112.0	122.1,105.1,114.0	122.9
IX	$\text{C}(\text{FH})_2\text{F}^{2+}$ (^2A)		98.0,112.0,111.1	120.5[2]
X	$\text{C}(\text{FH})_2\text{F}^{2+}$ TS (^2A)		107.9,100.9,117.7	119.5,164.3
XI	CF_3H^+ (^2A)		102.4[2],120.4	119.7
XII	CF_3H^+ TS (^2A)		91.3,99.6,112.1,99.6	136.2
XIII	$\text{CF}_2\text{HFH}^{2+}$ (^2A)		108.0,135.1,116.8	120.9,124.7
	CF_3^{2+} (^2A)		110.1[2],139.9	
	H_2 (^1A)			
	HCF_2^+ (^1A)	120.8[2]	118.4	
	HCF_2^+ (^3A)	93.9[2]	124.9	
	HF^+ (^2A)			
	F (^2P)			
	CF_2H^+ TS (^1A)	50.5,161.5	111	
	CF_2H^+ (^1A)	-	90.6	138.6

Table 4.3: Bond angles for all (QCISD) calculated structures. The symbols in the first column refer to labels used in Figures 4.1, 4.2, 4.3 and 4.4. Numbers in square brackets indicate the number of degenerate bond angles. No symmetry constraints were imposed during any of the geometry optimizations. All bond angles are given in degrees.

symbol	structure	total energy	zero-point energy	zero-point corrected energy	Q_1 -diagnostic
I	$H_2CF_3^{2+}$ (2A)	-336.9437745	0.024572	-336.9192025	0.0269
II	$H_2CF_3^{2+}$ TS (2A)	-336.9204905	0.023915	-336.8965755	0.0260
III	$HC(FH)F_2^{2+}$ (2A)	-337.0701787	0.026513	-337.0436657	0.0209
IV	$HC(FH)F_2^{2+}$ TS (2A)	-337.0069378	0.019647	-336.9872908	0.0200
V	HCF_3^+ (2A)	-337.1512063	0.019647	-337.1315593	0.0180
VI	HCF_3^+ TS (2A)	-337.1196899	0.020914	-337.0987759	0.0199
VII	HCF_2FH^{2+} TS (2A)	-337.0637402	0.026115	-337.0376252	0.0167
VIII	$HC(FH)F_2^{2+}$ TSb (2A)	-337.0409327	0.024630	-337.0163027	0.0402
IX	$C(FH)_2F^{2+}$ (2A)	-337.1160944	0.028492	-337.0876024	0.0245
X	$C(FH)_2F^{2+}$ TS (2A)	-337.0467039	0.021636	-337.0250679	0.0195
XI	CF_3H^+ (2A)	-337.1779872	0.020600	-337.1573872	0.0196
XII	CF_3H^+ TS (2A)	-337.0691993	0.015317	-337.0538823	0.0259
XIII	CF_2HFH^{2+} (2A)	-337.0860712	0.026682	-337.0593892	0.0227
	CF_3^{2+} (2A)	-335.7432934	0.011825	-335.7314684	0.0229
	H_2 (1A)	-1.1683403	0.010068	-1.1582723	0.0058
	HCF_2^+ (1A)	-237.5770649	0.021021	-237.5560439	0.0200
	HCF_2^+ (3A)	-237.3732153	0.012931	-237.3602843	0.0228
	HF^+ (2A)	-99.704935	0.006871	-99.698064	0.0069
	F (2P)	-99.5658041	-	-	0.0034
	CF_2H^+ TS (1A)	-237.4278733	0.012884	-237.4149893	0.0239
	CF_2H^+ (1A)	-237.5060605	0.016074	-237.4899865	0.0192

Table 4.4: Total energies, zero-point energies, zero-point corrected energies, and Q_1 -diagnostics for all structures. All energies are given in Hartrees. Zero-point energies were calculated at the QCISD/6-311G(d,p) level. Total energies and Q_1 -diagnostics were calculated at the QCISD(T) level.

QCISD level were virtually unchanged from those calculated at the B3LYP level, a large difference was noticed for the HCF_3^+ (structure V, Figure 4.1) ion. The largest differences were in the H-C bond length (1.32 Å at B3LYP and 2.74 Å at QCISD) and the F-C-F-F dihedral angle (144.7° at B3LYP and 178.7° at QCISD). Both structures are 2A_1 states. The difference in the B3LYP single point energies calculated for each structure is only 0.24 eV and the difference in the QCISD single point energy between the two structures is 0.25 eV. A geometry optimization was performed on this ion using the coupled cluster singles and doubles (CCSD) method and the same structure as that determined using QCISD was obtained. Given that, in general, post-Hartree-Fock methods such as CCSD and QCISD are likely to be more accurate than B3LYP, we tend to favour the *ab initio* geometry for structure HCF_3^+ .

It should also be noted that all attempts to optimize the geometry of the CF_3H^+ transition state (structure XII, Figure 4.3) directly were unsuccessful using QCISD. Thus, a potential energy surface scan was performed in which the optimized CF_3H^+ minimum (XI) was used as a starting structure and the C-F bond distance was held fixed over a series of increasing values whilst all other parameters were allowed to optimize. The structure at the point of maximum energy was taken as the starting guess for a QCISD transition state geometry optimization and frequency calculation. Although the geometry optimization was successful, the frequency calculation yielded three imaginary modes, the largest of which corresponds to the required C-F bond breaking (the other two modes correspond to H-C-F bend and twist).

Given our lack of success with other calculations in this area of the PES, we have decided to present structure XII as our best estimate of the C-F bond breaking transition state. A single-point QCISD(T) calculation was then also performed on this structure.

The Q_1 -diagnostics for each of the calculated stationary points are shown in Table 4.4 and, bar one, lie in the range 0.017-0.027. The largest Q_1 -diagnostic value (for structure VIII) is 0.040, still within the suggested threshold of 0.045 for open-shell systems. Given that we find good agreement between the B3LYP and QCISD methods with regards to the shapes of the potential energy surfaces and the geometries of the stationary points, it would indeed appear that T_1 - and Q_1 -diagnostic values of greater than 0.02 can be acceptable for open shell systems, as suggested previously. [97–99, 101].

Calculated Reaction Mechanisms

As can be seen in Figures 4.1, 4.2, 4.3 and 4.4, all four pathways we determined proceed *via* the same initial three stationary points. First, CF_3^{2+} and H_2 associate to form the $\text{H}_2\text{CF}_3^{2+}$ (structure I) dication complex, followed by an internal H-atom rearrangement *via* a transition state (structure II) to give $\text{HC}(\text{FH})\text{F}_2^{2+}$ (structure III). In two of the pathways, the $\text{HC}(\text{FH})\text{F}_2^{2+}$ complex then fragments immediately. This fragmentation occurs either *via* the loss of a proton followed by an F atom *via* two transition states to give the products $\text{HCF}_2^+ + \text{H}^+ + \text{F}$ (this pathway is called Proton Loss 1 (PL1) in Figure 4.1) or by simply losing an HF^+ molecule, again *via* a transition state, yielding the products $\text{HCF}_2^+ + \text{HF}^+$ (called HF^+ Loss 1 (HFL1) in

Figure 4.2).

The two other pathways require the $\text{HC}(\text{FH})\text{F}_2^{2+}$ complex to undergo another H-atom rearrangement before fragmentation occurs. This involves the migration of the H atom from the carbon in structure III to an available fluorine *via* a transition state (structure VIII) to give $\text{C}(\text{FH})_2\text{F}^{2+}$ (structure IX). One pathway then continues by loss of a proton then an F atom (Proton Loss 2 (PL2) in Figure 4.3) to give $\text{CF}_2\text{H}^+ + \text{H}^+ + \text{F}$, and the other proceeds by the loss of an HF^+ molecule (HF^+ Loss 2 (HFL2) in Figure 4.4) to give $\text{CF}_2\text{H}^+ + \text{HF}^+$. All of these fragmentations, as with the first two pathways, proceed *via* transition states. If the energy is available, the CF_2H^+ product can then overcome a 2.04 eV barrier in order to rearrange to HCF_2^+ , which is 1.80 eV more stable (note that this final rearrangement is not shown on Figures 4.3 and 4.4).

One would expect that the PL1 pathway would dominate the formation of $\text{HCF}_2^+ + \text{H}^+ + \text{F}$, as the largely exothermic charge separation occurs earlier in the mechanism than in the PL2 pathway. In addition, following charge separation, the barrier for the final neutral loss step is higher for PL2 than for PL1 (2.81 eV versus 0.91 eV, respectively). If one assumes a loss of 6 eV of internal energy in the form of kinetic energy upon charge separation, the internal energy of the CF_3H^+ complex in the PL2 pathway (structure XI) may well then not be enough to overcome this final neutral loss barrier, and the CF_3H^+ complex may instead fragment to different products and not contribute to the formation of CF_2H^+ .

One would also expect that the formation of the $\text{HCF}_2^+ + \text{HF}^+$ products

would be governed by the HFL1 pathway rather than HFL2, again due to charge separation occurring earlier in the mechanism. HFL1 is indeed the mechanism discussed in the Introduction, which was suggested by Tafadar *et al.* [46]. As noted in the Introduction, such a mechanistic pattern, involving complex formation followed by rearrangement and then fragmentation, has been seen before for the bond-forming reactions of $\text{CO}_2^{2+} + \text{H}_2$ [35], $\text{CF}_2^{2+} + \text{H}_2$ [55] and $\text{CF}_2^{2+} + \text{H}_2\text{O}$ [102] (see Chapter 2). As predicted by Tafadar *et al.*, X^+ formation is governed by the cleavage of an F-X bond, whereas the critical bond for XF^+ formation is C-F. This explains why an H/D isotope effect is observed for the formation of X^+ but not XF^+ . In addition, our calculations show that H^+ and HF^+ are formed *via* different pathways. This would explain why different collision energy dependencies have been observed experimentally for the formation of H^+ and HF^+ [42, 46].

Finally, in order to provide rationalization for the fact that the experimental ion intensities of XF^+ are approximately 5% of that of the XCF_2^+ ion, a series of Rice-Ramsperger-Kassel-Marcus (RRKM) calculations were performed in order to obtain rate constants for the fragmentation of the $\text{HC}(\text{FH})\text{F}_2^{2+}$ ion (structure III) [69]. These calculations showed that over a range of collision energies between 0.1 eV and 3.0 eV, the rates for the fragmentation of $\text{HC}(\text{FH})\text{F}_2^{2+}$ *via* proton loss are 15 to 20 times faster than *via* HF^+ loss. In addition to the above kinetic arguments, it has been shown previously [42] that product ions that are backward-scattered in the centre-of-mass frame may be detected less efficiently in the crossed-beam experiments of Tafadar *et al.* The dynamics of the fragmentation of the $\text{HC}(\text{FH})\text{F}_2^{2+}$ ion

to HCF_2^+ and HF^+ are not known. However, if HF^+ is predominantly back-scattered in the centre-of-mass frame, this would also contribute to the very weak HF^+ product ion intensities observed experimentally. Thus, the difference in the experimentally determined intensities of HF^+ and HCF_2^+ may involve apparatus factors as well as reflecting the preferential fragmentation of the collision complex.

4.3.2 Comparison With Prague Experimental Results

A series of angularly-resolved crossed-beam scattering experiments were performed by Žabka and Herman [95] to study collisions between CF_3^{2+} and D_2 at a collision energy of 1.16 eV. The details of the experimental apparatus have been previously discussed in the literature [2]. The products observed were CF_3^+ , CF_2^+ , DCF_2^+ , D^+ and CF_2^{2+} . No DF^+ signal was detected, presumably because the sensitivity of the apparatus was not sufficient to record the weak signal of this product kinematically expected to recoil mostly into the region of laboratory angles higher than 90° , inaccessible to the experiment. Earlier, Tafadar *et al.* showed that DF^+ was formed from $\text{CF}_3^{2+} + \text{D}_2$ collisions in very small amounts [46]. Žabka and Herman found that the two main channels they detected leading to products involve the formation of CF_3^+ and CF_2^+ and correspond to non-dissociative and dissociative electron transfer. The weakest channel they detected corresponds to the formation of the product ion DCF_2^+ . Repeated measurements of the energy distribution of this ion product at $T=1.16$ eV and a laboratory scattering angle $\Theta = 1.50^\circ$ (close to the angular maximum) allowed them to compile a

DCF₂⁺ product ion velocity distribution.

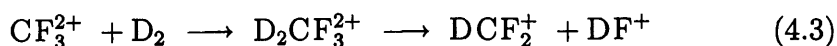
The velocity distribution is characterised by a strong forward-scattered peak corresponding to a DCF₂⁺ center-of-mass velocity of 750 m/s. There is also a second channel that exhibits symmetrical forward-backward scattering with peaks at a center-of-mass velocity of 340 m/s. These experimentally determined velocities of the peaks of DCF₂⁺ velocity distributions can be converted into translational energy releases which we can compare with the energetics predicted by our calculated PES's. For that we need to consider the different possible mechanisms for forming DCF₂⁺ as well as the various possible partner ions. These combinations of mechanism and products, and the corresponding translational energy releases as derived from the experimental velocities, are described below.

DCF₂⁺ 750 ms⁻¹ centre-of-mass velocity

In this section we consider the possible pathways for forming DCF₂⁺ following collisions of CF₃²⁺ with D₂ and within the constraints of those mechanisms, convert the centre-of-mass velocity of the DCF₂⁺ recorded experimentally by Žabka and Herman into a KER to compare with previous studies of such energy releases and with the release we calculate from our PESs.

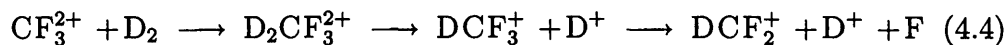
(a) DCF₂⁺ + F⁺ + D. The F⁺ ion has not been detected in the current, or any previous, studies of collisions of CF₃²⁺ with D₂. Hence, this pathway cannot be a significant source of DCF₂⁺.

(b) $\text{DCF}_2^+ + \text{DF}^+$. This is a two-body reaction and the corresponding KER we calculate from the experimental velocity of DCF_2^+ is 0.53 eV. This corresponds simply to the charge separation of $\text{D}_2\text{CF}_3^{2+}$ to DCF_2^+ and DF^+ :



This value of the KER appears unreasonably small, as a typical KER for the charge separation of a dication is approximately 3-5 eV [44].

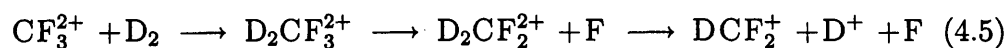
(c) $\text{DCF}_2^+ + \text{D}^+ + \text{F}$. In order to calculate the KER for the pathway that leads to these products, we first assume that DCF_2^+ is formed by loss of an F atom from DCF_3^+ following charge separation of $\text{D}_2\text{CF}_3^{2+}$ to $\text{DCF}_3^+ + \text{D}^+$:



This is, in effect, the mechanism PL1 that emerges from our theoretical investigations. As with pathway (b), to convert the measured velocity into a KER we consider the charge separation of $\text{D}_2\text{CF}_3^{2+}$ to $\text{DCF}_3^+ + \text{D}^+$, and assume that the KER of the subsequent neutral loss is negligible in comparison. The KER we calculate for this pathway from the velocity of DCF_2^+ is 7.55 eV, a value typical for the charge separation of a dication. This value also agrees very well with the KER value we determine from the calculated pathway PL1. Given the collision energy of 1.16 eV, and a total reaction exothermicity of 6.32 eV from the quantum chemical calculations,

the theoretical studies indicate a total of 7.48 eV energy is available for release. This value is in excellent agreement with the KER value of 7.55 eV we determine from the experimental velocity of DCF_2^+ .

There is also, in principle, the possibility that the $\text{DCF}_2^+ + \text{D}^+ + \text{F}$ products are formed *via* a different mechanism, i.e. complexation followed by neutral loss and then charge separation:



Again, assuming the energy release of the neutral loss process to be negligible in comparison with that of charge separation, the KER we calculate for this mechanism from the velocity of DCF_2^+ is 4.09 eV. However, we do not expect such a mechanism to predominate for the formation of $\text{DCF}_2^+ + \text{D}^+ + \text{F}$ since small dications, such as the $\text{D}_2\text{CF}_3^{2+}$ complex, tend to favour charge separation over neutral loss.

From the results discussed above, we conclude that the PL1 mechanism leading to $\text{DCF}_2^+ + \text{D}^+ + \text{F}$ in which $\text{D}_2\text{CF}_3^{2+}$ loses a proton followed by an F atom is predominant in the formation of 750 ms^{-1} DCF_2^+ ions. The strong forward scattering of the DCF_2^+ ion formed in this way is in agreement with the overall shape of the PES for this pathway (Figure 4.1). Specifically, the PES exhibits relatively shallow wells and a charge separation exit barrier of about 4 eV. Thus, most of the energy available in the reaction is likely to appear as the kinetic energy of the products.

DCF₂⁺ 340 ms⁻¹ centre-of-mass velocity

The same mechanisms as those described in the previous section for reaching each product asymptote will also be considered here.

(a) DCF₂⁺ + DF⁺. The KER we calculate from the velocity of DCF₂⁺ for forming DCF₂⁺ + DF⁺ via direct charge separation of a collision complex (pathway 4.3) is 0.1 eV. Again, with such a small KER value, it is unlikely that this pathway is governing the formation of the ‘slow’ DCF₂⁺.

(b) DCF₂⁺ + D⁺ + F. The KER we calculate from the velocity of DCF₂⁺ that corresponds to the formation of ‘slow’ DCF₂⁺ via pathway 4.4 is 1.55 eV. Although this value is also quite small, it may correspond to the formation of DCF₂⁺ in an excited state. From our quantum chemical calculations we determine that the formation of triplet DCF₂⁺ occurs with an exothermicity of 0.56 eV (see Figure 4.1) and is spin-allowed. Given the collision energy of 1.16 eV, the experimentally determined KER (1.55 eV) is in good agreement with the calculated energetics for such a pathway (0.56 eV calculated exothermicity + 1.16 eV COM collision energy = 1.72 eV). In this case it must be that much of the internal energy of the collision complex is used for electronic excitation of the DCF₂⁺.

As described above, there is also the possibility that the DCF₂⁺ + D⁺ + F products are formed *via* pathway 4.5 in which neutral loss occurs before charge separation. The KER we calculate from the velocity of DCF₂⁺ for such a mechanism is 0.84 eV. This value does not agree as well with our

quantum chemical results, and, as above, we would expect a small dicationic collision complex, such as $D_2CF_3^{2+}$, to favour charge separation over neutral loss.

It is also interesting to note that the 340 ms^{-1} DCF_2^+ signals involve both forward and backward scattering. Such signals are indicative of a slower reaction, as the complexes involved have enough time to reorient before fragmentation. The 750 ms^{-1} peak, however, is only forward-scattered, indicative of a faster process where reorientation is not possible. If indeed the 340 ms^{-1} peaks are due to the formation of DCF_2^+ in the triplet state, the slower fragmentation indicated by the experimental data may be due to a need for greater electronic reorganization in the final fragmentation step in which an F atom is lost from doublet DCF_3^+ to give triplet DCF_2^+ and F.

From the results discussed above, we tentatively propose that the 340 ms^{-1} DCF_2^+ peaks arise from the formation of DCF_2^+ in its ground triplet state, via pathway PL1, along with D^+ and F. As discussed at the end of Section 4.3.2, we believe that the 750 ms^{-1} DCF_2^+ peak corresponds to the formation of ground singlet $DCF_2^+ + D^+ + F$, also *via* the PL1 pathway.

4.4 Conclusions

Ab initio quantum chemical calculations have been performed to elucidate the stationary points on four distinct reactive pathways discovered on the potential energy surface for the bond-forming reaction of CF_3^{2+} with X_2 ($X = H, D$). We find that the H^+ and HF^+ product ions are formed *via*

two separate pathways, explaining previously-observed experimental isotope effects and collision energy dependencies. The reactive mechanism for the dominant pathway leading to the formation of $\text{HCF}_2^+ + \text{H}^+ + \text{F}$ supports a general pattern of reactivity that is emerging from recent studies of the bond-forming reactions of dications with neutral molecules. This involves the initial formation of a bound collision complex between the dication and the neutral, followed by internal rearrangement and then fragmentation to products. The energetics of this pathway were found to be in good agreement with the DCF_2^+ product ion velocity distributions obtained from a series of crossed-beam scattering experiments performed by Žabka and Herman [95] on the collision system $\text{CF}_3^{2+} + \text{D}_2$.

The QCISD *ab initio* calculations presented here generally agree well with comparative B3LYP and coupled cluster studies. This agreement suggests that single-reference techniques are adequate for the current systems. The T_1/Q_1 -diagnostic values found, although sometimes higher than the usually accepted 0.020 upper limit, are generally well below the 0.045 value proposed for open shell systems. Our results therefore support the use of the higher value for these diagnostics in open shell cases.

Chapter 5

Experimental cross sections and theoretical state-to-state probabilities for electron transfer between SF^{2+} and H_2O

5.1 Introduction

The electron transfer reactions of dications with neutrals have, to date, been the most extensively studied aspect of dication reactivity. Electron transfer pathways tend to dominate the reactivity of small dications with neutrals in most systems [1, 2, 51]. Early studies concentrated on high energy ($\sim\text{keV}$) collisions of CO^{2+} with rare gas atoms [13, 15, 16, 54] or CS_2^{2+} with small diatomics [19]. Later experiments explored the electron transfer reactivity of a host of previously unstudied atomic and molecular dications with neutrals at lower collision energies ($\sim\text{eV}$) [2, 38, 44, 45, 47, 103], as discussed in Section 1.2.1.

The electron transfer reactivity of dications has previously been explained

for a number of systems using the Landau-Zener model [71, 104]. This model, which is explained in detail in Section 1.3.3, can provide cross sections for the formation of charge transfer products by modelling the energies of the dication, neutral and the corresponding two monocations as pure polarization attraction and Coulombic repulsion, respectively. The cross section for forming a given product is then determined by the polarizability of the neutral collision partner and the energy of the product state relative to the reactant state, the reaction exothermicity. Hence the electronic, vibrational and rotational excitation of the product ions will have a direct effect on the reaction exothermicity and correspondingly the predicted reaction cross sections.

In the study described in this Chapter, a series of crossed-beam collision experiments were performed between SF^{2+} and H_2O . The products of the collisions were detected by TOFMS and the ion intensities converted to integral reaction cross sections using a new method previously used with success [47]. These integral reaction cross sections were then compared with calculated theoretical cross sections. A number of theoretical techniques were used in order to improve on the Landau-Zener model as it is typically implemented. The potential energy curves for a number of the excited states of SF^+ were calculated using multireference *ab initio* methods. These curves were then used to calculate the energies and vibrational wavefunctions of all vibrational levels in each bound electronic state of SF^+ . In this way, a more precise value of the reaction exothermicity can be obtained for each electronic and vibrational state of SF^+ . In addition, Franck-Condon factors were calculated for transitions from the lowest three vibrational levels of the

electronic ground state of SF^{2+} to various electronic and vibrational states of SF^+ . By multiplying the Franck-Condon factor for a given transition by its Landau-Zener cross section, a more realistic state-to-state probability could be obtained. It should be noted that rotational excitation was not taken into account in this study, that is, all species were assumed to be in their ground rotational states.

5.2 Details of the Experiment

A detailed description of the experimental setup used for the collision experiments and most of the subsequent data analysis procedures is given in Section 1.4.2. The experiments discussed in this Chapter made use of SF_6 as a precursor gas, which was ionized with 150 eV electrons. The pressure in the ion source was maintained at 4×10^{-6} mbar. H_2O was used as the neutral collision gas, and the pressure in the collision region was maintained at 11×10^{-6} mbar. Collision energies ranged from 5 to 11 eV in the laboratory frame, in 1 eV intervals.

The usual data analysis procedures used to correct for stray ions or ions formed from non-collisional processes, as well as for the dications missed at the detector due to the deadtime of the discriminator, were applied to the raw experimental data in the manner described in Section 1.4.3. However in this study, as it is necessary to compare the cross sections for the formation of both the S^+ and the SF^+ product ions, we must also take into account the experimental detection efficiency of each ion. In order to do so, we begin

by noting that the flux F of a given product ion can be expressed as the product of the ion's velocity v and its number density d :

$$F = vd \quad (5.1)$$

and the intensity I of the signal for this ion is:

$$I = Ald \quad (5.2)$$

where the product of the area A and the length l gives the volume of space in the interaction region that is imaged onto the detector of the TOFMS. By rearranging equation 5.2 in terms of d and substituting into equation 5.1 we have:

$$F = \frac{vI}{Al} \quad (5.3)$$

Since the flux is proportional to the absolute cross section, we can express the ratio of the absolute cross sections for S^+ and SF^+ as:

$$\frac{\sigma_{S^+}}{\sigma_{SF^+}} = \frac{v_{S^+} I_{S^+}}{l_{S^+}} \cdot \frac{l_{SF^+}}{v_{SF^+} I_{SF^+}} = \frac{v_{S^+}}{l_{S^+}} \cdot \frac{l_{SF^+}}{v_{SF^+}} \cdot \frac{I_{S^+}}{I_{SF^+}} \quad (5.4)$$

where v_i/l_i is the detection efficiency for product ion i . Then all that is necessary is to calculate the translational velocity v_{SF^+} of SF^+ and the length l_i in the TOF source region that can be imaged onto the detector for each ion. The velocity of SF^+ can be calculated in the following way:

First the velocity of the COM is calculated:

$$v_{\text{COM}} = \frac{m_{\text{SF}^{2+}} v_{\text{SF}^{2+}} + m_{\text{H}_2\text{O}} v_{\text{H}_2\text{O}}}{m_{\text{SF}^{2+}} + m_{\text{H}_2\text{O}}} \quad (5.5)$$

Next the COM velocity of SF^+ can be calculated by solving the following two equations:

$$Eq = \frac{1}{2} m_{\text{SF}^+} v_{\text{SF}^+}^2 + \frac{1}{2} m_{\text{H}_2\text{O}^+} v_{\text{H}_2\text{O}^+}^2 \quad (5.6)$$

$$0 = m_{\text{SF}^+} v_{\text{SF}^+} + m_{\text{H}_2\text{O}^+} v_{\text{H}_2\text{O}^+} \quad (5.7)$$

where E is the kinetic energy release for the collision which we estimate to be approximately 3 eV based on the calculated exothermicities for forming the product states with the highest theoretical cross sections (see Section 5.4.3 for details).

Following the collision of SF^{2+} with H_2O , if electron transfer populates an excited state of SF^+ that results in its immediate dissociation to S^+ and F , the kinetic energy of the SF^+ ion will be transmitted to the charged product, in this case S^+ . Hence, the velocity of the S^+ ion will be the same as that of the SF^+ ion as calculated above.

The length in the TOF source region that SF^+ and S^+ ions can be imaged onto the detector can be calculated using the mass of the product ion, the strength of the fields experienced by the ion in the TOFMS, and the geometry of the TOFMS. The field strengths and geometries of the TOFMS are given in Figure 5.1.

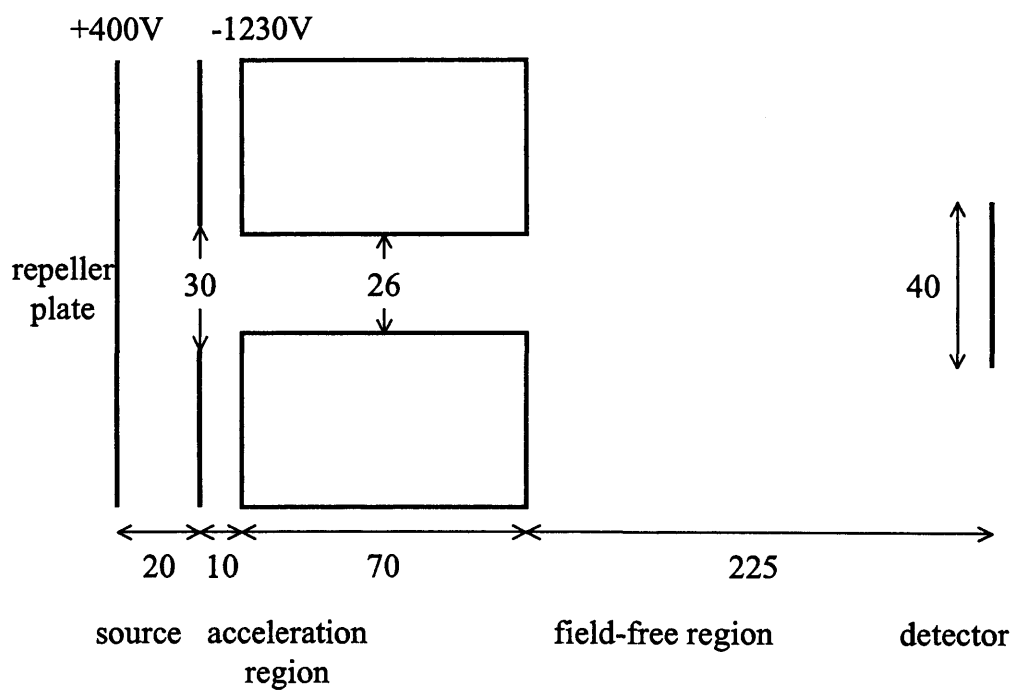


Figure 5.1: A schematic diagram giving the dimensions and voltages in the TOFMS (not to scale). All lengths are in mm.

5.3 Details of Calculations

Potential energy curves for the ground and low-lying excited states of SF⁺ and SF²⁺ were generated by performing a series of single-point energy calculations over a range of bond distances from 0.85-3.0 Å in steps of 0.05 Å. In all calculations, the state-averaged AQCC method was used with a full valence active space, coupled with an uncontracted basis set as implemented in Molpro v.2002.3 consisting of 16s11p3d2f1g functions for S atoms and 12s6p3d2f1g functions for F atoms. Calculations were attempted with the more efficient Dunning and ANO contracted basis sets, but they did not always yield smooth potentials. Hence, all results shown here are from calculations made with the uncontracted basis set described above.

C_{2v} symmetry was imposed for all calculations of diatomics. In order to determine the symmetry of each state in $C_{\infty v}$, descent in symmetry was applied. Non-degenerate A_1 and A_2 states correspond to Σ^+ and Σ^- states, respectively. Degenerate A_1 and A_2 states can be either Δ or Γ , but in this case assumed to be Δ . B_1 and B_2 states are always degenerate and correspond to either Π or Φ , but in this case assumed to be Π . The energies of product asymptotes were taken to be the sum of the two corresponding fragments calculated separately, with corrections for basis set superposition error (by means of counterpoise calculations). The MOLPRO v.2002.3 suite of programs was used for all quantum chemical calculations [88].

Using the potentials calculated quantum chemically, the number of vibrational levels in each bound potential, their energies and vibrational wavefunctions were calculated using the LEVEL program [105]. Franck-Condon

factors could then be calculated by evaluating the square of the integral of the overlap between the vibrational wavefunctions for the initial and final states, respectively. A FORTRAN90 program was written to evaluate these integrals which was based on an algorithm provided by E. Boleat [106]. The source is given in full in Appendix B.

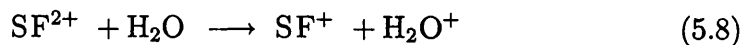
Landau-Zener cross sections for forming products in a given electronic and vibrational state were calculated using reaction window theory which is based on the Landau-Zener avoided crossing model. A Mathematica program written by S. D. Price [107] was used to calculate Landau-Zener cross sections using the reaction exoergicity and the polarizability of the neutral partner.

5.4 Results and Discussion

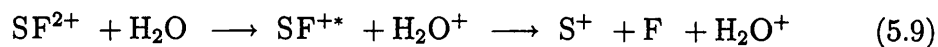
5.4.1 Experimental Results

The products detected following collisions of SF^{2+} with H_2O were SF^+ , H_2O^+ , S^+ , OSF^+ and HOSF^+ . This indicates that there are at least three different processes occurring following collision:

non-dissociative electron transfer:



dissociative electron transfer:



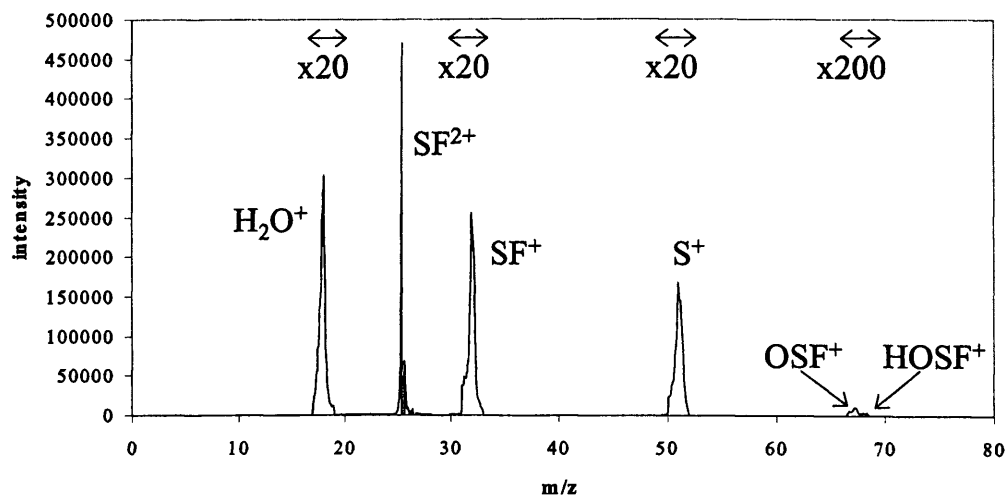
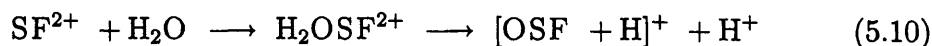


Figure 5.2: A typical raw mass spectrum recorded following collisions of SF^{2+} with H_2O .

bond-formation:



where SF^{2+} indicates that SF^+ is being formed in an excited state which then dissociates to S^+ and F . Note that no F^+ was detected.

A sample mass spectrum is given in Figure 5.2. As can be seen on the spectrum, the intensities of the electron transfer processes are much stronger than those of the bond-formation processes, as is typically the case. Drawing on the bond-forming mechanisms derived previously by Mrázek *et al.* for the $\text{CO}_2^{2+} + \text{D}_2$ system [35], Roithová *et al.* for the CHCl^{2+} system [48] and in Chapters 2 and 4 of this thesis for the $\text{CF}_2^{2+} + \text{H}_2\text{O}$ and $\text{CF}_3^{2+} + \text{H}_2$ systems, we can suggest that the mechanism for the formation of $[\text{OSF}$

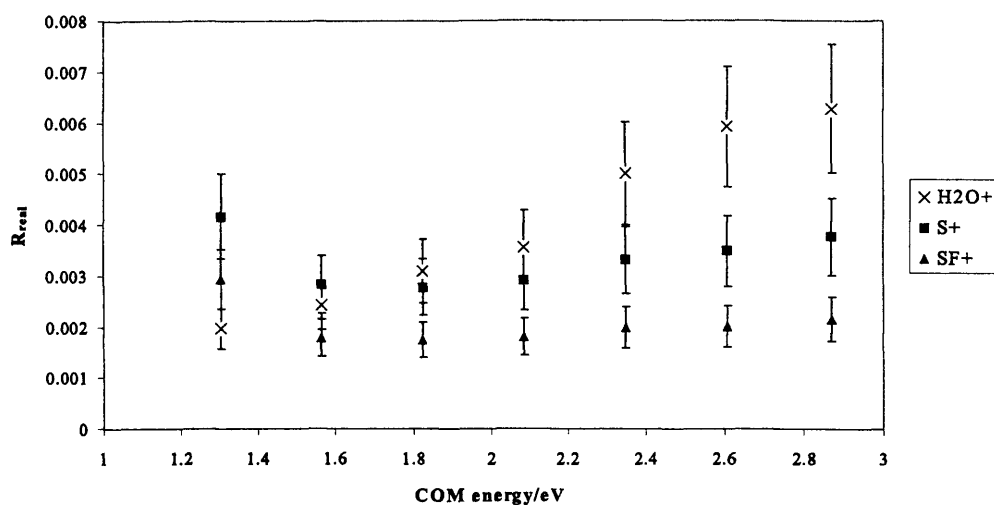


Figure 5.3: A plot of R_{real} as a function of centre-of-mass collision energy for the electron transfer products H_2O^+ , SF^+ and S^+ .

+ H^+ from SF^{2+} and H_2O involves the formation of an S-O bond to give $\text{H}_2\text{OSF}^{2+}$, followed by charge separation to give HOSF^+ , which can then lose another proton to give OSF^+ .

However, the focus of interest in this study is on the electron transfer processes. Figure 5.3 is a plot of R_{real} for the electron transfer products H_2O^+ , SF^+ and S^+ as a function of centre-of-mass collision energy. As can be seen on the Figure, R_{real} does not appear to have a strong dependence on the center-of-mass collision energy. Following the data analysis procedure described in Sections 1.4.3 and 5.2, the integral reaction cross section ratio S^+/SF^+ was determined to be 1.07 ± 0.28 .

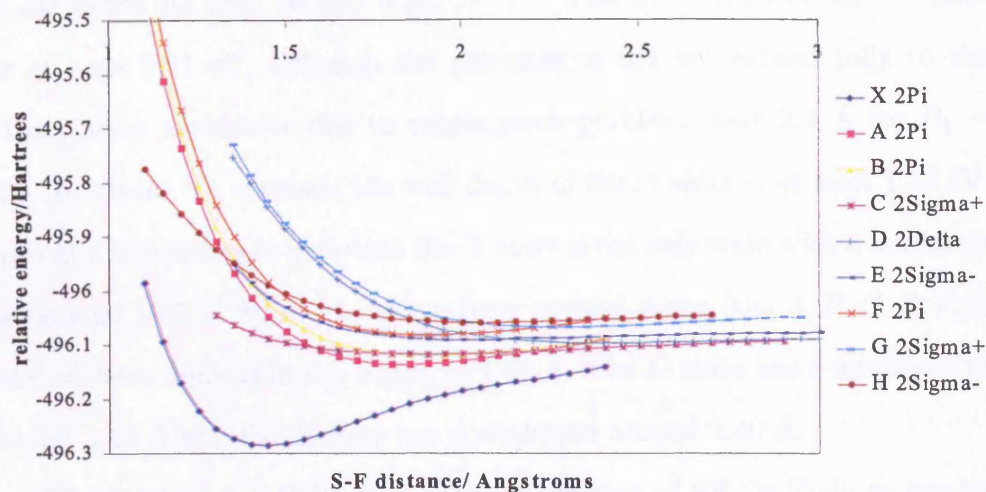


Figure 5.4: Potential energy curves for various low-lying states of SF²⁺.

5.4.2 Results of Calculations

Calculation of Potential Energy Curves

In order to determine the possible extents of initial electronic and vibrational excitation of SF²⁺ before its collision with H₂O, it was necessary to calculate the potential energy curves for the low-lying states of SF²⁺. These are shown in Figure 5.4. As can be seen, the equilibrium bond length for the ground X ²Π state of SF²⁺ is between 1.40 Å and 1.45 Å at approximately 1.43 Å. A previous computational geometry optimization at the MP2 level, using a triple zeta basis set with two *d*- and one *f*- polarization functions taken from Dunning's cc-pVTZ basis set, determined a bond length of 1.453 Å [108]. To our knowledge there exists, to date, no experimental measurement of this bond distance.

As can be seen on Figure 5.4, the ground X ²Π state of SF²⁺ lies about

4 eV below its first excited state $A\ ^2\Pi$. The well depth of the X state is at least 3.91 eV, although our calculations did not extend fully to the dissociation asymptote due to convergence problems past 2.4 Å for $B_1 = B_2$ (Π) states. In contrast, the well depth of the A state is at least 1.43 eV. It is also interesting to note that the X state is the only state with a minimum at around 1.43 Å. Many of the low-lying excited states (the A, B, C, E, F, H states) have minima in the region of 1.80 Å. The D state has a minimum at about 2.25 Å and the G state has a minimum around 2.40 Å.

The formation of SF^{2+} by electron ionization of SF_6 is likely to involve a vertical transition. We expect the ($v = 0, 1, 2$) levels of the dication to be the most populated since the equilibrium S-F bond lengths of SF_6 and SF^{2+} are relatively similar (1.56 Å [109] and 1.45 Å [108], respectively).

Finally, in order to calculate the FCFs for transitions from SF^{2+} to SF^+ following collisions of SF^{2+} with H_2O , the potential energy curves for some of the low-lying states of SF^+ were calculated and are plotted on Figure 5.5. The singlet and triplet curves are plotted separately for clarity in Figures 5.6 and 5.7, respectively. The ground state of SF^+ is shown to be $^3\Sigma^-$, which is in good agreement with previous calculations by Peterson *et al.* [110], Irikura *et al.* [111] and Lange *et al.* [108]. The first two excited states $^1\Delta$ and $^1\Sigma^+$ were found to lie approximately 1.03 eV and 1.93 eV above the ground state. This is in good agreement with the excitation energies of 1.0 eV and 1.8 eV to the $^1\Delta$ and $^1\Sigma^+$ states, respectively, estimated by Fisher *et al.* [112]. It is also interesting to note that the $X\ ^3\Sigma^-$, $B\ ^3\Delta$, $C\ ^3\Sigma^-$, $a\ ^1\Delta$, $b\ ^1\Sigma^+$, $c\ ^1\Sigma^-$ and $e\ ^1\Delta$ states are all bound (albeit in some cases loosely bound); only the Π

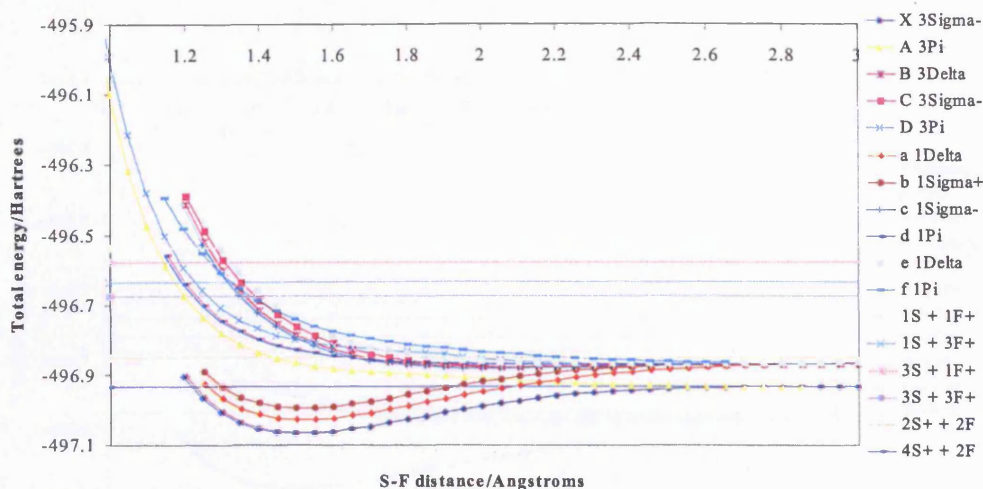


Figure 5.5: Potential Energy curves for various low-lying triplet and singlet states of SF^+ . Horizontal lines indicate dissociation product asymptotes.

states of SF^+ are dissociative.

The equilibrium geometry for the $^3\Sigma^-$ ground state of SF^+ lies between 1.50 and 1.55 Å. A previous CASSCF calculation by Peterson *et al.* with a basis set consisting of $(14s, 10p, 3d, 1f/11s, 8p, 3d, 1f)$ functions on the S atom and $(12s, 8p, 2d, 1f/9s, 6p, 2d, 1f)$ functions on the F atom resulted in an equilibrium S-F bond length of 1.506 Å for SF^+ [110]. An MP2/6-31G* calculation by Irikura *et al.* gave a value of 1.540 Å [111], and an MP2/TZVPP calculation by Lange *et al.* gave a value of 1.513 Å [108]. Our results are in good agreement with these values.

The horizontal lines on the plots on Figures 5.5 to 5.7 indicate the dissociation product asymptotes. All of the calculated potential energy curves for SF^+ were found to dissociate to either the $S^+ (^4S) + F (^2P)$ or the $S^+ (^2P) + F (^2P)$ asymptotes, the two lowest energy product states. The product

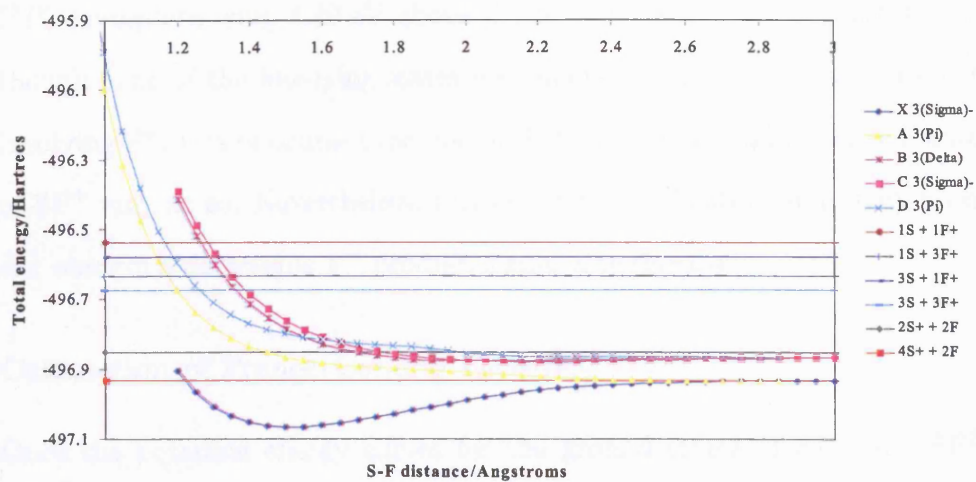


Figure 5.6: Potential Energy curves for various low-lying triplet states of SF^+ . Horizontal lines indicate dissociation product asymptotes.

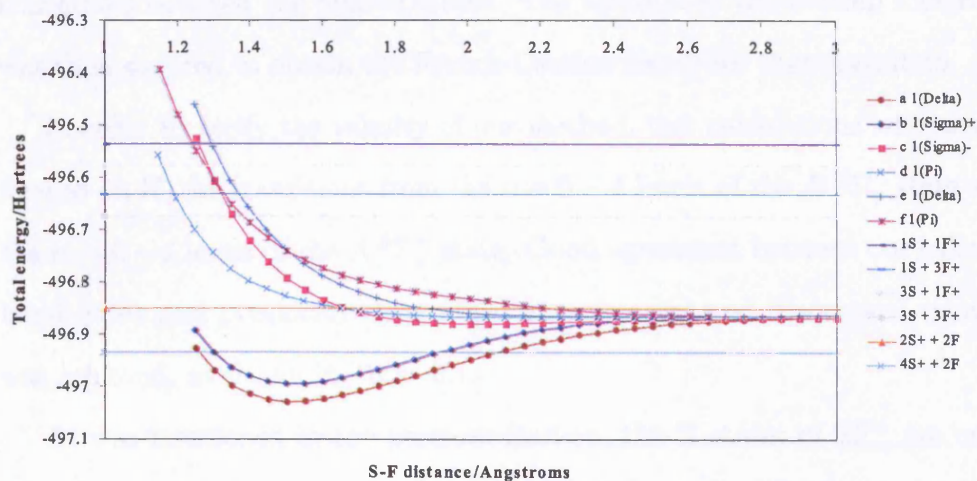


Figure 5.7: Potential Energy curves for various low-lying singlet states of SF^+ . Horizontal lines indicate dissociation product asymptotes.

asymptotes that involve F^+ were much higher in energy, the $S (^3P) + F^+$ (3P) asymptote lying 4.79 eV above the $S^+ (^2P) + F (^2P)$ asymptote. Although none of the low-lying states we calculate dissociate to any products involving F^+ , it is of course conceivable that some more highly excited states of SF^+ may do so. Nevertheless, this may be an indication as to why we do not observe a detectable F^+ product signal experimentally.

Calculation of Franck-Condon Factors

Once the potential energy curves for the ground states of SF^+ and SF^{2+} were calculated, as well as the low-lying excited states of SF^+ , the LEVEL code was used to calculate the number of vibrational levels for each (bound) state, their energies and vibrational wavefunctions. Using the vibrational wavefunctions generated by LEVEL, the overlap integrals were solved for transitions between the desired states. The solution of the overlap integral was then squared to obtain the Franck-Condon factor for that transition.

In order to verify the validity of our method, test calculations were performed on N_2 for transitions from the $v = 0 - 4$ levels of the $B ^3\Pi_g$ state to the $v' = 0 - 4$ levels of the $A ^3\Sigma_u^+$ state. Good agreement between our calculated FCFs and previously determined experimental and theoretical values was achieved, as shown in Table 5.1.

As was mentioned in the previous Section, the Π states of SF^+ are not bound, so FCFs for transitions to these states were not calculated and assumed to be 1. A discussion of the validity of this assumption is given in Section 5.4.3. However, FCFs were calculated for overlap between all existing

$v \setminus v'$	0	1	2	3	4	reference
0	3.40E-01	4.06E-01	2.00E-01	5.00E-02	6.00E-03	[113]
	4.06E-01	4.01E-01	1.58E-01	3.17E-02	3.47E-03	[114]
	3.38E-01	4.06E-01	1.97E-01	5.00E-02	7.00E-03	[115]
	4.10E-01	3.98E-01	1.62E-01	3.42E-02		[116]
	3.99E-01	3.96E-01	1.64E-01	3.61E-02		[117]
	4.40E-01	3.91E-01	1.40E-01	2.59E-02	2.67E-03	[118]
	3.89E-01	4.00E-01	1.70E-01	3.80E-02	4.79E-03	average
3.96E-01	4.00E-01	1.64E-01	3.54E-02	4.38E-03	this work	
1	3.23E-01	2.00E-03	2.12E-01	3.01E-01	1.34E-01	[113]
	3.27E-01	3.71E-03	2.85E-01	2.77E-01	9.18E-02	[114]
	3.24E-01	2.00E-03	2.12E-01	2.98E-01	1.31E-01	[115]
	3.31E-01	2.90E-03	2.74E-01	2.76E-01		[116]
	3.34E-01	2.80E-03	2.65E-01	2.77E-01		[117]
	3.28E-01	1.39E-03	3.11E-01	2.58E-01	7.71E-02	[118]
	3.28E-01	2.47E-03	2.60E-01	2.81E-01	1.08E-01	average
3.30E-01	2.09E-03	2.69E-01	2.79E-01	1.00E-01	this work	
2	1.90E-01	1.03E-01	1.13E-01	3.90E-02	2.73E-01	[113]
	1.64E-01	1.59E-01	6.59E-02	1.05E-01	3.06E-01	[114]
	1.90E-01	1.03E-01	1.13E-01	3.90E-02	2.73E-01	[115]
	1.66E-01	1.59E-01	6.88E-01	9.56E-02		[116]
	1.70E-01	1.64E-01	6.60E-02	8.98E-02		[117]
	1.50E-01	1.92E-01	4.26E-02	1.42E-01	3.02E-01	[118]
	1.72E-01	1.47E-01	1.81E-01	8.51E-02	2.89E-01	average
1.68E-01	1.55E-01	7.27E-02	8.91E-02	2.94E-01	this work	
3	8.80E-02	1.77E-01	2.00E-03	1.61E-01	1.00E-03	[113]
	6.67E-02	1.93E-01	2.25E-02	1.50E-01	1.11E-02	[114]
	8.80E-02	1.78E-01	1.00E-03	1.62E-01	2.00E-03	[115]
	6.69E-02	1.97E-01	2.21E-02	1.52E-01		[116]
	6.63E-02	2.07E-01	2.50E-02	1.42E-01		[117]
	5.56E-02	1.99E-01	4.62E-02	1.32E-01	2.93E-02	[118]
	7.19E-02	1.92E-01	1.98E-02	1.50E-01	1.09E-02	average
6.84E-02	1.96E-01	1.95E-02	1.54E-01	5.21E-03	this work	
4	3.60E-02	1.45E-01	7.40E-02	3.10E-02	1.13E-01	[113]
	2.44E-02	1.29E-01	1.22E-01	4.67E-03	1.53E-01	[114]
	3.60E-02	1.45E-01	7.70E-02	3.20E-02	1.14E-01	[115]
	1.84E-02	1.17E-01	1.49E-01	1.60E-06	1.60E-01	[118]
	2.87E-02	1.34E-01	1.06E-01	1.69E-02	1.35E-01	average
	2.47E-02	1.32E-01	1.21E-01	6.73E-03	1.49E-01	this work

Table 5.1: Comparison of Franck-Condon factors for $v = 0 - 4$ to $v' = 0 - 4$ transitions from the $B^3\Sigma_g^+$ to the $A^3\Sigma_u^+$ state of N_2 . Values in bold are from this work, all other values are from previous studies referenced in the final column. These data were taken from a compilation by López *et al.* [119].

levels of the ground state of SF^{2+} and all levels of the ground and excited states of SF^+ for which we have calculated bound potentials. The results of these calculations are given in full in Appendix C.

Looking at Figure 5.5, it can be seen that of the bound SF^+ states, the $X^3\Sigma^-$, $a^1\Delta$ and $b^1\Sigma^+$ states have minima around 1.5 Å, whereas the $B^3\Delta$, $C^3\Sigma^-$, $c^1\Sigma^-$ and $e^1\Delta$ states have minima around 2.0 Å. Therefore we would expect that for the former states, the $v' = v''$ transitions will be the strongest. For the latter states, we would expect high v' to low v'' transitions to be the strongest. Figures 5.8 and 5.9 are colour maps of the intensities of the calculated FCFs for transitions from $X^2\Pi \text{SF}^{2+}$ to $X^3\Sigma^- \text{SF}^+$ and $B^3\Delta \text{SF}^+$, respectively. FCF colour maps for transitions to the remaining a , b , C , c and e states of SF^+ are given in Appendix D. As can be seen on these Figures, the results support our predictions. It is interesting to note the “beats” of intensity that are apparent on all these maps as a result of the vibrational wavefunctions, which are sinusoidal in nature, overlapping in regions of high or low intensity.

Calculation of Landau-Zener Cross Sections

In order to calculate the LZ cross sections for transitions to a given electronic and vibrational state, it was necessary to determine the exoergicity for each transition. Figure 5.10 shows a distribution of LZ probabilities relative to the term energy for the transition from $X^2\Pi \text{SF}^{2+} + X^1A_1 \text{H}_2\text{O}$ to $X^3\Sigma^- \text{SF}^+ + \tilde{X}^2B_1 \text{H}_2\text{O}^+$, that is, the degree of vibrational or electronic excitation in the monocation state subtracted by the degree of vibrational or electronic

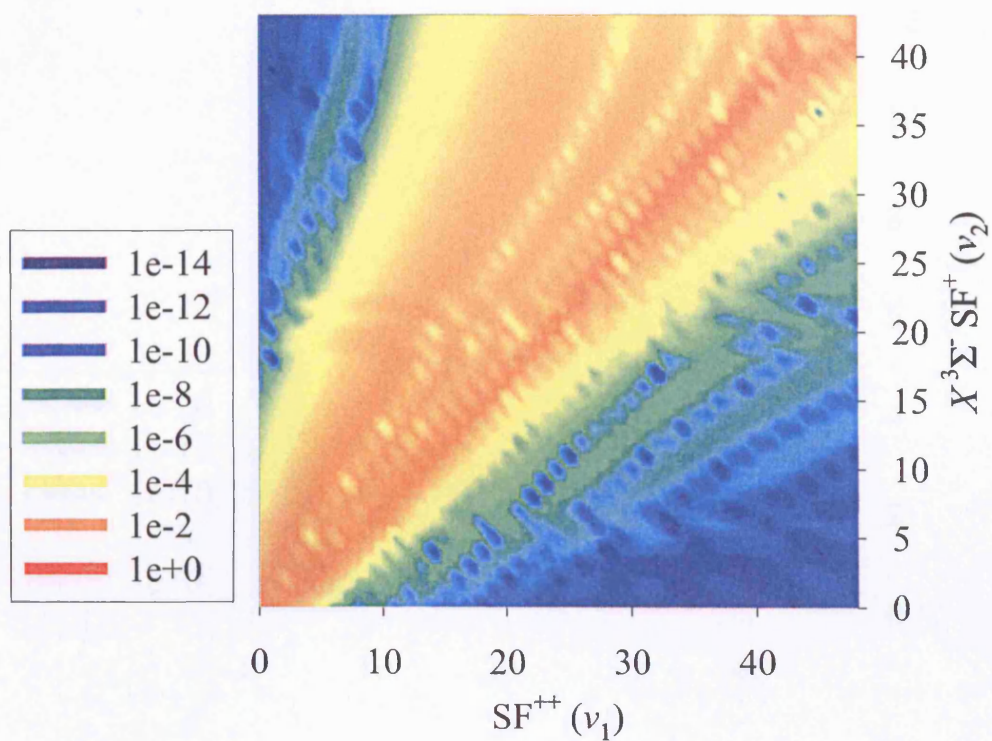


Figure 5.8: Franck-Condon factors for transitions from $X^2\Pi SF^{2+}$ to $X^3\Sigma^- SF^+$. The x - and y - axes are the vibrational levels of SF^{2+} and SF^+ , respectively. The intensities of the FCFs are plotted logarithmically on the z - axis using color with red as the most intense and blue as the least intense.

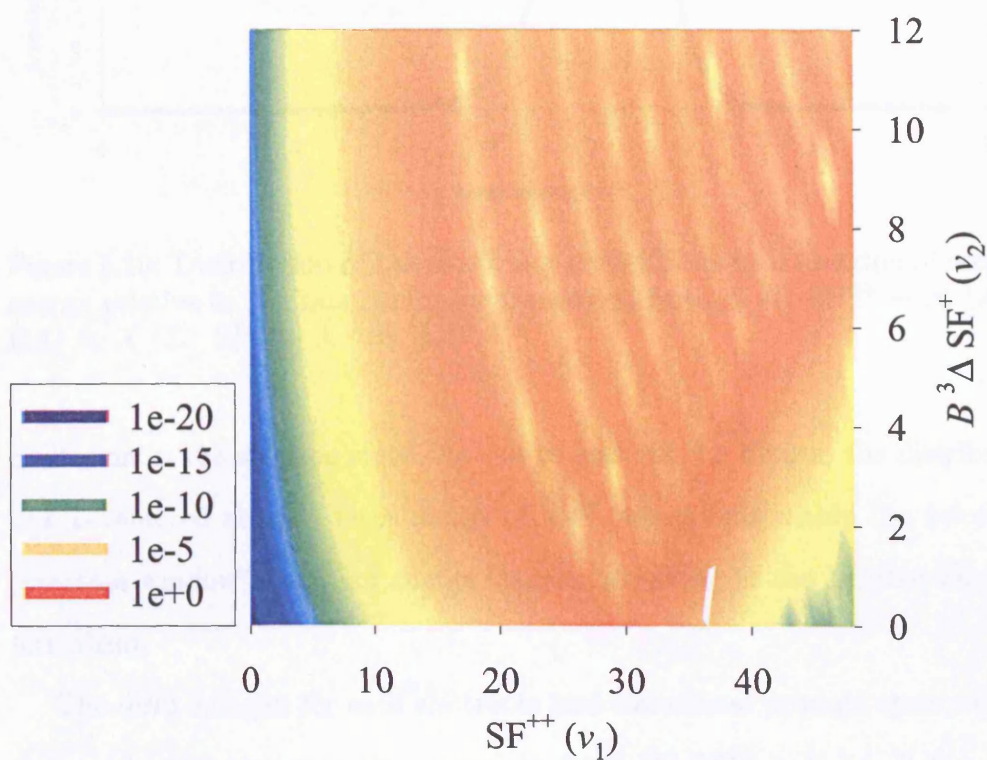


Figure 5.9: Franck-Condon factors for transitions from $X^2\Pi SF^{2+}$ to $B^3\Delta SF^+$. The x - and y - axes are the vibrational levels of SF^{2+} and SF^+ , respectively. The intensities of the FCFs are plotted logarithmically on the z - axis using color with red as the most intense and blue as the least intense.

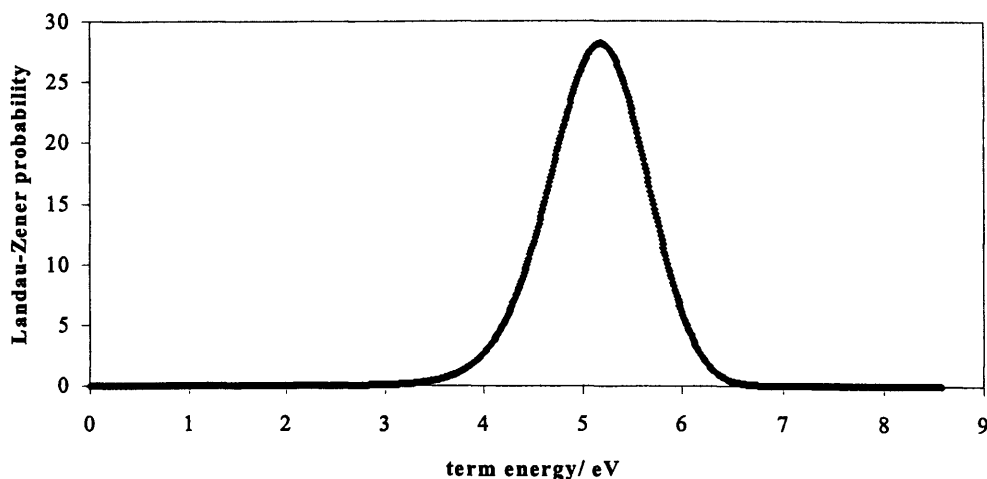


Figure 5.10: Distribution of Landau-Zener probabilities as a function of term energy relative to the exoergicity for transitions from $X^2\Pi SF^{2+} + X^1A_1 H_2O$ to $X^3\Sigma^- SF^+ + \tilde{X}^2B_1 H_2O^+$.

excitation in the dication state. As can be seen on the Figure, the distribution is centered about a term energy of 5 eV, which falls within the 4-6 eV “reaction window” range for charge transfer according to the Landau-Zener formalism.

The term energies for each electronic and vibrational product state were then calculated relative to the exoergicity for $X^2\Pi SF^{2+} + X^1A_1 H_2O \rightarrow X^3\Sigma^- SF^+ + \tilde{X}^2B_1 H_2O^+$. All of the SF^+ states discussed above were considered, as well as the \tilde{X}^2B_1 , \tilde{A}^2A_1 and \tilde{B}^2B_2 states of H_2O^+ . Upon examination of the photoelectron spectrum of water [120], the vibrational maximum is at about 1 eV for both the \tilde{A} and the \tilde{B} states. The \tilde{X} state maximum is at $v' = 0$, which is to be expected when one considers that the HOMO for ground state H_2O is non-bonding, therefore there should be a minimal change in geometry upon removal of one of these electrons to

form the ground state of H_2O^+ . Since the vibrational levels of the \widetilde{X} , \widetilde{A} and \widetilde{B} states of H_2O^+ were not calculated, when calculating term energies for forming given states of H_2O^+ along with SF^+ we have assumed that the $\widetilde{X}^2B_1 \text{H}_2\text{O}^+$ state is formed with no vibrational excitation, and the $\widetilde{A}^2A_1 \text{H}_2\text{O}^+$ and $\widetilde{B}^2B_2 \text{H}_2\text{O}^+$ states are formed with 1 eV vibrational excitation, according to the vibrational maxima in the photoelectron spectrum. In all cases we have assumed that the reactant state consists of SF^{2+} and H_2O in their ground electronic states.

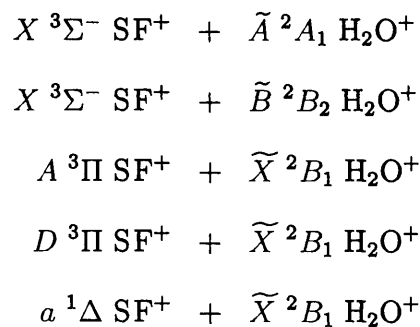
The vertical second IPs we have determined from our quantum chemical calculations for various states of SF^+ and vertical first IPs for H_2O to the \widetilde{X} , \widetilde{A} and \widetilde{B} states of H_2O^+ are shown in Table 5.2. The IPs of H_2O for ionization to the \widetilde{A} and \widetilde{B} states of H_2O^+ include 1 eV of vibrational excitation as described above. $v = 0$ was assumed for all other states of H_2O , H_2O^+ , SF^{2+} and SF^+ . The vertical second IPs of SF^+ were calculated at the equilibrium geometry of the dication, taken to be 1.45 Å (see Figure 5.4). To our knowledge, no previous data exists in the literature for the vertical second ionization potentials of SF^+ at the dication geometry. However, a previous computational study by Lange *et al.* [108] calculated a vertical second ionization potential from $X^3\Sigma^- \text{SF}^+$ to $X^2\Pi \text{SF}^{2+}$ at the geometry of SF_6 . They used the CISD method with the cc-pvdz basis set and calculated a value of 21.10 eV. The vertical ionization potential of H_2O to $\widetilde{X}^2B_1 \text{H}_2\text{O}^+$ was determined by Reutt *et al.* to be 12.62 eV from high resolution photoelectron spectroscopy experiments [121]. Our result of 12.64 eV is in good agreement with this value.

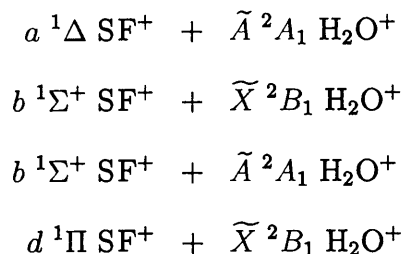
SF ⁺ state	IP/eV	H ₂ O ⁺ state	IP/eV
<i>X</i> ³ Σ ⁻	21.22	\widetilde{X} ² B ₁	12.64
<i>A</i> ³ Π	15.54	\widetilde{A} ² A ₁	15.75 ¹
<i>B</i> ³ Δ	12.84	\widetilde{B} ² B ₂	20.24 ¹
<i>C</i> ³ Σ ⁻	12.13		
<i>D</i> ³ Π	13.67		
<i>a</i> ¹ Δ	20.20		
<i>b</i> ¹ Σ ⁺	19.29		
<i>c</i> ¹ Σ ⁻	13.03		
<i>d</i> ¹ Π	14.47		
<i>e</i> ¹ Δ	11.44		
<i>f</i> ¹ Π	11.81		

¹IP includes 1 eV vibrational excitation.

Table 5.2: Vertical second ionization potentials from various states of SF⁺ and vertical first ionization potentials to the \widetilde{X} , \widetilde{A} and \widetilde{B} states of H₂O⁺.

Given these IPs along with the well depth for each SF⁺ state, a range of term energies was obtained for each possible electronic product state. The LZ probability distribution shown in Figure 5.10 was then used to determine which product states would possess a non-zero LZ cross section at any point in its range of term energies. The product states that gave non-zero LZ cross sections are listed below:





For each of these product states, term energies were calculated for each vibrational level of the electronic state of SF^+ in question and for the $v' = 0, 1, 2$ levels of SF^{2+} . The LZ probability distribution was used to obtain LZ cross sections for each specific electronic and vibrational state. For unbound SF^+ states only three term energies were calculated, corresponding simply to vertical transitions at 1.45 Å from the $v' = 0, 1, 2$ states of SF^{2+} . The calculated term energies and LZ cross sections are given in full in Appendices E and F, respectively. The LZ cross sections were then multiplied by the FCF for the corresponding transition to give a combined state-to-state probability. These probabilities are given for each product asymptote in Tables 5.3 to 5.5.

The probabilities were then summed over all vibrational levels of the given SF^+ state and these are shown in the final rows for each product state in Tables 5.3 to 5.5. These sums indicate the probabilities for forming a given $\text{SF}^+ + \text{H}_2\text{O}^+$ state from a SF^{2+} parent ion in the $v' = 0, 1$ or 2 vibrational level. A total probability for forming S^+ is then obtained by summing all of the probabilities for all the dissociative SF^+ product states: $A \ ^3\Pi \text{ SF}^+ + \tilde{X} \ ^2B_1 \text{ H}_2\text{O}^+$, $D \ ^3\Pi \text{ SF}^+ + \tilde{X} \ ^2B_1 \text{ H}_2\text{O}^+$ and $d \ ^1\Pi \text{ SF}^+ + \tilde{X} \ ^2B_1 \text{ H}_2\text{O}^+$. A total probability for forming SF^+ is obtained by summing the probabilities for all non-dissociative SF^+ product states: $X \ ^3\Sigma^- \text{ SF}^+ + \tilde{A} \ ^2A_1 \text{ H}_2\text{O}^+$,

$v'' \setminus v'$	$X^3\Sigma^- \text{SF}^+ + \tilde{A}^2A_1 \text{H}_2\text{O}^+$			$X^3\Sigma^- \text{SF}^+ + \tilde{B}^2B_2 \text{H}_2\text{O}^+$		
	0	1	2	0	1	2
0	2.84E-03	1.73E-03	3.40E-04	5.08E-02	6.89E-02	5.66E-02
1	2.47E-03	3.41E-04	1.62E-03	9.77E-03	3.33E-03	8.02E-02
2	1.37E-03	2.18E-03	4.39E-05	9.68E-04	4.32E-03	4.85E-04
3	6.38E-04	2.54E-03	9.51E-04	6.16E-05	6.88E-04	2.17E-03
4	2.67E-04	1.79E-03	2.29E-03	2.56E-06	5.70E-05	8.60E-04
5	1.03E-04	9.57E-04	2.35E-03	6.51E-08	3.13E-06	1.09E-04
6	1.34E-04	1.14E-03	2.57E-03	3.29E-09	2.00E-07	1.30E-05
7	1.10E-05	1.88E-04	9.45E-04	7.37E-12	1.34E-09	2.80E-07
8	3.03E-06	7.29E-05	4.65E-04	1.59E-14	7.39E-12	6.20E-09
9	7.30E-07	2.53E-05	2.08E-04	1.38E-17	2.00E-14	6.66E-11
10	2.02E-07	8.37E-06	8.63E-05	0	1.42E-17	2.86E-13
11	1.02E-07	2.91E-06	3.43E-05	0	0	3.61E-16
12	9.18E-08	1.26E-06	1.37E-05	0	0	0
13	8.40E-08	7.14E-07	5.70E-06	0	0	0
14	5.79E-08	5.07E-07	2.89E-06	0	0	0
15	2.11E-08	3.26E-07	1.65E-06	0	0	0
16	1.39E-09	1.52E-07	9.92E-07	0	0	0
17	2.36E-09	3.43E-08	5.22E-07	0	0	0
18	8.18E-09	1.74E-12	1.89E-07	0	0	0
19	9.04E-09	1.85E-08	1.32E-06	0	0	0
20	9.06E-09	8.98E-11	4.43E-07	0	0	0
21	1.41E-11	1.97E-08	3.74E-08	0	0	0
22	2.75E-10	3.16E-10	7.63E-09	0	0	0
23	2.07E-09	5.91E-11	2.31E-08	0	0	0
24	1.71E-09	4.38E-09	2.03E-09	0	0	0
25	6.58E-10	8.78E-09	3.59E-09	0	0	0
26	6.35E-11	8.62E-09	1.72E-08	0	0	0
27	2.60E-11	5.08E-09	2.41E-08	0	0	0
28	1.15E-10	1.67E-09	1.83E-08	0	0	0
29	9.68E-11	1.29E-10	7.91E-09	0	0	0
30	3.05E-11	1.42E-10	1.13E-09	0	0	0
31	6.88E-13	7.23E-10	2.09E-10	0	0	0
32	4.71E-12	1.15E-09	2.17E-09	0	0	0
33	7.91E-12	1.19E-09	3.69E-09	0	0	0
34	2.48E-12	9.47E-10	3.59E-09	0	0	0
35	4.46E-13	6.02E-10	2.43E-09	0	0	0
36	8.57E-12	3.06E-10	1.18E-09	0	0	0
37	2.16E-11	1.14E-10	3.62E-10	0	0	0
38	3.07E-11	2.37E-11	3.90E-11	0	0	0
39	3.20E-11	1.40E-13	9.73E-12	0	0	0
40	2.76E-11	7.38E-12	7.94E-11	0	0	0
41	2.05E-11	2.04E-11	1.41E-10	0	0	0
42	1.34E-11	2.77E-11	1.55E-10	0	0	0
43	6.92E-12	2.24E-11	1.14E-10	0	0	0
SUM	7.84E-03	1.10E-02	1.19E-02	6.16E-02	7.73E-02	1.40E-01

Table 5.3: Products of Landau-Zener cross sections and Franck-Condon factors for transitions from $(v' = 0, 1, 2) X^2\Pi \text{SF}^{2+}$ to all vibrational levels of $X^3\Sigma^- \text{SF}^+$ for the $X^3\Sigma^- \text{SF}^+ + \tilde{A}^2A_1 \text{H}_2\text{O}^+$ and $X^3\Sigma^- \text{SF}^+ + \tilde{B}^2B_2 \text{H}_2\text{O}^+$ product states.

vert. transition	$A^3\Pi SF^+ + \tilde{X}^2B_1 H_2O^+$			$D^3\Pi SF^+ + \tilde{X}^2B_1 H_2O^+$		
	0	1	2	0	1	2
SUM	16.400608	18.981652	23.683523	6.393E-09	7.014E-08	3.519E-06
	16.400608	18.981652	23.683523	6.393E-09	7.014E-08	3.519E-06
$v'' \setminus v'$	$a^1\Delta SF^+ + \tilde{X}^2B_1 H_2O^+$			$a^1\Delta SF^+ + \tilde{A}^2A_1 H_2O^+$		
	0	1	2	0	1	2
0	2.78E-04	1.87E-04	4.14E-05	7.55E-02	4.40E-02	7.49E-03
1	2.06E-04	2.92E-05	1.86E-04	7.25E-02	8.93E-03	4.27E-02
2	1.03E-04	1.63E-04	6.82E-06	4.54E-02	6.55E-02	2.05E-03
3	4.86E-05	1.76E-04	6.34E-05	2.70E-02	8.64E-02	2.41E-02
4	2.14E-05	1.21E-04	1.56E-04	1.44E-02	7.30E-02	7.39E-02
5	8.15E-06	6.47E-05	1.54E-04	6.49E-03	4.68E-02	9.01E-02
6	2.30E-06	2.70E-05	9.97E-05	2.09E-03	2.34E-02	7.16E-02
7	3.93E-07	9.03E-06	5.02E-05	4.01E-04	8.66E-03	4.11E-02
8	1.30E-08	2.17E-06	2.01E-05	1.43E-05	2.29E-03	1.94E-02
9	7.94E-09	3.19E-07	6.77E-06	9.40E-06	3.69E-04	7.03E-03
10	8.13E-09	1.76E-08	1.79E-06	9.66E-06	2.03E-05	1.99E-03
11	9.92E-12	3.75E-10	3.86E-07	1.10E-08	4.30E-07	4.45E-04
12	1.05E-08	7.39E-09	9.54E-08	1.11E-05	8.02E-06	1.10E-04
13	2.38E-08	4.09E-08	6.33E-08	2.17E-05	4.15E-05	7.00E-05
14	2.03E-08	7.94E-08	9.54E-08	1.56E-05	6.86E-05	9.78E-05
15	6.52E-09	7.55E-08	1.43E-07	4.13E-06	5.56E-05	1.29E-04
16	1.70E-11	3.65E-08	1.44E-07	8.09E-09	2.08E-05	1.10E-04
17	3.30E-09	3.42E-09	8.60E-08	1.17E-06	1.50E-06	5.39E-05
18	7.06E-09	4.67E-09	2.04E-08	1.77E-06	1.50E-06	1.00E-05
19	5.45E-09	2.23E-08	6.48E-10	9.23E-07	4.99E-06	2.37E-07
20	1.42E-09	2.66E-08	2.60E-08	1.61E-07	4.11E-06	6.75E-06
21	2.01E-11	1.47E-08	4.93E-08	1.42E-09	1.46E-06	9.01E-06
22	1.37E-09	1.86E-09	4.12E-08	5.87E-08	1.16E-07	4.92E-06
23	2.62E-09	1.49E-09	1.27E-08	6.43E-08	5.50E-08	9.88E-07
24	2.02E-09	9.78E-09	6.30E-11	2.84E-08	2.13E-07	3.07E-09
25	6.69E-10	1.54E-08	1.39E-08	5.18E-09	1.91E-07	4.07E-07
26	1.39E-11	1.30E-08	3.37E-08	5.92E-11	8.76E-08	5.73E-07
27	1.55E-10	5.65E-09	3.43E-08	3.49E-10	2.16E-08	3.38E-07
28	3.47E-10	5.80E-10	1.79E-08	3.86E-10	1.12E-09	9.83E-08
29	2.32E-10	8.15E-10	2.03E-09	1.33E-10	8.37E-10	6.20E-09
30	5.55E-11	5.15E-09	2.42E-09	1.59E-11	2.71E-09	3.84E-09
31	2.12E-12	9.83E-09	1.48E-08	2.91E-13	2.57E-09	1.23E-08
32	3.01E-12	1.15E-08	2.38E-08	1.91E-13	1.44E-09	1.05E-08
33	8.48E-11	8.92E-09	2.00E-08	2.46E-12	5.29E-10	4.37E-09
34	4.44E-10	4.23E-09	8.08E-09	5.96E-12	1.20E-10	9.19E-10
35	9.94E-10	4.67E-10	3.42E-10	6.09E-12	6.28E-12	1.83E-11
36	1.23E-09	7.43E-10	2.83E-09	3.30E-12	4.56E-12	7.41E-11
37	7.97E-10	5.39E-09	1.18E-08	8.88E-13	1.44E-11	1.58E-10
38	1.15E-10	1.16E-08	1.87E-08	5.09E-14	1.31E-11	1.15E-10
39	1.97E-10	1.59E-08	1.79E-08	3.68E-14	7.98E-12	5.41E-11
40	1.64E-09	1.54E-08	1.11E-08	1.23E-13	3.33E-12	1.43E-11
41	3.92E-09	1.09E-08	3.57E-09	1.12E-13	9.55E-13	2.09E-12
42	5.74E-09	4.96E-09	5.89E-11	5.79E-14	1.67E-13	1.69E-14
43	5.98E-09	8.40E-10	1.73E-09	1.97E-14	1.02E-14	2.06E-13
44	4.63E-09	1.68E-10	6.49E-09	5.56E-15	8.08E-16	3.56E-13
45	2.53E-09	2.49E-09	1.12E-08	1.02E-15	4.50E-15	2.70E-13
46	7.61E-10	6.08E-09	1.35E-08	1.22E-16	3.84E-15	1.37E-13
47	1.53E-11	9.12E-09	1.31E-08	7.00E-19	2.33E-15	6.33E-14
48	2.99E-10	1.05E-08	1.07E-08	4.67E-18	1.03E-15	2.35E-14
49	1.13E-09	1.01E-08	7.42E-09	5.52E-18	3.54E-16	7.19E-15
SUM	6.68E-04	7.80E-04	7.87E-04	2.44E-01	3.60E-01	3.82E-01

Table 5.4: Products of Landau-Zener cross sections and Franck-Condon factors for transitions from $(v' = 0, 1, 2) X^2\Pi SF^{2+}$ to all vibrational levels of $A^3\Pi SF^+$, $D^3\Pi SF^+$ and $a^1\Delta SF^+$ for the $A^3\Pi SF^+ + \tilde{A}^2A_1 H_2O^+$, $D^3\Pi SF^+ + \tilde{X}^2B_1 H_2O^+$, $a^1\Delta SF^+ + \tilde{X}^2B_1 H_2O^+$ and $a^1\Delta SF^+ + \tilde{A}^2A_1 H_2O^+$ product states.

vert. transition	$d^1\Pi SF^+ + \tilde{X}^2B_1 H_2O^+$					
	0	1	2			
SUM	4.68E-02	9.17E-02	2.76E-01			
	4.68E-02	9.17E-02	2.76E-01			
$v'' \setminus v'$	$b^1\Sigma^+ SF^+ + \tilde{X}^2B_1 H_2O^+$			$b^1\Sigma^+ SF^+ + \tilde{A}^2A_1 H_2O^+$		
	0	1	2	0	1	2
0	1.64E-03	1.11E-03	2.39E-04	1.80E+00	1.15E+00	2.10E-01
1	1.47E-03	1.28E-04	1.01E-03	1.68E+00	1.42E-01	1.01E+00
2	8.70E-04	1.12E-03	8.81E-05	1.04E+00	1.32E+00	9.65E-02
3	4.89E-04	1.49E-03	3.50E-04	5.50E-01	1.72E+00	4.02E-01
4	2.56E-04	1.25E-03	1.20E-03	2.65E-01	1.36E+00	1.39E+00
5	1.15E-04	8.06E-04	1.50E-03	1.07E-01	7.93E-01	1.66E+00
6	4.15E-05	4.05E-04	1.18E-03	3.13E-02	3.45E-01	1.22E+00
7	9.24E-06	1.61E-04	7.23E-04	5.54E-03	1.14E-01	6.33E-01
8	6.72E-07	4.85E-05	3.49E-04	3.05E-04	2.66E-02	2.54E-01
9	7.71E-08	9.85E-06	1.39E-04	2.48E-05	3.83E-03	7.94E-02
10	2.38E-07	8.54E-07	4.49E-05	5.11E-05	2.30E-04	1.91E-02
11	2.42E-08	1.05E-08	1.17E-05	3.27E-06	1.92E-06	3.50E-03
12	1.24E-07	5.19E-08	2.83E-06	1.01E-05	5.92E-06	5.86E-04
13	5.17E-07	6.08E-07	1.38E-06	2.48E-05	4.21E-05	1.81E-04
14	6.57E-07	1.76E-06	1.86E-06	1.71E-05	6.87E-05	1.52E-04
15	3.65E-07	2.33E-06	3.15E-06	5.14E-06	5.07E-05	1.54E-04
16	5.46E-08	1.68E-06	4.07E-06	3.95E-07	1.94E-05	1.13E-04
17	1.98E-08	5.24E-07	3.47E-06	7.02E-08	3.08E-06	5.20E-05
18	1.45E-07	9.60E-10	1.67E-06	2.48E-07	2.82E-09	1.30E-05
19	1.95E-07	2.92E-07	2.11E-07	1.56E-07	4.13E-07	8.69E-07
20	1.13E-07	6.92E-07	1.29E-07	4.20E-08	4.69E-07	2.59E-07
21	2.12E-08	6.60E-07	8.84E-07	3.52E-09	2.06E-07	8.64E-07
22	2.06E-09	3.07E-07	1.33E-06	1.45E-10	4.22E-08	6.08E-07
23	3.09E-08	3.48E-08	9.86E-07	8.75E-10	2.01E-09	2.15E-07
24	4.78E-08	2.56E-08	3.11E-07	5.75E-10	6.53E-10	3.01E-08
25	3.55E-08	1.55E-07	1.35E-09	1.57E-10	1.53E-09	5.77E-11
26	1.40E-08	2.36E-07	1.75E-07	2.33E-11	9.25E-10	3.25E-09
27	1.80E-09	2.07E-07	4.73E-07	1.18E-12	3.38E-10	3.73E-09
28	2.23E-10	1.18E-07	5.69E-07	4.88E-14	6.79E-11	1.94E-09
29	1.94E-09	3.82E-08	4.06E-07	1.46E-13	8.26E-12	5.84E-10
30	2.29E-09	2.74E-09	1.72E-07	5.53E-14	2.06E-13	9.88E-11
31	1.33E-09	4.01E-09	2.61E-08	1.12E-14	1.15E-13	5.70E-12
32	4.39E-10	2.01E-08	3.34E-09	1.18E-15	1.71E-13	2.94E-13
33	7.45E-11	3.40E-08	4.43E-08	5.83E-17	1.11E-13	1.51E-12
34	6.31E-12	3.85E-08	8.49E-08	1.62E-18	3.74E-14	1.22E-12
35	4.26E-12	3.50E-08	9.58E-08	3.26E-19	1.42E-14	5.61E-13
36	2.41E-11	2.73E-08	8.27E-08	6.50E-19	4.36E-15	2.24E-13
37	7.68E-11	1.91E-08	6.02E-08	6.80E-19	1.13E-15	8.86E-14
38	1.44E-10	1.24E-08	3.91E-08	5.25E-19	3.36E-16	3.06E-14
39	1.98E-10	7.82E-09	2.40E-08	2.79E-19	9.18E-17	9.70E-15
40	2.30E-10	4.92E-09	1.45E-08	1.68E-19	3.24E-17	3.72E-15
41	2.43E-10	3.12E-09	8.80E-09	1.27E-19	1.54E-17	1.40E-15
42	2.31E-10	1.93E-09	5.16E-09	5.94E-20	5.15E-18	6.47E-16
43	1.70E-10	1.01E-09	2.57E-09	3.08E-20	1.97E-18	2.52E-16
SUM	4.90E-03	6.53E-03	6.86E-03	5.47E+00	6.98E+00	6.97E+00

Table 5.5: Products of Landau-Zener cross sections and Franck-Condon factors for transitions from $(v' = 0, 1, 2) X^2\Pi SF^{2+}$ to all vibrational levels of $b^1\Sigma^+ SF^+$ and $d^1\Pi SF^+$ for the $d^1\Pi SF^+ + \tilde{X}^2B_1 H_2O^+$, $b^1\Sigma^+ SF^+ + \tilde{X}^2B_1 H_2O^+$ and $b^1\Sigma^+ SF^+ + \tilde{A}^2A_1 H_2O^+$ product states.

$X^3\Sigma^- \text{SF}^+ + \tilde{B}^2B_2 \text{H}_2\text{O}^+$, $a^1\Delta \text{SF}^+ + \tilde{X}^2B_1 \text{H}_2\text{O}^+$, $a^1\Delta \text{SF}^+ + \tilde{A}^2A_1 \text{H}_2\text{O}^+$, $b^1\Sigma^+ \text{SF}^+ + \tilde{X}^2B_1 \text{H}_2\text{O}^+$ and $b^1\Sigma^+ \text{SF}^+ + \tilde{A}^2A_1 \text{H}_2\text{O}^+$. The total probabilities for forming S^+ and SF^+ are 17.82 and 6.40, respectively. This gives a S^+/SF^+ ratio of 2.78; the experimentally determined value is 1.07.

5.4.3 Discussion

In calculating the theoretical S^+/SF^+ ratio, a number of approximations were made. First, we have assumed that the formation of SF^{2+} from SF_6 occurs by ionization of SF_6 in its ground electronic and vibrational state to SF^{2+} in its ground electronic state and first three vibrational levels ($v' = 0, 1, 2$). Since there is no energy source to excite our precursor SF_6 gas prior to electron impact, we would expect that most SF_6 molecules would be in their ground electronic and vibrational states. However, it is certainly likely that some more highly electronically and vibrationally excited states of SF^{2+} could be populated. As can be seen on Figure 5.4, all excited states of SF^{2+} calculated in this study have equilibrium bond lengths between 1.80 and 2.50 Å. This means that there will be greater Franck-Condon overlap with some of the more highly excited states of SF^+ that have equilibrium bond lengths in the region of 1.80 Å (see Figure 5.5). In addition, the greater excitation of SF^{2+} will result in the exothermicities for some $\text{SF}^+ + \text{H}_2\text{O}^+$ product states to fall outside the range of non-zero LZ cross sections (approximately 4-6 eV), and those for some new product states to enter this range. However, the probability of reaching a given $\text{SF}^+ + \text{H}_2\text{O}^+$ state from an excited SF^{2+} first depends on the lifetime of the excited dication. It is interesting to note

that of the excited states of SF^{2+} calculated in this study, all were bound (if loosely). It is key that the dication live long enough after its formation to survive the journey to the source of the TOFMS. Although this may be the case for some of the more (relatively) deeply bound states (such as the $A\ ^2\Pi$ and $B\ ^2\Pi$ states with well depths of 1.43 and 0.89 eV, respectively), it is unlikely for some of the more highly excited, and less bound, states of SF^{2+} .

Similarly, we have also not considered some of the more highly excited states of SF^+ , as we were limited by the number of states that it is possible to consider simultaneously in a state-averaged calculation. As with the excited states of SF^{2+} , including more states of SF^+ would be likely to increase both the yields of S^+ and of SF^+ . It is most likely that the theoretical yield of S^+ would increase more than that of SF^+ , since the more highly excited states of SF^+ are more likely to be dissociative. However, there would be a limit to the extent of the contribution of these more highly excited states, since the exothermicities for reaching product asymptotes containing these states would gradually decrease with the degree of excitation of the SF^+ until the LZ cross sections for their formation become 0.

Second, for simplicity we have not considered any excited states of H_2O , nor of H_2O^+ above the \tilde{B} state. As with SF_6 , we expect that with no external input of energy, the neutral water molecules will be in their ground state. In addition, it is important to note that no OH^+ (or O^+) was observed experimentally, so none of the dissociative states of H_2O^+ should be contributing to the S^+/SF^+ ratio. However, we have also not fully taken into account the

FCFs for transitions from H_2O to H_2O^+ . Although the $\widetilde{X}^2B_1 \text{H}_2\text{O}^+$ state is similar in geometry to neutral H_2O , the $\widetilde{A}^2A_1 \text{H}_2\text{O}^+$ state is linear with a bond length of 0.98 Å and the $\widetilde{B}^2B_2 \text{H}_2\text{O}^+$ state is very bent at 54.98° with a bond length of 1.140 Å [122–125]. Therefore, as discussed in Section 5.4.2, upon examination of the photoelectron spectrum of water we have assumed FCFs equal to 1 for all modes for transitions to the \widetilde{X} state with no vibrational excitation and to the \widetilde{A} and \widetilde{B} states with 1 eV excitation, as these appear to be where the vibrational maxima lie for each state, respectively.

Finally, it has been mentioned above that the FCFs for transitions from SF^{2+} to the dissociative (Π) states of SF^+ were assumed to be 1. Since all of the contributions to the theoretical S^+ intensity come from dissociative states, it is therefore likely that the S^+ intensity has been overestimated. In order to be more rigorous, a continuum wavefunction could be calculated for each dissociative state and the overlap integrals evaluated using these wavefunctions. It is expected that this is most likely the approximation with the greatest effect on the final S^+/SF^+ ratio and may explain why the theoretical ratio is greater than that derived from the experimental data.

The two largest contributions to the S^+/SF^+ ratio were from the $A^3\Pi \text{SF}^+ + \widetilde{X}^2B_1 \text{H}_2\text{O}^+$ and $b^1\Sigma^+ \text{SF}^+ + \widetilde{A}^2A_1 \text{H}_2\text{O}^+$ product states. The exothermicities for these two product states are 2.90 eV and 3.73 eV, respectively. When these exothermicities are weighted with their theoretical cross sections, this gives a kinetic energy release of about 3 eV. Therefore it is expected that the experimental kinetic energy release distribution would be centered about 3 eV. This could be measured using an experiment in which

the velocities of the product ions are measured, such as that of Herman [2] or of Price [89]. Hence, a value of 3 eV for the kinetic energy release for the charge transfer between SF^{2+} and H_2O was used for the calculation of the COM velocity of SF^+ , used as described in Section 5.2 in the conversion of experimental intensities to absolute relative cross sections.

It is interesting to note, as can be seen in Tables 5.3 to 5.5, that the largest contributions to the S^+ and SF^+ intensities come from excited states of both SF^+ and H_2O^+ , even relatively highly excited states (such as for the $b\ ^1\Sigma^+ \text{SF}^+ + \tilde{A}\ ^2A_1 \text{H}_2\text{O}^+$ product asymptote). In particular, the ground state product asymptote of $X\ ^3\Sigma^- \text{SF}^+ + \tilde{X}\ ^2B_1 \text{H}_2\text{O}^+$ does not contribute at all to the final SF^+ intensity. Therefore it appears that for such charge transfer pathways, highly electronically and vibrationally excited states may well play a significant role.

5.5 Conclusions

Crossed-beam TOFMS collision experiments were performed between SF^{2+} and H_2O . The product ions SF^+ , H_2O^+ , S^+ and $\text{OSF}^+(\text{HOSF}^+)$ were observed. No center-of-mass collision energy dependence was observed for the charge transfer products S^+ , SF^+ and H_2O^+ . Analysis of the intensities of the S^+ and SF^+ signals indicate that the experimental S^+/SF^+ ratio is 1.07.

Multireference quantum chemical calculations were performed in order to generate the potential energy curves for 9 of the low-lying states of SF^{2+} and

11 of the low-lying states of SF^+ . All of the 9 calculated states of SF^{2+} were found to be bound, and of the 11 calculated states of SF^+ only 4 states were unbound, all of Π symmetry.

The calculated potential energy curves were then used to determine the number of vibrational levels in each bound state, the vibrational wavefunctions for each level, and the Franck-Condon factors for various transitions between SF and SF^{2+} , and SF^{2+} and SF^+ . Term energies for each reactant and product state combination were calculated and used to determine the Landau-Zener cross section for each outcome. It was found that the ground product state $X^3\Sigma^- \text{SF}^+ + \widetilde{X}^2B_1 \text{H}_2\text{O}^+$ has a zero Landau-Zener probability for all vibrational levels of SF^+ .

The Franck-Condon factors and Landau-Zener cross-sections were then multiplied to give state-to-state probabilities. These probabilities were then summed over all SF^+ vibrational levels for each electronic product state and it was found that the product asymptotes with the highest probabilities (by several orders of magnitude) were the $A^3\Pi \text{SF}^+ + \widetilde{X}^2B_1 \text{H}_2\text{O}^+$, $a^1\Delta \text{SF}^+ + \widetilde{A}^2A_1 \text{H}_2\text{O}^+$ and $b^1\Sigma^+ \text{SF}^+ + \widetilde{A}^2A_1 \text{H}_2\text{O}^+$ states. The calculated probabilities for each product state were then used to determine a theoretical S^+/SF^+ ratio of 2.78, in good agreement with the value of 1.07 determined from the experimental data when one bears in mind the approximations made in the derivation of the theoretical ratio.

Appendix A

FORTRAN90 source code for a program written to calculate unimolecular dissociation rate constants using the RRKM/QET equation

```
-----  
!THIS PROGRAM CALCULATES UNIMOLECULAR DISSOCIATION RATE CONSTANTS.  
!INFO NEEDED: FREQUENCIES OF ALL BONDS, COLLISION ENERGY, ZP-CORRECTED  
! ENERGIES OF REACTANTS AND TS.  
program rrkm
```

```
implicit none
```

```
real, dimension(7):: E  
integer :: sum_of_states, density_of_states  
real :: rate_constant
```

```
interface
```

```
  subroutine sum_states(E,sum_of_states)  
    real, dimension(7), intent(in) :: E  
    integer, intent(out) :: sum_of_states  
  end subroutine sum_states  
  subroutine density_states(E,density_of_states)  
    real, dimension(7), intent(in) :: E
```

```
integer, intent(out) :: density_of_states
end subroutine density_states
end interface

!E(1) = COM collision energy
!E(2) = total internal energy of reactants
!E(3) = internal energy of starting structure
!E(4) = internal energy of transition state
!E(5) = total energy (E)
!E(6) = activation energy (Eo)
!E(7) = E - Eo

print*, "Enter the centre of mass collision energy in eV:"
read*, E(1)
print*, "Enter the energy of the reactants in Hartrees:"
read*, E(2)
print*, "Enter the energy of the minimum in Hartrees:"
read*, E(3)
print*, "Enter the energy of the transition state in Hartrees:"
read*, E(4)

E(1) = E(1)*1.602E-19          !convert eV to J
E(2:4) = E(2:4)*2625501.4025/(6.022*(10.0**(23))) !convert Hartrees to J
E(5) = E(2) - E(3) + E(1)
E(6) = E(4) - E(3)
E(7) = E(5) - E(6)

!convert energy (J) into frequency (cm-1)
E(5:7:2) = E(5:7:2)/(6.6260755*(10.0**(-34)))*2.99792458*(10.0**10)

call sum_states(E,sum_of_states)
call density_states(E,density_of_states)

!calculate the rate constant
rate_constant = sum_of_states/(density_of_states*6.6260755*(10.0**(-34)))

print*, "The rate constant is ", rate_constant

end program rrkm
```

```
subroutine sum_states(E,sum_of_states)

  implicit none

  !dummy variables
  real, dimension(7), intent(in) :: E
  integer, intent(out) :: sum_of_states

  !local variables
  integer :: i,j,s,energy
  integer, dimension(:), allocatable :: frequency,sum

  print*, "Enter the number of oscillators in " &
    & "the transition state structure:"
  read*,s

  energy = int(E(7))
  allocate(frequency(s))
  allocate(sum(energy))

  do i=1,s
    print*, "For the transition state: enter the frequency of " &
      & "oscillator ", i, " in (cm-1):"
    read*, frequency(i)
  end do

  sum(0) = 1
  sum(:) = 1

  do j=1,s
    do i=frequency(j),energy
      sum(i) = sum(i) + sum(i-frequency(j))
    end do
  end do

  sum_of_states = sum(energy)
  print*, "The sum of states at energy", energy, "is", sum_of_states

end subroutine sum_states
```

```
subroutine density_states(E,density_of_states)

  implicit none

  !dummy variables
  real, dimension(7), intent(in) :: E
  integer, intent(out) :: density_of_states

  !local variables
  integer :: i,j,s,energy
  integer, dimension(:), allocatable :: frequency,density

  print*, "Enter the number of oscillators for the parent structure:"
  read*,s

  energy = int(E(5))
  allocate(frequency(s))
  allocate(density(energy))

  do i=1,s
    print*, "For the parent structure: enter the frequency of " &
      & "oscillator ", i, " in (cm-1):"
    read*, frequency(i)
  end do

  density(:) = 0
  density(0) = 1

  do j=1,s
    do i=frequency(j),energy
      density(i) = density(i) + density(i-frequency(j))
    end do
  end do

  density_of_states = density(energy)
  print*, "The density of states for the parent ion at energy", &
    & energy, "is", density_of_states

end subroutine density_states
```

Appendix B

FORTRAN90 source code for a program written to calculate Franck-Condon factors from the vibrational wavefunctions of the initial and final states.

This program is based on an original F90 program written and kindly provided by E. Boleat [106].

```
!-----  
!program to calculate Franck-Condon overlaps  
!-----  
  
program franck_condon  
  
!you need to have 2 data files, one with the vib levels for v'' and another  
!for v'. Make sure that all the vib wfs are over the same values of r.  
  
implicit none  
  
real(kind=kind(1.0d0)), dimension(:,:), allocatable :: v  
real(kind=kind(1.0d0)), dimension(:,:), allocatable :: vv  
real, dimension(:), allocatable :: fcon !output  
real(kind=kind(1.0d0)) :: sum  
integer :: i,j,k,nv,nvv,np
```

```
print*, "Enter the highest vibrational level in first state to include:"
read*, nv

print*, "Enter the highest vibrational level in second state to include:"
read*, nvv

print*, "Enter the number of data points for each vibrational wavefunction:"
read*, np

allocate(v(0:nv,np))
allocate(vv(0:nvv,np))
allocate(fcon(0:nvv))

!get the data
open(1,file='v.txt')
open(2,file='vv.txt')

!read into matrix form
read(1,*)((v(j,i),i=1,np),j=0,nv)
read(2,*)((vv(k,i),i=1,np),k=0,nvv)

!open output file with format statements before do-loop
open(3,file='fcon.csv')
write(3,30)'fc factors'
30      format (a10)

!use do-loop to calculate fc factors with step size of 0.01

do k=0,nvv
write(3,33)'v+=',k
33      format (/, a3, i2, /)
      do j=0,nv
      sum=0.0
          do i=1,np
          sum=sum+0.5*(0.01*(v(j,i)*vv(k,i)+v(j,(i+1))*vv(k,(i+1))))
          end do
      fcon(k)=(sum)**2!square of sum
      !output to file
      write(3,4) fcon(k)
4      format (21(e14.8,1x), /)
```

```
        end do  
end do  
  
end program franck_condon
```

Appendix C

Calculated Franck-Condon factors

$v' \setminus v$	0	1	2	3	4	5	6
0	0.4536719	0.3188265	0.0958802	0.0193226	0.0025984	0.0001791	1.963E-07
1	0.3656573	0.0982097	0.3191348	0.1905317	0.0580761	0.0104582	0.0009574
2	0.1412348	0.3260099	2.966E-06	0.2063878	0.2389428	0.1056544	0.0252617
3	0.0333839	0.1923782	0.2098654	0.0422114	0.0947984	0.2372978	0.1506569
4	0.0053984	0.0540261	0.2472652	0.0940639	0.1017076	0.0256795	0.2005733
5	0.0006059	0.0094204	0.1015933	0.2504755	0.0242551	0.1335946	0.0007956
6	4.524E-05	0.0010553	0.0229041	0.1479091	0.2185145	0.0004882	0.1332885
7	2.448E-06	7.067E-05	0.0031096	0.0419049	0.1844075	0.1716621	0.0076315
8	6.517E-08	3.139E-06	0.0002351	0.0066263	0.0641985	0.2085236	0.1234694
9	1.08E-09	2.927E-08	9.238E-06	0.0005477	0.0114786	0.0875926	0.2211659
10	2.678E-10	1.013E-08	8.17E-08	1.899E-05	0.0009931	0.0173247	0.1104635
11	1.147E-11	2.456E-09	3.319E-08	5.011E-08	2.918E-05	0.0015097	0.0236835
12	3.025E-10	1.508E-10	4.508E-10	7.236E-08	2.533E-09	3.498E-05	0.0020183
13	1.567E-10	7.06E-10	4.554E-10	3.398E-12	1.277E-07	2.713E-07	3.238E-05
14	1.958E-12	1.381E-09	1.66E-09	3.073E-09	1.614E-10	2.002E-07	1.586E-06
15	1.796E-11	4.112E-10	1.645E-09	2.533E-09	4.927E-09	1.629E-10	3.078E-07
16	1.212E-11	4.957E-12	3.241E-10	9.698E-10	5.516E-09	4.658E-09	2.673E-09
17	2.514E-12	2.233E-10	1.142E-10	1.968E-10	1.133E-09	5.079E-09	3.024E-09
18	4.528E-12	2.617E-10	5.708E-10	5.84E-11	1.04E-11	1.015E-09	2.038E-09
19	1.4E-11	9.834E-11	3.473E-10	7.288E-10	4.79E-10	3.553E-10	2.806E-10
20	8.166E-12	4.849E-13	4.86E-11	8.92E-10	1.05E-09	1.888E-09	4.298E-10
21	2.318E-12	4.859E-11	1.892E-12	2.814E-10	1.231E-09	1.683E-09	1.756E-09
22	4.001E-11	9.21E-11	2.6E-11	4.528E-13	5.677E-10	7.671E-10	1.484E-09
23	5.577E-11	4.559E-11	3.977E-11	7.752E-11	5.114E-12	1.522E-10	3.972E-10
24	1.385E-11	1.173E-12	3.518E-11	1.297E-10	2.924E-10	1.986E-11	1.242E-12
25	5.874E-12	1.455E-11	1.596E-11	1.18E-10	6.318E-10	4.348E-10	2.771E-10
26	4.934E-11	3.285E-11	1.239E-12	8.828E-11	4.951E-10	9.65E-10	6.096E-10
27	5.718E-11	2.077E-11	1.832E-12	4.69E-11	2.066E-10	9.238E-10	7.059E-10
28	1.782E-11	2.654E-12	5.54E-12	8.916E-12	4.307E-11	3.958E-10	5.637E-10
29	5.5E-13	1.962E-12	3.325E-12	1.775E-12	1.543E-13	2.922E-11	2.836E-10
30	2.269E-11	1.14E-11	2.677E-13	2.209E-11	2.115E-11	4.69E-11	4.596E-11
31	3.92E-11	1.515E-11	3.967E-13	3.885E-11	7.691E-11	1.873E-10	1.907E-11
32	2.596E-11	9.661E-12	1.123E-12	3.58E-11	1.341E-10	2.389E-10	1.887E-10
33	4.957E-12	2.416E-12	4.588E-13	2.191E-11	1.493E-10	2.024E-10	3.619E-10
34	9.797E-13	5.552E-14	5.379E-14	9.788E-12	1.087E-10	1.42E-10	3.817E-10
35	1.167E-11	3.207E-12	1.61E-12	3.28E-12	4.591E-11	8.856E-11	2.646E-10
36	1.99E-11	7.971E-12	4.362E-12	7.042E-13	5.897E-12	4.52E-11	1.229E-10
37	1.679E-11	1.032E-11	6.102E-12	1.135E-14	2.14E-12	1.293E-11	3.354E-11
38	7.298E-12	8.985E-12	5.587E-12	2.918E-13	1.733E-11	3.37E-15	2.193E-12
39	6.683E-13	5.294E-12	3.211E-12	1.351E-12	2.977E-11	1.23E-11	2.511E-12
40	1.017E-12	1.713E-12	7.931E-13	3.049E-12	3.121E-11	4.204E-11	1.342E-11
41	5.676E-12	3.086E-14	3.457E-14	4.984E-12	2.502E-11	6.991E-11	2.699E-11
42	9.816E-12	8.728E-13	1.643E-12	6.454E-12	1.708E-11	7.962E-11	4.25E-11
43	1.019E-11	3.648E-12	5.175E-12	6.931E-12	1.056E-11	6.65E-11	5.932E-11
44	6.664E-12	6.787E-12	8.84E-12	6.074E-12	6.033E-12	3.878E-11	7.131E-11
45	2.254E-12	8.139E-12	1.006E-11	4.161E-12	3.089E-12	1.39E-11	6.81E-11
46	1.606E-13	7.204E-12	8.44E-12	2.33E-12	1.342E-12	2.442E-12	5.136E-11
47	2.743E-13	5.732E-12	6.307E-12	1.186E-12	4.377E-13	2.109E-15	3.483E-11
48	1.472E-12	3.344E-12	3.309E-12	4.04E-13	1.395E-14	8.982E-13	1.626E-11

Table C.1: Franck-Condon factors for transitions from $X^2\Pi$ SF ($v = 0 - 6$) to $X^2\Pi$ SF²⁺ ($v' = 0 - 48$).

$v' \setminus v$	7	8	9	10	11	12	13
0	6.129E-06	4.468E-06	1.21E-06	8.703E-08	1.592E-08	5.459E-08	2.725E-08
1	8.201E-06	2.061E-05	1.892E-05	5.916E-06	6.975E-07	8.144E-10	9.587E-08
2	0.0031334	8.305E-05	3.321E-05	4.989E-05	2.023E-05	3.718E-06	1.204E-07
3	0.0471224	0.0077161	0.0003931	3.09E-05	9.963E-05	5.188E-05	1.252E-05
4	0.1833488	0.0740283	0.0155045	0.0012468	8.735E-06	0.0001534	0.0001051
5	0.1473151	0.1991379	0.1026518	0.026993	0.003118	8.777E-06	0.000184
6	0.0064924	0.0939391	0.1969987	0.129119	0.0419946	0.0065518	0.0001621
7	0.1114041	0.0267113	0.0501741	0.1798642	0.1499403	0.0596846	0.0120595
8	0.0294519	0.0809521	0.0489594	0.0204197	0.1526584	0.1630848	0.0787976
9	0.0820267	0.0541284	0.0515182	0.0664069	0.0044738	0.1205548	0.167475
10	0.2252819	0.0502452	0.0749504	0.0280829	0.0763355	1.164E-06	0.0884046
11	0.1318803	0.2234476	0.0282613	0.0894166	0.0121504	0.078705	0.0034996
12	0.0300944	0.1510961	0.219196	0.0143309	0.0974254	0.0032877	0.0748926
13	0.002409	0.0358955	0.1682162	0.2145127	0.0063379	0.0999603	0.0001123
14	1.982E-05	0.0025789	0.0406318	0.1834931	0.2112859	0.0022868	0.0982772
15	4.899E-06	4.27E-06	0.0024696	0.0438997	0.1972121	0.2106232	0.0006001
16	4.029E-07	1.071E-05	2.253E-06	0.002062	0.0453487	0.2092795	0.2135017
17	2.395E-08	3.918E-07	1.898E-05	3.764E-05	0.0014223	0.0447247	0.2195098
18	6.833E-10	7.97E-08	1.915E-07	2.771E-05	0.0001335	0.0007013	0.0417124
19	8.944E-10	8.677E-12	1.849E-07	6.314E-10	3.28E-05	0.0003031	0.000136
20	2.775E-10	6.256E-10	9.427E-11	3.249E-07	5.641E-07	2.972E-05	0.000532
21	1.016E-10	9.751E-10	1.688E-09	4.173E-09	4.36E-07	3.068E-06	1.671E-05
22	7.248E-10	3.371E-10	1.391E-09	2.875E-09	2.287E-08	4.104E-07	8.492E-06
23	5.479E-10	5.321E-11	1.035E-09	2.641E-09	3.021E-09	8.347E-08	1.542E-07
24	9.293E-11	3.545E-10	1.897E-10	1.934E-09	3.442E-09	1.786E-09	2.006E-07
25	1.587E-11	1.152E-10	3.19E-11	6.681E-10	2.836E-09	5.619E-09	5.144E-10
26	2.07E-10	1.595E-11	1.497E-10	2.329E-11	1.769E-09	3.19E-09	6.516E-09
27	4.523E-10	1.911E-10	2.771E-11	4.9E-11	3.261E-10	2.026E-09	3.932E-09
28	5.59E-10	2.881E-10	4.375E-11	6.179E-11	1.791E-11	7.278E-10	1.911E-09
29	4.332E-10	2.816E-10	2.163E-10	5.898E-12	1.955E-10	7.759E-12	7.808E-10
30	1.902E-10	2.365E-10	2.547E-10	1.647E-11	1.598E-10	2.587E-10	7.582E-11
31	2.316E-11	1.521E-10	1.531E-10	6.521E-11	4.717E-11	5.132E-10	9.847E-11
32	1.539E-11	4.524E-11	5.247E-11	6.828E-11	2.713E-12	3.477E-10	4.774E-10
33	1.223E-10	9.902E-13	5.71E-12	2.757E-11	1.794E-12	1.064E-10	6.026E-10
34	2.538E-10	8.128E-11	4.461E-12	6.242E-13	4.929E-12	9.507E-12	3.8E-10
35	3.342E-10	2.354E-10	4.517E-11	1.158E-11	2.315E-12	8.187E-13	1.133E-10
36	3.246E-10	3.517E-10	1.285E-10	4.206E-11	5.488E-14	4.577E-12	4.814E-12
37	2.373E-10	3.654E-10	2.297E-10	7.273E-11	6.185E-12	3.777E-12	9.772E-12
38	1.214E-10	2.878E-10	2.946E-10	9.877E-11	2.12E-11	1.468E-12	2.25E-11
39	3.324E-11	1.724E-10	2.82E-10	1.207E-10	3.772E-11	2.995E-14	1.36E-11
40	3.43E-13	6.999E-11	1.999E-10	1.331E-10	4.823E-11	1.494E-12	2.285E-12
41	1.434E-11	1.07E-11	9.696E-11	1.26E-10	5.158E-11	8.561E-12	4.121E-13
42	4.946E-11	2.964E-12	2.224E-11	9.393E-11	5.054E-11	2.222E-11	5.418E-12
43	8.297E-11	4.021E-11	3.715E-13	4.537E-11	4.637E-11	3.909E-11	1.319E-11
44	1.002E-10	1.009E-10	2.995E-11	6.289E-12	3.728E-11	5.013E-11	2.219E-11
45	9.591E-11	1.453E-10	8.145E-11	4.17E-12	2.224E-11	4.715E-11	3.019E-11
46	7.941E-11	1.505E-10	1.176E-10	3.099E-11	7.805E-12	3.43E-11	3.359E-11
47	6.824E-11	1.45E-10	1.457E-10	6.804E-11	4.526E-13	2.274E-11	3.533E-11
48	4.989E-11	1.116E-10	1.413E-10	9.056E-11	2.779E-12	1.037E-11	2.86E-11

Table C.2: Franck-Condon factors for transitions from $X^2\Pi$ SF ($v = 7 - 13$) to $X^2\Pi$ SF²⁺ ($v' = 0 - 48$).

$v' \setminus v$	14	15	16	17	18	19	20
0	2.118E-09	1.878E-09	5.415E-09	2.937E-09	1.679E-10	5.354E-10	1.532E-09
1	7.341E-08	1.595E-08	2.456E-12	3.234E-09	3.008E-09	4.308E-10	2.744E-10
2	1.092E-07	1.995E-07	9.727E-08	1.727E-08	3.154E-11	1.797E-09	1.076E-09
3	9.87E-07	7.296E-08	4.198E-07	3.251E-07	1.181E-07	1.867E-08	1.345E-10
4	3.184E-05	3.947E-06	3.077E-09	6.971E-07	7.872E-07	4.023E-07	1.093E-07
5	0.000177	6.661E-05	1.136E-05	1.53E-07	8.665E-07	1.42E-06	8.87E-07
6	0.0001647	0.0002532	0.0001195	2.699E-05	1.487E-06	6.18E-07	1.939E-06
7	0.0007062	9.359E-05	0.0003141	0.0001921	5.632E-05	6.3E-06	1.109E-07
8	0.0199147	0.0019432	1.492E-05	0.0003375	0.0002789	0.0001038	1.789E-05
9	0.0975213	0.0300061	0.0041847	2.317E-05	0.0003019	0.0003617	0.0001695
10	0.1632886	0.1138218	0.0418395	0.0077089	0.0002719	0.0002043	0.0004159
11	0.0598376	0.1518729	0.1262761	0.0547586	0.0127099	0.0009659	7.869E-05
12	0.0113251	0.0367847	0.1351734	0.1339755	0.067847	0.0191797	0.0023194
13	0.0671713	0.0205336	0.0198845	0.1155449	0.1366785	0.0801272	0.0269252
14	0.000841	0.0576092	0.0292011	0.0087574	0.0949873	0.1345738	0.0906822
15	0.0938093	0.0037582	0.047773	0.0362314	0.0025616	0.0751513	0.128299
16	9.632E-05	0.0878132	0.007572	0.0385963	0.041213	0.0001592	0.0572251
17	0.2208662	1.488E-05	0.0811168	0.011413	0.0306078	0.044125	0.0004065
18	0.2271908	0.2335806	4.12E-05	0.0741796	0.0147628	0.0240344	0.0452426
19	0.0362311	0.2315871	0.252133	0.0003066	0.0671633	0.0173812	0.0188432
20	4.163E-05	0.0285713	0.2314604	0.2766725	0.0014028	0.0600791	0.019208
21	0.0007658	0.0007426	0.0194782	0.2250631	0.3067669	0.0044283	0.0527653
22	1.999E-06	0.0009119	0.0024482	0.0103182	0.2106048	0.3412793	0.0110287
23	1.612E-05	7.277E-06	0.0008673	0.0050864	0.0030381	0.1866042	0.3776278
24	2.082E-08	2.217E-05	6.46E-05	0.0005912	0.0081558	1.298E-06	0.1528525
25	3.296E-07	1.037E-06	2.043E-05	0.0001951	0.000194	0.0106696	0.0033738
26	2.056E-08	3.315E-07	4.674E-06	8.94E-06	0.0003754	3.523E-06	0.0114125
27	3.765E-09	9.93E-08	9.531E-08	1.101E-05	4.783E-08	0.0005119	0.0004889
28	4.499E-09	5.235E-11	2.378E-07	1.066E-07	1.643E-05	2.582E-05	0.0004783
29	2.087E-09	5.276E-09	1.218E-08	3.015E-07	1.792E-06	1.393E-05	0.0001192
30	1.016E-09	2.627E-09	3.641E-09	7.807E-08	1.372E-07	6.449E-06	3.127E-06
31	2.623E-10	1.182E-09	4.586E-09	2.18E-11	2.086E-07	3.873E-08	1.202E-05
32	3.41E-12	6.065E-10	1.808E-09	4.648E-09	1.892E-08	2.705E-07	1.379E-06
33	2.555E-10	1.251E-10	6.869E-10	2.826E-09	1.181E-09	1.082E-07	8.393E-08
34	5.08E-10	3.101E-11	2.279E-10	9.297E-10	3.383E-09	3.911E-09	2.362E-07
35	4.903E-10	3.727E-10	5.7E-12	2.558E-10	1.351E-09	2.017E-09	5.425E-08
36	3.01E-10	6.619E-10	1.391E-10	2.207E-11	3.488E-10	2.3E-09	7.566E-10
37	1.154E-10	6.244E-10	5.557E-10	4.496E-11	6.549E-11	6.322E-10	1.851E-09
38	1.89E-11	3.95E-10	8.745E-10	3.085E-10	1.589E-12	8.044E-11	1.561E-09
39	1.745E-13	1.781E-10	8.407E-10	6.717E-10	1.352E-10	8.736E-13	3.607E-10
40	7.909E-12	5.401E-11	5.533E-10	9.149E-10	4.528E-10	2.726E-11	1.621E-11
41	8.433E-12	7.323E-12	2.554E-10	9.049E-10	7.833E-10	1.65E-10	1.502E-11
42	1.879E-12	1.834E-13	7.684E-11	6.712E-10	9.544E-10	4.591E-10	8.471E-11
43	7.69E-13	4.164E-12	9.873E-12	3.526E-10	8.987E-10	8.214E-10	2.347E-10
44	8.256E-12	4.5E-12	2.104E-13	1.06E-10	6.483E-10	1.016E-09	5.089E-10
45	1.539E-11	9.857E-13	4.763E-12	8.518E-12	3.356E-10	8.878E-10	7.977E-10
46	1.656E-11	2.374E-13	6.82E-12	2.479E-12	1.2E-10	5.949E-10	9.043E-10
47	1.632E-11	3.119E-12	6.482E-12	1.449E-11	2.569E-11	3.696E-10	9.109E-10
48	1.378E-11	6.43E-12	4.001E-12	1.883E-11	3.881E-14	1.7E-10	6.919E-10

Table C.3: Franck-Condon factors for transitions from $X^2\Pi$ SF ($v = 7 - 13$) to $X^2\Pi$ SF $^{2+}$ ($v' = 0 - 48$).

$v' \setminus v''$	0	1	2	3	4	5	6	7	8
0	5.06E-01	3.15E-01	1.23E-01	3.97E-02	1.14E-02	2.96E-03	2.58E-03	1.45E-04	2.61E-05
1	3.73E-01	5.30E-02	2.41E-01	1.91E-01	9.22E-02	3.47E-02	2.78E-02	3.14E-03	8.04E-04
2	1.05E-01	3.69E-01	7.01E-03	1.08E-01	1.83E-01	1.29E-01	9.94E-02	2.46E-02	8.33E-03
3	1.42E-02	2.15E-01	2.44E-01	7.22E-02	2.48E-02	1.33E-01	1.16E-01	8.79E-02	4.17E-02
4	9.56E-04	4.38E-02	2.90E-01	1.22E-01	1.30E-01	5.57E-05	7.89E-03	1.29E-01	1.04E-01
5	2.36E-05	3.80E-03	8.50E-02	3.19E-01	4.24E-02	1.52E-01	7.73E-02	3.21E-02	1.02E-01
6	2.01E-08	1.19E-04	9.18E-03	1.31E-01	3.12E-01	6.09E-03	6.26E-02	4.05E-02	6.78E-03
7	4.14E-09	7.44E-08	3.31E-04	1.72E-02	1.76E-01	2.84E-01	6.61E-02	1.15E-01	6.80E-02
8	3.76E-10	4.13E-09	2.41E-07	6.79E-04	2.75E-02	2.17E-01	8.47E-02	1.40E-02	8.09E-02
9	3.22E-09	2.36E-09	1.27E-07	3.69E-07	1.14E-03	3.95E-02	3.06E-01	2.02E-01	3.53E-02
10	2.62E-09	1.27E-08	1.38E-08	6.16E-07	1.71E-07	1.68E-03	1.35E-01	2.83E-01	1.61E-01
11	7.88E-11	4.05E-09	2.03E-08	2.79E-08	1.71E-06	9.38E-08	1.43E-02	6.68E-02	3.07E-01
12	4.53E-10	8.82E-11	2.89E-09	1.78E-08	3.65E-08	3.75E-06	1.31E-04	2.74E-03	8.11E-02
13	5.39E-10	2.11E-09	1.61E-09	6.44E-10	1.06E-08	5.28E-08	2.32E-05	1.45E-05	3.12E-03
14	7.24E-11	1.51E-09	5.24E-09	4.77E-09	1.73E-12	2.63E-09	7.23E-07	1.16E-05	4.68E-05
15	2.79E-11	1.21E-10	2.40E-09	8.01E-09	8.81E-09	1.37E-09	1.46E-07	1.67E-07	1.75E-05
16	9.44E-11	1.60E-10	4.08E-11	2.90E-09	1.15E-08	1.47E-08	1.97E-08	1.14E-08	4.18E-07
17	4.17E-11	4.06E-10	5.48E-10	1.23E-11	3.87E-09	1.56E-08	9.67E-09	1.24E-08	2.98E-08
18	1.13E-12	1.88E-10	8.56E-10	8.79E-10	1.26E-11	4.55E-09	8.10E-11	2.03E-08	2.15E-08
19	6.15E-12	4.93E-12	3.09E-10	1.28E-09	1.33E-09	1.18E-11	4.80E-09	1.59E-08	2.27E-08
20	1.06E-11	4.10E-11	1.42E-12	5.19E-10	2.24E-09	2.60E-09	7.78E-09	3.79E-09	1.83E-08
21	5.34E-12	7.94E-11	9.89E-11	2.10E-11	1.24E-09	3.89E-09	3.55E-09	8.34E-11	5.49E-09
22	8.18E-13	4.06E-11	1.53E-10	6.95E-11	1.76E-10	2.03E-09	2.29E-10	2.97E-09	9.54E-13
23	5.15E-14	3.16E-12	6.48E-11	1.58E-10	4.35E-11	2.40E-10	4.95E-10	4.33E-09	2.77E-09
24	8.01E-13	4.83E-12	1.77E-12	1.04E-10	3.19E-10	1.27E-10	1.78E-09	2.58E-09	5.42E-09
25	1.36E-12	1.76E-11	1.53E-11	2.56E-11	3.89E-10	7.07E-10	1.80E-09	5.57E-10	4.28E-09
26	1.30E-12	1.70E-11	3.41E-11	2.13E-13	2.23E-10	8.41E-10	7.08E-10	8.24E-12	1.60E-09
27	7.59E-13	6.92E-12	2.15E-11	4.58E-12	5.40E-11	4.70E-10	1.64E-11	4.23E-10	1.09E-10
28	1.63E-13	3.33E-13	2.97E-12	7.41E-12	1.62E-14	9.59E-11	2.28E-10	7.30E-10	1.83E-10
29	1.82E-14	1.66E-12	1.61E-12	4.19E-12	2.52E-11	3.51E-12	6.09E-10	5.77E-10	7.56E-10
30	4.19E-13	6.25E-12	1.02E-11	1.04E-12	5.83E-11	1.04E-10	5.90E-10	2.41E-10	9.69E-10
31	1.02E-12	8.34E-12	1.31E-11	8.60E-14	6.44E-11	1.97E-10	3.04E-10	3.07E-11	7.17E-10
32	1.28E-12	6.13E-12	7.60E-12	1.34E-14	4.68E-11	1.89E-10	6.90E-11	8.31E-12	3.18E-10
33	9.77E-13	2.29E-12	1.30E-12	1.73E-13	2.30E-11	1.11E-10	2.94E-14	6.82E-11	5.78E-11
34	3.82E-13	7.03E-14	3.87E-13	8.79E-13	6.06E-12	3.56E-11	4.50E-11	1.07E-10	1.88E-12
35	1.28E-14	9.06E-13	4.22E-12	1.91E-12	6.94E-14	1.62E-12	1.20E-10	9.47E-11	5.89E-11
36	1.73E-13	3.59E-12	8.29E-12	2.32E-12	2.32E-12	7.10E-12	1.68E-10	5.36E-11	1.19E-10
37	7.49E-13	5.81E-12	9.09E-12	1.65E-12	7.71E-12	2.93E-11	1.64E-10	1.67E-11	1.31E-10
38	1.34E-12	6.06E-12	6.56E-12	4.71E-13	1.22E-11	4.66E-11	1.15E-10	6.68E-13	1.00E-10
39	1.53E-12	4.35E-12	2.78E-12	1.68E-14	1.37E-11	4.97E-11	5.13E-11	3.68E-12	5.55E-11
40	1.24E-12	1.96E-12	3.07E-13	1.01E-12	1.24E-11	4.00E-11	8.45E-12	1.44E-11	2.00E-11
41	6.72E-13	2.66E-13	3.44E-13	3.20E-12	9.38E-12	2.45E-11	1.61E-12	2.21E-11	2.57E-12
42	1.55E-13	1.77E-13	2.58E-12	5.53E-12	5.80E-12	1.04E-11	2.26E-11	2.24E-11	6.37E-13
43	1.16E-14	1.69E-12	5.80E-12	6.87E-12	2.62E-12	1.77E-12	5.08E-11	1.61E-11	6.80E-12
44	3.85E-13	3.94E-12	8.10E-12	6.29E-12	5.44E-13	2.61E-13	6.53E-11	7.22E-12	1.34E-11
45	1.01E-12	5.29E-12	7.83E-12	3.98E-12	1.36E-14	3.86E-12	5.70E-11	1.19E-12	1.45E-11
46	1.42E-12	5.01E-12	5.64E-12	1.67E-12	6.18E-13	7.85E-12	3.81E-11	7.46E-14	1.09E-11
47	1.63E-12	4.19E-12	3.51E-12	3.58E-13	1.78E-12	1.11E-11	2.40E-11	1.77E-12	7.02E-12
48	1.39E-12	2.56E-12	1.37E-12	9.51E-15	2.89E-12	1.15E-11	1.15E-11	4.09E-12	3.01E-12

Table C.4: Franck-Condon factors for transitions from $X^2\Pi$ SF²⁺ ($v' = 0 - 48$) to $X^3\Sigma^-$ SF⁺ ($v'' = 0 - 8$).

$v' \backslash v''$	9	10	11	12	13	14	15
0	4.24E-06	7.89E-07	2.66E-07	1.61E-07	1.02E-07	4.77E-08	1.22E-08
1	1.89E-04	4.21E-05	9.82E-06	2.84E-06	1.12E-06	5.36E-07	2.41E-07
2	2.54E-03	7.17E-04	1.92E-04	5.14E-05	1.49E-05	5.05E-06	2.02E-06
3	1.67E-02	5.92E-03	1.93E-03	5.92E-04	1.77E-04	5.41E-05	1.78E-05
4	5.92E-02	2.76E-02	1.12E-02	4.14E-03	1.43E-03	4.72E-04	1.55E-04
5	1.08E-01	7.40E-02	3.99E-02	1.84E-02	7.60E-03	2.90E-03	1.06E-03
6	6.94E-02	1.00E-01	8.32E-02	5.17E-02	2.69E-02	1.23E-02	5.20E-03
7	4.15E-05	3.95E-02	8.45E-02	8.56E-02	6.13E-02	3.57E-02	1.82E-02
8	8.65E-02	6.81E-03	1.72E-02	6.44E-02	8.14E-02	6.75E-02	4.42E-02
9	4.94E-02	9.36E-02	2.08E-02	4.21E-03	4.38E-02	7.19E-02	6.96E-02
10	5.75E-02	2.50E-02	9.05E-02	3.65E-02	8.58E-06	2.58E-02	5.90E-02
11	1.25E-01	7.65E-02	9.16E-03	8.00E-02	5.01E-02	2.75E-03	1.21E-02
12	3.27E-01	9.49E-02	9.00E-02	1.44E-03	6.54E-02	5.93E-02	9.96E-03
13	9.51E-02	3.44E-01	7.09E-02	9.77E-02	1.91E-04	4.96E-02	6.35E-02
14	3.29E-03	1.08E-01	3.57E-01	5.27E-02	1.00E-01	3.47E-03	3.49E-02
15	1.16E-04	3.19E-03	1.20E-01	3.70E-01	3.94E-02	9.83E-02	9.39E-03
16	2.41E-05	2.46E-04	2.79E-03	1.30E-01	3.82E-01	3.01E-02	9.32E-02
17	1.05E-06	2.93E-05	4.62E-04	2.12E-03	1.37E-01	3.95E-01	2.41E-02
18	5.61E-08	2.40E-06	3.07E-05	7.91E-04	1.28E-03	1.42E-01	4.09E-01
19	4.35E-08	8.05E-08	5.09E-06	2.62E-05	1.24E-03	4.70E-04	1.44E-01
20	3.00E-08	8.32E-08	6.35E-08	1.00E-05	1.52E-05	1.81E-03	1.26E-05
21	2.15E-08	3.65E-08	1.34E-07	8.84E-09	1.79E-05	2.63E-06	2.45E-03
22	6.47E-09	2.05E-08	4.24E-08	1.96E-07	5.19E-08	2.83E-05	3.96E-06
23	5.32E-13	5.65E-09	1.77E-08	5.64E-08	2.70E-07	5.83E-07	3.94E-05
24	3.54E-09	1.62E-11	4.85E-09	1.79E-08	9.08E-08	3.15E-07	2.45E-06
25	7.38E-09	4.17E-09	8.43E-13	5.34E-09	2.23E-08	1.57E-07	2.56E-07
26	6.44E-09	8.36E-09	3.39E-09	9.16E-11	6.51E-09	3.31E-08	2.58E-07
27	2.87E-09	7.45E-09	7.65E-09	2.14E-09	4.74E-10	7.63E-09	5.59E-08
28	3.77E-10	3.60E-09	7.61E-09	6.34E-09	1.17E-09	8.50E-10	9.98E-09
29	1.19E-10	6.45E-10	4.28E-09	7.55E-09	5.35E-09	5.59E-10	1.17E-09
30	9.56E-10	4.83E-11	1.12E-09	5.31E-09	7.69E-09	4.26E-09	2.54E-10
31	1.52E-09	9.22E-10	2.30E-12	2.11E-09	6.47E-09	7.57E-09	3.24E-09
32	1.37E-09	1.78E-09	5.54E-10	2.28E-10	3.45E-09	7.63E-09	6.77E-09
33	8.09E-10	1.86E-09	1.50E-09	1.49E-10	9.35E-10	5.04E-09	7.98E-09
34	2.81E-10	1.29E-09	1.92E-09	9.92E-10	6.55E-12	2.05E-09	6.42E-09
35	2.46E-11	5.82E-10	1.64E-09	1.71E-09	4.22E-10	2.97E-10	3.52E-09
36	2.42E-11	1.24E-10	9.84E-10	1.82E-09	1.30E-09	6.14E-11	1.08E-09
37	1.39E-10	4.73E-13	3.68E-10	1.39E-09	1.85E-09	7.32E-10	3.95E-11
38	2.35E-10	9.72E-11	4.36E-11	7.76E-10	1.80E-09	1.54E-09	2.66E-10
39	2.53E-10	2.50E-10	1.96E-11	2.69E-10	1.30E-09	1.95E-09	1.06E-09
40	2.01E-10	3.46E-10	1.62E-10	2.36E-11	6.99E-10	1.82E-09	1.76E-09
41	1.22E-10	3.47E-10	3.20E-10	2.85E-11	2.37E-10	1.33E-09	2.03E-09
42	5.25E-11	2.75E-10	4.07E-10	1.80E-10	1.97E-11	7.24E-10	1.86E-09
43	1.11E-11	1.68E-10	3.97E-10	3.57E-10	3.14E-11	2.41E-10	1.36E-09
44	4.93E-14	6.78E-11	2.99E-10	4.50E-10	1.88E-10	1.43E-11	7.28E-10
45	8.14E-12	1.12E-11	1.65E-10	4.02E-10	3.43E-10	3.81E-11	2.28E-10
46	1.81E-11	2.54E-13	6.55E-11	2.78E-10	3.91E-10	1.58E-10	1.95E-11
47	2.52E-11	1.10E-11	1.67E-11	1.77E-10	3.92E-10	2.86E-10	1.65E-11
48	2.47E-11	2.55E-11	1.40E-13	8.22E-11	3.02E-10	3.39E-10	1.09E-10

Table C.5: Franck-Condon factors for transitions from $X^2\Pi$ SF²⁺ ($v' = 0 - 48$) to $X^3\Sigma^-$ SF⁺ ($v'' = 9 - 15$).

$v' \backslash v''$	16	17	18	19	20	21	22
0	5.72E-10	6.97E-10	1.76E-09	1.48E-09	1.15E-09	1.38E-12	2.16E-11
1	7.96E-08	1.27E-08	4.67E-13	3.75E-09	1.35E-11	2.30E-09	2.93E-11
2	8.46E-07	3.13E-07	8.03E-08	4.16E-07	1.01E-07	6.49E-09	1.02E-09
3	6.52E-06	2.55E-06	9.72E-07	5.14E-06	1.94E-06	3.68E-09	1.85E-07
4	5.22E-05	1.86E-05	7.05E-06	3.86E-05	1.64E-05	3.01E-07	2.60E-06
5	3.73E-04	1.32E-04	4.79E-05	2.27E-04	1.00E-04	2.73E-06	1.93E-05
6	2.06E-03	7.86E-04	2.95E-04	1.09E-03	5.00E-04	1.69E-05	1.06E-04
7	8.40E-03	3.62E-03	1.48E-03	4.13E-03	2.04E-03	9.32E-05	4.79E-04
8	2.48E-02	1.25E-02	5.81E-03	1.22E-02	6.66E-03	4.56E-04	1.81E-03
9	5.11E-02	3.15E-02	1.73E-02	2.71E-02	1.69E-02	1.87E-03	5.57E-03
10	6.75E-02	5.56E-02	3.77E-02	4.38E-02	3.25E-02	6.19E-03	1.38E-02
11	4.46E-02	6.16E-02	5.74E-02	4.67E-02	4.48E-02	1.62E-02	2.66E-02
12	3.67E-03	3.07E-02	5.29E-02	2.56E-02	3.93E-02	3.25E-02	3.84E-02
13	1.91E-02	1.91E-04	1.86E-02	1.49E-03	1.50E-02	4.78E-02	3.82E-02
14	6.31E-02	2.83E-02	8.35E-04	1.16E-02	2.84E-05	4.65E-02	2.09E-02
15	2.25E-02	5.90E-02	3.59E-02	4.04E-02	1.88E-02	2.22E-02	1.90E-03
16	1.64E-02	1.29E-02	5.23E-02	2.84E-02	4.00E-02	4.40E-04	6.35E-03
17	8.59E-02	2.35E-02	6.24E-03	4.69E-05	1.92E-02	1.57E-02	2.95E-02
18	2.06E-02	7.74E-02	2.98E-02	3.16E-02	7.95E-04	4.47E-02	3.12E-02
19	4.25E-01	1.93E-02	6.81E-02	4.90E-02	3.60E-02	2.78E-02	5.70E-03
20	1.41E-01	4.43E-01	1.99E-02	9.18E-04	4.19E-02	5.68E-05	7.14E-03
21	3.52E-04	1.34E-01	4.63E-01	2.76E-02	3.01E-05	4.20E-02	3.94E-02
22	3.07E-03	2.03E-03	1.23E-01	2.54E-01	2.24E-02	4.05E-02	2.90E-02
23	5.08E-05	3.49E-03	5.60E-03	3.73E-01	2.76E-01	3.54E-02	1.36E-03
24	4.64E-05	1.91E-04	3.56E-03	1.51E-03	3.62E-01	5.23E-01	1.03E-02
25	7.07E-06	4.33E-05	4.82E-04	1.91E-02	1.05E-04	6.35E-02	3.38E-01
26	7.71E-08	1.59E-05	2.63E-05	1.43E-04	2.21E-02	3.02E-02	3.11E-01
27	3.80E-07	4.67E-08	2.90E-05	6.67E-04	9.49E-04	9.50E-04	1.56E-02
28	1.03E-07	4.56E-07	1.10E-06	1.20E-04	6.15E-04	2.29E-03	2.12E-02
29	1.57E-08	1.96E-07	3.67E-07	1.20E-06	2.60E-04	1.06E-04	5.84E-03
30	1.72E-09	3.20E-08	3.39E-07	8.27E-06	2.02E-06	3.93E-05	9.15E-05
31	5.21E-11	3.02E-09	7.47E-08	1.63E-06	9.17E-06	2.86E-05	6.02E-04
32	2.22E-09	8.96E-14	8.07E-09	6.66E-09	4.16E-06	2.00E-06	1.07E-04
33	5.72E-09	1.29E-09	1.34E-10	7.60E-08	2.66E-07	2.25E-07	2.79E-07
34	7.75E-09	4.17E-09	7.47E-10	6.33E-08	3.52E-08	5.04E-07	9.85E-06
35	7.16E-09	6.80E-09	2.97E-09	2.63E-08	9.28E-08	1.82E-07	4.01E-06
36	4.81E-09	7.49E-09	5.42E-09	1.03E-08	5.12E-08	2.82E-08	3.21E-07
37	2.22E-09	6.02E-09	6.86E-09	4.39E-09	1.91E-08	1.03E-09	2.53E-08
38	4.94E-10	3.53E-09	6.60E-09	1.54E-09	6.53E-09	6.00E-10	1.05E-07
39	2.81E-12	1.35E-09	4.88E-09	1.40E-10	2.07E-09	2.36E-09	6.74E-08
40	4.72E-10	1.80E-10	2.64E-09	2.34E-10	3.70E-10	3.88E-09	2.55E-08
41	1.31E-09	6.12E-11	8.63E-10	1.48E-09	2.10E-11	5.15E-09	7.79E-09
42	1.99E-09	6.57E-10	4.85E-11	3.06E-09	7.38E-10	5.92E-09	2.19E-09
43	2.23E-09	1.53E-09	1.89E-10	4.19E-09	2.21E-09	5.75E-09	4.27E-10
44	1.92E-09	2.19E-09	9.30E-10	4.33E-09	3.65E-09	4.44E-09	7.08E-13
45	1.25E-09	2.21E-09	1.64E-09	3.40E-09	4.05E-09	2.48E-09	3.93E-10
46	6.29E-10	1.71E-09	1.88E-09	2.10E-09	3.38E-09	9.64E-10	1.12E-09
47	2.60E-10	1.24E-09	1.95E-09	1.14E-09	2.62E-09	2.19E-10	1.92E-09
48	4.77E-11	6.74E-10	1.57E-09	3.76E-10	1.56E-09	2.10E-13	2.28E-09

Table C.6: Franck-Condon factors for transitions from $X^2\Pi SF^{2+}$ ($v' = 0 - 48$) to $X^3\Sigma^- SF^+$ ($v'' = 16 - 22$).

$v' \setminus v''$	23	24	25	26	27	28	29
0	1.36E-10	9.50E-11	3.20E-11	2.73E-12	1.04E-12	4.28E-12	3.48E-12
1	4.43E-12	2.77E-10	4.78E-10	4.06E-10	2.16E-10	6.59E-11	4.80E-12
2	2.43E-09	1.75E-10	2.52E-10	1.03E-09	1.25E-09	8.49E-10	3.32E-10
3	6.44E-09	4.94E-09	1.53E-09	2.84E-11	4.04E-10	1.11E-09	1.25E-09
4	2.76E-09	2.29E-09	6.58E-09	5.13E-09	1.68E-09	3.67E-11	5.17E-10
5	2.74E-07	4.90E-08	1.61E-09	2.38E-09	5.30E-09	3.30E-09	5.95E-10
6	2.57E-06	8.99E-07	2.61E-07	5.30E-08	4.25E-09	2.51E-10	1.64E-09
7	1.55E-05	6.36E-06	2.53E-06	9.29E-07	2.96E-07	7.32E-08	1.09E-08
8	7.98E-05	3.40E-05	1.46E-05	6.25E-06	2.58E-06	9.90E-07	3.38E-07
9	3.62E-04	1.59E-04	7.01E-05	3.13E-05	1.40E-05	6.21E-06	2.67E-06
10	1.41E-03	6.48E-04	2.97E-04	1.36E-04	6.31E-05	2.95E-05	1.38E-05
11	4.52E-03	2.25E-03	1.09E-03	5.24E-04	2.52E-04	1.21E-04	5.90E-05
12	1.18E-02	6.46E-03	3.40E-03	1.74E-03	8.80E-04	4.42E-04	2.22E-04
13	2.45E-02	1.51E-02	8.80E-03	4.90E-03	2.65E-03	1.41E-03	7.41E-04
14	3.89E-02	2.81E-02	1.86E-02	1.15E-02	6.76E-03	3.85E-03	2.15E-03
15	4.44E-02	4.00E-02	3.11E-02	2.18E-02	1.43E-02	8.91E-03	5.36E-03
16	3.09E-02	4.00E-02	3.94E-02	3.30E-02	2.47E-02	1.72E-02	1.13E-02
17	7.12E-03	2.28E-02	3.42E-02	3.72E-02	3.36E-02	2.69E-02	1.98E-02
18	1.99E-03	2.72E-03	1.54E-02	2.78E-02	3.36E-02	3.28E-02	2.80E-02
19	2.59E-02	5.18E-03	4.47E-04	9.25E-03	2.11E-02	2.89E-02	3.07E-02
20	3.98E-02	2.92E-02	9.05E-03	6.28E-05	4.59E-03	1.48E-02	2.34E-02
21	1.45E-02	3.55E-02	3.11E-02	1.30E-02	1.19E-03	1.57E-03	9.32E-03
22	2.36E-03	9.60E-03	3.06E-02	3.14E-02	1.66E-02	3.37E-03	1.57E-04
23	4.50E-02	4.14E-03	5.89E-03	2.55E-02	3.05E-02	1.94E-02	6.14E-03
24	2.41E-02	4.55E-02	5.98E-03	3.24E-03	2.06E-02	2.86E-02	2.13E-02
25	6.26E-02	1.69E-02	4.57E-02	7.71E-03	1.49E-03	1.60E-02	2.58E-02
26	5.44E-01	8.30E-02	1.07E-02	4.56E-02	9.27E-03	4.85E-04	1.19E-02
27	1.99E-02	5.42E-01	1.08E-01	5.65E-03	4.54E-02	1.07E-02	4.77E-05
28	5.13E-02	5.51E-03	5.29E-01	1.37E-01	2.11E-03	4.48E-02	1.20E-02
29	4.07E-04	5.81E-02	9.24E-06	5.04E-01	1.70E-01	2.60E-04	4.39E-02
30	2.82E-03	2.86E-03	5.97E-02	4.79E-03	4.69E-01	2.04E-01	1.75E-04
31	8.49E-04	2.23E-03	7.91E-03	5.51E-02	1.92E-02	4.27E-01	2.37E-01
32	1.43E-06	1.48E-03	1.17E-03	1.52E-02	4.52E-02	4.05E-02	3.83E-01
33	4.76E-05	6.95E-05	2.07E-03	2.04E-04	2.36E-02	3.22E-02	6.42E-02
34	2.09E-05	3.18E-05	2.98E-04	2.34E-03	1.34E-04	3.10E-02	1.90E-02
35	1.33E-06	3.66E-05	5.15E-06	7.23E-04	2.08E-03	1.67E-03	3.57E-02
36	2.33E-07	6.87E-06	4.57E-05	1.14E-05	1.27E-03	1.33E-03	5.00E-03
37	5.45E-07	2.32E-08	1.85E-05	3.67E-05	1.20E-04	1.74E-03	4.67E-04
38	2.39E-07	4.97E-07	1.55E-06	3.36E-05	1.20E-05	3.84E-04	1.93E-03
39	4.72E-08	4.47E-07	1.38E-07	7.46E-06	4.28E-05	1.37E-06	7.81E-04
40	2.82E-09	1.50E-07	5.70E-07	1.39E-07	1.90E-05	3.60E-05	5.63E-05
41	4.68E-10	2.33E-08	3.39E-07	3.93E-07	2.38E-06	3.28E-05	1.48E-05
42	2.64E-09	3.83E-10	9.39E-08	5.44E-07	3.07E-08	9.03E-06	4.09E-05
43	4.21E-09	1.61E-09	9.99E-09	2.46E-07	5.77E-07	3.90E-07	2.00E-05
44	5.25E-09	3.83E-09	1.18E-10	4.95E-08	4.51E-07	3.16E-07	2.82E-06
45	5.47E-09	4.61E-09	2.83E-09	2.33E-09	1.44E-07	5.74E-07	7.77E-09
46	4.77E-09	4.60E-09	3.95E-09	7.42E-10	2.32E-08	3.00E-07	4.46E-07
47	4.07E-09	4.71E-09	4.39E-09	3.11E-09	8.63E-10	1.02E-07	4.84E-07
48	2.75E-09	4.03E-09	4.08E-09	3.89E-09	9.88E-10	1.73E-08	2.37E-07

Table C.7: Franck-Condon factors for transitions from $X^2\Pi$ SF $^{2+}$ ($v' = 0 - 48$) to $X^3\Sigma^-$ SF $^{+}$ ($v'' = 23 - 29$).

$v' \setminus v''$	30	31	32	33	34	35	36
0	1.08E-12	2.46E-14	1.73E-13	3.02E-13	1.00E-13	1.93E-14	4.00E-13
1	5.09E-12	2.57E-11	4.10E-11	4.35E-11	3.58E-11	2.40E-11	1.29E-11
2	4.43E-11	7.75E-12	7.82E-11	1.31E-10	1.28E-10	8.78E-11	4.36E-11
3	8.87E-10	4.30E-10	1.30E-10	1.36E-11	2.61E-12	2.11E-11	3.31E-11
4	1.66E-09	2.25E-09	2.05E-09	1.40E-09	7.29E-10	2.71E-10	5.33E-11
5	1.10E-10	1.43E-09	2.88E-09	3.39E-09	2.92E-09	1.98E-09	1.07E-09
6	1.04E-09	8.62E-11	2.50E-10	1.28E-09	2.28E-09	2.68E-09	2.46E-09
7	2.45E-10	4.26E-10	6.05E-10	1.41E-10	4.08E-11	5.49E-10	1.29E-09
8	9.50E-08	1.92E-08	1.85E-09	3.52E-12	2.22E-10	1.05E-10	3.89E-12
9	1.09E-06	4.07E-07	1.35E-07	3.81E-08	8.45E-09	1.29E-09	1.11E-10
10	6.42E-06	2.93E-06	1.30E-06	5.47E-07	2.17E-07	8.07E-08	2.78E-08
11	2.90E-05	1.43E-05	7.06E-06	3.46E-06	1.67E-06	7.91E-07	3.67E-07
12	1.13E-04	5.77E-05	2.99E-05	1.56E-05	8.20E-06	4.32E-06	2.28E-06
13	3.89E-04	2.06E-04	1.10E-04	5.93E-05	3.24E-05	1.80E-05	1.01E-05
14	1.19E-03	6.52E-04	3.60E-04	2.00E-04	1.13E-04	6.42E-05	3.72E-05
15	3.14E-03	1.82E-03	1.05E-03	6.03E-04	3.49E-04	2.05E-04	1.22E-04
16	7.14E-03	4.40E-03	2.67E-03	1.61E-03	9.69E-04	5.86E-04	3.58E-04
17	1.37E-02	9.14E-03	5.92E-03	3.77E-03	2.37E-03	1.49E-03	9.42E-04
18	2.19E-02	1.60E-02	1.12E-02	7.63E-03	5.09E-03	3.35E-03	2.20E-03
19	2.81E-02	2.32E-02	1.80E-02	1.32E-02	9.43E-03	6.57E-03	4.52E-03
20	2.74E-02	2.69E-02	2.36E-02	1.93E-02	1.49E-02	1.11E-02	8.09E-03
21	1.78E-02	2.31E-02	2.45E-02	2.29E-02	1.97E-02	1.60E-02	1.25E-02
22	4.97E-03	1.24E-02	1.82E-02	2.11E-02	2.10E-02	1.91E-02	1.63E-02
23	1.66E-04	1.96E-03	7.60E-03	1.33E-02	1.69E-02	1.81E-02	1.74E-02
24	9.06E-03	1.31E-03	3.39E-04	3.84E-03	8.59E-03	1.24E-02	1.43E-02
25	2.21E-02	1.17E-02	3.23E-03	3.95E-05	1.32E-03	4.65E-03	7.97E-03
26	2.25E-02	2.19E-02	1.39E-02	5.56E-03	8.55E-04	1.19E-04	1.81E-03
27	8.43E-03	1.89E-02	2.08E-02	1.54E-02	7.91E-03	2.48E-03	1.80E-04
28	4.63E-05	5.53E-03	1.52E-02	1.89E-02	1.59E-02	9.92E-03	4.53E-03
29	1.33E-02	3.73E-04	3.25E-03	1.15E-02	1.63E-02	1.55E-02	1.13E-02
30	4.21E-02	1.47E-02	9.53E-04	1.59E-03	8.08E-03	1.32E-02	1.41E-02
31	1.66E-03	3.91E-02	1.65E-02	1.76E-03	5.29E-04	5.08E-03	9.88E-03
32	2.70E-01	4.20E-03	3.44E-02	1.87E-02	2.83E-03	4.24E-05	2.65E-03
33	3.42E-01	2.99E-01	6.85E-03	2.75E-02	2.13E-02	4.32E-03	9.29E-05
34	8.54E-02	3.09E-01	3.25E-01	8.34E-03	1.87E-02	2.37E-02	6.48E-03
35	8.50E-03	9.97E-02	2.89E-01	3.46E-01	7.30E-03	9.36E-03	2.46E-02
36	3.69E-02	2.15E-03	1.04E-01	2.87E-01	3.58E-01	3.41E-03	2.18E-03
37	9.59E-03	3.45E-02	1.88E-05	9.79E-02	3.09E-01	3.53E-01	3.03E-06
38	5.86E-06	1.44E-02	3.00E-02	9.82E-04	8.02E-02	3.60E-01	3.16E-01
39	1.71E-03	3.51E-04	1.82E-02	2.49E-02	3.62E-03	5.28E-02	4.42E-01
40	1.20E-03	1.18E-03	1.54E-03	2.04E-02	2.07E-02	7.15E-03	2.16E-02
41	2.17E-04	1.50E-03	5.84E-04	3.24E-03	2.09E-02	1.87E-02	1.21E-02
42	3.57E-08	4.74E-04	1.60E-03	1.74E-04	4.85E-03	1.97E-02	2.07E-02
43	3.71E-05	1.90E-05	7.55E-04	1.51E-03	1.75E-05	5.82E-03	1.65E-02
44	3.11E-05	2.30E-05	7.98E-05	9.65E-04	1.31E-03	3.61E-07	6.16E-03
45	8.06E-06	3.66E-05	6.52E-06	1.69E-04	1.05E-03	1.00E-03	2.99E-09
46	5.27E-07	1.59E-05	3.22E-05	4.95E-07	2.82E-04	1.04E-03	6.09E-04
47	1.06E-07	3.55E-06	2.57E-05	2.11E-05	2.18E-05	4.36E-04	1.02E-03
48	4.39E-07	1.13E-07	9.04E-06	2.79E-05	5.98E-06	6.31E-05	5.42E-04

Table C.8: Franck-Condon factors for transitions from $X^2\Pi$ SF²⁺ ($v' = 0 - 48$) to $X^3\Sigma^-$ SF⁺ ($v'' = 30 - 36$).

$v' \setminus v''$	37	38	39	40	41	42	43
0	1.09E-12	1.68E-12	1.91E-12	1.76E-12	1.41E-12	9.70E-13	5.28E-13
1	5.14E-12	1.14E-12	7.23E-15	4.04E-13	1.19E-12	1.69E-12	1.43E-12
2	1.39E-11	1.56E-12	4.06E-13	3.49E-12	6.38E-12	7.33E-12	5.50E-12
3	3.27E-11	2.54E-11	1.70E-11	1.03E-11	5.91E-12	3.23E-12	1.51E-12
4	4.21E-14	2.20E-11	5.84E-11	8.18E-11	8.63E-11	7.57E-11	4.94E-11
5	4.39E-10	1.17E-10	8.93E-12	6.00E-12	3.28E-11	5.16E-11	4.48E-11
6	1.88E-09	1.24E-09	7.25E-10	3.76E-10	1.75E-10	7.29E-11	2.50E-11
7	1.84E-09	2.02E-09	1.87E-09	1.54E-09	1.15E-09	7.98E-10	4.45E-10
8	2.34E-10	6.91E-10	1.12E-09	1.36E-09	1.36E-09	1.17E-09	7.61E-10
9	1.01E-11	2.54E-11	1.08E-10	2.49E-10	3.82E-10	4.38E-10	3.42E-10
10	8.99E-09	2.81E-09	9.29E-10	3.73E-10	2.02E-10	1.39E-10	8.92E-11
11	1.67E-07	7.51E-08	3.37E-08	1.53E-08	7.17E-09	3.46E-09	1.52E-09
12	1.21E-06	6.39E-07	3.41E-07	1.84E-07	1.00E-07	5.49E-08	2.63E-08
13	5.73E-06	3.30E-06	1.92E-06	1.13E-06	6.70E-07	3.95E-07	2.00E-07
14	2.20E-05	1.32E-05	8.00E-06	4.93E-06	3.06E-06	1.88E-06	9.79E-07
15	7.35E-05	4.51E-05	2.81E-05	1.78E-05	1.13E-05	7.07E-06	3.75E-06
16	2.21E-04	1.38E-04	8.79E-05	5.65E-05	3.65E-05	2.31E-05	1.24E-05
17	5.98E-04	3.83E-04	2.48E-04	1.62E-04	1.06E-04	6.79E-05	3.67E-05
18	1.44E-03	9.51E-04	6.30E-04	4.19E-04	2.78E-04	1.81E-04	9.82E-05
19	3.09E-03	2.10E-03	1.43E-03	9.74E-04	6.58E-04	4.33E-04	2.38E-04
20	5.79E-03	4.10E-03	2.89E-03	2.02E-03	1.39E-03	9.29E-04	5.16E-04
21	9.45E-03	7.01E-03	5.12E-03	3.69E-03	2.61E-03	1.78E-03	1.00E-03
22	1.32E-02	1.04E-02	7.94E-03	5.93E-03	4.32E-03	3.01E-03	1.72E-03
23	1.55E-02	1.31E-02	1.06E-02	8.27E-03	6.24E-03	4.46E-03	2.59E-03
24	1.46E-02	1.36E-02	1.19E-02	9.82E-03	7.74E-03	5.72E-03	3.40E-03
25	1.02E-02	1.11E-02	1.07E-02	9.63E-03	8.05E-03	6.21E-03	3.80E-03
26	4.21E-03	6.18E-03	7.23E-03	7.34E-03	6.69E-03	5.49E-03	3.49E-03
27	2.75E-04	1.51E-03	2.86E-03	3.75E-03	4.01E-03	3.64E-03	2.47E-03
28	1.27E-03	7.21E-05	1.56E-04	7.27E-04	1.24E-03	1.44E-03	1.12E-03
29	6.54E-03	2.99E-03	9.72E-04	1.52E-04	1.55E-06	9.16E-05	1.47E-04
30	1.17E-02	8.04E-03	4.77E-03	2.46E-03	1.11E-03	4.27E-04	1.30E-04
31	1.18E-02	1.09E-02	8.58E-03	5.98E-03	3.81E-03	2.24E-03	1.09E-03
32	6.53E-03	8.90E-03	9.13E-03	7.90E-03	6.07E-03	4.23E-03	2.36E-03
33	9.69E-04	3.55E-03	5.69E-03	6.47E-03	6.03E-03	4.84E-03	2.98E-03
34	6.73E-04	1.18E-04	1.35E-03	2.78E-03	3.56E-03	3.48E-03	2.42E-03
35	9.64E-03	1.92E-03	8.17E-05	1.92E-04	7.97E-04	1.23E-03	1.07E-03
36	2.17E-02	1.36E-02	4.24E-03	8.78E-04	6.35E-05	2.31E-05	1.01E-04
37	3.64E-05	1.34E-02	1.60E-02	7.94E-03	2.88E-03	9.01E-04	2.33E-04
38	8.20E-03	1.76E-03	3.35E-03	1.22E-02	1.07E-02	6.00E-03	2.55E-03
39	2.29E-01	4.53E-02	7.94E-04	6.11E-05	2.94E-03	6.27E-03	4.92E-03
40	5.42E-01	9.67E-02	1.09E-01	4.34E-03	6.64E-04	1.53E-04	1.29E-04
41	9.85E-04	5.94E-01	9.81E-04	1.24E-01	4.85E-02	4.86E-03	3.30E-05
42	2.07E-02	1.18E-02	4.76E-01	1.04E-01	2.04E-02	6.94E-02	3.90E-02
43	3.12E-02	3.85E-02	5.30E-02	1.74E-01	2.81E-01	6.71E-02	1.32E-03
44	9.37E-03	6.25E-02	7.01E-02	5.93E-02	6.40E-04	1.08E-01	1.21E-01
45	7.41E-03	5.03E-04	1.39E-01	9.17E-02	6.52E-03	3.40E-02	3.49E-03
46	4.14E-05	1.31E-02	1.03E-02	2.44E-01	3.90E-02	2.05E-02	8.01E-04
47	4.12E-04	1.74E-04	2.24E-02	4.84E-02	2.43E-01	5.35E-03	1.05E-02
48	6.72E-04	5.47E-04	4.32E-04	4.53E-02	1.50E-01	1.52E-01	6.06E-02

Table C.9: Franck-Condon factors for transitions from $X^2\Pi$ SF²⁺ ($v' = 0 - 48$) to $X^3\Sigma^-$ SF⁺ ($v'' = 37 - 43$).

$v' \setminus v''$	0	1	2	3	4	5	6
0	8.00E-20	5.66E-18	9.30E-17	6.23E-16	2.97E-15	1.16E-14	3.63E-14
1	5.96E-18	3.70E-16	5.95E-15	3.79E-14	1.74E-13	6.63E-13	2.00E-12
2	2.09E-16	1.17E-14	1.83E-13	1.12E-12	4.94E-12	1.82E-11	5.31E-11
3	4.61E-15	2.38E-13	3.62E-12	2.12E-11	9.05E-11	3.22E-10	9.08E-10
4	7.36E-14	3.56E-12	5.21E-11	2.94E-10	1.21E-09	4.13E-09	1.12E-08
5	9.09E-13	4.15E-11	5.84E-10	3.17E-09	1.24E-08	4.09E-08	1.07E-07
6	9.10E-12	3.93E-10	5.30E-09	2.75E-08	1.03E-07	3.25E-07	8.15E-07
7	7.64E-11	3.12E-09	4.01E-08	1.98E-07	7.10E-07	2.13E-06	5.10E-06
8	5.48E-10	2.11E-08	2.57E-07	1.21E-06	4.10E-06	1.17E-05	2.66E-05
9	3.42E-09	1.24E-07	1.42E-06	6.33E-06	2.03E-05	5.45E-05	1.17E-04
10	1.88E-08	6.33E-07	6.85E-06	2.87E-05	8.60E-05	2.17E-04	4.40E-04
11	9.18E-08	2.86E-06	2.89E-05	1.13E-04	3.16E-04	7.43E-04	1.41E-03
12	4.02E-07	1.15E-05	1.08E-04	3.93E-04	1.01E-03	2.20E-03	3.84E-03
13	1.59E-06	4.15E-05	3.58E-04	1.20E-03	2.82E-03	5.58E-03	8.89E-03
14	5.71E-06	1.34E-04	1.06E-03	3.22E-03	6.83E-03	1.21E-02	1.74E-02
15	1.87E-05	3.93E-04	2.79E-03	7.60E-03	1.43E-02	2.24E-02	2.80E-02
16	5.65E-05	1.04E-03	6.54E-03	1.57E-02	2.56E-02	3.43E-02	3.61E-02
17	1.57E-04	2.50E-03	1.37E-02	2.84E-02	3.88E-02	4.23E-02	3.50E-02
18	4.05E-04	5.47E-03	2.55E-02	4.41E-02	4.80E-02	3.94E-02	2.21E-02
19	9.75E-04	1.09E-02	4.18E-02	5.78E-02	4.62E-02	2.38E-02	5.34E-03
20	2.20E-03	1.98E-02	6.02E-02	6.18E-02	3.06E-02	5.37E-03	6.95E-04
21	4.69E-03	3.27E-02	7.48E-02	5.05E-02	9.57E-03	9.75E-04	1.48E-02
22	9.45E-03	4.92E-02	7.80E-02	2.68E-02	3.42E-05	1.72E-02	3.15E-02
23	1.80E-02	6.69E-02	6.51E-02	4.85E-03	1.27E-02	3.69E-02	2.72E-02
24	3.25E-02	8.10E-02	3.85E-02	1.78E-03	3.61E-02	3.42E-02	6.57E-03
25	5.46E-02	8.45E-02	1.10E-02	2.13E-02	4.31E-02	1.08E-02	1.85E-03
26	8.44E-02	7.13E-02	7.33E-05	4.45E-02	2.26E-02	5.99E-04	2.16E-02
27	1.18E-01	4.20E-02	1.53E-02	4.40E-02	9.20E-04	2.05E-02	2.92E-02
28	1.45E-01	1.05E-02	4.47E-02	1.74E-02	1.16E-02	3.57E-02	8.28E-03
29	1.54E-01	9.41E-04	5.77E-02	1.97E-05	4.00E-02	1.61E-02	2.69E-03
30	1.40E-01	2.89E-02	3.62E-02	2.24E-02	3.65E-02	3.42E-04	2.74E-02
31	1.07E-01	8.04E-02	4.58E-03	5.64E-02	5.12E-03	2.61E-02	2.61E-02
32	6.86E-02	1.19E-01	8.43E-03	4.76E-02	1.03E-02	4.11E-02	8.56E-04
33	3.64E-02	1.20E-01	5.57E-02	8.30E-03	5.24E-02	1.01E-02	1.91E-02
34	1.57E-02	8.95E-02	1.03E-01	8.46E-03	5.24E-02	7.35E-03	4.16E-02
35	5.43E-03	5.06E-02	1.10E-01	6.51E-02	8.80E-03	5.20E-02	1.07E-02
36	1.49E-03	2.19E-02	7.99E-02	1.17E-01	1.15E-02	5.05E-02	8.78E-03
37	3.31E-04	7.29E-03	4.19E-02	1.15E-01	7.72E-02	5.50E-03	5.55E-02
38	5.90E-05	1.91E-03	1.64E-02	7.53E-02	1.27E-01	1.83E-02	4.67E-02
39	7.99E-06	4.07E-04	4.96E-03	3.53E-02	1.14E-01	8.88E-02	2.44E-03
40	1.04E-06	6.96E-05	1.21E-03	1.25E-02	6.84E-02	1.28E-01	2.53E-02
41	1.68E-07	9.94E-06	2.43E-04	3.55E-03	2.99E-02	1.04E-01	9.07E-02
42	5.88E-09	1.62E-06	4.24E-05	8.45E-04	1.03E-02	5.79E-02	1.13E-01
43	1.31E-10	2.42E-07	8.52E-06	2.01E-04	3.27E-03	2.65E-02	8.91E-02
44	4.84E-09	3.64E-08	2.53E-06	6.44E-05	1.20E-03	1.24E-02	6.11E-02
45	7.24E-11	5.52E-08	1.07E-06	2.91E-05	5.71E-04	6.78E-03	4.36E-02
46	8.88E-11	1.88E-08	4.66E-07	1.04E-05	2.26E-04	3.16E-03	2.66E-02
47	9.43E-10	1.47E-09	8.89E-09	4.76E-07	1.92E-05	5.14E-04	7.63E-03
48	5.10E-10	5.23E-10	7.93E-08	7.78E-07	4.67E-06	4.83E-07	6.11E-04

Table C.10: Franck-Condon factors for transitions from $X^2\Pi SF^{2+}$ ($v' = 0 - 48$) to $B^3\Delta SF^+$ ($v'' = 0 - 6$).

$v' \setminus v''$	7	8	9	10	11	12
0	9.20E-14	1.96E-13	3.54E-13	5.56E-13	7.57E-13	7.78E-13
1	4.92E-12	1.02E-11	1.81E-11	2.78E-11	3.73E-11	3.78E-11
2	1.27E-10	2.57E-10	4.44E-10	6.67E-10	8.80E-10	8.81E-10
3	2.10E-09	4.14E-09	6.97E-09	1.03E-08	1.33E-08	1.31E-08
4	2.52E-08	4.80E-08	7.87E-08	1.13E-07	1.43E-07	1.39E-07
5	2.31E-07	4.27E-07	6.80E-07	9.51E-07	1.18E-06	1.13E-06
6	1.69E-06	3.01E-06	4.65E-06	6.32E-06	7.66E-06	7.17E-06
7	1.01E-05	1.74E-05	2.58E-05	3.41E-05	4.03E-05	3.69E-05
8	5.05E-05	8.27E-05	1.18E-04	1.51E-04	1.73E-04	1.55E-04
9	2.11E-04	3.29E-04	4.52E-04	5.54E-04	6.14E-04	5.35E-04
10	7.46E-04	1.10E-03	1.44E-03	1.69E-03	1.80E-03	1.52E-03
11	2.23E-03	3.09E-03	3.81E-03	4.26E-03	4.35E-03	3.54E-03
12	5.63E-03	7.27E-03	8.37E-03	8.80E-03	8.51E-03	6.63E-03
13	1.19E-02	1.41E-02	1.50E-02	1.46E-02	1.32E-02	9.70E-03
14	2.08E-02	2.21E-02	2.11E-02	1.86E-02	1.53E-02	1.04E-02
15	2.92E-02	2.68E-02	2.21E-02	1.69E-02	1.20E-02	7.13E-03
16	3.11E-02	2.31E-02	1.50E-02	8.68E-03	4.49E-03	1.87E-03
17	2.24E-02	1.11E-02	4.04E-03	8.20E-04	6.25E-06	1.73E-04
18	7.46E-03	8.06E-04	2.88E-04	2.25E-03	4.17E-03	4.33E-03
19	1.58E-05	3.69E-03	8.78E-03	1.14E-02	1.12E-02	8.17E-03
20	9.32E-03	1.69E-02	1.80E-02	1.44E-02	9.59E-03	4.98E-03
21	2.45E-02	2.16E-02	1.29E-02	5.42E-03	1.43E-03	1.23E-04
22	2.37E-02	9.19E-03	1.16E-03	2.22E-04	2.17E-03	3.31E-03
23	6.54E-03	3.67E-05	4.54E-03	9.68E-03	1.12E-02	8.45E-03
24	1.19E-03	1.18E-02	1.76E-02	1.52E-02	9.45E-03	4.18E-03
25	1.81E-02	2.26E-02	1.35E-02	4.37E-03	4.07E-04	1.11E-04
26	2.53E-02	9.67E-03	4.37E-04	1.54E-03	5.39E-03	6.24E-03
27	7.24E-03	4.44E-04	8.28E-03	1.34E-02	1.20E-02	6.88E-03
28	2.33E-03	1.62E-02	1.79E-02	9.65E-03	2.70E-03	1.82E-04
29	2.28E-02	1.87E-02	4.30E-03	3.87E-05	2.93E-03	4.90E-03
30	1.99E-02	1.01E-03	3.99E-03	1.17E-02	1.22E-02	7.35E-03
31	1.92E-04	1.14E-02	1.90E-02	1.15E-02	3.10E-03	1.34E-04
32	1.79E-02	2.35E-02	6.37E-03	2.89E-05	3.85E-03	6.21E-03
33	2.94E-02	2.84E-03	4.24E-03	1.41E-02	1.36E-02	6.83E-03
34	2.68E-03	1.18E-02	2.27E-02	1.12E-02	1.44E-03	1.66E-04
35	1.64E-02	2.98E-02	5.93E-03	9.55E-04	8.53E-03	9.87E-03
36	4.15E-02	3.89E-03	8.01E-03	2.05E-02	1.43E-02	4.43E-03
37	9.61E-03	1.51E-02	2.94E-02	9.17E-03	6.77E-07	2.98E-03
38	1.11E-02	4.11E-02	5.37E-03	4.67E-03	1.69E-02	1.36E-02
39	5.85E-02	9.48E-03	1.26E-02	2.89E-02	1.33E-02	1.37E-03
40	4.51E-02	1.09E-02	4.16E-02	9.11E-03	1.30E-03	9.23E-03
41	2.37E-03	5.72E-02	1.43E-02	6.74E-03	2.65E-02	1.71E-02
42	1.83E-02	4.93E-02	3.34E-03	3.83E-02	1.99E-02	1.14E-03
43	6.41E-02	9.17E-03	3.61E-02	2.78E-02	7.26E-05	8.34E-03
44	9.41E-02	3.26E-03	4.85E-02	1.84E-03	1.47E-02	2.06E-02
45	1.12E-01	4.39E-02	2.53E-02	1.15E-02	3.16E-02	9.70E-03
46	1.07E-01	1.19E-01	5.51E-06	4.86E-02	1.39E-02	8.20E-04
47	5.61E-02	1.45E-01	4.38E-02	3.45E-02	2.29E-03	2.05E-02
48	1.74E-02	1.22E-01	1.86E-01	2.91E-03	4.44E-02	1.10E-02

Table C.11: Franck-Condon factors for transitions from $X \ ^2\Pi \ SF^{2+}$ ($v' = 0 - 48$) to $B \ ^3\Delta \ SF^+$ ($v'' = 7 - 12$).

$v' \setminus v''$	0	1	2	3	4	5	6	7	8
0	3.41E-21	4.49E-20	3.56E-19	1.75E-18	5.67E-18	1.26E-17	2.36E-17	3.68E-17	5.44E-17
1	3.41E-19	4.28E-18	3.20E-17	1.49E-16	4.62E-16	1.01E-15	1.83E-15	2.82E-15	4.12E-15
2	1.61E-17	1.92E-16	1.36E-15	6.03E-15	1.80E-14	3.87E-14	6.78E-14	1.03E-13	1.49E-13
3	4.72E-16	5.39E-15	3.64E-14	1.55E-13	4.47E-13	9.42E-13	1.61E-12	2.42E-12	3.44E-12
4	1.02E-14	1.11E-13	7.13E-13	2.91E-12	8.10E-12	1.67E-11	2.78E-11	4.11E-11	5.76E-11
5	1.71E-13	1.77E-12	1.08E-11	4.23E-11	1.14E-10	2.28E-10	3.71E-10	5.39E-10	7.42E-10
6	2.33E-12	2.27E-11	1.32E-10	4.96E-10	1.29E-09	2.50E-09	3.97E-09	5.66E-09	7.66E-09
7	2.66E-11	2.45E-10	1.35E-09	4.84E-09	1.21E-08	2.27E-08	3.51E-08	4.90E-08	6.52E-08
8	2.60E-10	2.24E-09	1.17E-08	3.99E-08	9.54E-08	1.74E-07	2.61E-07	3.55E-07	4.63E-07
9	2.20E-09	1.77E-08	8.68E-08	2.81E-07	6.44E-07	1.13E-06	1.65E-06	2.19E-06	2.79E-06
10	1.63E-08	1.22E-07	5.60E-07	1.72E-06	3.74E-06	6.30E-06	8.89E-06	1.15E-05	1.43E-05
11	1.07E-07	7.35E-07	3.16E-06	9.10E-06	1.88E-05	3.04E-05	4.13E-05	5.18E-05	6.28E-05
12	6.22E-07	3.93E-06	1.57E-05	4.22E-05	8.25E-05	1.27E-04	1.65E-04	2.01E-04	2.36E-04
13	3.24E-06	1.87E-05	6.84E-05	1.71E-04	3.14E-04	4.57E-04	5.70E-04	6.66E-04	7.60E-04
14	1.52E-05	7.87E-05	2.63E-04	6.09E-04	1.04E-03	1.42E-03	1.69E-03	1.89E-03	2.07E-03
15	6.38E-05	2.95E-04	8.92E-04	1.88E-03	2.97E-03	3.78E-03	4.23E-03	4.51E-03	4.74E-03
16	2.41E-04	9.85E-04	2.65E-03	5.05E-03	7.24E-03	8.51E-03	8.89E-03	8.92E-03	8.90E-03
17	8.19E-04	2.90E-03	6.87E-03	1.16E-02	1.49E-02	1.59E-02	1.52E-02	1.42E-02	1.32E-02
18	2.50E-03	7.53E-03	1.53E-02	2.24E-02	2.52E-02	2.37E-02	2.03E-02	1.71E-02	1.46E-02
19	6.79E-03	1.70E-02	2.89E-02	3.55E-02	3.36E-02	2.67E-02	1.95E-02	1.41E-02	1.02E-02
20	1.64E-02	3.31E-02	4.50E-02	4.39E-02	3.24E-02	1.98E-02	1.09E-02	5.67E-03	2.77E-03
21	3.51E-02	5.40E-02	5.49E-02	3.83E-02	1.86E-02	6.33E-03	1.30E-03	3.34E-05	2.50E-04
22	6.55E-02	7.14E-02	4.78E-02	1.83E-02	2.61E-03	1.15E-04	2.27E-03	4.63E-03	6.28E-03
23	1.06E-01	7.19E-02	2.31E-02	9.36E-04	3.21E-03	1.00E-02	1.28E-02	1.25E-02	1.10E-02
24	1.45E-01	4.78E-02	1.33E-03	8.54E-03	2.15E-02	2.14E-02	1.51E-02	9.14E-03	4.97E-03
25	1.68E-01	1.28E-02	1.05E-02	3.49E-02	2.92E-02	1.33E-02	3.65E-03	3.48E-04	1.39E-04
26	1.61E-01	1.16E-03	4.80E-02	4.11E-02	1.08E-02	1.32E-04	2.18E-03	5.98E-03	8.45E-03
27	1.28E-01	3.66E-02	6.88E-02	1.41E-02	9.69E-04	1.22E-02	1.73E-02	1.56E-02	1.17E-02
28	8.39E-02	1.02E-01	4.19E-02	1.37E-03	2.62E-02	2.87E-02	1.62E-02	6.29E-03	1.39E-03
29	4.62E-02	1.50E-01	3.59E-03	3.58E-02	4.16E-02	1.30E-02	6.25E-04	1.26E-03	5.23E-03
30	2.18E-02	1.51E-01	1.46E-02	6.62E-02	1.46E-02	8.26E-04	1.15E-02	1.73E-02	1.65E-02
31	8.91E-03	1.15E-01	7.64E-02	4.15E-02	2.02E-03	2.69E-02	2.77E-02	1.55E-02	5.54E-03
32	3.03E-03	6.99E-02	1.34E-01	2.72E-03	3.89E-02	3.81E-02	1.01E-02	1.34E-04	2.59E-03
33	8.22E-04	3.44E-02	1.44E-01	1.75E-02	6.29E-02	9.46E-03	2.22E-03	1.43E-02	1.98E-02
34	1.91E-04	1.38E-02	1.12E-01	8.06E-02	3.23E-02	4.81E-03	2.91E-02	2.69E-02	1.33E-02
35	4.52E-05	4.62E-03	6.71E-02	1.32E-01	4.62E-04	4.27E-02	3.43E-02	7.36E-03	5.59E-05
36	9.21E-06	1.35E-03	3.24E-02	1.35E-01	2.43E-02	5.86E-02	6.72E-03	3.55E-03	1.75E-02
37	8.54E-07	3.48E-04	1.32E-02	1.00E-01	8.44E-02	2.69E-02	5.69E-03	3.00E-02	2.73E-02
38	1.26E-07	7.62E-05	4.65E-03	5.96E-02	1.25E-01	2.25E-04	4.01E-02	3.41E-02	7.23E-03
39	1.25E-07	1.53E-05	1.44E-03	2.98E-02	1.24E-01	2.04E-02	5.57E-02	8.65E-03	2.83E-03
40	5.11E-10	3.48E-06	4.05E-04	1.29E-02	9.45E-02	6.86E-02	3.18E-02	2.16E-03	2.69E-02
41	8.56E-09	5.69E-07	1.08E-04	4.93E-03	5.88E-02	1.03E-01	4.02E-03	2.69E-02	3.66E-02
42	1.27E-08	5.22E-08	2.58E-05	1.73E-03	3.11E-02	1.03E-01	3.54E-03	4.62E-02	1.83E-02
43	3.07E-10	3.68E-08	6.31E-06	6.08E-04	1.55E-02	8.38E-02	2.44E-02	3.99E-02	1.47E-03
44	8.27E-09	1.08E-08	2.50E-06	2.53E-04	8.53E-03	6.74E-02	5.28E-02	2.12E-02	3.82E-03
45	3.33E-09	1.09E-11	1.22E-06	1.38E-04	5.55E-03	6.05E-02	9.38E-02	3.87E-03	2.49E-02
46	3.67E-10	4.53E-09	3.98E-07	6.37E-05	3.22E-03	4.92E-02	1.38E-01	4.93E-03	5.25E-02
47	3.50E-09	2.61E-10	4.10E-08	8.34E-06	8.29E-04	2.25E-02	1.26E-01	5.24E-02	3.84E-02
48	2.27E-09	2.57E-09	2.04E-08	1.67E-07	4.78E-05	6.54E-03	9.73E-02	1.74E-01	3.74E-04

Table C.12: Franck-Condon factors for transitions from $X^2\Pi$ SF $^{2+}$ ($v' = 0 - 48$) to $C^3\Sigma^-$ SF $^+$ ($v'' = 0 - 8$).

$v' \setminus v''$	9	10	11	12	13	14	15
0	7.86E-17	1.04E-16	1.30E-16	1.55E-16	1.76E-16	1.90E-16	1.83E-16
1	5.80E-15	7.57E-15	9.43E-15	1.12E-14	1.26E-14	1.35E-14	1.30E-14
2	2.05E-13	2.65E-13	3.28E-13	3.86E-13	4.32E-13	4.58E-13	4.38E-13
3	4.66E-12	5.96E-12	7.29E-12	8.51E-12	9.48E-12	9.97E-12	9.47E-12
4	7.67E-11	9.70E-11	1.17E-10	1.36E-10	1.50E-10	1.57E-10	1.48E-10
5	9.74E-10	1.22E-09	1.46E-09	1.67E-09	1.83E-09	1.89E-09	1.77E-09
6	9.90E-09	1.22E-08	1.44E-08	1.64E-08	1.77E-08	1.82E-08	1.70E-08
7	8.28E-08	1.01E-07	1.17E-07	1.32E-07	1.41E-07	1.44E-07	1.33E-07
8	5.79E-07	6.92E-07	7.96E-07	8.81E-07	9.35E-07	9.42E-07	8.64E-07
9	3.42E-06	4.02E-06	4.55E-06	4.96E-06	5.21E-06	5.19E-06	4.72E-06
10	1.72E-05	1.98E-05	2.20E-05	2.37E-05	2.45E-05	2.42E-05	2.17E-05
11	7.36E-05	8.32E-05	9.09E-05	9.62E-05	9.80E-05	9.53E-05	8.49E-05
12	2.70E-04	2.98E-04	3.19E-04	3.31E-04	3.32E-04	3.18E-04	2.80E-04
13	8.43E-04	9.07E-04	9.48E-04	9.63E-04	9.47E-04	8.92E-04	7.74E-04
14	2.23E-03	2.32E-03	2.36E-03	2.34E-03	2.25E-03	2.08E-03	1.77E-03
15	4.89E-03	4.92E-03	4.84E-03	4.66E-03	4.36E-03	3.93E-03	3.29E-03
16	8.74E-03	8.41E-03	7.94E-03	7.35E-03	6.65E-03	5.82E-03	4.74E-03
17	1.22E-02	1.11E-02	9.88E-03	8.68E-03	7.48E-03	6.27E-03	4.91E-03
18	1.23E-02	1.02E-02	8.35E-03	6.75E-03	5.37E-03	4.17E-03	3.06E-03
19	7.34E-03	5.14E-03	3.51E-03	2.33E-03	1.50E-03	9.29E-04	5.40E-04
20	1.16E-03	3.54E-04	4.23E-05	1.03E-05	1.11E-04	2.44E-04	3.33E-04
21	9.94E-04	1.82E-03	2.50E-03	2.95E-03	3.15E-03	3.09E-03	2.72E-03
22	7.15E-03	7.31E-03	6.96E-03	6.30E-03	5.45E-03	4.51E-03	3.46E-03
23	8.95E-03	6.87E-03	5.01E-03	3.50E-03	2.33E-03	1.49E-03	8.82E-04
24	2.31E-03	8.13E-04	1.51E-04	4.11E-07	1.10E-04	3.00E-04	4.39E-04
25	1.14E-03	2.37E-03	3.37E-03	3.96E-03	4.14E-03	3.93E-03	3.35E-03
26	9.29E-03	8.84E-03	7.66E-03	6.20E-03	4.75E-03	3.45E-03	2.33E-03
27	7.59E-03	4.27E-03	2.04E-03	7.56E-04	1.68E-04	3.04E-06	3.55E-05
28	8.53E-06	5.38E-04	1.74E-03	2.87E-03	3.59E-03	3.81E-03	3.47E-03
29	8.42E-03	9.73E-03	9.42E-03	8.13E-03	6.45E-03	4.76E-03	3.22E-03
30	1.23E-02	7.61E-03	3.91E-03	1.57E-03	4.12E-04	2.56E-05	3.09E-05
31	7.78E-04	9.90E-05	1.42E-03	3.15E-03	4.40E-03	4.89E-03	4.53E-03
32	7.81E-03	1.11E-02	1.17E-02	1.03E-02	8.01E-03	5.65E-03	3.58E-03
33	1.72E-02	1.11E-02	5.57E-03	1.98E-03	3.48E-04	1.97E-06	2.18E-04
34	3.23E-03	1.76E-05	1.29E-03	3.91E-03	5.95E-03	6.72E-03	6.15E-03
35	5.29E-03	1.16E-02	1.41E-02	1.28E-02	9.73E-03	6.41E-03	3.67E-03
36	2.20E-02	1.68E-02	8.89E-03	3.10E-03	4.48E-04	3.27E-05	5.38E-04
37	1.18E-02	1.68E-03	2.89E-04	3.36E-03	6.65E-03	8.20E-03	7.67E-03
38	2.56E-04	7.33E-03	1.43E-02	1.56E-02	1.27E-02	8.37E-03	4.58E-03
39	1.81E-02	2.32E-02	1.66E-02	7.61E-03	1.90E-03	4.84E-05	3.34E-04
40	2.88E-02	1.28E-02	1.61E-03	5.19E-04	4.29E-03	7.64E-03	8.33E-03
41	1.15E-02	2.63E-06	6.00E-03	1.39E-02	1.58E-02	1.27E-02	7.92E-03
42	1.95E-05	1.11E-02	2.07E-02	1.80E-02	9.70E-03	3.19E-03	4.08E-04
43	1.05E-02	2.36E-02	1.74E-02	5.78E-03	2.80E-04	8.65E-04	3.13E-03
44	2.53E-02	1.95E-02	4.25E-03	1.39E-04	4.34E-03	8.49E-03	8.95E-03
45	2.97E-02	5.56E-03	9.74E-04	9.45E-03	1.40E-02	1.17E-02	6.76E-03
46	1.37E-02	1.69E-03	1.71E-02	2.03E-02	1.14E-02	3.17E-03	1.55E-04
47	5.01E-04	2.29E-02	2.39E-02	7.85E-03	1.14E-04	2.23E-03	5.72E-03
48	4.44E-02	2.54E-02	9.94E-04	3.75E-03	1.01E-02	1.04E-02	6.91E-03

Table C.13: Franck-Condon factors for transitions from $X \ ^2\Pi \ SF^{2+}$ ($v' = 0 - 48$) to $C \ ^3\Sigma^- \ SF^+$ ($v'' = 9 - 15$).

$v' \setminus v''$	0	1	2	3	4	5	6	7	8
0	5.06E-01	3.04E-01	1.23E-01	4.56E-02	1.57E-02	4.64E-03	1.02E-03	1.31E-04	3.27E-06
1	3.79E-01	4.82E-02	2.21E-01	1.88E-01	1.03E-01	4.29E-02	1.40E-02	3.56E-03	6.55E-04
2	1.02E-01	3.81E-01	1.15E-02	8.73E-02	1.73E-01	1.37E-01	7.04E-02	2.74E-02	8.52E-03
3	1.30E-02	2.21E-01	2.41E-01	8.31E-02	1.56E-02	1.23E-01	1.43E-01	9.26E-02	4.36E-02
4	9.11E-04	4.17E-02	3.08E-01	1.07E-01	1.33E-01	1.51E-04	7.14E-02	1.29E-01	1.06E-01
5	1.61E-05	3.55E-03	8.67E-02	3.34E-01	3.22E-02	1.45E-01	1.38E-02	3.13E-02	1.03E-01
6	4.06E-07	1.11E-04	8.79E-03	1.38E-01	3.17E-01	3.74E-03	1.34E-01	3.86E-02	7.60E-03
7	3.00E-07	1.62E-06	3.36E-04	1.67E-02	1.83E-01	2.85E-01	1.04E-03	1.10E-01	6.32E-02
8	1.83E-09	6.37E-08	1.60E-06	6.76E-04	2.62E-02	2.22E-01	2.49E-01	1.16E-02	8.12E-02
9	9.99E-08	1.57E-07	2.98E-07	1.27E-06	1.03E-03	3.62E-02	2.54E-01	2.14E-01	2.86E-02
10	7.23E-08	3.67E-07	6.75E-07	2.38E-06	1.87E-06	1.31E-03	4.64E-02	2.83E-01	1.81E-01
11	1.38E-09	8.99E-08	5.38E-07	1.28E-06	6.39E-06	5.71E-06	1.47E-03	5.68E-02	3.08E-01
12	1.51E-08	7.14E-09	4.33E-08	5.13E-07	1.71E-06	1.20E-05	1.81E-05	1.49E-03	6.70E-02
13	1.63E-08	6.52E-08	6.20E-08	2.68E-09	3.94E-07	2.15E-06	1.83E-05	5.09E-05	1.37E-03
14	1.82E-09	3.79E-08	1.41E-07	1.63E-07	7.75E-09	2.56E-07	2.51E-06	2.40E-05	1.22E-04
15	1.22E-09	1.44E-09	5.24E-08	2.10E-07	2.79E-07	6.02E-08	9.24E-08	2.92E-06	2.86E-05
16	3.35E-09	6.60E-09	1.49E-11	5.76E-08	2.94E-07	4.52E-07	1.81E-07	1.55E-08	4.18E-06
17	1.30E-09	1.19E-08	1.96E-08	5.35E-10	7.96E-08	4.13E-07	6.03E-07	2.70E-07	2.97E-09
18	6.64E-12	4.38E-09	2.38E-08	3.05E-08	4.13E-10	1.02E-07	4.54E-07	6.23E-07	3.43E-07
19	3.30E-10	1.03E-11	6.47E-09	3.31E-08	4.32E-08	2.35E-09	8.95E-08	4.51E-07	6.97E-07
20	4.32E-10	1.59E-09	9.34E-11	9.76E-09	5.76E-08	7.83E-08	8.03E-09	9.87E-08	5.46E-07
21	1.54E-10	2.43E-09	4.11E-09	2.95E-12	2.61E-08	1.04E-07	1.02E-07	3.30E-09	1.57E-07
22	5.70E-12	1.07E-09	4.72E-09	3.41E-09	2.08E-09	4.87E-08	1.22E-07	8.47E-08	4.43E-11
23	1.69E-11	4.39E-11	1.49E-09	4.85E-09	2.39E-09	4.04E-09	5.46E-08	1.19E-07	7.56E-08
24	4.10E-11	2.23E-10	1.08E-13	2.24E-09	9.06E-09	5.15E-09	4.15E-09	6.81E-08	1.48E-07
25	3.68E-11	6.22E-10	7.72E-10	2.25E-10	9.05E-09	2.07E-08	6.13E-09	1.33E-08	1.17E-07
26	2.24E-11	5.40E-10	1.26E-09	9.08E-11	4.35E-09	2.21E-08	2.35E-08	5.14E-10	4.38E-08
27	9.86E-12	1.89E-10	6.86E-10	3.80E-10	7.43E-10	1.11E-08	2.46E-08	1.25E-08	2.97E-09
28	1.77E-12	2.83E-12	7.02E-11	2.90E-10	4.30E-11	1.77E-09	1.23E-08	1.99E-08	5.09E-09
29	5.19E-13	7.59E-11	8.01E-11	6.97E-11	8.12E-10	2.87E-10	1.97E-09	1.49E-08	2.07E-08
30	8.08E-12	2.22E-10	3.92E-10	7.89E-14	1.42E-09	3.26E-09	3.05E-10	5.77E-09	2.61E-08
31	2.10E-11	2.61E-10	4.88E-10	2.57E-11	1.35E-09	5.44E-09	3.54E-09	5.62E-10	1.90E-08
32	2.95E-11	1.73E-10	2.91E-10	2.60E-11	8.66E-10	4.87E-09	5.90E-09	3.84E-10	8.19E-09
33	2.56E-11	5.46E-11	5.87E-11	2.44E-12	3.73E-10	2.70E-09	5.21E-09	2.15E-09	1.41E-09
34	1.23E-11	3.34E-13	7.25E-12	1.17E-11	8.05E-11	7.67E-10	2.78E-09	3.09E-09	7.15E-11
35	1.15E-12	3.27E-11	1.27E-10	5.97E-11	8.58E-15	1.21E-11	7.00E-10	2.54E-09	1.64E-09
36	2.84E-12	1.07E-10	2.70E-10	9.89E-11	5.10E-11	2.68E-10	1.18E-13	1.30E-09	3.24E-09
37	1.75E-11	1.62E-10	3.11E-10	9.10E-11	1.44E-10	8.80E-10	4.33E-10	3.26E-10	3.52E-09
38	3.52E-11	1.62E-10	2.33E-10	4.53E-11	2.20E-10	1.30E-09	1.19E-09	3.32E-13	2.66E-09
39	4.38E-11	1.13E-10	1.07E-10	5.24E-12	2.53E-10	1.31E-09	1.62E-09	1.78E-10	1.43E-09
40	3.80E-11	4.93E-11	1.60E-11	7.86E-12	2.41E-10	1.00E-09	1.53E-09	4.95E-10	4.77E-10
41	2.23E-11	6.57E-12	6.49E-12	5.81E-11	1.96E-10	5.83E-10	1.07E-09	6.72E-10	4.56E-11
42	6.29E-12	4.52E-12	7.13E-11	1.31E-10	1.36E-10	2.28E-10	5.28E-10	6.27E-10	3.29E-11
43	4.21E-14	4.27E-11	1.70E-10	1.91E-10	7.29E-11	3.07E-11	1.31E-10	4.15E-10	2.18E-10
44	9.10E-12	9.96E-11	2.43E-10	1.99E-10	2.28E-11	1.23E-11	1.12E-13	1.64E-10	3.80E-10
45	2.72E-11	1.35E-10	2.36E-10	1.45E-10	6.86E-13	1.10E-10	1.02E-10	1.78E-11	3.83E-10
46	4.00E-11	1.29E-10	1.70E-10	7.44E-11	6.27E-12	2.07E-10	2.58E-10	8.71E-12	2.70E-10
47	4.75E-11	1.10E-10	1.06E-10	2.61E-11	2.84E-11	2.84E-10	3.99E-10	7.21E-11	1.63E-10
48	4.14E-11	6.92E-11	4.20E-11	1.49E-12	5.43E-11	2.89E-10	4.28E-10	1.43E-10	6.43E-11

Table C.14: Franck-Condon factors for transitions from $X^2\Pi SF^{2+}$ ($v' = 0 - 48$) to $a^1\Delta SF^+$ ($v'' = 0 - 8$).

$v' \setminus v''$	9	10	11	12	13	14	15	16
0	1.50E-06	1.13E-06	9.73E-10	7.66E-07	1.23E-06	7.34E-07	1.70E-07	3.05E-10
1	7.24E-05	2.88E-06	4.52E-08	6.44E-07	2.63E-06	3.61E-06	2.48E-06	8.30E-07
2	2.14E-03	4.27E-04	6.88E-05	1.25E-05	6.03E-06	6.72E-06	7.16E-06	5.20E-06
3	1.65E-02	5.23E-03	1.42E-03	3.38E-04	8.16E-05	2.78E-05	1.66E-05	1.29E-05
4	6.03E-02	2.71E-02	1.03E-02	3.38E-03	9.92E-04	2.82E-04	9.09E-05	3.96E-05
5	1.10E-01	7.46E-02	3.93E-02	1.72E-02	6.54E-03	2.23E-03	7.20E-04	2.39E-04
6	7.20E-02	1.03E-01	8.40E-02	5.10E-02	2.54E-02	1.09E-02	4.24E-03	1.52E-03
7	1.51E-05	4.31E-02	8.79E-02	8.68E-02	6.05E-02	3.40E-02	1.65E-02	7.10E-03
8	8.09E-02	4.68E-03	2.07E-02	6.89E-02	8.34E-02	6.71E-02	4.25E-02	2.28E-02
9	5.32E-02	8.90E-02	1.64E-02	6.64E-03	4.90E-02	7.54E-02	7.03E-02	4.97E-02
10	4.68E-02	3.02E-02	8.84E-02	3.03E-02	5.31E-04	3.13E-02	6.41E-02	6.94E-02
11	1.50E-01	6.28E-02	1.41E-02	8.11E-02	4.30E-02	8.69E-04	1.72E-02	5.10E-02
12	3.31E-01	1.24E-01	7.46E-02	4.57E-03	6.97E-02	5.26E-02	5.58E-03	7.43E-03
13	7.63E-02	3.50E-01	1.04E-01	8.18E-02	4.49E-04	5.66E-02	5.83E-02	1.25E-02
14	1.09E-03	8.44E-02	3.68E-01	8.89E-02	8.48E-02	3.81E-04	4.39E-02	6.02E-02
15	2.47E-04	6.84E-04	9.02E-02	3.85E-01	7.85E-02	8.39E-02	2.88E-03	3.27E-02
16	3.15E-05	4.48E-04	2.56E-04	9.30E-02	4.02E-01	7.21E-02	7.98E-02	6.68E-02
17	6.50E-06	2.85E-05	7.47E-04	5.06E-06	9.29E-02	4.20E-01	7.03E-02	7.35E-02
18	6.72E-10	9.68E-06	1.81E-05	1.14E-03	2.38E-04	8.92E-02	4.36E-01	7.31E-02
19	5.54E-07	1.16E-08	1.45E-05	5.32E-06	1.57E-03	1.38E-03	8.10E-02	4.53E-01
20	8.99E-07	8.45E-07	8.38E-12	2.20E-05	5.32E-07	1.98E-03	3.95E-03	6.84E-02
21	6.74E-07	1.03E-06	9.93E-07	1.53E-07	3.12E-05	2.68E-05	2.23E-03	8.44E-03
22	2.00E-07	6.84E-07	1.04E-06	1.00E-06	1.03E-06	3.78E-05	1.25E-04	2.16E-03
23	2.71E-10	1.90E-07	6.37E-07	1.09E-06	9.72E-07	3.48E-06	3.65E-05	3.48E-04
24	9.49E-08	1.20E-12	1.88E-07	6.66E-07	1.29E-06	7.74E-07	8.82E-06	2.36E-05
25	2.04E-07	1.07E-07	9.49E-10	2.34E-07	7.83E-07	1.56E-06	3.06E-07	1.81E-05
26	1.80E-07	2.29E-07	8.28E-08	1.15E-08	3.10E-07	9.51E-07	1.77E-06	1.11E-08
27	8.12E-08	2.11E-07	2.06E-07	4.61E-08	3.65E-08	3.89E-07	1.16E-06	1.70E-06
28	1.13E-08	1.05E-07	2.14E-07	1.69E-07	1.99E-08	6.87E-08	4.80E-07	1.41E-06
29	2.83E-09	2.03E-08	1.27E-07	2.16E-07	1.37E-07	5.30E-09	1.08E-07	6.10E-07
30	2.55E-08	8.46E-10	3.71E-08	1.60E-07	2.19E-07	1.06E-07	1.37E-11	1.63E-07
31	4.16E-08	2.36E-08	5.74E-10	6.94E-08	1.98E-07	2.13E-07	7.20E-08	5.72E-09
32	3.79E-08	4.73E-08	1.25E-08	1.06E-08	1.15E-07	2.30E-07	1.88E-07	3.80E-08
33	2.23E-08	5.04E-08	3.86E-08	1.85E-09	3.67E-08	1.65E-07	2.42E-07	1.48E-07
34	7.66E-09	3.56E-08	5.15E-08	2.26E-08	1.64E-09	7.68E-08	2.08E-07	2.28E-07
35	6.34E-10	1.64E-08	4.50E-08	4.39E-08	7.49E-09	1.65E-08	1.25E-07	2.31E-07
36	7.05E-10	3.64E-09	2.76E-08	4.96E-08	3.04E-08	1.10E-10	4.70E-08	1.70E-07
37	3.85E-09	5.03E-12	1.08E-08	3.98E-08	4.77E-08	1.47E-08	5.52E-09	8.90E-08
38	6.43E-09	2.62E-09	1.50E-09	2.31E-08	4.96E-08	3.78E-08	2.73E-09	2.70E-08
39	6.86E-09	6.90E-09	3.60E-10	8.55E-09	3.84E-08	5.22E-08	2.23E-08	1.02E-09
40	5.45E-09	9.55E-09	3.99E-09	1.02E-09	2.22E-08	5.18E-08	4.45E-08	6.77E-09
41	3.31E-09	9.53E-09	8.40E-09	4.75E-10	8.57E-09	4.01E-08	5.68E-08	2.86E-08
42	1.42E-09	7.49E-09	1.10E-08	4.18E-09	1.19E-09	2.40E-08	5.58E-08	5.09E-08
43	2.93E-10	4.52E-09	1.09E-08	8.92E-09	3.92E-10	9.63E-09	4.37E-08	6.34E-08
44	3.24E-12	1.81E-09	8.30E-09	1.17E-08	4.15E-09	1.36E-09	2.57E-08	6.00E-08
45	2.50E-10	2.93E-10	4.57E-09	1.08E-08	8.39E-09	3.16E-10	9.75E-09	4.29E-08
46	5.39E-10	8.57E-12	1.78E-09	7.68E-09	9.96E-09	3.04E-09	1.74E-09	2.40E-08
47	7.39E-10	3.11E-10	4.37E-10	5.04E-09	1.03E-08	6.59E-09	1.55E-11	1.17E-08
48	7.10E-10	7.24E-10	1.80E-12	2.39E-09	8.07E-09	8.51E-09	1.62E-09	3.27E-09

Table C.15: Franck-Condon factors for transitions from $X \ ^2\Pi \ SF^{2+}$ ($v' = 0 - 48$) to $a \ ^1\Delta \ SF^+$ ($v'' = 9 - 16$).

$v' \setminus v''$	17	18	19	20	21	22	23	24
0	4.19E-08	6.29E-08	3.40E-08	6.41E-09	6.30E-11	3.09E-09	4.11E-09	2.29E-09
1	5.53E-08	5.33E-08	1.79E-07	1.54E-07	5.94E-08	5.42E-09	3.01E-09	1.43E-08
2	2.24E-06	3.79E-07	8.51E-09	2.40E-07	3.30E-07	1.92E-07	4.28E-08	1.53E-10
3	9.00E-06	4.51E-06	1.26E-06	5.66E-08	1.26E-07	3.65E-07	3.25E-07	1.38E-07
4	2.33E-05	1.49E-05	8.30E-06	3.27E-06	6.10E-07	8.17E-10	2.66E-07	4.61E-07
5	9.22E-05	4.50E-05	2.58E-05	1.46E-05	6.68E-06	1.93E-06	1.42E-07	1.08E-07
6	5.36E-04	2.01E-04	8.77E-05	4.44E-05	2.37E-05	1.16E-05	4.34E-06	9.08E-07
7	2.80E-03	1.05E-03	4.00E-04	1.65E-04	7.67E-05	3.91E-05	2.00E-05	9.13E-06
8	1.07E-02	4.59E-03	1.86E-03	7.40E-04	3.06E-04	1.37E-04	6.77E-05	3.51E-05
9	2.91E-02	1.50E-02	6.99E-03	3.05E-03	1.29E-03	5.48E-04	2.44E-04	1.17E-04
10	5.45E-02	3.51E-02	1.97E-02	9.99E-03	4.70E-03	2.10E-03	9.24E-04	4.14E-04
11	6.49E-02	5.71E-02	4.04E-02	2.47E-02	1.35E-02	6.75E-03	3.19E-03	1.47E-03
12	3.78E-02	5.79E-02	5.74E-02	4.45E-02	2.93E-02	1.71E-02	9.14E-03	4.59E-03
13	1.92E-03	2.60E-02	4.94E-02	5.53E-02	4.69E-02	3.32E-02	2.08E-02	1.18E-02
14	2.01E-02	2.24E-05	1.62E-02	4.03E-02	5.13E-02	4.76E-02	3.63E-02	2.42E-02
15	5.89E-02	2.71E-02	9.09E-04	8.81E-03	3.12E-02	4.58E-02	4.66E-02	3.83E-02
16	2.34E-02	5.54E-02	3.28E-02	3.64E-03	3.85E-03	2.29E-02	3.94E-02	4.42E-02
17	1.10E-02	1.60E-02	5.04E-02	3.68E-02	7.35E-03	1.04E-03	1.57E-02	3.27E-02
18	6.56E-02	1.54E-02	1.04E-02	4.48E-02	3.91E-02	1.14E-02	2.66E-05	9.95E-03
19	8.06E-02	5.65E-02	1.95E-02	6.61E-03	3.91E-02	4.00E-02	1.52E-02	3.68E-04
20	4.68E-01	9.30E-02	4.64E-02	2.32E-02	4.10E-03	3.36E-02	3.97E-02	1.85E-02
21	5.24E-02	4.79E-01	1.11E-01	3.59E-02	2.67E-02	2.55E-03	2.85E-02	3.85E-02
22	1.52E-02	3.44E-02	4.83E-01	1.36E-01	2.53E-02	3.02E-02	1.65E-03	2.40E-02
23	1.68E-03	2.40E-02	1.70E-02	4.75E-01	1.70E-01	1.54E-02	3.42E-02	1.21E-03
24	7.31E-04	8.64E-04	3.40E-02	3.89E-03	4.52E-01	2.10E-01	6.97E-03	3.92E-02
25	4.44E-06	1.25E-03	1.08E-04	4.33E-02	3.04E-04	4.09E-01	2.56E-01	1.42E-03
26	2.96E-05	7.04E-06	1.79E-03	2.75E-04	4.91E-02	1.13E-02	3.47E-01	3.03E-01
27	1.34E-06	3.71E-05	9.35E-05	2.06E-03	2.60E-03	4.83E-02	4.01E-02	2.66E-01
28	1.18E-06	6.66E-06	3.08E-05	3.50E-04	1.79E-03	8.17E-03	3.93E-02	8.54E-02
29	1.68E-06	3.13E-07	1.76E-05	9.11E-06	8.25E-04	9.33E-04	1.71E-02	2.37E-02
30	8.19E-07	1.80E-06	1.58E-07	3.09E-05	4.68E-06	1.42E-03	6.85E-05	2.74E-02
31	2.50E-07	1.14E-06	1.44E-06	3.37E-06	3.56E-05	1.04E-04	1.82E-03	6.01E-04
32	2.78E-08	4.04E-07	1.52E-06	5.09E-07	1.30E-05	1.99E-05	4.20E-04	1.60E-03
33	1.11E-08	7.62E-08	6.68E-07	1.73E-06	8.27E-08	2.73E-05	1.83E-08	9.68E-04
34	9.67E-08	3.14E-11	1.74E-07	1.07E-06	1.32E-06	3.38E-06	3.44E-05	5.58E-05
35	1.91E-07	4.97E-08	1.21E-08	3.62E-07	1.50E-06	2.94E-07	1.39E-05	1.95E-05
36	2.31E-07	1.40E-07	1.53E-08	6.23E-08	7.01E-07	1.58E-06	4.37E-07	2.85E-05
37	2.03E-07	2.06E-07	8.73E-08	9.30E-11	1.88E-07	1.17E-06	8.74E-07	5.92E-06
38	1.34E-07	2.16E-07	1.64E-07	4.05E-08	1.59E-08	4.52E-07	1.52E-06	1.57E-09
39	6.26E-08	1.74E-07	2.05E-07	1.13E-07	8.88E-09	9.33E-08	8.87E-07	1.20E-06
40	1.52E-08	1.07E-07	1.96E-07	1.74E-07	6.37E-08	1.31E-09	2.92E-07	1.34E-06
41	3.33E-12	4.61E-08	1.50E-07	1.99E-07	1.30E-07	2.40E-08	4.35E-08	6.83E-07
42	1.08E-08	8.87E-09	8.96E-08	1.83E-07	1.82E-07	8.56E-08	1.10E-09	1.96E-07
43	3.51E-08	5.57E-10	3.57E-08	1.36E-07	1.99E-07	1.51E-07	4.35E-08	1.64E-08
44	5.76E-08	1.59E-08	4.53E-09	7.50E-08	1.73E-07	1.91E-07	1.10E-07	1.02E-08
45	6.36E-08	3.82E-08	1.92E-09	2.51E-08	1.14E-07	1.82E-07	1.55E-07	6.07E-08
46	5.36E-08	5.05E-08	1.50E-08	2.78E-09	5.76E-08	1.39E-07	1.61E-07	1.03E-07
47	4.24E-08	5.71E-08	3.22E-08	1.11E-09	2.34E-08	9.99E-08	1.57E-07	1.36E-07
48	2.59E-08	4.98E-08	4.24E-08	1.03E-08	3.93E-09	5.43E-08	1.21E-07	1.38E-07

Table C.16: Franck-Condon factors for transitions from $X^2\Pi SF^{2+}$ ($v' = 0 - 48$) to $a^1\Delta SF^+$ ($v'' = 17 - 24$).

$v' \backslash v''$	25	26	27	28	29	30	31	32
0	5.50E-10	8.64E-12	7.04E-11	1.17E-10	6.02E-11	1.12E-11	3.37E-13	3.81E-13
1	1.63E-08	9.95E-09	3.27E-09	2.47E-10	2.66E-10	1.29E-09	1.93E-09	1.78E-09
2	2.43E-08	4.25E-08	3.26E-08	1.24E-08	1.06E-09	9.63E-10	4.51E-09	5.61E-09
3	1.70E-08	4.39E-09	3.17E-08	4.17E-08	2.88E-08	1.13E-08	1.76E-09	4.83E-11
4	3.50E-07	1.34E-07	1.18E-08	1.10E-08	5.53E-08	7.69E-08	6.22E-08	3.22E-08
5	4.59E-07	5.04E-07	2.77E-07	6.02E-08	9.14E-10	5.39E-08	1.11E-07	1.14E-07
6	1.00E-08	1.78E-07	3.88E-07	3.28E-07	1.38E-07	1.41E-08	1.12E-08	6.62E-08
7	3.16E-06	5.80E-07	6.30E-10	1.67E-07	3.18E-07	2.57E-07	1.04E-07	9.21E-09
8	1.75E-05	7.47E-06	2.30E-06	3.17E-07	8.83E-09	2.04E-07	3.02E-07	2.11E-07
9	5.92E-05	3.02E-05	1.42E-05	5.61E-06	1.54E-06	1.61E-07	1.96E-08	1.66E-07
10	1.95E-04	9.72E-05	5.00E-05	2.52E-05	1.16E-05	4.50E-06	1.24E-06	1.51E-07
11	6.75E-04	3.20E-04	1.59E-04	8.25E-05	4.34E-05	2.21E-05	1.03E-05	4.07E-06
12	2.22E-03	1.06E-03	5.14E-04	2.58E-04	1.35E-04	7.25E-05	3.89E-05	2.01E-05
13	6.30E-03	3.22E-03	1.61E-03	8.03E-04	4.10E-04	2.16E-04	1.17E-04	6.48E-05
14	1.47E-02	8.31E-03	4.47E-03	2.34E-03	1.21E-03	6.30E-04	3.36E-04	1.85E-04
15	2.73E-02	1.76E-02	1.05E-02	5.96E-03	3.26E-03	1.75E-03	9.37E-04	5.09E-04
16	3.92E-02	2.98E-02	2.04E-02	1.28E-02	7.64E-03	4.37E-03	2.44E-03	1.35E-03
17	4.07E-02	3.89E-02	3.15E-02	2.28E-02	1.51E-02	9.44E-03	5.64E-03	3.28E-03
18	2.61E-02	3.63E-02	3.75E-02	3.24E-02	2.47E-02	1.72E-02	1.13E-02	7.05E-03
19	5.63E-03	2.01E-02	3.15E-02	3.52E-02	3.23E-02	2.60E-02	1.91E-02	1.31E-02
20	1.63E-03	2.68E-03	1.47E-02	2.65E-02	3.22E-02	3.15E-02	2.67E-02	2.05E-02
21	2.11E-02	3.42E-03	9.20E-04	1.03E-02	2.17E-02	2.87E-02	2.99E-02	2.67E-02
22	3.66E-02	2.29E-02	5.41E-03	1.22E-04	6.74E-03	1.72E-02	2.50E-02	2.77E-02
23	2.01E-02	3.44E-02	2.40E-02	7.33E-03	3.60E-05	4.10E-03	1.33E-02	2.13E-02
24	1.11E-03	1.67E-02	3.21E-02	2.44E-02	9.03E-03	4.31E-04	2.24E-03	9.89E-03
25	4.58E-02	1.35E-03	1.37E-02	2.99E-02	2.43E-02	1.04E-02	1.11E-03	1.03E-03
26	1.66E-04	5.46E-02	2.07E-03	1.11E-02	2.79E-02	2.38E-02	1.15E-02	1.92E-03
27	3.44E-01	4.49E-03	6.66E-02	3.60E-03	8.65E-03	2.62E-02	2.29E-02	1.22E-02
28	1.77E-01	3.72E-01	1.49E-02	8.24E-02	6.51E-03	6.37E-03	2.49E-02	2.18E-02
29	1.40E-01	9.26E-02	3.77E-01	3.07E-02	1.03E-01	1.16E-02	4.20E-03	2.40E-02
30	7.40E-03	1.90E-01	2.90E-02	3.55E-01	4.91E-02	1.27E-01	2.00E-02	2.23E-03
31	3.50E-02	7.58E-06	2.18E-01	7.11E-04	3.04E-01	6.57E-02	1.54E-01	3.27E-02
32	4.27E-03	3.53E-02	1.11E-02	2.13E-01	1.34E-02	2.31E-01	7.57E-02	1.82E-01
33	7.15E-04	1.18E-02	2.61E-02	4.40E-02	1.72E-01	5.98E-02	1.51E-01	7.54E-02
34	1.52E-03	1.11E-06	2.15E-02	1.12E-02	9.13E-02	1.07E-01	1.21E-01	7.87E-02
35	3.16E-04	1.60E-03	1.29E-03	2.84E-02	5.66E-04	1.35E-01	4.38E-02	1.72E-01
36	1.71E-08	8.31E-04	9.14E-04	6.27E-03	2.76E-02	5.73E-03	1.56E-01	5.17E-03
37	3.19E-05	6.70E-05	1.37E-03	5.66E-05	1.45E-02	1.78E-02	3.18E-02	1.42E-01
38	1.91E-05	1.17E-05	3.57E-04	1.45E-03	7.41E-04	2.24E-02	5.02E-03	7.16E-02
39	2.27E-06	3.15E-05	5.12E-06	8.81E-04	7.83E-04	4.77E-03	2.44E-02	2.23E-04
40	1.93E-07	1.21E-05	2.44E-05	1.30E-04	1.34E-03	2.32E-05	1.20E-02	1.80E-02
41	1.32E-06	7.78E-07	2.68E-05	1.42E-06	5.01E-04	1.25E-03	8.78E-04	1.92E-02
42	1.19E-06	4.72E-07	7.60E-06	3.08E-05	3.65E-05	1.03E-03	5.31E-04	4.84E-03
43	5.40E-07	1.41E-06	1.50E-07	2.17E-05	1.24E-05	2.50E-04	1.37E-03	1.20E-08
44	1.19E-07	1.03E-06	8.13E-07	4.06E-06	3.26E-05	2.07E-06	6.63E-04	1.13E-03
45	2.37E-09	3.73E-07	1.30E-06	2.74E-09	1.46E-05	2.37E-05	8.34E-05	1.07E-03
46	1.66E-08	6.93E-08	7.73E-07	8.11E-07	2.12E-06	2.61E-05	9.77E-07	3.51E-04
47	5.82E-08	1.09E-09	3.19E-07	1.12E-06	4.51E-09	1.20E-05	2.35E-05	4.31E-05
48	9.00E-08	1.49E-08	6.71E-08	7.02E-07	6.39E-07	2.08E-06	2.30E-05	1.77E-06

Table C.17: Franck-Condon factors for transitions from $X^2\Pi SF^{2+}$ ($v' = 0 - 48$) to $a^1\Delta SF^+$ ($v'' = 25 - 32$).

$v' \setminus v''$	33	34	35	36	37	38	39	40
0	8.92E-12	3.83E-11	7.29E-11	7.80E-11	4.42E-11	5.74E-12	8.92E-12	6.87E-11
1	1.13E-09	4.33E-10	4.03E-11	5.45E-11	3.41E-10	6.55E-10	7.97E-10	7.07E-10
2	3.70E-09	1.21E-09	4.22E-11	2.90E-10	1.01E-09	1.37E-09	1.16E-09	6.36E-10
3	1.17E-09	1.76E-09	1.34E-09	6.42E-10	1.87E-10	2.43E-11	5.87E-14	6.96E-13
4	9.08E-09	3.17E-10	1.64E-09	5.68E-09	7.82E-09	7.17E-09	4.93E-09	2.56E-09
5	7.44E-08	2.96E-08	4.33E-09	5.74E-10	7.33E-09	1.36E-08	1.47E-08	1.14E-08
6	1.04E-07	9.61E-08	6.01E-08	2.40E-08	3.92E-09	2.19E-10	4.75E-09	9.63E-09
7	1.19E-08	6.41E-08	1.04E-07	1.05E-07	7.56E-08	3.89E-08	1.25E-08	1.10E-09
8	6.96E-08	1.47E-09	2.56E-08	8.87E-08	1.33E-07	1.34E-07	1.02E-07	5.90E-08
9	2.05E-07	1.20E-07	2.57E-08	1.70E-09	4.55E-08	1.09E-07	1.49E-07	1.49E-07
10	4.84E-09	8.44E-08	1.06E-07	5.53E-08	6.59E-09	7.40E-09	5.29E-08	1.09E-07
11	1.21E-06	1.95E-07	7.58E-10	3.16E-08	4.92E-08	2.48E-08	1.30E-09	1.02E-08
12	9.48E-06	3.87E-06	1.25E-06	2.62E-07	1.59E-08	5.54E-09	1.77E-08	9.18E-09
13	3.54E-05	1.86E-05	8.97E-06	3.84E-06	1.37E-06	3.68E-07	5.79E-08	1.43E-09
14	1.04E-04	5.88E-05	3.28E-05	1.76E-05	8.84E-06	4.03E-06	1.62E-06	5.50E-07
15	2.84E-04	1.62E-04	9.39E-05	5.46E-05	3.13E-05	1.74E-05	9.17E-06	4.53E-06
16	7.51E-04	4.25E-04	2.46E-04	1.46E-04	8.71E-05	5.23E-05	3.10E-05	1.79E-05
17	1.88E-03	1.08E-03	6.23E-04	3.67E-04	2.20E-04	1.35E-04	8.33E-05	5.17E-05
18	4.27E-03	2.53E-03	1.50E-03	8.87E-04	5.33E-04	3.26E-04	2.03E-04	1.28E-04
19	8.53E-03	5.37E-03	3.31E-03	2.02E-03	1.23E-03	7.55E-04	4.70E-04	2.98E-04
20	1.47E-02	1.00E-02	6.56E-03	4.19E-03	2.64E-03	1.65E-03	1.04E-03	6.63E-04
21	2.15E-02	1.61E-02	1.14E-02	7.77E-03	5.14E-03	3.35E-03	2.17E-03	1.40E-03
22	2.61E-02	2.20E-02	1.72E-02	1.27E-02	8.94E-03	6.14E-03	4.13E-03	2.75E-03
23	2.52E-02	2.49E-02	2.20E-02	1.79E-02	1.37E-02	1.00E-02	7.12E-03	4.96E-03
24	1.77E-02	2.24E-02	2.33E-02	2.15E-02	1.81E-02	1.44E-02	1.09E-02	8.04E-03
25	7.10E-03	1.44E-02	1.95E-02	2.13E-02	2.05E-02	1.80E-02	1.48E-02	1.17E-02
26	3.42E-04	4.90E-03	1.14E-02	1.66E-02	1.92E-02	1.92E-02	1.75E-02	1.49E-02
27	2.75E-03	4.13E-05	3.20E-03	8.82E-03	1.39E-02	1.69E-02	1.77E-02	1.67E-02
28	1.26E-02	3.52E-03	1.71E-05	1.96E-03	6.64E-03	1.14E-02	1.46E-02	1.59E-02
29	2.05E-02	1.28E-02	4.20E-03	1.77E-04	1.08E-03	4.85E-03	9.12E-03	1.24E-02
30	2.38E-02	1.90E-02	1.28E-02	4.77E-03	4.50E-04	5.12E-04	3.40E-03	7.14E-03
31	7.10E-04	2.41E-02	1.75E-02	1.26E-02	5.22E-03	7.86E-04	1.75E-04	2.27E-03
32	5.07E-02	6.18E-06	2.50E-02	1.59E-02	1.23E-02	5.57E-03	1.15E-03	2.21E-05
33	2.07E-01	7.43E-02	6.41E-04	2.67E-02	1.43E-02	1.19E-02	5.85E-03	1.52E-03
34	6.39E-02	2.24E-01	1.03E-01	3.19E-03	2.91E-02	1.28E-02	1.14E-02	6.06E-03
35	2.78E-02	4.44E-02	2.30E-01	1.35E-01	8.14E-03	3.21E-02	1.14E-02	1.08E-02
36	1.94E-01	3.34E-03	2.30E-02	2.23E-01	1.69E-01	1.57E-02	3.56E-02	1.02E-02
37	4.57E-03	1.81E-01	1.33E-03	6.62E-03	2.04E-01	2.01E-01	2.58E-02	3.89E-02
38	9.92E-02	3.70E-02	1.40E-01	1.17E-02	4.84E-05	1.76E-01	2.30E-01	3.78E-02
39	1.08E-01	4.73E-02	8.32E-02	8.83E-02	2.34E-02	4.17E-03	1.45E-01	2.55E-01
40	1.23E-02	1.22E-01	9.74E-03	1.21E-01	4.30E-02	2.94E-02	1.62E-02	1.15E-01
41	6.98E-03	4.07E-02	1.08E-01	5.44E-04	1.35E-01	1.40E-02	2.81E-02	3.13E-02
42	2.19E-02	1.39E-04	7.42E-02	7.57E-02	1.71E-02	1.28E-01	1.87E-03	2.24E-02
43	1.13E-02	1.80E-02	4.57E-03	9.83E-02	4.10E-02	4.48E-02	1.08E-01	1.07E-04
44	9.36E-04	1.73E-02	9.76E-03	2.00E-02	1.04E-01	1.53E-02	6.90E-02	8.49E-02
45	4.07E-04	4.06E-03	1.91E-02	1.97E-03	4.06E-02	8.95E-02	1.63E-03	8.27E-02
46	1.11E-03	2.48E-05	9.02E-03	1.48E-02	8.11E-04	6.02E-02	5.83E-02	2.69E-03
47	8.10E-04	6.26E-04	1.61E-03	1.44E-02	7.04E-03	1.22E-02	7.49E-02	2.82E-02
48	2.56E-04	9.70E-04	1.42E-05	5.43E-03	1.39E-02	4.81E-04	3.02E-02	6.45E-02

Table C.18: Franck-Condon factors for transitions from $X \ ^2\Pi \ SF^{2+}$ ($v' = 0 - 48$) to $a \ ^1\Delta \ SF^+$ ($v'' = 33 - 40$).

$v' \setminus v''$	41	42	43	44	45	46	47	48	49
0	1.55E-10	2.16E-10	2.19E-10	1.66E-10	8.99E-11	2.71E-11	5.50E-13	1.10E-11	4.21E-11
1	4.61E-10	1.97E-10	3.21E-11	6.16E-12	8.96E-11	2.17E-10	3.24E-10	3.75E-10	3.63E-10
2	1.85E-10	2.78E-12	7.50E-11	2.66E-10	4.37E-10	5.11E-10	4.82E-10	3.85E-10	2.65E-10
3	2.14E-13	7.67E-12	2.45E-11	3.98E-11	4.35E-11	3.46E-11	1.96E-11	6.75E-12	5.59E-13
4	9.16E-10	1.45E-10	6.57E-12	1.70E-10	3.86E-10	5.28E-10	5.68E-10	5.24E-10	4.32E-10
5	6.59E-09	2.65E-09	5.30E-10	6.70E-13	3.46E-10	9.11E-10	1.32E-09	1.44E-09	1.32E-09
6	1.11E-08	9.32E-09	6.02E-09	2.95E-09	9.59E-10	1.09E-10	3.26E-11	2.92E-10	5.66E-10
7	8.20E-10	4.94E-09	8.50E-09	9.54E-09	8.33E-09	6.02E-09	3.67E-09	1.87E-09	7.65E-10
8	2.43E-08	5.31E-09	8.68E-12	2.42E-09	6.89E-09	1.01E-08	1.09E-08	9.83E-09	7.72E-09
9	1.17E-07	7.37E-08	3.61E-08	1.20E-08	1.52E-09	2.94E-10	3.30E-09	6.81E-09	8.86E-09
10	1.45E-07	1.48E-07	1.24E-07	8.70E-08	5.11E-08	2.41E-08	8.22E-09	1.33E-09	2.23E-11
11	4.96E-08	9.75E-08	1.32E-07	1.41E-07	1.28E-07	1.01E-07	7.01E-08	4.33E-08	2.35E-08
12	2.59E-11	1.08E-08	4.25E-08	8.18E-08	1.13E-07	1.28E-07	1.25E-07	1.08E-07	8.47E-08
13	1.62E-09	1.05E-09	6.80E-10	1.13E-08	3.47E-08	6.41E-08	8.97E-08	1.04E-07	1.05E-07
14	1.48E-07	2.93E-08	4.60E-09	1.78E-09	4.22E-09	1.26E-08	2.74E-08	4.51E-08	5.97E-08
15	2.05E-06	8.48E-07	3.17E-07	1.10E-07	3.92E-08	1.84E-08	1.43E-08	1.67E-08	2.21E-08
16	1.00E-05	5.35E-06	2.72E-06	1.31E-06	6.08E-07	2.77E-07	1.30E-07	6.68E-08	4.02E-08
17	3.18E-05	1.92E-05	1.14E-05	6.55E-06	3.67E-06	2.01E-06	1.08E-06	5.82E-07	3.16E-07
18	8.21E-05	5.26E-05	3.36E-05	2.13E-05	1.33E-05	8.20E-06	5.00E-06	3.01E-06	1.79E-06
19	1.92E-04	1.26E-04	8.28E-05	5.49E-05	3.64E-05	2.40E-05	1.58E-05	1.03E-05	6.65E-06
20	4.28E-04	2.80E-04	1.86E-04	1.26E-04	8.53E-05	5.84E-05	4.00E-05	2.74E-05	1.86E-05
21	9.12E-04	5.99E-04	3.99E-04	2.70E-04	1.85E-04	1.28E-04	8.93E-05	6.25E-05	4.35E-05
22	1.83E-03	1.22E-03	8.18E-04	5.55E-04	3.81E-04	2.64E-04	1.86E-04	1.31E-04	9.22E-05
23	3.40E-03	2.32E-03	1.59E-03	1.09E-03	7.51E-04	5.24E-04	3.69E-04	2.61E-04	1.84E-04
24	5.78E-03	4.09E-03	2.87E-03	2.01E-03	1.41E-03	9.89E-04	7.01E-04	4.98E-04	3.52E-04
25	8.85E-03	6.55E-03	4.77E-03	3.44E-03	2.46E-03	1.77E-03	1.27E-03	9.07E-04	6.46E-04
26	1.21E-02	9.50E-03	7.24E-03	5.42E-03	4.01E-03	2.94E-03	2.15E-03	1.56E-03	1.13E-03
27	1.47E-02	1.23E-02	9.94E-03	7.79E-03	5.98E-03	4.53E-03	3.40E-03	2.53E-03	1.85E-03
28	1.56E-02	1.42E-02	1.22E-02	1.01E-02	8.16E-03	6.42E-03	4.97E-03	3.79E-03	2.83E-03
29	1.41E-02	1.43E-02	1.34E-02	1.19E-02	1.01E-02	8.32E-03	6.69E-03	5.26E-03	4.03E-03
30	1.03E-02	1.22E-02	1.28E-02	1.23E-02	1.12E-02	9.78E-03	8.23E-03	6.72E-03	5.30E-03
31	5.43E-03	8.34E-03	1.03E-02	1.12E-02	1.11E-02	1.03E-02	9.20E-03	7.85E-03	6.42E-03
32	1.41E-03	3.98E-03	6.56E-03	8.48E-03	9.51E-03	9.70E-03	9.24E-03	8.32E-03	7.11E-03
33	9.57E-06	7.85E-04	2.78E-03	4.98E-03	6.76E-03	7.84E-03	8.19E-03	7.92E-03	7.14E-03
34	1.88E-03	1.05E-04	3.59E-04	1.81E-03	3.61E-03	5.18E-03	6.20E-03	6.60E-03	6.39E-03
35	6.23E-03	2.23E-03	2.83E-04	1.05E-04	1.06E-03	2.45E-03	3.74E-03	4.63E-03	4.96E-03
36	1.01E-02	6.36E-03	2.58E-03	5.24E-04	3.94E-06	5.17E-04	1.50E-03	2.49E-03	3.15E-03
37	9.39E-03	9.20E-03	6.46E-03	2.92E-03	8.20E-04	3.49E-05	1.70E-04	7.72E-04	1.44E-03
38	4.15E-02	9.06E-03	8.20E-03	6.49E-03	3.26E-03	1.17E-03	1.82E-04	1.33E-05	2.74E-04
39	5.09E-02	4.25E-02	9.41E-03	7.04E-03	6.50E-03	3.54E-03	1.57E-03	4.50E-04	2.95E-05
40	2.76E-01	6.37E-02	4.04E-02	1.10E-02	5.63E-03	6.49E-03	3.85E-03	1.87E-03	8.18E-04
41	9.09E-02	2.95E-01	7.26E-02	3.24E-02	1.53E-02	4.19E-03	5.87E-03	4.58E-03	2.17E-03
42	4.35E-02	7.91E-02	3.13E-01	6.99E-02	1.70E-02	2.34E-02	4.30E-03	3.81E-03	4.89E-03
43	1.64E-02	4.70E-02	8.60E-02	3.30E-01	5.00E-02	2.60E-03	2.81E-02	8.83E-03	2.51E-03
44	1.97E-03	1.14E-02	3.84E-02	1.19E-01	3.42E-01	2.27E-02	7.84E-04	1.81E-02	1.63E-02
45	5.93E-02	4.99E-03	5.98E-03	2.17E-02	1.77E-01	3.51E-01	6.42E-03	4.72E-03	4.69E-03
46	8.54E-02	3.20E-02	9.73E-03	1.19E-03	1.01E-02	2.29E-01	3.65E-01	8.97E-04	7.69E-03
47	1.94E-02	8.38E-02	1.29E-02	1.25E-02	1.66E-04	9.44E-03	2.58E-01	3.41E-01	3.47E-03
48	5.73E-03	3.68E-02	6.58E-02	2.02E-03	8.51E-03	1.65E-04	5.56E-03	3.19E-01	3.27E-01

Table C.19: Franck-Condon factors for transitions from $X^2\Pi SF^{2+}$ ($v' = 0 - 48$) to $a^1\Delta SF^+$ ($v'' = 41 - 49$).

$v' \setminus v''$	0	1	2	3	4	5	6	7	8
0	4.82E-01	3.09E-01	1.31E-01	5.09E-02	1.86E-02	5.93E-03	1.45E-03	2.25E-04	1.13E-05
1	3.87E-01	3.24E-02	2.04E-01	1.90E-01	1.12E-01	5.02E-02	1.78E-02	4.96E-03	1.03E-03
2	1.14E-01	3.63E-01	2.28E-02	6.58E-02	1.62E-01	1.43E-01	8.04E-02	3.39E-02	1.15E-02
3	1.63E-02	2.38E-01	2.05E-01	1.04E-01	5.27E-03	1.03E-01	1.42E-01	1.02E-01	5.23E-02
4	1.33E-03	5.15E-02	3.18E-01	7.16E-02	1.46E-01	4.77E-03	4.99E-02	1.20E-01	1.12E-01
5	3.53E-05	5.27E-03	1.05E-01	3.26E-01	1.10E-02	1.43E-01	2.94E-02	1.51E-02	8.65E-02
6	8.67E-08	2.28E-04	1.32E-02	1.63E-01	2.89E-01	4.68E-04	1.18E-01	5.88E-02	6.94E-04
7	3.20E-07	1.39E-07	7.13E-04	2.55E-02	2.13E-01	2.38E-01	1.39E-02	8.44E-02	8.16E-02
8	1.03E-09	7.54E-08	3.42E-07	1.54E-03	4.04E-02	2.51E-01	1.89E-01	3.68E-02	5.14E-02
9	1.06E-07	1.75E-07	2.68E-07	4.11E-06	2.59E-03	5.65E-02	2.80E-01	1.44E-01	6.17E-02
10	7.12E-08	3.80E-07	6.80E-07	2.25E-06	1.08E-05	3.72E-03	7.34E-02	3.03E-01	1.04E-01
11	8.41E-10	8.03E-08	5.30E-07	1.16E-06	6.26E-06	1.44E-05	4.82E-03	9.12E-02	3.20E-02
12	1.67E-08	1.12E-08	2.87E-08	4.67E-07	1.32E-06	1.24E-05	1.18E-05	5.88E-03	1.10E-01
13	1.64E-08	7.03E-08	7.97E-08	1.44E-10	3.13E-07	1.35E-06	2.09E-05	4.14E-06	6.87E-03
14	1.51E-09	3.64E-08	1.48E-07	1.99E-07	2.97E-08	1.64E-07	1.23E-06	3.11E-05	2.33E-07
15	1.51E-09	7.54E-10	4.66E-08	2.11E-07	3.29E-07	1.15E-07	2.76E-08	1.03E-06	4.43E-05
16	3.53E-09	8.01E-09	2.55E-10	4.50E-08	2.82E-07	5.16E-07	2.79E-07	6.23E-09	1.19E-06
17	1.23E-09	1.23E-08	2.36E-08	3.13E-09	5.68E-08	3.90E-07	6.89E-07	3.97E-07	5.42E-08
18	2.32E-13	3.99E-09	2.45E-08	3.76E-08	4.11E-09	7.04E-08	4.28E-07	7.06E-07	4.67E-07
19	3.88E-10	2.07E-12	5.47E-09	3.31E-08	5.27E-08	1.01E-08	5.48E-08	4.07E-07	7.52E-07
20	4.43E-10	1.86E-09	3.61E-10	7.26E-09	5.57E-08	9.46E-08	2.51E-08	5.22E-08	4.74E-07
21	1.38E-10	2.52E-09	5.07E-09	2.31E-10	2.00E-08	1.03E-07	1.32E-07	2.13E-08	8.82E-08
22	2.15E-12	1.01E-09	5.08E-09	4.93E-09	5.49E-10	4.03E-08	1.28E-07	1.20E-07	8.22E-09
23	2.21E-11	2.44E-11	1.37E-09	5.28E-09	3.96E-09	1.50E-09	4.54E-08	1.26E-07	1.11E-07
24	4.17E-11	2.68E-10	1.85E-11	1.82E-09	9.55E-09	8.25E-09	9.62E-10	5.44E-08	1.55E-07
25	3.31E-11	6.60E-10	1.03E-09	4.26E-11	7.84E-09	2.31E-08	1.21E-08	4.85E-09	9.71E-08
26	1.88E-11	5.46E-10	1.49E-09	3.16E-10	3.06E-09	2.15E-08	3.01E-08	4.48E-09	2.52E-08
27	8.41E-12	1.84E-10	7.54E-10	6.10E-10	3.08E-10	9.44E-09	2.65E-08	2.00E-08	2.23E-11
28	1.77E-12	1.90E-12	6.32E-11	3.31E-10	1.49E-10	1.04E-09	1.10E-08	2.29E-08	1.13E-08
29	2.86E-13	8.09E-11	1.12E-10	3.69E-11	8.56E-10	6.25E-10	9.60E-10	1.32E-08	2.50E-08
30	6.74E-12	2.29E-10	4.81E-10	2.10E-11	1.19E-09	3.81E-09	1.08E-09	3.30E-09	2.45E-08
31	1.93E-11	2.70E-10	5.83E-10	9.58E-11	9.98E-10	5.61E-09	5.30E-09	7.84E-13	1.42E-08
32	2.89E-11	1.81E-10	3.46E-10	8.01E-11	5.87E-10	4.66E-09	7.32E-09	1.64E-09	4.32E-09
33	2.66E-11	5.93E-11	7.24E-11	1.43E-11	2.39E-10	2.40E-09	5.75E-09	3.76E-09	1.79E-10
34	1.37E-11	7.12E-13	6.70E-12	9.03E-12	5.10E-11	6.01E-10	2.69E-09	3.96E-09	7.45E-10
35	1.71E-12	3.09E-11	1.39E-10	7.90E-11	2.07E-14	7.97E-13	4.98E-10	2.55E-09	2.67E-09
36	2.20E-12	1.07E-10	3.03E-10	1.48E-10	2.80E-11	3.22E-10	3.08E-11	9.30E-10	3.59E-09
37	1.65E-11	1.67E-10	3.55E-10	1.50E-10	8.51E-11	9.14E-10	7.34E-10	7.89E-11	3.07E-09
38	3.51E-11	1.71E-10	2.73E-10	8.74E-11	1.40E-10	1.28E-09	1.61E-09	9.93E-11	1.82E-09
39	4.52E-11	1.23E-10	1.31E-10	1.95E-11	1.77E-10	1.26E-09	1.99E-09	5.49E-10	6.90E-10
40	4.04E-11	5.64E-11	2.33E-11	2.04E-12	1.87E-10	9.47E-10	1.75E-09	9.34E-10	9.77E-11
41	2.45E-11	9.09E-12	4.26E-12	5.03E-11	1.73E-10	5.46E-10	1.15E-09	1.01E-09	1.58E-11
42	7.51E-12	3.18E-12	6.97E-11	1.38E-10	1.39E-10	2.14E-10	5.22E-10	7.87E-10	1.99E-10
43	1.33E-16	4.04E-11	1.78E-10	2.20E-10	9.21E-11	2.97E-11	1.05E-10	4.27E-10	4.01E-10
44	8.41E-12	1.00E-10	2.62E-10	2.43E-10	4.20E-11	1.03E-11	5.04E-12	1.16E-10	4.58E-10
45	2.70E-11	1.40E-10	2.62E-10	1.89E-10	7.80E-12	9.84E-11	1.51E-10	3.71E-13	3.41E-10
46	4.08E-11	1.37E-10	1.94E-10	1.05E-10	4.06E-13	1.89E-10	3.29E-10	5.18E-11	1.77E-10
47	4.93E-11	1.20E-10	1.25E-10	4.29E-11	1.35E-11	2.64E-10	4.78E-10	1.69E-10	6.87E-11
48	4.36E-11	7.69E-11	5.26E-11	5.42E-12	3.74E-11	2.72E-10	4.95E-10	2.59E-10	9.00E-12

Table C.20: Franck-Condon factors for transitions from $X \ ^2\Pi \ SF^{2+}$ ($v' = 0 - 48$) to $b \ ^1\Sigma^+ \ SF^+$ ($v'' = 0 - 8$).

$v' \setminus v''$	9	10	11	12	13	14	15	16	17
0	8.80E-07	1.84E-06	1.26E-07	4.32E-07	1.26E-06	1.07E-06	4.14E-07	4.34E-08	1.11E-08
1	1.39E-04	8.18E-06	7.05E-08	2.34E-07	1.91E-06	3.69E-06	3.40E-06	1.71E-06	3.75E-07
2	3.16E-03	7.01E-04	1.24E-04	2.11E-05	6.95E-06	6.49E-06	7.66E-06	6.87E-06	4.08E-06
3	2.15E-02	7.40E-03	2.18E-03	5.64E-04	1.39E-04	4.16E-05	2.05E-05	1.53E-05	1.19E-05
4	6.99E-02	3.42E-02	1.41E-02	5.04E-03	1.60E-03	4.78E-04	1.50E-04	5.90E-05	3.16E-05
5	1.09E-01	8.31E-02	4.80E-02	2.30E-02	9.50E-03	3.52E-03	1.21E-03	4.14E-04	1.54E-04
6	5.23E-02	9.53E-02	8.94E-02	6.03E-02	3.29E-02	1.55E-02	6.53E-03	2.54E-03	9.47E-04
7	3.58E-03	2.43E-02	7.42E-02	8.74E-02	6.87E-02	4.27E-02	2.27E-02	1.08E-02	4.63E-03
8	9.25E-02	1.72E-02	6.87E-03	5.11E-02	7.82E-02	7.25E-02	5.15E-02	3.06E-02	1.59E-02
9	2.48E-02	9.10E-02	3.47E-02	1.79E-04	2.99E-02	6.43E-02	7.16E-02	5.78E-02	3.81E-02
10	8.32E-02	7.80E-03	8.01E-02	5.03E-02	2.40E-03	1.37E-02	4.83E-02	6.58E-02	6.05E-02
11	7.12E-02	9.83E-02	5.45E-04	6.39E-02	6.09E-02	1.05E-02	3.81E-03	3.25E-02	5.62E-02
12	3.33E-01	4.55E-02	1.06E-01	1.21E-03	4.61E-02	6.53E-02	2.12E-02	8.75E-05	1.88E-02
13	1.28E-01	3.40E-01	2.71E-02	1.07E-01	7.27E-03	2.96E-02	6.39E-02	3.17E-02	1.45E-03
14	7.68E-03	1.46E-01	3.45E-01	1.49E-02	1.03E-01	1.63E-02	1.64E-02	5.81E-02	4.01E-02
15	1.61E-05	8.16E-03	1.64E-01	3.48E-01	7.39E-03	9.47E-02	2.61E-02	7.35E-03	4.94E-02
16	6.22E-05	7.62E-05	8.19E-03	1.79E-01	3.52E-01	3.08E-03	8.44E-02	3.50E-02	2.09E-03
17	1.80E-06	8.12E-05	2.21E-04	7.68E-03	1.92E-01	3.57E-01	1.03E-03	7.32E-02	4.24E-02
18	1.80E-07	2.82E-06	9.63E-05	4.98E-04	6.62E-03	2.04E-01	3.63E-01	2.66E-04	6.23E-02
19	6.80E-07	4.79E-07	4.92E-06	1.05E-04	9.51E-04	5.08E-03	2.12E-01	3.73E-01	5.77E-05
20	9.32E-07	1.02E-06	7.52E-07	9.88E-06	1.04E-04	1.62E-03	3.23E-03	2.16E-01	3.86E-01
21	5.91E-07	1.05E-06	1.26E-06	7.26E-07	1.96E-05	8.41E-05	2.52E-03	1.40E-03	2.16E-01
22	1.20E-07	6.00E-07	1.02E-06	1.43E-06	4.56E-07	3.52E-05	4.63E-05	3.61E-03	1.68E-04
23	7.42E-09	1.08E-07	5.35E-07	9.91E-07	1.73E-06	1.05E-07	5.70E-05	7.36E-06	4.77E-03
24	1.41E-07	1.37E-08	9.57E-08	5.21E-07	1.11E-06	2.16E-06	1.01E-07	8.27E-05	1.10E-05
25	2.21E-07	1.72E-07	1.20E-08	1.17E-07	5.76E-07	1.36E-06	2.49E-06	1.89E-06	1.05E-04
26	1.61E-07	2.66E-07	1.59E-07	2.51E-09	1.64E-07	6.62E-07	1.71E-06	2.38E-06	8.32E-06
27	5.62E-08	2.00E-07	2.59E-07	1.18E-07	6.40E-10	2.10E-07	7.61E-07	2.15E-06	1.58E-06
28	2.86E-09	7.77E-08	2.13E-07	2.33E-07	8.02E-08	7.80E-09	2.51E-07	9.05E-07	2.62E-06
29	9.19E-09	6.81E-09	9.68E-08	2.23E-07	2.10E-07	5.27E-08	2.02E-08	2.96E-07	1.15E-06
30	3.39E-08	7.27E-09	1.53E-08	1.27E-07	2.41E-07	1.88E-07	3.12E-08	3.81E-08	3.68E-07
31	4.35E-08	3.77E-08	2.26E-09	3.60E-08	1.70E-07	2.56E-07	1.61E-07	1.32E-08	6.39E-08
32	3.35E-08	5.63E-08	2.90E-08	3.94E-10	7.12E-08	2.15E-07	2.56E-07	1.24E-07	2.12E-09
33	1.63E-08	5.02E-08	5.43E-08	1.38E-08	1.04E-08	1.18E-07	2.49E-07	2.37E-07	8.18E-08
34	3.90E-09	2.98E-08	5.75E-08	4.17E-08	2.18E-09	3.49E-08	1.67E-07	2.65E-07	1.97E-07
35	4.81E-12	1.06E-08	4.16E-08	5.65E-08	2.47E-08	9.92E-10	7.23E-08	2.08E-07	2.58E-07
36	1.92E-09	1.04E-09	2.03E-08	5.11E-08	4.86E-08	9.55E-09	1.32E-08	1.16E-07	2.36E-07
37	5.17E-09	7.84E-10	5.18E-09	3.31E-08	5.65E-08	3.51E-08	7.38E-10	3.89E-08	1.60E-07
38	6.82E-09	5.06E-09	2.52E-11	1.45E-08	4.73E-08	5.46E-08	1.93E-08	2.80E-09	7.56E-08
39	6.22E-09	9.08E-09	2.45E-09	2.92E-09	2.93E-08	5.78E-08	4.50E-08	5.36E-09	1.86E-08
40	4.26E-09	1.04E-08	7.56E-09	5.08E-11	1.24E-08	4.65E-08	6.05E-08	2.86E-08	1.78E-11
41	2.15E-09	9.04E-09	1.14E-08	3.22E-09	2.36E-09	2.87E-08	6.03E-08	5.31E-08	1.16E-08
42	6.67E-10	6.17E-09	1.24E-08	8.48E-09	9.56E-11	1.24E-08	4.80E-08	6.68E-08	3.72E-08
43	3.75E-11	3.10E-09	1.05E-08	1.26E-08	3.51E-09	2.32E-09	2.96E-08	6.52E-08	6.19E-08
44	1.10E-10	8.65E-10	6.76E-09	1.33E-08	8.97E-09	1.58E-10	1.21E-08	4.93E-08	7.26E-08
45	4.53E-10	2.32E-11	2.97E-09	1.03E-08	1.22E-08	3.59E-09	1.99E-09	2.73E-08	6.30E-08
46	6.55E-10	1.68E-10	7.78E-10	6.18E-09	1.16E-08	7.52E-09	7.50E-11	1.08E-08	4.31E-08
47	7.31E-10	6.44E-10	4.17E-11	3.29E-09	1.01E-08	1.06E-08	2.42E-09	2.74E-09	2.72E-08
48	6.01E-10	1.01E-09	1.29E-10	1.11E-09	6.76E-09	1.07E-08	5.76E-09	1.87E-11	1.23E-08

Table C.21: Franck-Condon factors for transitions from $X \ ^2\Pi \ SF^{2+}$ ($v' = 0 - 48$) to $b \ ^1\Sigma^+ \ SF^+$ ($v'' = 9 - 17$).

$v' \setminus v''$	18	19	20	21	22	23	24	25	26
0	5.96E-08	5.76E-08	2.50E-08	3.59E-09	2.69E-10	3.17E-09	4.02E-09	2.50E-09	8.36E-10
1	5.01E-10	1.09E-07	1.91E-07	1.38E-07	4.89E-08	4.30E-09	2.56E-09	1.27E-08	1.62E-08
2	1.38E-06	1.27E-07	5.67E-08	2.88E-07	3.24E-07	1.82E-07	4.54E-08	1.54E-10	1.62E-08
3	7.59E-06	3.35E-06	7.65E-07	8.05E-09	1.68E-07	3.70E-07	3.26E-07	1.58E-07	3.39E-08
4	2.05E-05	1.31E-05	7.01E-06	2.61E-06	4.45E-07	3.61E-09	2.51E-07	4.43E-07	3.83E-07
5	6.91E-05	3.81E-05	2.31E-05	1.31E-05	6.02E-06	1.81E-06	1.71E-07	6.15E-08	3.73E-07
6	3.59E-04	1.50E-04	7.30E-05	3.99E-05	2.22E-05	1.13E-05	4.58E-06	1.20E-06	8.20E-08
7	1.87E-03	7.44E-04	3.08E-04	1.39E-04	7.02E-05	3.81E-05	2.07E-05	1.03E-05	4.23E-06
8	7.50E-03	3.30E-03	1.40E-03	5.99E-04	2.68E-04	1.30E-04	6.88E-05	3.80E-05	2.06E-05
9	2.17E-02	1.12E-02	5.37E-03	2.46E-03	1.11E-03	5.07E-04	2.43E-04	1.25E-04	6.76E-05
10	4.41E-02	2.77E-02	1.56E-02	8.15E-03	4.01E-03	1.91E-03	9.05E-04	4.38E-04	2.22E-04
11	5.95E-02	4.85E-02	3.35E-02	2.05E-02	1.15E-02	6.08E-03	3.07E-03	1.52E-03	7.59E-04
12	4.45E-02	5.53E-02	5.05E-02	3.82E-02	2.54E-02	1.53E-02	8.64E-03	4.65E-03	2.43E-03
13	8.61E-03	3.24E-02	4.85E-02	4.99E-02	4.14E-02	2.97E-02	1.93E-02	1.16E-02	6.68E-03
14	6.33E-03	2.40E-03	2.12E-02	3.99E-02	4.67E-02	4.26E-02	3.31E-02	2.31E-02	1.49E-02
15	4.54E-02	1.31E-02	5.43E-05	1.20E-02	3.05E-02	4.13E-02	4.17E-02	3.52E-02	2.64E-02
16	3.94E-02	4.75E-02	2.03E-02	9.49E-04	5.25E-03	2.13E-02	3.44E-02	3.88E-02	3.57E-02
17	7.35E-05	2.93E-02	4.64E-02	2.66E-02	4.18E-03	1.31E-03	1.32E-02	2.68E-02	3.42E-02
18	4.79E-02	6.20E-04	2.03E-02	4.30E-02	3.13E-02	8.78E-03	2.19E-06	6.78E-03	1.91E-02
19	5.17E-02	5.14E-02	2.92E-03	1.29E-02	3.78E-02	3.41E-02	1.38E-02	9.44E-04	2.45E-03
20	2.51E-05	4.20E-02	5.31E-02	6.19E-03	7.23E-03	3.16E-02	3.49E-02	1.86E-02	3.55E-03
21	4.04E-01	7.09E-05	3.32E-02	5.32E-02	9.80E-03	3.34E-03	2.52E-02	3.37E-02	2.23E-02
22	2.11E-01	4.24E-01	3.32E-04	2.57E-02	5.22E-02	1.34E-02	1.04E-03	1.90E-02	3.10E-02
23	2.60E-04	2.01E-01	4.48E-01	1.19E-03	1.93E-02	5.03E-02	1.66E-02	7.18E-05	1.34E-02
24	5.80E-03	2.45E-03	1.84E-01	4.73E-01	3.20E-03	1.38E-02	4.79E-02	1.93E-02	1.73E-04
25	1.30E-04	6.40E-03	7.49E-03	1.62E-01	5.00E-01	7.02E-03	9.29E-03	4.50E-02	2.15E-02
26	1.12E-04	4.59E-04	6.26E-03	1.58E-02	1.34E-01	5.26E-01	1.32E-02	5.64E-03	4.19E-02
27	2.29E-05	9.06E-05	1.08E-03	5.23E-03	2.73E-02	1.04E-01	5.49E-01	2.22E-02	2.92E-03
28	3.83E-07	4.76E-05	4.19E-05	2.02E-03	3.43E-03	4.08E-02	7.39E-02	5.67E-01	3.40E-02
29	2.94E-06	2.34E-07	7.82E-05	9.23E-07	3.16E-03	1.40E-03	5.47E-02	4.65E-02	5.78E-01
30	1.56E-06	2.75E-06	4.46E-06	1.02E-04	5.16E-05	4.20E-03	9.33E-05	6.64E-02	2.47E-02
31	5.03E-07	2.13E-06	1.70E-06	1.76E-05	9.90E-05	3.11E-04	4.77E-03	5.45E-04	7.38E-02
32	1.06E-07	7.50E-07	2.73E-06	2.46E-07	4.23E-05	6.00E-05	8.72E-04	4.54E-03	3.50E-03
33	9.08E-10	1.78E-07	1.18E-06	2.92E-06	7.80E-07	7.31E-05	9.04E-06	1.72E-03	3.48E-03
34	4.43E-08	1.27E-08	3.16E-07	1.81E-06	2.19E-06	7.94E-06	9.38E-05	1.90E-05	2.67E-03
35	1.48E-07	1.62E-08	4.27E-08	5.78E-07	2.51E-06	6.32E-07	2.61E-05	8.48E-05	1.92E-04
36	2.29E-07	9.77E-08	1.93E-09	1.10E-07	1.04E-06	2.80E-06	2.12E-07	5.37E-05	4.34E-05
37	2.43E-07	1.87E-07	5.49E-08	2.42E-09	2.54E-07	1.72E-06	2.13E-06	5.20E-06	7.92E-05
38	1.95E-07	2.32E-07	1.38E-07	2.36E-08	2.58E-08	5.50E-07	2.40E-06	6.11E-07	1.98E-05
39	1.18E-07	2.16E-07	2.03E-07	9.22E-08	4.41E-09	9.60E-08	1.06E-06	2.59E-06	1.97E-07
40	4.83E-08	1.57E-07	2.20E-07	1.63E-07	5.26E-08	9.74E-10	2.67E-07	1.76E-06	1.79E-06
41	8.06E-09	8.69E-08	1.89E-07	2.05E-07	1.21E-07	2.37E-08	2.59E-08	6.19E-07	2.36E-06
42	1.08E-09	3.09E-08	1.30E-07	2.07E-07	1.81E-07	8.35E-08	4.85E-09	1.15E-07	1.20E-06
43	1.93E-08	2.52E-09	6.57E-08	1.69E-07	2.11E-07	1.51E-07	5.27E-08	1.26E-09	3.28E-07
44	4.72E-08	4.73E-09	1.76E-08	1.06E-07	1.94E-07	1.97E-07	1.17E-07	2.61E-08	2.94E-08
45	6.45E-08	2.56E-08	1.35E-10	4.40E-08	1.36E-07	1.93E-07	1.62E-07	7.94E-08	5.66E-09
46	6.33E-08	4.39E-08	6.54E-09	9.61E-09	7.44E-08	1.50E-07	1.67E-07	1.16E-07	4.20E-08
47	5.76E-08	5.77E-08	2.28E-08	3.00E-11	3.46E-08	1.11E-07	1.62E-07	1.46E-07	8.32E-08
48	4.11E-08	5.65E-08	3.69E-08	5.22E-09	8.41E-09	6.20E-08	1.25E-07	1.43E-07	1.07E-07

Table C.22: Franck-Condon factors for transitions from $X^2\Pi$ SF²⁺ ($v' = 0 - 48$) to $b^1\Sigma^+$ SF⁺ ($v'' = 18 - 26$).

$v' \setminus v''$	27	28	29	30	31	32	33	34	35
0	9.31E-11	1.04E-11	8.14E-11	8.95E-11	4.98E-11	1.59E-11	2.65E-12	2.24E-13	1.53E-13
1	1.21E-08	6.01E-09	1.75E-09	1.15E-10	1.58E-10	7.57E-10	1.24E-09	1.38E-09	1.24E-09
2	3.71E-08	3.75E-08	2.33E-08	8.75E-09	1.21E-09	1.42E-10	1.78E-09	3.24E-09	3.56E-09
3	3.51E-12	1.60E-08	3.40E-08	3.55E-08	2.52E-08	1.31E-08	4.88E-09	1.08E-09	4.25E-11
4	2.00E-07	5.34E-08	9.38E-10	1.44E-08	4.39E-08	5.96E-08	5.64E-08	4.26E-08	2.71E-08
5	5.03E-07	3.80E-07	1.75E-07	3.66E-08	1.21E-10	2.54E-08	6.08E-08	7.85E-08	7.55E-08
6	6.40E-08	2.82E-07	3.55E-07	2.65E-07	1.27E-07	3.21E-08	4.69E-10	9.31E-09	2.92E-08
7	1.21E-06	1.35E-07	1.73E-08	1.69E-07	2.62E-07	2.35E-07	1.49E-07	6.78E-08	1.92E-08
8	1.02E-05	4.27E-06	1.31E-06	1.95E-07	1.56E-09	1.04E-07	1.98E-07	2.09E-07	1.62E-07
9	3.74E-05	2.02E-05	1.00E-05	4.37E-06	1.52E-06	3.51E-07	2.23E-08	1.56E-08	7.20E-08
10	1.18E-04	6.56E-05	3.69E-05	2.04E-05	1.07E-05	5.21E-06	2.26E-06	8.39E-07	2.47E-07
11	3.89E-04	2.07E-04	1.16E-04	6.66E-05	3.90E-05	2.27E-05	1.29E-05	7.08E-06	3.73E-06
12	1.27E-03	6.69E-04	3.63E-04	2.04E-04	1.19E-04	7.14E-05	4.36E-05	2.67E-05	1.64E-05
13	3.71E-03	2.03E-03	1.12E-03	6.22E-04	3.56E-04	2.10E-04	1.28E-04	7.96E-05	5.05E-05
14	9.14E-03	5.39E-03	3.11E-03	1.79E-03	1.03E-03	6.05E-04	3.63E-04	2.24E-04	1.42E-04
15	1.83E-02	1.19E-02	7.44E-03	4.54E-03	2.73E-03	1.64E-03	9.96E-04	6.14E-04	3.86E-04
16	2.89E-02	2.13E-02	1.48E-02	9.77E-03	6.28E-03	3.97E-03	2.50E-03	1.58E-03	1.00E-03
17	3.45E-02	3.00E-02	2.37E-02	1.74E-02	1.22E-02	8.26E-03	5.49E-03	3.61E-03	2.37E-03
18	2.83E-02	3.15E-02	2.96E-02	2.50E-02	1.95E-02	1.44E-02	1.03E-02	7.16E-03	4.92E-03
19	1.21E-02	2.17E-02	2.71E-02	2.76E-02	2.49E-02	2.06E-02	1.61E-02	1.20E-02	8.75E-03
20	3.02E-04	6.40E-03	1.51E-02	2.15E-02	2.41E-02	2.32E-02	2.04E-02	1.67E-02	1.31E-02
21	7.14E-03	1.72E-04	2.42E-03	9.12E-03	1.55E-02	1.93E-02	2.01E-02	1.86E-02	1.60E-02
22	2.48E-02	1.10E-02	1.70E-03	3.44E-04	4.36E-03	9.74E-03	1.38E-02	1.56E-02	1.54E-02
23	2.72E-02	2.57E-02	1.46E-02	4.35E-03	1.21E-04	1.25E-03	4.85E-03	8.36E-03	1.05E-02
24	8.63E-03	2.26E-02	2.51E-02	1.73E-02	7.54E-03	1.47E-03	2.39E-05	1.49E-03	3.81E-03
25	1.06E-03	4.92E-03	1.77E-02	2.30E-02	1.88E-02	1.06E-02	3.90E-03	5.83E-04	5.27E-05
26	2.32E-02	2.48E-03	2.26E-03	1.29E-02	1.98E-02	1.88E-02	1.29E-02	6.72E-03	2.49E-03
27	3.84E-02	2.44E-02	4.23E-03	6.41E-04	8.40E-03	1.58E-02	1.73E-02	1.39E-02	9.08E-03
28	1.12E-03	3.44E-02	2.53E-02	6.17E-03	1.28E-05	4.64E-03	1.13E-02	1.43E-02	1.33E-02
29	4.83E-02	2.12E-04	2.97E-02	2.59E-02	8.21E-03	3.06E-04	1.85E-03	6.86E-03	1.03E-02
30	5.83E-01	6.40E-02	1.90E-06	2.41E-02	2.62E-02	1.03E-02	1.41E-03	2.87E-04	3.11E-03
31	1.02E-02	5.83E-01	7.94E-02	1.46E-04	1.76E-02	2.59E-02	1.25E-02	3.19E-03	8.29E-05
32	7.54E-02	2.56E-03	5.84E-01	9.21E-02	2.02E-04	1.07E-02	2.43E-02	1.46E-02	5.45E-03
33	8.99E-03	7.11E-02	1.52E-04	5.89E-01	9.85E-02	1.04E-05	4.55E-03	2.02E-02	1.64E-02
34	1.95E-03	1.62E-02	6.21E-02	7.15E-05	6.04E-01	9.39E-02	6.82E-04	8.48E-04	1.29E-02
35	3.42E-03	5.82E-04	2.37E-02	5.04E-02	2.92E-05	6.33E-01	7.26E-02	5.93E-03	1.55E-06
36	6.00E-04	3.68E-03	1.85E-06	3.00E-02	3.76E-02	8.02E-04	6.71E-01	3.43E-02	2.03E-02
37	2.67E-06	1.21E-03	3.35E-03	4.43E-04	3.45E-02	2.49E-02	9.93E-03	6.90E-01	1.04E-03
38	8.46E-05	2.83E-05	1.88E-03	2.58E-03	1.58E-03	3.75E-02	1.26E-02	4.48E-02	6.29E-01
39	4.34E-05	6.05E-05	1.80E-04	2.41E-03	1.69E-03	2.66E-03	4.11E-02	2.29E-03	1.24E-01
40	4.65E-06	6.70E-05	2.10E-05	4.64E-04	2.67E-03	9.33E-04	2.75E-03	4.91E-02	2.04E-03
41	3.94E-07	1.71E-05	7.74E-05	1.11E-10	8.12E-04	2.67E-03	4.27E-04	1.34E-03	6.93E-02
42	2.39E-06	2.78E-07	3.63E-05	6.87E-05	2.53E-05	1.12E-03	2.58E-03	1.17E-04	5.93E-05
43	1.90E-06	1.60E-06	3.86E-06	5.55E-05	4.77E-05	8.70E-05	1.25E-03	2.69E-03	4.84E-05
44	7.01E-07	2.36E-06	4.57E-07	1.16E-05	6.68E-05	2.70E-05	1.46E-04	1.08E-03	3.86E-03
45	1.21E-07	1.17E-06	2.19E-06	3.29E-08	2.15E-05	6.56E-05	1.27E-05	2.01E-04	4.04E-04
46	2.30E-09	3.27E-07	1.60E-06	1.29E-06	1.69E-06	3.14E-05	5.29E-05	5.99E-06	3.83E-04
47	1.49E-08	5.16E-08	7.43E-07	1.89E-06	2.83E-07	6.77E-06	4.12E-05	4.26E-05	2.62E-06
48	4.78E-08	3.17E-11	1.92E-07	1.14E-06	1.44E-06	8.61E-08	1.32E-05	3.58E-05	5.09E-05

Table C.23: Franck-Condon factors for transitions from $X \ ^2\Pi \ SF^{2+}$ ($v' = 0 - 48$) to $b \ ^1\Sigma^+ \ SF^+$ ($v'' = 27 - 35$).

$v' \setminus v''$	36	37	38	39	40	41	42	43
0	8.74E-13	2.85E-12	5.46E-12	7.61E-12	9.02E-12	9.69E-12	9.30E-12	6.99E-12
1	9.73E-10	6.86E-10	4.52E-10	2.87E-10	1.82E-10	1.17E-10	7.34E-11	3.88E-11
2	3.01E-09	2.16E-09	1.39E-09	8.52E-10	5.16E-10	3.13E-10	1.84E-10	9.16E-11
3	9.81E-11	3.42E-10	4.75E-10	4.89E-10	4.46E-10	3.87E-10	3.15E-10	2.07E-10
4	1.50E-08	7.33E-09	3.22E-09	1.29E-09	4.61E-10	1.34E-10	2.17E-11	1.54E-13
5	6.06E-08	4.32E-08	2.85E-08	1.81E-08	1.16E-08	7.55E-09	4.81E-09	2.60E-09
6	4.30E-08	4.63E-08	4.21E-08	3.51E-08	2.83E-08	2.27E-08	1.75E-08	1.11E-08
7	1.48E-09	1.10E-09	6.07E-09	1.04E-08	1.29E-08	1.38E-08	1.32E-08	9.73E-09
8	1.02E-07	5.37E-08	2.45E-08	9.70E-09	3.22E-09	7.31E-10	3.72E-11	3.75E-11
9	1.03E-07	1.00E-07	8.07E-08	5.92E-08	4.21E-08	2.98E-08	2.03E-08	1.15E-08
10	4.67E-08	1.79E-09	3.10E-09	1.10E-08	1.59E-08	1.78E-08	1.70E-08	1.23E-08
11	1.90E-06	9.33E-07	4.51E-07	2.20E-07	1.11E-07	5.74E-08	2.94E-08	1.31E-08
12	9.95E-06	6.03E-06	3.67E-06	2.28E-06	1.48E-06	9.98E-07	6.71E-07	3.84E-07
13	3.25E-05	2.11E-05	1.38E-05	9.24E-06	6.42E-06	4.63E-06	3.30E-06	1.99E-06
14	9.15E-05	6.01E-05	4.01E-05	2.74E-05	1.95E-05	1.44E-05	1.05E-05	6.44E-06
15	2.48E-04	1.62E-04	1.08E-04	7.39E-05	5.27E-05	3.90E-05	2.86E-05	1.76E-05
16	6.47E-04	4.23E-04	2.81E-04	1.92E-04	1.37E-04	1.01E-04	7.40E-05	4.56E-05
17	1.56E-03	1.04E-03	6.95E-04	4.77E-04	3.40E-04	2.52E-04	1.85E-04	1.14E-04
18	3.35E-03	2.28E-03	1.56E-03	1.09E-03	7.82E-04	5.84E-04	4.30E-04	2.66E-04
19	6.25E-03	4.41E-03	3.10E-03	2.20E-03	1.61E-03	1.22E-03	9.05E-04	5.63E-04
20	9.90E-03	7.31E-03	5.32E-03	3.88E-03	2.90E-03	2.23E-03	1.68E-03	1.06E-03
21	1.31E-02	1.02E-02	7.76E-03	5.86E-03	4.49E-03	3.52E-03	2.70E-03	1.72E-03
22	1.39E-02	1.17E-02	9.40E-03	7.40E-03	5.87E-03	4.72E-03	3.69E-03	2.38E-03
23	1.11E-02	1.04E-02	9.08E-03	7.58E-03	6.28E-03	5.22E-03	4.20E-03	2.76E-03
24	5.64E-03	6.49E-03	6.45E-03	5.89E-03	5.21E-03	4.55E-03	3.80E-03	2.57E-03
25	9.01E-04	1.97E-03	2.68E-03	2.95E-03	2.95E-03	2.81E-03	2.50E-03	1.77E-03
26	4.97E-04	1.58E-06	1.71E-04	4.77E-04	7.22E-04	8.76E-04	9.11E-04	7.13E-04
27	4.92E-03	2.24E-03	8.35E-04	2.37E-04	3.65E-05	1.85E-07	2.24E-05	4.22E-05
28	1.02E-02	6.83E-03	4.21E-03	2.48E-03	1.45E-03	8.50E-04	4.81E-04	2.30E-04
29	1.09E-02	9.47E-03	7.31E-03	5.33E-03	3.83E-03	2.78E-03	1.96E-03	1.15E-03
30	6.04E-03	7.34E-03	7.12E-03	6.15E-03	5.08E-03	4.13E-03	3.22E-03	2.05E-03
31	6.99E-04	2.39E-03	3.60E-03	4.01E-03	3.93E-03	3.63E-03	3.11E-03	2.13E-03
32	1.13E-03	8.77E-06	3.21E-04	9.25E-04	1.38E-03	1.64E-03	1.66E-03	1.26E-03
33	8.03E-03	3.07E-03	8.71E-04	1.25E-04	1.55E-06	9.13E-05	2.15E-04	2.41E-04
34	1.60E-02	1.05E-02	5.51E-03	2.68E-03	1.27E-03	5.73E-04	2.30E-04	7.13E-05
35	4.61E-03	1.13E-02	1.09E-02	7.66E-03	4.93E-03	3.13E-03	1.93E-03	1.02E-03
36	3.86E-05	3.24E-04	3.56E-03	6.41E-03	6.82E-03	5.92E-03	4.54E-03	2.77E-03
37	3.60E-02	3.83E-03	1.62E-05	8.94E-05	8.47E-04	1.98E-03	2.68E-03	2.29E-03
38	3.77E-02	2.23E-02	1.85E-02	3.68E-03	3.11E-04	1.41E-05	1.70E-05	5.85E-05
39	4.13E-01	1.91E-01	2.07E-03	1.19E-02	1.43E-02	7.78E-03	3.02E-03	8.93E-04
40	2.22E-01	1.06E-01	2.85E-01	1.07E-01	1.25E-02	1.92E-04	4.47E-03	5.09E-03
41	2.51E-02	2.14E-01	9.32E-03	9.31E-02	1.70E-01	1.24E-01	5.81E-02	1.86E-02
42	1.12E-01	5.13E-02	5.59E-02	1.16E-01	1.76E-02	8.41E-03	4.97E-02	5.75E-02
43	9.83E-03	1.64E-01	1.69E-02	4.34E-03	2.66E-02	6.89E-02	5.33E-02	1.96E-02
44	3.34E-03	5.96E-02	1.36E-01	1.64E-02	7.55E-03	8.00E-03	1.09E-07	4.90E-03
45	1.05E-02	3.23E-02	1.39E-01	1.59E-02	7.04E-02	2.15E-02	1.87E-04	2.05E-03
46	1.97E-04	3.98E-02	1.15E-01	9.43E-02	3.47E-02	4.75E-03	3.28E-02	2.56E-02
47	7.38E-04	4.21E-03	9.83E-02	1.32E-01	9.95E-04	4.84E-02	3.13E-02	4.58E-03
48	6.95E-06	1.19E-03	2.54E-02	2.13E-01	8.08E-02	2.98E-02	1.49E-03	1.19E-02

Table C.24: Franck-Condon factors for transitions from $X \ ^2\Pi \text{ SF}^{2+}$ ($v' = 0 - 48$) to $b \ ^1\Sigma^+ \text{ SF}^+$ ($v'' = 36 - 43$).

$v' \setminus v''$	0	1	2	3	4	5	6	7
0	2.59E-16	4.10E-15	3.12E-14	1.59E-13	6.00E-13	1.77E-12	4.24E-12	8.41E-12
1	1.59E-14	2.35E-13	1.71E-12	8.34E-12	3.02E-11	8.59E-11	1.99E-10	3.83E-10
2	4.70E-13	6.53E-12	4.54E-11	2.11E-10	7.31E-10	2.00E-09	4.47E-09	8.34E-09
3	8.94E-12	1.17E-10	7.75E-10	3.43E-09	1.14E-08	2.98E-08	6.41E-08	1.15E-07
4	1.24E-10	1.53E-09	9.60E-09	4.03E-08	1.27E-07	3.19E-07	6.57E-07	1.14E-06
5	1.34E-09	1.56E-08	9.18E-08	3.64E-07	1.09E-06	2.60E-06	5.12E-06	8.53E-06
6	1.17E-08	1.27E-07	7.03E-07	2.62E-06	7.40E-06	1.67E-05	3.14E-05	5.00E-05
7	8.53E-08	8.62E-07	4.44E-06	1.55E-05	4.10E-05	8.73E-05	1.55E-04	2.35E-04
8	5.27E-07	4.93E-06	2.35E-05	7.63E-05	1.88E-04	3.74E-04	6.25E-04	8.96E-04
9	2.81E-06	2.41E-05	1.06E-04	3.16E-04	7.20E-04	1.33E-03	2.07E-03	2.78E-03
10	1.30E-05	1.02E-04	4.07E-04	1.11E-03	2.31E-03	3.92E-03	5.63E-03	7.03E-03
11	5.31E-05	3.73E-04	1.34E-03	3.30E-03	6.22E-03	9.56E-03	1.25E-02	1.43E-02
12	1.91E-04	1.20E-03	3.83E-03	8.37E-03	1.40E-02	1.91E-02	2.22E-02	2.26E-02
13	6.13E-04	3.36E-03	9.41E-03	1.79E-02	2.59E-02	3.06E-02	3.06E-02	2.68E-02
14	1.75E-03	8.28E-03	1.98E-02	3.19E-02	3.86E-02	3.75E-02	3.04E-02	2.10E-02
15	4.49E-03	1.78E-02	3.53E-02	4.62E-02	4.42E-02	3.24E-02	1.83E-02	7.77E-03
16	1.03E-02	3.33E-02	5.25E-02	5.23E-02	3.52E-02	1.54E-02	3.31E-03	2.34E-06
17	2.11E-02	5.37E-02	6.31E-02	4.21E-02	1.47E-02	9.69E-04	1.73E-03	7.65E-03
18	3.88E-02	7.33E-02	5.73E-02	1.89E-02	3.47E-04	5.65E-03	1.61E-02	1.97E-02
19	6.39E-02	8.24E-02	3.40E-02	9.89E-04	8.78E-03	2.42E-02	2.51E-02	1.57E-02
20	9.40E-02	7.21E-02	7.56E-03	7.86E-03	3.09E-02	2.93E-02	1.27E-02	1.77E-03
21	1.23E-01	4.33E-02	1.43E-03	3.42E-02	3.56E-02	1.09E-02	1.67E-05	4.82E-03
22	1.42E-01	1.14E-02	2.55E-02	4.75E-02	1.37E-02	3.95E-04	1.25E-02	2.00E-02
23	1.44E-01	5.11E-04	5.81E-02	2.73E-02	2.60E-04	1.96E-02	2.68E-02	1.45E-02
24	1.28E-01	2.50E-02	6.30E-02	1.46E-02	2.24E-02	3.36E-02	1.19E-02	1.17E-04
25	9.88E-02	7.48E-02	3.14E-02	1.34E-02	4.43E-02	1.29E-02	6.77E-04	1.29E-02
26	6.52E-02	1.20E-01	1.33E-03	5.25E-02	2.44E-02	1.32E-03	2.28E-02	2.39E-02
27	3.65E-02	1.33E-01	1.70E-02	6.02E-02	3.58E-05	3.00E-02	2.86E-02	4.77E-03
28	1.72E-02	1.12E-01	7.49E-02	2.21E-02	2.61E-02	4.03E-02	3.06E-03	6.84E-03
29	6.71E-03	7.33E-02	1.26E-01	6.06E-04	6.28E-02	7.92E-03	1.27E-02	3.01E-02
30	2.16E-03	3.79E-02	1.32E-01	4.27E-02	4.21E-02	9.23E-03	4.21E-02	1.35E-02
31	5.69E-04	1.56E-02	9.74E-02	1.10E-01	1.95E-03	5.48E-02	2.00E-02	2.57E-03
32	1.23E-04	5.14E-03	5.38E-02	1.38E-01	2.43E-02	5.46E-02	1.53E-03	3.55E-02
33	2.17E-05	1.37E-03	2.29E-02	1.11E-01	9.59E-02	8.51E-03	4.34E-02	3.11E-02
34	3.18E-06	2.96E-04	7.72E-03	6.47E-02	1.38E-01	1.27E-02	6.17E-02	2.90E-04
35	3.93E-07	5.33E-05	2.10E-03	2.86E-02	1.20E-01	8.06E-02	1.82E-02	2.88E-02
36	4.19E-08	8.11E-06	4.71E-04	9.98E-03	7.34E-02	1.33E-01	3.86E-03	6.34E-02
37	3.98E-09	1.07E-06	8.98E-05	2.86E-03	3.42E-02	1.26E-01	5.94E-02	3.30E-02
38	3.47E-10	1.28E-07	1.50E-05	6.94E-04	1.29E-02	8.33E-02	1.19E-01	8.80E-05
39	2.88E-11	1.43E-08	2.27E-06	1.48E-04	4.07E-03	4.27E-02	1.28E-01	3.02E-02
40	2.98E-12	1.49E-09	3.18E-07	2.85E-05	1.12E-03	1.80E-02	9.64E-02	8.92E-02
41	9.25E-14	1.38E-10	4.11E-08	4.99E-06	2.74E-04	6.45E-03	5.58E-02	1.17E-01
42	8.50E-16	1.41E-11	4.81E-09	8.21E-07	6.17E-05	2.05E-03	2.67E-02	1.01E-01
43	7.45E-14	7.44E-13	7.21E-10	1.54E-07	1.48E-05	6.48E-04	1.18E-02	6.99E-02
44	1.64E-14	5.73E-13	2.73E-10	4.78E-08	4.89E-06	2.50E-04	5.74E-03	4.79E-02
45	2.55E-15	1.73E-12	1.57E-10	2.53E-08	2.36E-06	1.26E-04	3.35E-03	3.65E-02
46	8.91E-14	6.91E-15	6.49E-11	9.74E-09	9.09E-07	5.29E-05	1.70E-03	2.46E-02
47	9.12E-14	1.21E-15	2.15E-13	9.66E-11	3.87E-08	5.31E-06	3.26E-04	8.39E-03
48	8.81E-15	1.19E-17	2.13E-11	1.52E-09	6.30E-08	7.89E-07	1.67E-06	1.22E-03

Table C.25: Franck-Condon factors for transitions from $X^2\Pi$ SF $^{2+}$ ($v' = 0 - 48$) to $c^1\Sigma^-$ SF $^+$ ($v'' = 0 - 7$).

$v' \setminus v''$	8	9	10	11	12	13	14
0	1.41E-11	2.07E-11	2.79E-11	3.55E-11	4.25E-11	4.72E-11	4.63E-11
1	6.25E-10	8.98E-10	1.19E-09	1.49E-09	1.76E-09	1.93E-09	1.87E-09
2	1.32E-08	1.86E-08	2.41E-08	2.97E-08	3.45E-08	3.74E-08	3.59E-08
3	1.78E-07	2.44E-07	3.09E-07	3.73E-07	4.27E-07	4.56E-07	4.32E-07
4	1.70E-06	2.27E-06	2.81E-06	3.32E-06	3.73E-06	3.92E-06	3.67E-06
5	1.23E-05	1.59E-05	1.91E-05	2.22E-05	2.44E-05	2.52E-05	2.33E-05
6	6.93E-05	8.64E-05	1.01E-04	1.14E-04	1.23E-04	1.25E-04	1.13E-04
7	3.12E-04	3.75E-04	4.25E-04	4.66E-04	4.90E-04	4.86E-04	4.33E-04
8	1.13E-03	1.30E-03	1.42E-03	1.51E-03	1.54E-03	1.49E-03	1.30E-03
9	3.32E-03	3.64E-03	3.81E-03	3.89E-03	3.83E-03	3.59E-03	3.06E-03
10	7.84E-03	8.09E-03	8.03E-03	7.82E-03	7.39E-03	6.68E-03	5.52E-03
11	1.46E-02	1.40E-02	1.30E-02	1.19E-02	1.07E-02	9.19E-03	7.27E-03
12	2.09E-02	1.82E-02	1.54E-02	1.30E-02	1.07E-02	8.53E-03	6.31E-03
13	2.13E-02	1.59E-02	1.16E-02	8.44E-03	5.99E-03	4.12E-03	2.65E-03
14	1.29E-02	7.14E-03	3.69E-03	1.73E-03	6.82E-04	1.95E-04	2.57E-05
15	2.18E-03	2.15E-04	7.13E-05	6.17E-04	1.29E-03	1.80E-03	1.92E-03
16	1.44E-03	3.84E-03	5.63E-03	6.59E-03	6.77E-03	6.28E-03	5.16E-03
17	1.17E-02	1.25E-02	1.14E-02	9.55E-03	7.47E-03	5.48E-03	3.68E-03
18	1.65E-02	1.12E-02	6.70E-03	3.58E-03	1.64E-03	6.03E-04	1.50E-04
19	6.53E-03	1.59E-03	6.06E-05	2.51E-04	1.04E-03	1.78E-03	2.07E-03
20	2.41E-04	2.79E-03	5.40E-03	6.90E-03	7.19E-03	6.53E-03	5.17E-03
21	1.11E-02	1.29E-02	1.13E-02	8.56E-03	5.77E-03	3.50E-03	1.87E-03
22	1.62E-02	9.03E-03	3.69E-03	9.42E-04	4.03E-05	1.32E-04	4.93E-04
23	3.29E-03	8.43E-06	1.24E-03	3.48E-03	5.10E-03	5.61E-03	4.98E-03
24	3.67E-03	9.22E-03	1.12E-02	1.02E-02	7.82E-03	5.22E-03	3.03E-03
25	1.84E-02	1.39E-02	7.32E-03	2.71E-03	5.06E-04	2.29E-07	2.39E-04
26	9.77E-03	1.19E-03	2.61E-04	2.51E-03	4.81E-03	5.85E-03	5.40E-03
27	8.30E-04	7.49E-03	1.17E-02	1.16E-02	8.89E-03	5.68E-03	3.04E-03
28	1.93E-02	1.73E-02	9.25E-03	3.08E-03	3.52E-04	8.50E-05	6.99E-04
29	1.57E-02	2.24E-03	3.16E-04	3.67E-03	6.86E-03	7.89E-03	6.79E-03
30	1.24E-04	8.49E-03	1.47E-02	1.38E-02	9.32E-03	4.81E-03	1.87E-03
31	2.21E-02	2.17E-02	1.01E-02	2.06E-03	4.13E-06	1.23E-03	2.69E-03
32	2.36E-02	2.84E-03	1.08E-03	7.23E-03	1.13E-02	1.10E-02	8.07E-03
33	1.30E-04	1.09E-02	2.02E-02	1.66E-02	8.56E-03	2.68E-03	3.21E-04
34	2.39E-02	2.91E-02	1.15E-02	8.92E-04	1.03E-03	4.82E-03	6.81E-03
35	3.92E-02	5.67E-03	1.91E-03	1.24E-02	1.69E-02	1.37E-02	7.90E-03
36	6.48E-03	9.61E-03	2.66E-02	2.08E-02	7.86E-03	9.23E-04	1.57E-04
37	1.15E-02	3.97E-02	1.84E-02	9.86E-04	2.76E-03	9.53E-03	1.15E-02
38	5.43E-02	2.20E-02	2.08E-04	1.43E-02	2.23E-02	1.65E-02	7.63E-03
39	5.13E-02	1.34E-04	2.59E-02	2.95E-02	1.15E-02	8.75E-04	7.42E-04
40	1.13E-02	2.88E-02	3.85E-02	7.45E-03	1.04E-03	1.06E-02	1.46E-02
41	3.02E-03	5.66E-02	1.17E-02	3.95E-03	2.25E-02	2.30E-02	1.17E-02
42	3.47E-02	4.00E-02	1.02E-03	2.83E-02	2.67E-02	7.71E-03	1.08E-04
43	6.75E-02	1.00E-02	2.07E-02	3.27E-02	7.26E-03	5.71E-04	7.49E-03
44	8.85E-02	2.44E-04	4.00E-02	1.46E-02	6.13E-04	1.28E-02	1.61E-02
45	1.10E-01	2.08E-02	4.27E-02	2.04E-04	1.65E-02	2.24E-02	1.02E-02
46	1.17E-01	8.13E-02	1.87E-02	1.57E-02	3.41E-02	1.07E-02	3.24E-05
47	7.35E-02	1.36E-01	1.32E-03	4.66E-02	1.46E-02	7.12E-04	1.12E-02
48	3.33E-02	1.72E-01	9.26E-02	2.92E-02	7.13E-03	2.45E-02	1.35E-02

Table C.26: Franck-Condon factors for transitions from $X^2\Pi$ SF $^{2+}$ ($v' = 0 - 48$) to $c^1\Sigma^-$ SF $^+$ ($v'' = 8 - 14$).

$v' \setminus v''$	0	1	2	3	4	5	6	7
0	9.00E-32	1.02E-29	3.80E-28	3.35E-27	2.16E-26	1.26E-25	3.32E-25	1.45E-24
1	6.89E-29	3.18E-27	7.72E-26	6.20E-25	3.66E-24	1.92E-23	5.30E-23	2.08E-22
2	9.60E-27	3.37E-25	6.42E-24	4.83E-23	2.67E-22	1.29E-21	3.68E-21	1.32E-20
3	5.70E-25	1.76E-23	2.89E-22	2.08E-21	1.10E-20	5.01E-20	1.46E-19	4.92E-19
4	2.55E-23	6.79E-22	9.52E-21	6.54E-20	3.30E-19	1.42E-18	4.21E-18	1.33E-17
5	8.01E-22	1.88E-20	2.30E-19	1.52E-18	7.38E-18	3.02E-17	9.08E-17	2.72E-16
6	1.92E-20	4.02E-19	4.36E-18	2.77E-17	1.30E-16	5.11E-16	1.55E-15	4.44E-15
7	3.68E-19	6.93E-18	6.78E-17	4.16E-16	1.91E-15	7.20E-15	2.18E-14	6.02E-14
8	5.75E-18	9.83E-17	8.84E-16	5.26E-15	2.36E-14	8.61E-14	2.58E-13	6.92E-13
9	7.46E-17	1.18E-15	9.91E-15	5.73E-14	2.51E-13	8.93E-13	2.64E-12	6.90E-12
10	8.25E-16	1.22E-14	9.76E-14	5.49E-13	2.36E-12	8.16E-12	2.37E-11	6.04E-11
11	7.91E-15	1.10E-13	8.54E-13	4.69E-12	1.97E-11	6.63E-11	1.88E-10	4.70E-10
12	6.71E-14	8.98E-13	6.74E-12	3.60E-11	1.47E-10	4.85E-10	1.34E-09	3.27E-09
13	5.11E-13	6.60E-12	4.82E-11	2.51E-10	9.99E-10	3.19E-09	8.63E-09	2.05E-08
14	3.53E-12	4.43E-11	3.15E-10	1.59E-09	6.16E-09	1.91E-08	5.01E-08	1.16E-07
15	2.24E-11	2.73E-10	1.89E-09	9.23E-09	3.46E-08	1.04E-07	2.65E-07	5.93E-07
16	1.31E-10	1.55E-09	1.04E-08	4.91E-08	1.78E-07	5.16E-07	1.27E-06	2.75E-06
17	7.13E-10	8.16E-09	5.27E-08	2.40E-07	8.37E-07	2.34E-06	5.55E-06	1.16E-05
18	3.60E-09	3.98E-08	2.47E-07	1.08E-06	3.62E-06	9.70E-06	2.21E-05	4.44E-05
19	1.69E-08	1.80E-07	1.07E-06	4.49E-06	1.43E-05	3.67E-05	7.99E-05	1.54E-04
20	7.42E-08	7.57E-07	4.31E-06	1.72E-05	5.21E-05	1.27E-04	2.63E-04	4.80E-04
21	3.04E-07	2.96E-06	1.60E-05	6.04E-05	1.73E-04	3.99E-04	7.79E-04	1.35E-03
22	1.16E-06	1.07E-05	5.50E-05	1.95E-04	5.26E-04	1.13E-03	2.08E-03	3.37E-03
23	4.14E-06	3.63E-05	1.74E-04	5.78E-04	1.45E-03	2.90E-03	4.93E-03	7.42E-03
24	1.38E-05	1.13E-04	5.08E-04	1.56E-03	3.59E-03	6.61E-03	1.03E-02	1.42E-02
25	4.29E-05	3.28E-04	1.36E-03	3.81E-03	7.98E-03	1.33E-02	1.86E-02	2.29E-02
26	1.24E-04	8.75E-04	3.30E-03	8.36E-03	1.57E-02	2.31E-02	2.84E-02	3.03E-02
27	3.32E-04	2.14E-03	7.27E-03	1.63E-02	2.67E-02	3.39E-02	3.52E-02	3.08E-02
28	8.26E-04	4.81E-03	1.44E-02	2.81E-02	3.88E-02	4.04E-02	3.29E-02	2.09E-02
29	1.90E-03	9.83E-03	2.55E-02	4.17E-02	4.64E-02	3.64E-02	1.99E-02	6.18E-03
30	4.05E-03	1.82E-02	3.98E-02	5.21E-02	4.29E-02	2.11E-02	4.31E-03	1.59E-04
31	7.97E-03	3.06E-02	5.40E-02	5.25E-02	2.69E-02	4.27E-03	9.78E-04	1.07E-02
32	1.45E-02	4.60E-02	6.22E-02	3.94E-02	7.38E-03	1.23E-03	1.50E-02	2.56E-02
33	2.44E-02	6.16E-02	5.86E-02	1.78E-02	2.34E-04	1.67E-02	3.01E-02	2.35E-02
34	3.80E-02	7.27E-02	4.19E-02	1.60E-03	1.35E-02	3.41E-02	2.55E-02	6.11E-03
35	5.47E-02	7.41E-02	1.86E-02	4.27E-03	3.52E-02	3.13E-02	6.23E-03	1.33E-03
36	7.28E-02	6.32E-02	1.96E-03	2.52E-02	4.15E-02	1.05E-02	1.53E-03	1.86E-02
37	8.98E-02	4.21E-02	3.37E-03	4.63E-02	2.38E-02	2.14E-04	2.03E-02	2.81E-02
38	1.03E-01	1.86E-02	2.32E-02	4.71E-02	2.65E-03	1.66E-02	3.24E-02	1.18E-02
39	1.09E-01	2.66E-03	4.83E-02	2.59E-02	5.10E-03	3.66E-02	1.69E-02	1.55E-04
40	1.06E-01	1.55E-03	6.04E-02	3.68E-03	2.93E-02	3.02E-02	2.07E-04	1.67E-02
41	9.35E-02	1.51E-02	5.03E-02	2.92E-03	4.45E-02	6.95E-03	1.18E-02	3.06E-02
42	7.42E-02	3.44E-02	2.65E-02	2.17E-02	3.21E-02	1.25E-03	3.11E-02	1.62E-02
43	5.58E-02	5.08E-02	6.78E-03	3.92E-02	9.66E-03	1.70E-02	2.70E-02	5.17E-04
44	4.51E-02	6.69E-02	1.11E-05	4.46E-02	4.51E-06	3.18E-02	8.39E-03	7.01E-03
45	4.24E-02	9.33E-02	1.11E-02	3.73E-02	1.29E-02	3.02E-02	4.49E-04	2.47E-02
46	3.67E-02	1.17E-01	5.33E-02	1.19E-02	4.60E-02	7.58E-03	2.15E-02	2.21E-02
47	1.82E-02	9.18E-02	1.04E-01	4.08E-03	4.41E-02	5.26E-03	3.42E-02	4.80E-04
48	5.98E-03	5.76E-02	1.54E-01	9.84E-02	7.67E-04	4.25E-02	1.42E-03	1.52E-02

Table C.27: Franck-Condon factors for transitions from $X^2\Pi SF^{2+}$ ($v' = 0 - 48$) to $e^1\Delta SF^+$ ($v'' = 0 - 7$).

$v' \setminus v''$	8	9	10	11	12	13	14	15
0	4.72E-24	1.06E-23	2.82E-23	5.65E-23	1.34E-22	2.35E-22	3.62E-22	7.23E-22
1	6.26E-22	1.42E-21	3.51E-21	7.01E-21	1.55E-20	2.70E-20	4.23E-20	7.83E-20
2	3.75E-20	8.54E-20	1.99E-19	3.96E-19	8.21E-19	1.43E-18	2.27E-18	3.95E-18
3	1.33E-18	3.04E-18	6.82E-18	1.34E-17	2.66E-17	4.61E-17	7.37E-17	1.23E-16
4	3.47E-17	7.87E-17	1.70E-16	3.33E-16	6.34E-16	1.09E-15	1.75E-15	2.81E-15
5	6.88E-16	1.55E-15	3.26E-15	6.29E-15	1.16E-14	1.97E-14	3.16E-14	4.95E-14
6	1.09E-14	2.43E-14	5.00E-14	9.53E-14	1.72E-13	2.89E-13	4.61E-13	7.06E-13
7	1.45E-13	3.18E-13	6.41E-13	1.20E-12	2.13E-12	3.54E-12	5.59E-12	8.43E-12
8	1.64E-12	3.53E-12	6.99E-12	1.29E-11	2.25E-11	3.69E-11	5.75E-11	8.55E-11
9	1.60E-11	3.39E-11	6.60E-11	1.20E-10	2.05E-10	3.32E-10	5.11E-10	7.49E-10
10	1.37E-10	2.85E-10	5.46E-10	9.77E-10	1.64E-09	2.61E-09	3.96E-09	5.72E-09
11	1.05E-09	2.13E-09	4.00E-09	7.01E-09	1.16E-08	1.81E-08	2.70E-08	3.85E-08
12	7.12E-09	1.42E-08	2.60E-08	4.48E-08	7.25E-08	1.11E-07	1.63E-07	2.29E-07
13	4.35E-08	8.45E-08	1.52E-07	2.55E-07	4.05E-07	6.10E-07	8.76E-07	1.21E-06
14	2.39E-07	4.53E-07	7.94E-07	1.30E-06	2.02E-06	2.98E-06	4.20E-06	5.66E-06
15	1.19E-06	2.19E-06	3.74E-06	5.98E-06	9.05E-06	1.30E-05	1.79E-05	2.37E-05
16	5.35E-06	9.56E-06	1.58E-05	2.46E-05	3.62E-05	5.08E-05	6.82E-05	8.80E-05
17	2.18E-05	3.76E-05	6.03E-05	9.09E-05	1.30E-04	1.77E-04	2.31E-04	2.90E-04
18	8.02E-05	1.33E-04	2.06E-04	3.00E-04	4.14E-04	5.45E-04	6.89E-04	8.40E-04
19	2.66E-04	4.24E-04	6.29E-04	8.79E-04	1.17E-03	1.48E-03	1.81E-03	2.13E-03
20	7.92E-04	1.20E-03	1.70E-03	2.28E-03	2.89E-03	3.51E-03	4.11E-03	4.64E-03
21	2.10E-03	3.02E-03	4.05E-03	5.14E-03	6.19E-03	7.15E-03	7.95E-03	8.54E-03
22	4.93E-03	6.65E-03	8.36E-03	9.94E-03	1.12E-02	1.22E-02	1.27E-02	1.28E-02
23	1.01E-02	1.26E-02	1.46E-02	1.61E-02	1.67E-02	1.67E-02	1.60E-02	1.49E-02
24	1.75E-02	1.99E-02	2.09E-02	2.07E-02	1.94E-02	1.72E-02	1.46E-02	1.18E-02
25	2.52E-02	2.52E-02	2.32E-02	1.97E-02	1.56E-02	1.14E-02	7.60E-03	4.58E-03
26	2.84E-02	2.37E-02	1.76E-02	1.15E-02	6.35E-03	2.74E-03	7.14E-04	1.40E-05
27	2.26E-02	1.38E-02	6.44E-03	1.86E-03	7.33E-05	4.57E-04	2.09E-03	4.12E-03
28	9.55E-03	2.31E-03	2.38E-06	1.45E-03	4.71E-03	8.05E-03	1.04E-02	1.12E-02
29	2.39E-04	1.56E-03	6.58E-03	1.16E-02	1.44E-02	1.44E-02	1.23E-02	9.15E-03
30	5.69E-03	1.35E-02	1.80E-02	1.75E-02	1.34E-02	8.12E-03	3.65E-03	9.24E-04
31	2.01E-02	2.17E-02	1.62E-02	8.40E-03	2.45E-03	6.26E-05	7.95E-04	3.17E-03
32	2.29E-02	1.24E-02	3.10E-03	3.02E-07	2.32E-03	6.76E-03	1.03E-02	1.16E-02
33	8.41E-03	2.97E-04	2.43E-03	9.18E-03	1.41E-02	1.46E-02	1.14E-02	6.82E-03
34	2.44E-04	8.00E-03	1.66E-02	1.79E-02	1.26E-02	5.61E-03	1.05E-03	5.80E-05
35	1.40E-02	2.18E-02	1.69E-02	6.89E-03	6.33E-04	8.19E-04	4.84E-03	8.91E-03
36	2.50E-02	1.39E-02	2.10E-03	7.63E-04	6.91E-03	1.27E-02	1.38E-02	1.06E-02
37	1.15E-02	1.43E-04	5.23E-03	1.47E-02	1.69E-02	1.15E-02	4.41E-03	4.17E-04
38	9.73E-05	1.09E-02	2.02E-02	1.57E-02	5.42E-03	1.24E-04	1.97E-03	6.87E-03
39	1.53E-02	2.34E-02	1.21E-02	1.02E-03	1.98E-03	9.36E-03	1.38E-02	1.22E-02
40	2.64E-02	9.52E-03	2.25E-05	7.94E-03	1.65E-02	1.48E-02	7.02E-03	1.05E-03
41	1.02E-02	6.33E-04	1.40E-02	2.03E-02	1.13E-02	1.56E-03	8.30E-04	6.30E-03
42	3.29E-04	1.68E-02	2.19E-02	7.89E-03	2.25E-07	5.88E-03	1.37E-02	1.42E-02
43	1.41E-02	2.29E-02	6.80E-03	4.94E-04	1.04E-02	1.68E-02	1.18E-02	3.34E-03
44	2.38E-02	8.26E-03	6.70E-04	1.24E-02	1.67E-02	7.84E-03	4.25E-04	1.98E-03
45	1.26E-02	4.58E-04	1.41E-02	1.61E-02	4.36E-03	2.71E-04	6.48E-03	1.16E-02
46	1.28E-04	1.76E-02	1.66E-02	1.51E-03	3.51E-03	1.27E-02	1.20E-02	4.54E-03
47	1.96E-02	1.80E-02	2.13E-04	9.18E-03	1.66E-02	7.77E-03	1.88E-04	2.97E-03
48	1.36E-02	1.56E-05	1.03E-02	1.50E-02	3.43E-03	1.24E-03	1.02E-02	1.29E-02

Table C.28: Franck-Condon factors for transitions from $X^2\Pi SF^{2+}$ ($v' = 0 - 48$) to $e^1\Delta SF^+$ ($v'' = 8 - 15$).

$v' \setminus v''$	16	17	18	19	20	21	22
0	1.13E-21	1.56E-21	2.01E-21	2.71E-21	3.89E-21	4.22E-21	3.69E-21
1	1.21E-19	1.69E-19	2.20E-19	2.93E-19	3.97E-19	4.32E-19	3.74E-19
2	6.03E-18	8.45E-18	1.11E-17	1.47E-17	1.90E-17	2.07E-17	1.77E-17
3	1.85E-16	2.61E-16	3.46E-16	4.50E-16	5.66E-16	6.17E-16	5.23E-16
4	4.18E-15	5.88E-15	7.81E-15	1.01E-14	1.23E-14	1.35E-14	1.13E-14
5	7.30E-14	1.02E-13	1.35E-13	1.73E-13	2.09E-13	2.27E-13	1.89E-13
6	1.03E-12	1.43E-12	1.89E-12	2.39E-12	2.84E-12	3.07E-12	2.55E-12
7	1.21E-11	1.67E-11	2.19E-11	2.74E-11	3.24E-11	3.47E-11	2.86E-11
8	1.22E-10	1.65E-10	2.15E-10	2.67E-10	3.12E-10	3.33E-10	2.72E-10
9	1.05E-09	1.41E-09	1.82E-09	2.23E-09	2.59E-09	2.74E-09	2.23E-09
10	7.93E-09	1.05E-08	1.34E-08	1.63E-08	1.87E-08	1.96E-08	1.58E-08
11	5.25E-08	6.88E-08	8.64E-08	1.04E-07	1.18E-07	1.22E-07	9.83E-08
12	3.07E-07	3.97E-07	4.92E-07	5.83E-07	6.55E-07	6.74E-07	5.36E-07
13	1.59E-06	2.03E-06	2.47E-06	2.89E-06	3.21E-06	3.27E-06	2.58E-06
14	7.35E-06	9.18E-06	1.10E-05	1.27E-05	1.39E-05	1.40E-05	1.09E-05
15	3.01E-05	3.69E-05	4.35E-05	4.93E-05	5.32E-05	5.28E-05	4.09E-05
16	1.09E-04	1.31E-04	1.52E-04	1.69E-04	1.79E-04	1.75E-04	1.34E-04
17	3.51E-04	4.11E-04	4.65E-04	5.06E-04	5.27E-04	5.07E-04	3.83E-04
18	9.89E-04	1.13E-03	1.24E-03	1.32E-03	1.34E-03	1.27E-03	9.44E-04
19	2.42E-03	2.67E-03	2.86E-03	2.96E-03	2.93E-03	2.70E-03	1.98E-03
20	5.08E-03	5.40E-03	5.57E-03	5.57E-03	5.35E-03	4.80E-03	3.43E-03
21	8.91E-03	9.04E-03	8.91E-03	8.53E-03	7.87E-03	6.80E-03	4.72E-03
22	1.26E-02	1.20E-02	1.11E-02	1.00E-02	8.76E-03	7.19E-03	4.79E-03
23	1.33E-02	1.16E-02	9.84E-03	8.09E-03	6.43E-03	4.83E-03	2.98E-03
24	9.13E-03	6.75E-03	4.76E-03	3.19E-03	2.01E-03	1.17E-03	5.62E-04
25	2.40E-03	1.01E-03	2.73E-04	1.23E-05	4.78E-05	2.05E-04	2.81E-04
26	2.53E-04	1.02E-03	1.95E-03	2.78E-03	3.33E-03	3.42E-03	2.65E-03
27	5.91E-03	7.12E-03	7.65E-03	7.52E-03	6.86E-03	5.71E-03	3.79E-03
28	1.08E-02	9.49E-03	7.68E-03	5.78E-03	4.05E-03	2.60E-03	1.37E-03
29	5.90E-03	3.23E-03	1.40E-03	3.90E-04	2.42E-05	4.02E-05	1.45E-04
30	8.43E-06	4.15E-04	1.49E-03	2.66E-03	3.51E-03	3.76E-03	2.95E-03
31	5.72E-03	7.50E-03	8.17E-03	7.81E-03	6.73E-03	5.21E-03	3.21E-03
32	1.07E-02	8.43E-03	5.74E-03	3.36E-03	1.64E-03	6.24E-04	1.56E-04
33	2.91E-03	6.39E-04	2.15E-07	4.60E-04	1.34E-03	2.06E-03	1.94E-03
34	1.65E-03	4.15E-03	6.20E-03	7.15E-03	6.96E-03	5.84E-03	3.78E-03
35	1.08E-02	1.01E-02	7.83E-03	5.12E-03	2.80E-03	1.23E-03	3.84E-04
36	5.89E-03	2.09E-03	2.37E-04	1.15E-04	9.32E-04	1.82E-03	1.88E-03
37	4.62E-04	2.90E-03	5.58E-03	7.14E-03	7.23E-03	6.09E-03	3.88E-03
38	1.04E-02	1.07E-02	8.44E-03	5.34E-03	2.65E-03	9.47E-04	1.99E-04
39	7.18E-03	2.50E-03	2.15E-04	2.51E-04	1.47E-03	2.63E-03	2.58E-03
40	2.96E-04	3.12E-03	6.37E-03	8.02E-03	7.70E-03	5.99E-03	3.50E-03
41	1.10E-02	1.14E-02	8.43E-03	4.53E-03	1.62E-03	2.52E-04	5.70E-07
42	8.65E-03	2.71E-03	8.38E-05	7.42E-04	2.77E-03	4.27E-03	3.83E-03
43	8.94E-08	2.45E-03	6.64E-03	9.03E-03	8.68E-03	6.47E-03	3.52E-03
44	7.76E-03	1.10E-02	9.61E-03	5.80E-03	2.30E-03	4.32E-04	1.77E-06
45	1.00E-02	4.71E-03	7.87E-04	1.06E-04	1.54E-03	3.09E-03	3.07E-03
46	1.16E-04	1.56E-03	5.22E-03	7.29E-03	6.77E-03	4.69E-03	2.32E-03
47	8.82E-03	1.01E-02	6.69E-03	2.51E-03	2.70E-04	1.19E-04	6.14E-04
48	6.49E-03	6.86E-04	6.78E-04	3.87E-03	6.17E-03	6.01E-03	3.85E-03

Table C.29: Franck-Condon factors for transitions from $X^2\Pi$ SF $^{2+}$ ($v' = 0 - 48$) to $e^1\Delta$ SF $^+$ ($v'' = 16 - 22$).

Appendix D

Colour maps of Franck-Condon factors for transitions from $X^2\Pi$ SF²⁺ to $C^3\Sigma^-$ SF⁺, $a^1\Delta$ SF⁺, $b^1\Sigma^+$ SF⁺, $c^1\Sigma^-$ SF⁺ and $e^1\Delta$ SF⁺.

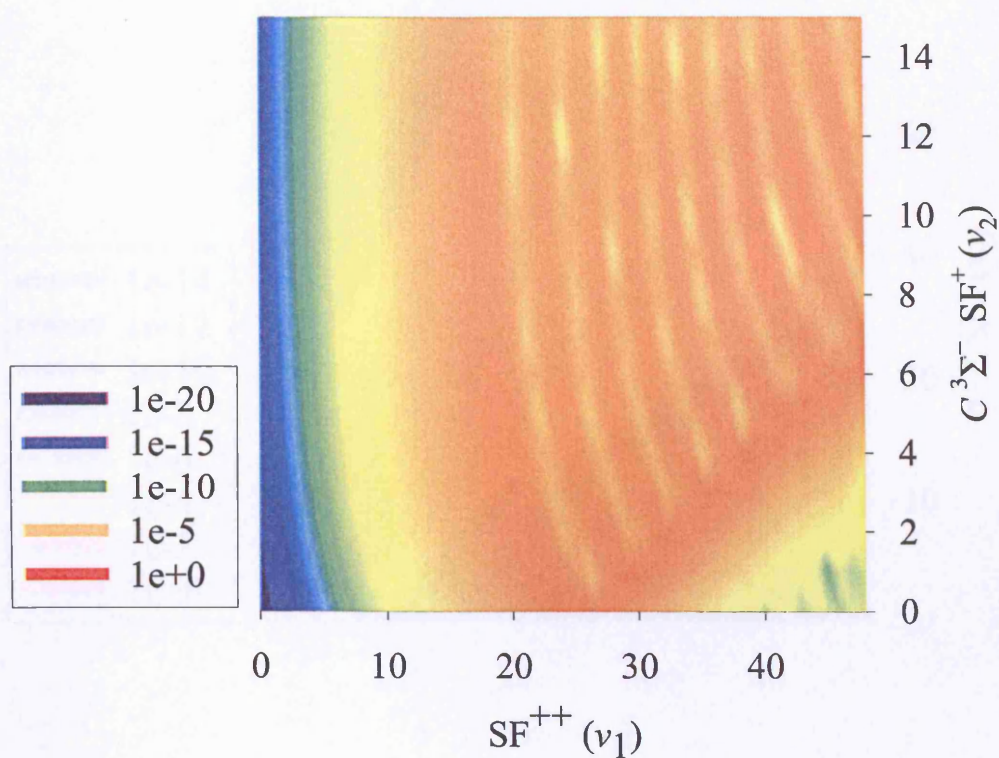


Figure D.1: Franck-Condon factors for transitions from $X^2\Pi SF^{2+}$ to $C^3\Sigma^- SF^+$. The x - and y - axes are the vibrational levels of SF^{2+} and SF^+ , respectively. The intensities of the FCFs are plotted logarithmically on the z - axis using color with red as the most intense and blue as the least intense.

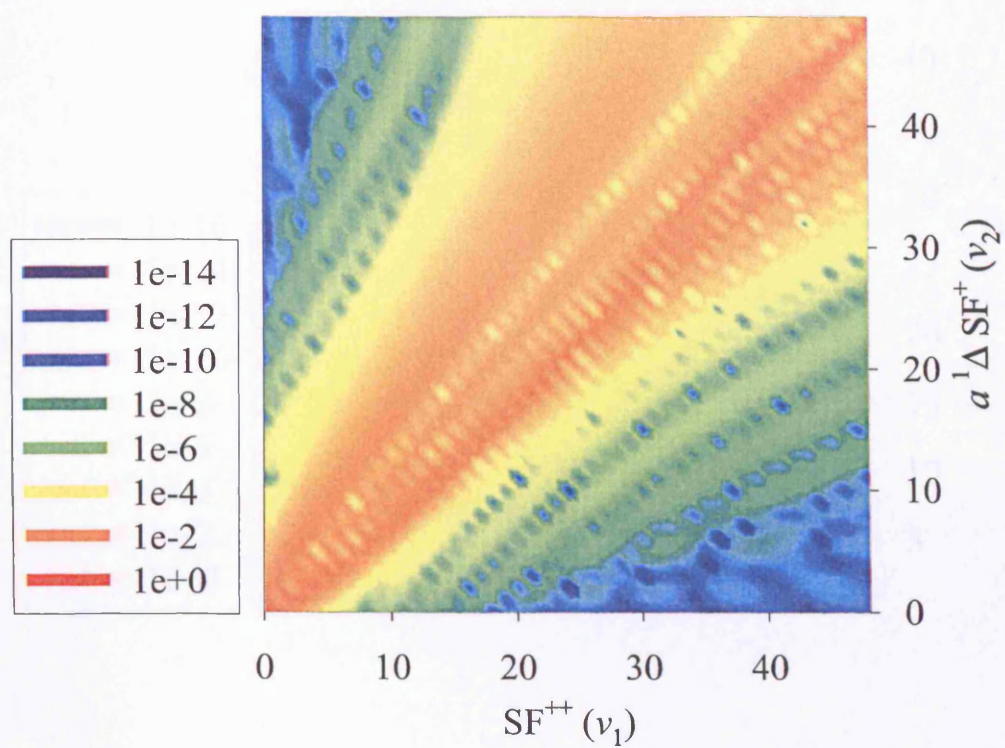


Figure D.2: Franck-Condon factors for transitions from $X \ ^2\Pi \text{SF}^{2+}$ to $a \ ^1\Delta \text{SF}^+$. The x - and y - axes are the vibrational levels of SF^{2+} and SF^+ , respectively. The intensities of the FCFs are plotted logarithmically on the z - axis using color with red as the most intense and blue as the least intense.

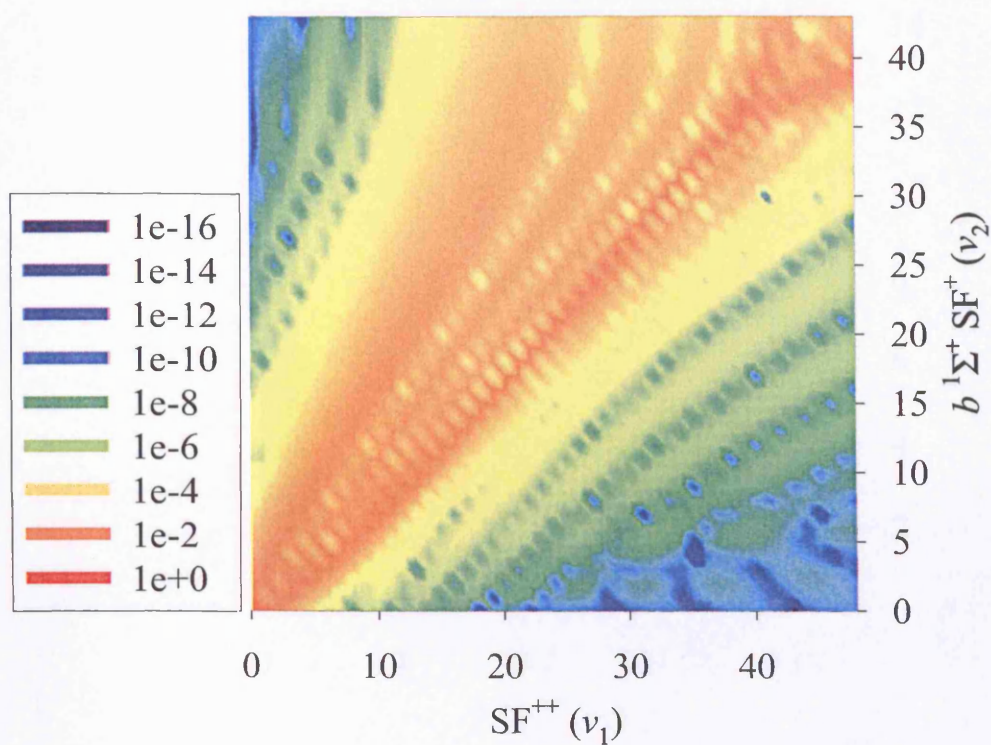


Figure D.3: Franck-Condon factors for transitions from $X^2\Pi SF^{2+}$ to $b^1\Sigma^+ SF^+$. The x - and y - axes are the vibrational levels of SF^{2+} and SF^+ , respectively. The intensities of the FCFs are plotted logarithmically on the z - axis using color with red as the most intense and blue as the least intense.

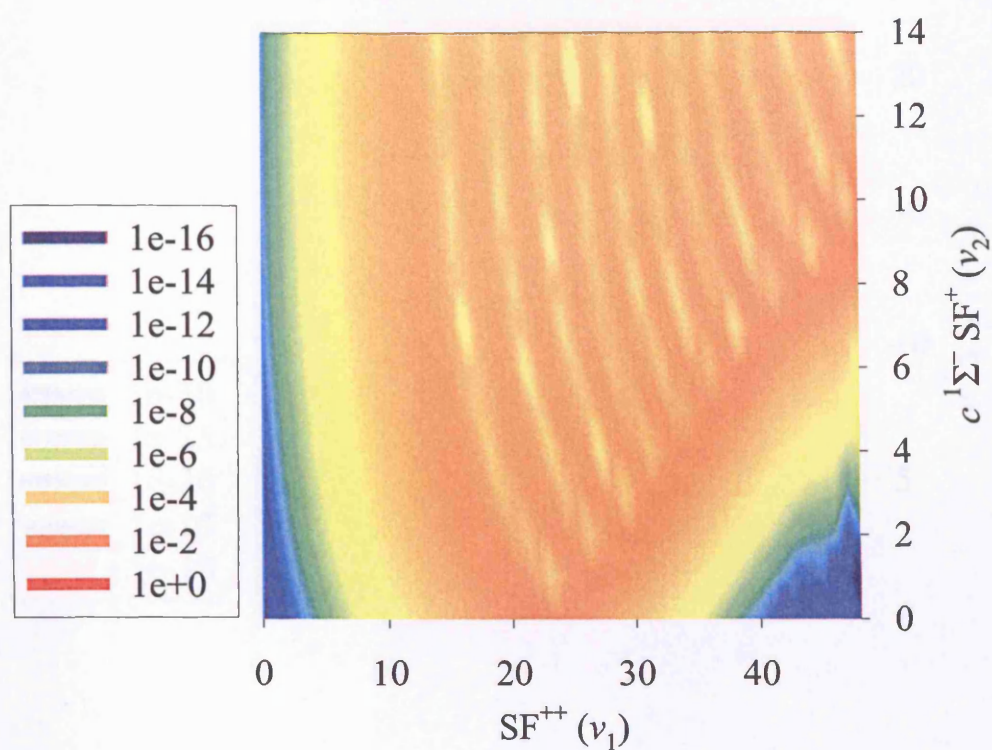


Figure D.4: Franck-Condon factors for transitions from $X^2\Pi SF^{2+}$ to $c^1\Sigma^- SF^+$. The x - and y - axes are the vibrational levels of SF^{2+} and SF^+ , respectively. The intensities of the FCFs are plotted logarithmically on the z - axis using color with red as the most intense and blue as the least intense.

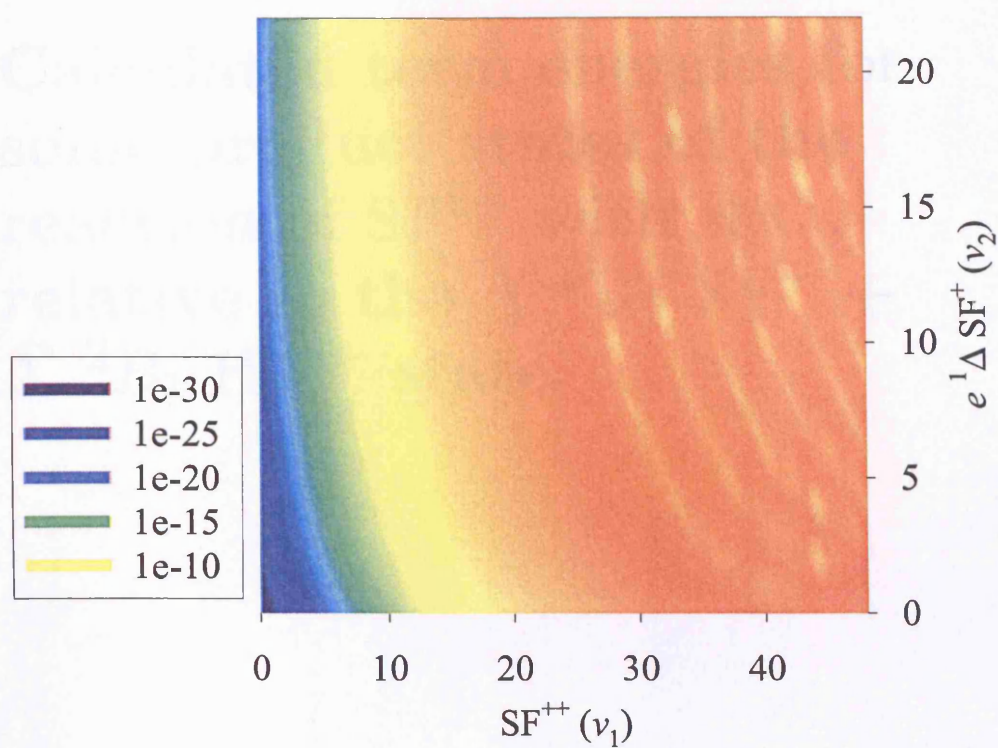


Figure D.5: Franck-Condon factors for transitions from $X^2\Pi SF^{2+}$ to $e^1\Delta SF^+$. The x - and y - axes are the vibrational levels of SF^{2+} and SF^+ , respectively. The intensities of the FCFs are plotted logarithmically on the z - axis using color with red as the most intense and blue as the least intense.

Appendix E

Calculated term energies for some product states of the reaction of SF^{2+} with H_2O , relative to the $X^3\Sigma^- SF^+ + \bar{X}^2B_1 H_2O^+$ state.

v ₁	v ₂		v ₃		v ₄	v ₅	v ₆
	0	1	0	1			
1	4.15	4.25	4.35	4.45	4.55	4.65	4.75
2	4.25	4.35	4.45	4.55	4.65	4.75	4.85
3	4.35	4.45	4.55	4.65	4.75	4.85	4.95
4	4.45	4.55	4.65	4.75	4.85	4.95	5.05
5	4.55	4.65	4.75	4.85	4.95	5.05	5.15
6	4.65	4.75	4.85	4.95	5.05	5.15	5.25
7	4.75	4.85	4.95	5.05	5.15	5.25	5.35
8	4.85	4.95	5.05	5.15	5.25	5.35	5.45
9	4.95	5.05	5.15	5.25	5.35	5.45	5.55
10	5.05	5.15	5.25	5.35	5.45	5.55	5.65
11	5.15	5.25	5.35	5.45	5.55	5.65	5.75
12	5.25	5.35	5.45	5.55	5.65	5.75	5.85
13	5.35	5.45	5.55	5.65	5.75	5.85	5.95
14	5.45	5.55	5.65	5.75	5.85	5.95	6.05
15	5.55	5.65	5.75	5.85	5.95	6.05	6.15
16	5.65	5.75	5.85	5.95	6.05	6.15	6.25
17	5.75	5.85	5.95	6.05	6.15	6.25	6.35
18	5.85	5.95	6.05	6.15	6.25	6.35	6.45
19	5.95	6.05	6.15	6.25	6.35	6.45	6.55
20	6.05	6.15	6.25	6.35	6.45	6.55	6.65
21	6.15	6.25	6.35	6.45	6.55	6.65	6.75
22	6.25	6.35	6.45	6.55	6.65	6.75	6.85
23	6.35	6.45	6.55	6.65	6.75	6.85	6.95
24	6.45	6.55	6.65	6.75	6.85	6.95	7.05
25	6.55	6.65	6.75	6.85	6.95	7.05	7.15
26	6.65	6.75	6.85	6.95	7.05	7.15	7.25
27	6.75	6.85	6.95	7.05	7.15	7.25	7.35
28	6.85	6.95	7.05	7.15	7.25	7.35	7.45
29	6.95	7.05	7.15	7.25	7.35	7.45	7.55
30	7.05	7.15	7.25	7.35	7.45	7.55	7.65
31	7.15	7.25	7.35	7.45	7.55	7.65	7.75
32	7.25	7.35	7.45	7.55	7.65	7.75	7.85
33	7.35	7.45	7.55	7.65	7.75	7.85	7.95
34	7.45	7.55	7.65	7.75	7.85	7.95	8.05
35	7.55	7.65	7.75	7.85	7.95	8.05	8.15
36	7.65	7.75	7.85	7.95	8.05	8.15	8.25
37	7.75	7.85	7.95	8.05	8.15	8.25	8.35
38	7.85	7.95	8.05	8.15	8.25	8.35	8.45
39	7.95	8.05	8.15	8.25	8.35	8.45	8.55
40	8.05	8.15	8.25	8.35	8.45	8.55	8.65
41	8.15	8.25	8.35	8.45	8.55	8.65	8.75
42	8.25	8.35	8.45	8.55	8.65	8.75	8.85
43	8.35	8.45	8.55	8.65	8.75	8.85	8.95
44	8.45	8.55	8.65	8.75	8.85	8.95	9.05
45	8.55	8.65	8.75	8.85	8.95	9.05	9.15
46	8.65	8.75	8.85	8.95	9.05	9.15	9.25
47	8.75	8.85	8.95	9.05	9.15	9.25	9.35
48	8.85	8.95	9.05	9.15	9.25	9.35	9.45
49	8.95	9.05	9.15	9.25	9.35	9.45	9.55
50	9.05	9.15	9.25	9.35	9.45	9.55	9.65
51	9.15	9.25	9.35	9.45	9.55	9.65	9.75
52	9.25	9.35	9.45	9.55	9.65	9.75	9.85
53	9.35	9.45	9.55	9.65	9.75	9.85	9.95
54	9.45	9.55	9.65	9.75	9.85	9.95	10.05
55	9.55	9.65	9.75	9.85	9.95	10.05	10.15
56	9.65	9.75	9.85	9.95	10.05	10.15	10.25
57	9.75	9.85	9.95	10.05	10.15	10.25	10.35
58	9.85	9.95	10.05	10.15	10.25	10.35	10.45
59	9.95	10.05	10.15	10.25	10.35	10.45	10.55
60	10.05	10.15	10.25	10.35	10.45	10.55	10.65
61	10.15	10.25	10.35	10.45	10.55	10.65	10.75
62	10.25	10.35	10.45	10.55	10.65	10.75	10.85
63	10.35	10.45	10.55	10.65	10.75	10.85	10.95
64	10.45	10.55	10.65	10.75	10.85	10.95	11.05
65	10.55	10.65	10.75	10.85	10.95	11.05	11.15
66	10.65	10.75	10.85	10.95	11.05	11.15	11.25
67	10.75	10.85	10.95	11.05	11.15	11.25	11.35
68	10.85	10.95	11.05	11.15	11.25	11.35	11.45
69	10.95	11.05	11.15	11.25	11.35	11.45	11.55
70	11.05	11.15	11.25	11.35	11.45	11.55	11.65
71	11.15	11.25	11.35	11.45	11.55	11.65	11.75
72	11.25	11.35	11.45	11.55	11.65	11.75	11.85
73	11.35	11.45	11.55	11.65	11.75	11.85	11.95
74	11.45	11.55	11.65	11.75	11.85	11.95	12.05
75	11.55	11.65	11.75	11.85	11.95	12.05	12.15
76	11.65	11.75	11.85	11.95	12.05	12.15	12.25
77	11.75	11.85	11.95	12.05	12.15	12.25	12.35
78	11.85	11.95	12.05	12.15	12.25	12.35	12.45
79	11.95	12.05	12.15	12.25	12.35	12.45	12.55
80	12.05	12.15	12.25	12.35	12.45	12.55	12.65
81	12.15	12.25	12.35	12.45	12.55	12.65	12.75
82	12.25	12.35	12.45	12.55	12.65	12.75	12.85
83	12.35	12.45	12.55	12.65	12.75	12.85	12.95
84	12.45	12.55	12.65	12.75	12.85	12.95	13.05
85	12.55	12.65	12.75	12.85	12.95	13.05	13.15
86	12.65	12.75	12.85	12.95	13.05	13.15	13.25
87	12.75	12.85	12.95	13.05	13.15	13.25	13.35
88	12.85	12.95	13.05	13.15	13.25	13.35	13.45
89	12.95	13.05	13.15	13.25	13.35	13.45	13.55
90	13.05	13.15	13.25	13.35	13.45	13.55	13.65
91	13.15	13.25	13.35	13.45	13.55	13.65	13.75
92	13.25	13.35	13.45	13.55	13.65	13.75	13.85
93	13.35	13.45	13.55	13.65	13.75	13.85	13.95
94	13.45	13.55	13.65	13.75	13.85	13.95	14.05
95	13.55	13.65	13.75	13.85	13.95	14.05	14.15
96	13.65	13.75	13.85	13.95	14.05	14.15	14.25
97	13.75	13.85	13.95	14.05	14.15	14.25	14.35
98	13.85	13.95	14.05	14.15	14.25	14.35	14.45
99	13.95	14.05	14.15	14.25	14.35	14.45	14.55
100	14.05	14.15	14.25	14.35	14.45	14.55	14.65

TABLE E.1. Calculated term energies (in eV) for some vibrational levels of the $X^3\Sigma^- SF^+ + \bar{X}^2B_1 H_2O^+$ product states, relative to the $X^3\Sigma^- SF^+ + \bar{X}^2B_1 H_2O^+$ state.

$v'' \setminus v'$	$X^3\Sigma^- \text{SF}^+ + \tilde{A}^2A_1 \text{H}_2\text{O}^+$			$X^3\Sigma^- \text{SF}^+ + \tilde{B}^2B_2 \text{H}_2\text{O}^+$		
	0	1	2	0	1	2
0	2.17	2.10	1.96	6.66	6.59	6.45
1	2.30	2.23	2.09	6.79	6.72	6.58
2	2.42	2.35	2.21	6.91	6.84	6.70
3	2.54	2.47	2.33	7.03	6.96	6.82
4	2.66	2.59	2.45	7.15	7.08	6.94
5	2.78	2.71	2.57	7.27	7.20	7.06
6	2.89	2.82	2.69	7.38	7.31	7.18
7	3.01	2.94	2.80	7.50	7.43	7.29
8	3.12	3.05	2.92	7.61	7.54	7.40
9	3.23	3.16	3.03	7.72	7.65	7.52
10	3.34	3.28	3.14	7.83	7.76	7.63
11	3.45	3.38	3.25	7.94	7.87	7.74
12	3.56	3.49	3.35	8.05	7.98	7.84
13	3.67	3.60	3.46	8.16	8.09	7.95
14	3.77	3.70	3.56	8.26	8.19	8.05
15	3.87	3.80	3.67	8.36	8.29	8.16
16	3.97	3.90	3.77	8.46	8.39	8.26
17	4.07	4.00	3.87	8.56	8.49	8.36
18	4.17	4.10	3.96	8.66	8.59	8.45
19	4.27	4.20	4.06	8.76	8.69	8.55
20	4.36	4.29	4.15	8.85	8.78	8.64
21	4.45	4.38	4.24	8.94	8.87	8.73
22	4.54	4.47	4.33	9.03	8.96	8.82
23	4.63	4.56	4.42	9.12	9.05	8.91
24	4.72	4.65	4.51	9.20	9.14	9.00
25	4.80	4.73	4.59	9.29	9.22	9.08
26	4.88	4.81	4.67	9.37	9.30	9.16
27	4.96	4.89	4.75	9.45	9.38	9.24
28	5.04	4.97	4.83	9.53	9.46	9.32
29	5.11	5.04	4.90	9.60	9.53	9.39
30	5.18	5.11	4.98	9.67	9.60	9.47
31	5.25	5.18	5.04	9.74	9.67	9.53
32	5.32	5.25	5.11	9.81	9.74	9.60
33	5.38	5.31	5.17	9.87	9.80	9.66
34	5.44	5.37	5.23	9.93	9.86	9.72
35	5.49	5.42	5.29	9.98	9.91	9.78
36	5.55	5.48	5.34	10.03	9.97	9.83
37	5.59	5.52	5.39	10.08	10.01	9.88
38	5.64	5.57	5.43	10.13	10.06	9.92
39	5.67	5.60	5.47	10.16	10.09	9.96
40	5.71	5.64	5.50	10.20	10.13	9.99
41	5.74	5.67	5.53	10.22	10.16	10.02
42	5.76	5.69	5.55	10.25	10.18	10.04
43	5.77	5.70	5.57	10.26	10.19	10.06

Table E.1: Term energies, in eV, for some vibrational levels of the $X^3\Sigma^- \text{SF}^+ + \tilde{A}^2A_1 \text{H}_2\text{O}^+$ and $X^3\Sigma^- \text{SF}^+ + \tilde{B}^2B_2 \text{H}_2\text{O}^+$ product states, relative to the $X^3\Sigma^- \text{SF}^+ + \tilde{X}^2B_1 \text{H}_2\text{O}^+$ state.

vert. transition	$A^3\Pi SF^+ + \tilde{X}^2B_1 H_2O^+$			$D^3\Pi SF^+ + \tilde{X}^2B_1 H_2O^+$		
	0	1	2	0	1	2
	5.68	5.62	5.48	7.55	7.48	7.35
$v'' \setminus v'$	$a^1\Delta SF^+ + \tilde{X}^2B_1 H_2O^+$			$a^1\Delta SF^+ + \tilde{A}^2A_1 H_2O^+$		
	0	1	2	0	1	2
0	1.08	1.02	0.88	3.20	3.13	2.99
1	1.21	1.14	1.00	3.32	3.25	3.12
2	1.34	1.27	1.13	3.45	3.38	3.24
3	1.46	1.39	1.25	3.57	3.50	3.37
4	1.58	1.51	1.38	3.70	3.63	3.49
5	1.70	1.63	1.49	3.81	3.74	3.61
6	1.82	1.75	1.61	3.93	3.86	3.72
7	1.93	1.86	1.72	4.04	3.98	3.84
8	2.05	1.98	1.84	4.16	4.09	3.95
9	2.16	2.09	1.95	4.27	4.20	4.06
10	2.27	2.20	2.06	4.38	4.31	4.18
11	2.38	2.31	2.17	4.49	4.42	4.29
12	2.49	2.42	2.28	4.60	4.53	4.40
13	2.60	2.53	2.39	4.71	4.64	4.50
14	2.70	2.63	2.50	4.82	4.75	4.61
15	2.81	2.74	2.60	4.92	4.85	4.71
16	2.91	2.84	2.70	5.02	4.95	4.82
17	3.01	2.94	2.81	5.13	5.06	4.92
18	3.11	3.04	2.91	5.23	5.16	5.02
19	3.21	3.14	3.01	5.32	5.26	5.12
20	3.31	3.24	3.10	5.42	5.35	5.22
21	3.40	3.34	3.20	5.52	5.45	5.31
22	3.50	3.43	3.29	5.61	5.54	5.40
23	3.59	3.52	3.38	5.70	5.64	5.50
24	3.68	3.61	3.48	5.80	5.73	5.59
25	3.77	3.70	3.57	5.88	5.82	5.68
26	3.86	3.79	3.65	5.97	5.90	5.77
27	3.95	3.88	3.74	6.06	5.99	5.85
28	4.03	3.96	3.82	6.14	6.07	5.94
29	4.11	4.04	3.91	6.23	6.16	6.02
30	4.19	4.13	3.99	6.31	6.24	6.10
31	4.27	4.21	4.07	6.39	6.32	6.18
32	4.35	4.28	4.15	6.46	6.40	6.26
33	4.43	4.36	4.22	6.54	6.47	6.33
34	4.50	4.43	4.30	6.61	6.55	6.41
35	4.57	4.50	4.37	6.69	6.62	6.48
36	4.64	4.58	4.44	6.76	6.69	6.55
37	4.71	4.64	4.51	6.83	6.76	6.62
38	4.78	4.71	4.57	6.89	6.82	6.69
39	4.84	4.77	4.64	6.96	6.89	6.75
40	4.91	4.84	4.70	7.02	6.95	6.81
41	4.96	4.90	4.76	7.08	7.01	6.87
42	5.02	4.95	4.82	7.14	7.07	6.93
43	5.08	5.01	4.87	7.19	7.12	6.98
44	5.13	5.06	4.92	7.24	7.17	7.04
45	5.18	5.11	4.97	7.29	7.22	7.09
46	5.23	5.16	5.02	7.34	7.27	7.13
47	5.27	5.20	5.06	7.38	7.31	7.18
48	5.31	5.24	5.10	7.42	7.35	7.22
49	5.35	5.28	5.14	7.46	7.39	7.25

Table E.2: Term energies, in eV, for some vibrational levels of the $A^3\Pi SF^+ + \tilde{X}^2B_1 H_2O^+$, $D^3\Pi SF^+ + \tilde{X}^2B_1 H_2O^+$, $a^1\Delta SF^+ + \tilde{X}^2B_1 H_2O^+$ and $a^1\Delta SF^+ + \tilde{A}^2A_1 H_2O^+$ product states, relative to the $X^3\Sigma^- SF^+ + \tilde{X}^2B_1 H_2O^+$ state.

vert. transition	$d^1\Pi\text{ SF}^+ + \tilde{X}^2B_1\text{ H}_2\text{O}^+$					
	0	1	2			
$v''\backslash v'$	$b^1\Sigma^+\text{ SF}^+ + \tilde{X}^2B_1\text{ H}_2\text{O}^+$			$b^1\Sigma^+\text{ SF}^+ + \tilde{A}^2A_1\text{ H}_2\text{O}^+$		
	0	1	2	0	1	2
0	1.99	1.92	1.78	4.10	4.03	3.90
1	2.11	2.04	1.91	4.23	4.16	4.02
2	2.24	2.17	2.03	4.35	4.28	4.15
3	2.36	2.29	2.16	4.48	4.41	4.27
4	2.48	2.41	2.28	4.60	4.53	4.39
5	2.60	2.53	2.39	4.71	4.64	4.51
6	2.71	2.64	2.51	4.83	4.76	4.62
7	2.83	2.76	2.62	4.94	4.87	4.73
8	2.94	2.87	2.73	5.05	4.98	4.85
9	3.05	2.98	2.84	5.16	5.09	4.96
10	3.16	3.09	2.95	5.27	5.20	5.07
11	3.27	3.20	3.06	5.38	5.31	5.17
12	3.37	3.30	3.17	5.49	5.42	5.28
13	3.48	3.41	3.27	5.59	5.52	5.38
14	3.58	3.51	3.38	5.69	5.63	5.49
15	3.68	3.61	3.48	5.80	5.73	5.59
16	3.78	3.71	3.58	5.90	5.83	5.69
17	3.88	3.81	3.67	5.99	5.93	5.79
18	3.98	3.91	3.77	6.09	6.02	5.88
19	4.07	4.00	3.87	6.19	6.12	5.98
20	4.17	4.10	3.96	6.28	6.21	6.07
21	4.26	4.19	4.05	6.37	6.30	6.16
22	4.34	4.28	4.14	6.46	6.39	6.25
23	4.43	4.36	4.22	6.54	6.47	6.34
24	4.52	4.45	4.31	6.63	6.56	6.42
25	4.60	4.53	4.39	6.71	6.64	6.50
26	4.68	4.61	4.47	6.79	6.72	6.58
27	4.76	4.69	4.55	6.87	6.80	6.66
28	4.83	4.76	4.62	6.94	6.87	6.74
29	4.90	4.83	4.69	7.01	6.95	6.81
30	4.97	4.90	4.76	7.08	7.01	6.88
31	5.04	4.97	4.83	7.15	7.08	6.94
32	5.10	5.03	4.89	7.21	7.14	7.00
33	5.15	5.09	4.95	7.27	7.20	7.06
34	5.21	5.14	5.00	7.32	7.25	7.11
35	5.25	5.19	5.05	7.37	7.30	7.16
36	5.30	5.23	5.09	7.41	7.34	7.20
37	5.33	5.26	5.13	7.45	7.38	7.24
38	5.36	5.29	5.16	7.48	7.41	7.27
39	5.39	5.32	5.18	7.50	7.43	7.29
40	5.41	5.34	5.20	7.52	7.45	7.31
41	5.43	5.36	5.22	7.54	7.47	7.33
42	5.44	5.37	5.23	7.55	7.48	7.35
43	5.45	5.38	5.24	7.56	7.49	7.36

Table E.3: Term energies, in eV, for some vibrational levels of the $d^1\Pi\text{ SF}^+ + \tilde{X}^2B_1\text{ H}_2\text{O}^+$, $b^1\Sigma^+\text{ SF}^+ + \tilde{X}^2B_1\text{ H}_2\text{O}^+$ and $b^1\Sigma^+\text{ SF}^+ + \tilde{A}^2A_1\text{ H}_2\text{O}^+$ product states, relative to the $X^3\Sigma^-\text{ SF}^+ + \tilde{X}^2B_1\text{ H}_2\text{O}^+$ state.

Appendix F

Landau-Zener cross sections for some product states of the reaction of SF^{2+} with H_2O , relative to the $X \ ^3\Sigma^- \text{SF}^+ + \bar{X} \ ^2B_1 \text{H}_2\text{O}^+$ state.

$v'' \setminus v'$	$X^3\Sigma^- \text{ SF}^+ + \tilde{A}^2A_1 \text{ H}_2\text{O}^+$			$X^3\Sigma^- \text{ SF}^+ + \tilde{B}^2B_2 \text{ H}_2\text{O}^+$		
	0	1	2	0	1	2
0	5.61E-03	4.64E-03	3.24E-03	1.00E-01	1.84E-01	5.39E-01
1	7.84E-03	6.44E-03	4.41E-03	3.10E-02	6.29E-02	2.17E-01
2	1.11E-02	9.06E-03	6.26E-03	7.84E-03	1.80E-02	6.92E-02
3	1.61E-02	1.33E-02	8.80E-03	1.55E-03	3.61E-03	2.01E-02
4	2.35E-02	1.94E-02	1.26E-02	2.25E-04	6.17E-04	4.71E-03
5	3.48E-02	2.76E-02	1.82E-02	2.20E-05	9.02E-05	8.47E-04
6	5.21E-02	4.11E-02	2.59E-02	1.27E-06	7.21E-06	1.31E-04
7	7.61E-02	5.97E-02	3.84E-02	5.08E-08	4.26E-07	1.14E-05
8	1.16E-01	9.07E-02	5.58E-02	6.09E-10	9.20E-09	7.44E-07
9	1.72E-01	1.34E-01	8.17E-02	3.25E-12	1.06E-10	2.62E-08
10	2.57E-01	1.99E-01	1.20E-01	0	3.37E-13	3.99E-10
11	3.83E-01	2.97E-01	1.79E-01	0	0	1.88E-12
12	5.71E-01	4.43E-01	2.66E-01	0	0	0
13	8.20E-01	6.37E-01	3.83E-01	0	0	0
14	1.22E+00	9.47E-01	5.71E-01	0	0	0
15	1.73E+00	1.35E+00	8.20E-01	0	0	0
16	2.43E+00	1.92E+00	1.17E+00	0	0	0
17	3.39E+00	2.69E+00	1.67E+00	0	0	0
18	4.65E+00	3.73E+00	2.35E+00	0	0	0
19	6.10E+00	4.95E+00	3.17E+00	0	0	0
20	7.88E+00	6.66E+00	4.37E+00	0	0	0
21	1.03E+01	8.55E+00	5.75E+00	0	0	0
22	1.27E+01	1.08E+01	7.46E+00	0	0	0
23	1.52E+01	1.33E+01	9.51E+00	0	0	0
24	1.80E+01	1.58E+01	1.16E+01	0	0	0
25	2.06E+01	1.84E+01	1.42E+01	0	0	0
26	2.33E+01	2.12E+01	1.67E+01	0	0	0
27	2.51E+01	2.36E+01	1.93E+01	0	0	0
28	2.68E+01	2.53E+01	2.15E+01	0	0	0
29	2.78E+01	2.69E+01	2.38E+01	0	0	0
30	2.82E+01	2.78E+01	2.56E+01	0	0	0
31	2.79E+01	2.82E+01	2.69E+01	0	0	0
32	2.73E+01	2.80E+01	2.77E+01	0	0	0
33	2.62E+01	2.74E+01	2.81E+01	0	0	0
34	2.48E+01	2.64E+01	2.81E+01	0	0	0
35	2.31E+01	2.51E+01	2.77E+01	0	0	0
36	2.15E+01	2.37E+01	2.70E+01	0	0	0
37	1.97E+01	2.21E+01	2.60E+01	0	0	0
38	1.83E+01	2.08E+01	2.51E+01	0	0	0
39	1.68E+01	1.93E+01	2.40E+01	0	0	0
40	1.57E+01	1.83E+01	2.28E+01	0	0	0
41	1.46E+01	1.71E+01	2.21E+01	0	0	0
42	1.38E+01	1.64E+01	2.11E+01	0	0	0
43	1.31E+01	1.57E+01	2.08E+01	0	0	0

Table F.1: Landau-Zener cross sections for forming the $X^3\Sigma^- \text{ SF}^+ + \tilde{A}^2A_1 \text{ H}_2\text{O}^+$ and $X^3\Sigma^- \text{ SF}^+ + \tilde{B}^2B_2 \text{ H}_2\text{O}^+$ product states with varying degrees of vibrational excitation.

vert. transition	$A^3\Pi SF^+ + \tilde{X}^2B_1 H_2O^+$			$D^3\Pi SF^+ + \tilde{X}^2B_1 H_2O^+$		
	0	1	2	0	1	2
$v'' \setminus v'$	$a^1\Delta SF^+ + \tilde{X}^2B_1 H_2O^+$			$a^1\Delta SF^+ + \tilde{A}^2A_1 H_2O^+$		
	0	1	2	0	1	2
0	5.50E-04	4.95E-04	4.06E-04	1.49E-01	1.16E-01	7.35E-02
1	6.79E-04	6.05E-04	4.88E-04	2.39E-01	1.85E-01	1.12E-01
2	8.36E-04	7.39E-04	5.95E-04	3.69E-01	2.97E-01	1.79E-01
3	1.07E-03	9.34E-04	7.26E-04	5.92E-01	4.59E-01	2.76E-01
4	1.36E-03	1.18E-03	9.00E-04	9.13E-01	7.10E-01	4.27E-01
5	1.76E-03	1.51E-03	1.13E-03	1.40E+00	1.09E+00	6.60E-01
6	2.25E-03	1.92E-03	1.42E-03	2.05E+00	1.67E+00	1.02E+00
7	3.01E-03	2.54E-03	1.84E-03	3.07E+00	2.43E+00	1.50E+00
8	3.97E-03	3.32E-03	2.36E-03	4.37E+00	3.50E+00	2.27E+00
9	5.31E-03	4.41E-03	3.16E-03	6.28E+00	5.10E+00	3.28E+00
10	7.20E-03	6.09E-03	4.18E-03	8.55E+00	7.05E+00	4.65E+00
11	1.02E-02	8.31E-03	5.61E-03	1.13E+01	9.51E+00	6.47E+00
12	1.38E-02	1.15E-02	7.62E-03	1.45E+01	1.25E+01	8.79E+00
13	1.94E-02	1.56E-02	1.05E-02	1.77E+01	1.58E+01	1.16E+01
14	2.76E-02	2.20E-02	1.42E-02	2.12E+01	1.90E+01	1.45E+01
15	3.84E-02	3.04E-02	2.00E-02	2.44E+01	2.24E+01	1.80E+01
16	5.58E-02	4.39E-02	2.76E-02	2.66E+01	2.51E+01	2.12E+01
17	7.88E-02	6.18E-02	3.84E-02	2.79E+01	2.71E+01	2.41E+01
18	1.12E-01	8.76E-02	5.39E-02	2.81E+01	2.81E+01	2.64E+01
19	1.60E-01	1.25E-01	7.61E-02	2.71E+01	2.79E+01	2.78E+01
20	2.22E-01	1.72E-01	1.08E-01	2.51E+01	2.66E+01	2.81E+01
21	3.19E-01	2.47E-01	1.49E-01	2.24E+01	2.45E+01	2.73E+01
22	4.43E-01	3.43E-01	2.14E-01	1.90E+01	2.15E+01	2.56E+01
23	6.37E-01	4.94E-01	2.97E-01	1.57E+01	1.83E+01	2.31E+01
24	8.81E-01	6.85E-01	4.12E-01	1.24E+01	1.49E+01	2.01E+01
25	1.22E+00	9.47E-01	5.71E-01	9.42E+00	1.17E+01	1.68E+01
26	1.61E+00	1.30E+00	7.91E-01	6.85E+00	8.81E+00	1.35E+01
27	2.20E+00	1.73E+00	1.05E+00	4.97E+00	6.59E+00	1.04E+01
28	2.97E+00	2.35E+00	1.45E+00	3.31E+00	4.56E+00	7.94E+00
29	3.85E+00	3.07E+00	1.92E+00	2.21E+00	3.15E+00	5.86E+00
30	4.95E+00	3.98E+00	2.51E+00	1.41E+00	2.09E+00	3.99E+00
31	6.28E+00	5.10E+00	3.28E+00	8.63E-01	1.33E+00	2.72E+00
32	7.88E+00	6.47E+00	4.24E+00	5.02E-01	8.09E-01	1.88E+00
33	9.51E+00	7.88E+00	5.42E+00	2.76E-01	4.67E-01	1.18E+00
34	1.16E+01	9.76E+00	6.66E+00	1.56E-01	2.76E-01	7.57E-01
35	1.36E+01	1.16E+01	8.10E+00	8.36E-02	1.56E-01	4.35E-01
36	1.58E+01	1.36E+01	9.76E+00	4.23E-02	8.36E-02	2.55E-01
37	1.80E+01	1.58E+01	1.16E+01	2.01E-02	4.23E-02	1.56E-01
38	2.00E+01	1.77E+01	1.36E+01	8.87E-03	2.01E-02	8.36E-02
39	2.21E+01	2.00E+01	1.55E+01	4.13E-03	1.00E-02	4.68E-02
40	2.38E+01	2.18E+01	1.74E+01	1.80E-03	4.71E-03	2.24E-02
41	2.53E+01	2.36E+01	1.93E+01	7.24E-04	2.07E-03	1.13E-02
42	2.66E+01	2.51E+01	2.12E+01	2.68E-04	8.47E-04	6.10E-03
43	2.74E+01	2.62E+01	2.30E+01	9.02E-05	3.18E-04	2.75E-03
44	2.79E+01	2.72E+01	2.44E+01	3.34E-05	1.31E-04	1.34E-03
45	2.81E+01	2.78E+01	2.56E+01	1.14E-05	5.02E-05	6.17E-04
46	2.81E+01	2.81E+01	2.64E+01	4.49E-06	1.77E-05	2.68E-04
47	2.78E+01	2.82E+01	2.72E+01	1.27E-06	7.21E-06	1.31E-04
48	2.73E+01	2.80E+01	2.77E+01	4.26E-07	2.75E-06	6.12E-05
49	2.68E+01	2.78E+01	2.80E+01	1.31E-07	9.76E-07	2.72E-05

Table F.2: Landau-Zener cross sections for forming the $A^3\Pi SF^+ + \tilde{X}^2B_1 H_2O^+$, $D^3\Pi SF^+ + \tilde{X}^2B_1 H_2O^+$, $a^1\Delta SF^+ + \tilde{X}^2B_1 H_2O^+$ and $a^1\Delta SF^+ + \tilde{A}^2A_1 H_2O^+$ product states with varying degrees of vibrational excitation.

vert. transition	$d \ ^1\Pi \text{ SF}^+ + \tilde{X} \ ^2B_1 \text{ H}_2\text{O}^+$					
	0	1	2			
$v'' \setminus v'$	$b \ ^1\Sigma^+ \text{ SF}^+ + \tilde{X} \ ^2B_1 \text{ H}_2\text{O}^+$			$b \ ^1\Sigma^+ \text{ SF}^+ + \tilde{A} \ ^2A_1 \text{ H}_2\text{O}^+$		
	0	1	2	0	1	2
0	3.40E-03	2.86E-03	2.10E-03	3.73E+00	2.97E+00	1.85E+00
1	4.77E-03	3.97E-03	2.79E-03	5.42E+00	4.37E+00	2.78E+00
2	6.62E-03	5.46E-03	3.87E-03	7.88E+00	6.47E+00	4.24E+00
3	9.61E-03	7.84E-03	5.31E-03	1.08E+01	9.02E+00	6.10E+00
4	1.38E-02	1.11E-02	7.41E-03	1.42E+01	1.22E+01	8.55E+00
5	1.94E-02	1.61E-02	1.05E-02	1.80E+01	1.58E+01	1.16E+01
6	2.85E-02	2.27E-02	1.46E-02	2.15E+01	1.93E+01	1.52E+01
7	4.11E-02	3.25E-02	2.13E-02	2.46E+01	2.30E+01	1.87E+01
8	5.97E-02	4.70E-02	3.04E-02	2.71E+01	2.58E+01	2.21E+01
9	8.76E-02	7.10E-02	4.39E-02	2.81E+01	2.76E+01	2.51E+01
10	1.29E-01	1.04E-01	6.40E-02	2.78E+01	2.82E+01	2.72E+01
11	1.92E-01	1.49E-01	9.40E-02	2.60E+01	2.73E+01	2.81E+01
12	2.86E-01	2.22E-01	1.34E-01	2.34E+01	2.53E+01	2.78E+01
13	4.12E-01	3.19E-01	1.99E-01	1.97E+01	2.21E+01	2.60E+01
14	6.14E-01	4.76E-01	2.86E-01	1.60E+01	1.86E+01	2.34E+01
15	8.81E-01	6.85E-01	4.12E-01	1.24E+01	1.49E+01	2.01E+01
16	1.26E+00	9.81E-01	5.92E-01	9.11E+00	1.14E+01	1.64E+01
17	1.79E+00	1.40E+00	8.50E-01	6.34E+00	8.22E+00	1.28E+01
18	2.43E+00	1.92E+00	1.22E+00	4.17E+00	5.63E+00	9.42E+00
19	3.39E+00	2.69E+00	1.67E+00	2.72E+00	3.81E+00	6.85E+00
20	4.51E+00	3.61E+00	2.27E+00	1.68E+00	2.45E+00	4.56E+00
21	5.93E+00	4.80E+00	3.07E+00	9.81E-01	1.50E+00	3.00E+00
22	7.67E+00	6.28E+00	4.10E+00	5.39E-01	8.63E-01	1.88E+00
23	9.76E+00	8.10E+00	5.42E+00	2.76E-01	4.67E-01	1.18E+00
24	1.19E+01	1.00E+01	6.85E+00	1.43E-01	2.55E-01	6.63E-01
25	1.42E+01	1.22E+01	8.79E+00	6.29E-02	1.20E-01	3.75E-01
26	1.67E+01	1.45E+01	1.08E+01	2.79E-02	5.71E-02	2.00E-01
27	1.93E+01	1.71E+01	1.27E+01	1.27E-02	2.79E-02	1.00E-01
28	2.15E+01	1.96E+01	1.52E+01	4.71E-03	1.13E-02	5.17E-02
29	2.38E+01	2.18E+01	1.74E+01	1.80E-03	4.71E-03	2.50E-02
30	2.56E+01	2.38E+01	1.96E+01	6.17E-04	1.80E-03	1.13E-02
31	2.68E+01	2.53E+01	2.15E+01	2.25E-04	7.24E-04	4.71E-03
32	2.76E+01	2.66E+01	2.36E+01	7.44E-05	2.25E-04	2.07E-03
33	2.81E+01	2.75E+01	2.49E+01	2.20E-05	9.02E-05	8.47E-04
34	2.82E+01	2.80E+01	2.62E+01	7.21E-06	2.72E-05	3.77E-04
35	2.79E+01	2.82E+01	2.69E+01	2.14E-06	1.14E-05	1.58E-04
36	2.75E+01	2.81E+01	2.75E+01	7.44E-07	4.49E-06	7.44E-05
37	2.70E+01	2.79E+01	2.79E+01	2.39E-07	1.65E-06	4.10E-05
38	2.64E+01	2.75E+01	2.81E+01	9.62E-08	7.44E-07	2.20E-05
39	2.60E+01	2.73E+01	2.82E+01	3.66E-08	3.20E-07	1.14E-05
40	2.56E+01	2.70E+01	2.82E+01	1.86E-08	1.77E-07	7.21E-06
41	2.51E+01	2.66E+01	2.81E+01	1.31E-08	1.31E-07	4.49E-06
42	2.48E+01	2.62E+01	2.81E+01	6.39E-09	7.01E-08	3.52E-06
43	2.43E+01	2.60E+01	2.80E+01	4.41E-09	5.08E-08	2.75E-06

Table F.3: Landau-Zener cross sections for forming the $d \ ^1\Pi \text{ SF}^+ + \tilde{X} \ ^2B_1 \text{ H}_2\text{O}^+$, $b \ ^1\Sigma^+ \text{ SF}^+ + \tilde{X} \ ^2B_1 \text{ H}_2\text{O}^+$ and $b \ ^1\Sigma^+ \text{ SF}^+ + \tilde{A} \ ^2A_1 \text{ H}_2\text{O}^+$ product states with varying degrees of vibrational excitation.

Bibliography

- [1] S. D. Price. *J. Chem. Soc., Faraday Trans.*, 93:2451, 1997.
- [2] Z. Herman. *Int. Rev. Phys. Chem.*, 15:299, 1996.
- [3] M. R. Bruce and R. A. Bonham. *Int. J. Mass Spectrom.*, 123:97, 1993.
- [4] P. Calandra, C. S. S. O'Connor, and S. D. Price. *J. Chem. Phys.*, 112:10821, 2000.
- [5] S. Harper, P. Calandra, and S. D. Price. *Phys. Chem. Chem. Phys.*, 3:741, 2001.
- [6] M. R. Bruce, C. Ma, and R. A. Bonham. *Chem. Phys. Lett.*, 190:285, 1992.
- [7] B. G. Lindsay, M. A. Mangan, H. C. Straub, and R. F. Stebbings. *J. Chem. Phys.*, 112:9404, 2000.
- [8] H. C. Straub, B. G. Lindsay, K. A. Smith, and R. F. Stebbings. *J. Chem. Phys.*, 108:109, 1998.
- [9] H. C. Straub, B. G. Lindsay, K. A. Smith, and R. F. Stebbings. *J. Chem. Phys.*, 105:4015, 1996.
- [10] Friedlander, Kallman, Lasareff, and Rosen. *Physik. Z.*, 76:60, 1932.
- [11] C. E. Melton and G. F. Wells. *J. Chem. Phys.*, 27:1132, 1957.
- [12] J. H. Bearman, F. Ranjbar, H. Harris, and J. Leventhal. *Chem. Phys. Lett.*, 42:335, 1976.
- [13] J. M. Curtis and R. K. Boyd. *J. Chem. Phys.*, 80:1150, 1984.
- [14] Z. Herman, P. Jonathan, A. G. Brenton, and J. H. Beynon. *Chem. Phys. Lett.*, 141:433, 1987.

- [15] M. Hamdan and A. G. Brenton. *J. Phys. B: At. Mol. Opt. Phys.*, 22:L45, 1989.
- [16] V. Krishnamurthi, K. Nagesha, V. R. Marathe, and D. Mathur. *Phys. Rev. A*, 44:5460, 1991.
- [17] M. Guilhaus, R. G. Kingston, A. G. Brenton, and J. H. Beynon. *Org. Mass Spectrom.*, 20:565, 1985.
- [18] K. Vékey, A. G. Brenton, and J. H. Beynon. *J. Phys. Chem.*, 90:3569, 1986.
- [19] D. Mathur, R. G. Kingston, F. M. Harris, A. G. Brenton, and J. H. Beynon. *J. Phys. B: At. Mol. Phys.*, 20:1811, 1987.
- [20] C. J. Reid, F. M. Harris, and J. H. Beynon. *Int. J. Mass Spectrom. Ion Processes*, 82:151, 1988.
- [21] Z. Herman, P. Jonathan, A. G. Brenton, and J. H. Beynon. *Chem. Phys.*, 126:377, 1988.
- [22] C. J. Reid, J. A. Ballantine, and F. M. Harris. *Int. J. Mass Spectrom.*, 93:23, 1989.
- [23] D. Smith, N. G. Adams, E. Alge, H. Villinger, and W. Lindinger. *J. Phys. B.*, 13:2787, 1980.
- [24] N. G. Adams, D. Smith, and D. Grief. *J. Phys. B: Atom. Molec. Phys.*, 12:791, 1979.
- [25] D. Smith, D. Grief, and N. G. Adams. *Int. J. Mass Spectrom. Ion Phys.*, 30:271, 1979.
- [26] A. A. Viggiano, F. Howorka, J. H. Futrell, J. A. Davison, I. Dotan, D. L. Albritton, and F. C. Fehsenfeld. *J. Chem. Phys.*, 71:2734, 1979.
- [27] W. Lindinger, E. Alge, H. Störi, M. Pahl, and R. N. Varney. *J. Chem. Phys.*, 67:3495, 1977.
- [28] R. Johnsen and M. A. Biondi. *Phys. Rev. A*, 18:996, 1978.
- [29] B. Friedrich and Z. Herman. *Chem. Phys. Lett.*, 107:375, 1984.
- [30] J. O. K. Pedersen and P. Hvelplund. *J. Phys. B: At. Mol. Phys.*, 20:L317, 1987.

- [31] S. D. Price, M. Manning, and S. R. Leone. *J. Am. Chem. Soc.*, 116:8673, 1994.
- [32] H. R. Koslowski, H. Lebius, V. Staemmler, R. Fink, K. Wiesemann, and B. A. Huber. *J. Phys. B: At. Mol. Opt. Phys.*, 24:5023, 1991.
- [33] M. Farník, Z. Herman, T. Ruhaltinger, J. P. Toennies, and R. G. Wang. *Chem. Phys. Lett.*, 206:376, 1993.
- [34] Y. Y. Lee, S. R. Leone, P. H. Champkin, N. Kaltsoyannis, and S. D. Price. *J. Chem. Phys.*, 106:7981, 1997.
- [35] L. Mrázek, J. Žabka, Z. Dolejšek, J. Hrušák, and Z. Herman. *J. Phys. Chem.*, 104:7294, 2000.
- [36] J. Roithová, R. Thissen, J. Žabka, P. Franceschi, O. Dutuit, and Z. Herman. *Int. J. Mass Spectrom.*, 228:487, 2003.
- [37] B. K. Chatterjee and R. Johnsen. *J. Chem. Phys.*, 91:1378, 1989.
- [38] W. Lu, P. Tosi, and D. Bassi. *J. Chem. Phys.*, 112:4648, 2000.
- [39] K. A. Newson, N. Tafadar, and S. D. Price. *J. Chem. Soc., Faraday Trans.*, 94:2735, 1998.
- [40] K. A. Newson and S. D. Price. *Chem. Phys. Lett.*, 269:93, 1997.
- [41] Z. Dolejšek, M. Farník, and Z. Herman. *Chem. Phys. Lett.*, 235:99, 1995.
- [42] N. Tafadar, D. Kearney, and S. D. Price. *J. Chem. Phys.*, 115:8819, 2001.
- [43] K. A. Newson and S. D. Price. *Chem. Phys. Lett.*, 294:223, 1998.
- [44] Z. Herman, J. Žabka, Z. Dolejšek, and Farník. *Int. J. Mass Spec.*, 192:191, 1999.
- [45] P. Tosi, R. Correale, W. Lu, S. Falcinelli, and D. Bassi. *Phys. Rev. Lett.*, 82:450, 1999.
- [46] N. Tafadar and S. D. Price. *Int. J. Mass Spectrom.*, 223-224:547, 2003.
- [47] D. J. A. Kearney and S. D. Price. *Phys. Chem. Chem. Phys.*, 5:1575, 2003.

- [48] J. Roithová, J. Hrušák, and Z. Herman. *J. Phys. Chem. A*, 107:7355, 2003.
- [49] P. Tosi, W. Lu, R. Correale, and D. Bassi. *Chem. Phys. Lett.*, 310:180, 1999.
- [50] D. Ascenzi, P. Franceschi, P. Tosi, D. Bassi, M. Kaczorowska, and J. N. Harvey. *J. Chem. Phys.*, 118:2159, 2003.
- [51] D. Schröder and H. Schwarz. *J. Phys. Chem. A*, 103:7385, 1999.
- [52] J. B. Hasted, S. M. Iqbal, and M. M. Yousaf. *J. Phys. B: Atom. Molec. Phys.*, 4:343, 1971.
- [53] W. B. Maier II. *J. Chem. Phys.*, 60:1974, 1974.
- [54] S. A. Rogers, S. D. Price, and S. R. Leone. *J. Chem. Phys.*, 98:280, 1993.
- [55] J. Hrušák. *Personal Communications*, 2001.
- [56] C. Møller and M.S. Plesset. *Phys. Rev.*, 46:618, 1934.
- [57] J.D. Watts and R.J. Bartlett. *Int. J. Quantum Chem.*, S27:51, 1993.
- [58] T. J. Lee and P. R. Taylor. *Int. J. Quantum Chem.*, S23:199, 1989.
- [59] P. Hohenberg and W. Kohn. *Phys. Rev.*, 136:B864, 1964.
- [60] W. Kohn and L. J. Sham. *Phys. Rev.*, 140:A1133, 1965.
- [61] S.J. Vosko, L. Wilk, and M. Nusair. *Can. J. Phys.*, 58:1200, 1980.
- [62] J.P. Perdew and Y. Wang. *Phys. Rev. B*, 45:13244, 1992.
- [63] J. P. Perdew and Y. Wang. *Phys. Rev. B*, 33:8800, 1989.
- [64] A. D. Becke. *Phys. Rev. B*, 38, 1988.
- [65] J. P. Perdew. *Phys. Rev. B*, 33:8822, 1986.
- [66] J. P. Perdew. *Phys. Rev. B*, 34:7406, 1986.
- [67] C. Lee, W. Yang, and R. G. Parr. *Phys. Rev. B*, 37:785, 1988.
- [68] T. Baer and W. Hase. *Unimolecular Reaction Dynamics*, chapter 6. Oxford University Press, New York, 1996.

- [69] T. Baer and Mayer P. M. *J. Am. Soc. Mass Spectrom.*, 8:103, 1997.
- [70] L. Landau. *Phys. Z. Sov.*, 2:46, 1932.
- [71] C. Zener. *Proc. Roy. Soc. Lond. Ser. A*, 137:696, 1932.
- [72] E. C. G. Stueckelberg. *Helv. Phys. Acta*, 5:369, 1932.
- [73] R. E. Olson, F. T. Smith, and E. Bauer. *Appl. Opt.*, 10:1848, 1971.
- [74] B. Numerov. *Publ. Obs. Central Astrophys. Russ.*, 2:188, 1933.
- [75] D Bassi, P Tosi, and R Schlögl. *J. Vac. Sci. Technol. A*, 16:114, 1998.
- [76] M. J. Frisch, G. W. Trucks, H. B. Schlegel, G. E. Scuseria, M. A. Rob, J. R. Cheeseman, V. G. Zakrzewski, J. A. Montgomery, R. E. Stratmann, J. C. Burant, S. Dapprich, J. M. Millam, A. D. Daniels, K. N. Kudin, M. C. Strain, O. Farkas, J. Tomasi, V. Barone, M. Cossi, R. Cammi, B. Mennucci, C. Pomelli, C. Adamo, S. Clifford, J. Ochterski, G. A. Petersson, P. Y. Ayala, Q. Cui, K. Morokuma, D. K. Malick, A. D. Rabuck, K. Raghavachari, J. B. Foresman, J. Cioslowski, J. V. Ortiz, B. B. Stefanov, G. Liu, A. Liashenko, P. Piskorz, I. Komaromi, R. Gomperts, R. L. Martin, D. J. Fox, T. Keith, M. A. Al-Laham, C. Y. Peng, A. Nanayakkara, C. Gonzales, M. Challacombe, P. M. W. Gill, B. G. Johnson, W. Chen, M. W. Wong, J. L. Andres, M. Head-Gordon, E. S. Replogle, and J. A. Pople. 1998. Pittsburgh.
- [77] A. D. Becke. *J. Chem. Phys.*, 98:5648, 1993.
- [78] G. E. Scuseria and T. J. Lee. *J. Chem. Phys.*, 93:5851, 1990.
- [79] T. Beyer and D. F. Swinehart. *Commun. ACM*, 16:379, 1973.
- [80] S. M. Harper, S. W. P. Hu, and S. D. Price. *J. Chem. Phys.*, 121:3507, 2004.
- [81] J. Hrušák, Z. Herman, N. Sändig, and W. Koch. *Int. J. Mass Spectrom.*, 201:269, 2000.
- [82] J. Hrušák. *Chemical Physics Letters*, 338:189, 2001.
- [83] N. Lambert, D. Kearney, N. Kaltsoyannis, and S. D. Price. *J. Am. Chem. Soc.*, 126:3658, 2004.
- [84] H.-J. Werner and P. J. Knowles. *J. Chem. Phys.*, 82:5053, 1985.

- [85] P. J. Knowles and H.-J. Werner. *Chem. Phys. Lett.*, 115:259, 1985.
- [86] H.-J. Werner and P. J. Knowles. *J. Chem. Phys.*, 89:5803, 1988.
- [87] P. J. Knowles and H.-J. Werner. *Chem. Phys. Lett.*, 145:514, 1988.
- [88] MOLPRO is a package of *ab initio* programs written by H.-J. Werner and P. J. Knowles, with contributions from R. D. Amos, A. Bernhardsson, A. Berning, P. Celani, D. L. Cooper, M. J. O. Deegan, A. J. Dobbyn, F. Eckert, C. Hampel, G. Hetzer, T. Korona, R. Lindh, A. W. Lloyd, S. J. McNicholas, F. R. Manby, W. Meyer, M. E. Mura, A. Nicklass, P. Palmieri, R. Pitzer, G. Rauhut, M. Sch'utz, H. Stoll, A. J. Stone, R. Tarroni and T. Thorsteinsson.
- [89] W.-P. Hu, S. M. Harper, and S. D. Price. *Meas. Sci. Technol.*, 13:1512, 2002.
- [90] K. M. Ervin and P. B. Armentrout. *J. Chem. Phys.*, 85:6380, 1986.
- [91] K. M. Ervin and P. B. Armentrout. *J. Chem. Phys.*, 86:6240, 1987.
- [92] K. M. Ervin and P. B. Armentrout. *J. Chem. Phys.*, 90:118, 1989.
- [93] M. Larsson. *Comm. Atom. Molec. Phys.*, 29:39, 1993.
- [94] D. M. Curtis and J. H. D. Eland. *Int. J. Mass Spectrom. Ion. Proc.*, 63:241, 1985.
- [95] N. Lambert, N. Kaltsoyannis, S. D. Price, J. Žabka, and Z. Herman. Bond-forming reactions of dications with molecules: A computational and experimental study of the mechanisms for the formation of HCF_2^+ from CF_3^{2+} and H_2 . *Phys. Chem. Chem. Phys.*, submitted, 2005.
- [96] *Gaussian 03, Revision B.04*, M. J. Frisch, G. W. Trucks, H. B. Schlegel, G. E. Scuseria, M. A. Robb, J. R. Cheeseman, J. A. Montgomery, Jr., T. Vreven, K. N. Kudin, J. C. Burant, J. M. Millam, S. S. Iyengar, J. Tomasi, V. Barone, B. Mennucci, M. Cossi, G. Scalmani, N. Rega, G. A. Petersson, H. Nakatsuji, M. Hada, M. Ehara, K. Toyota, R. Fukuda, J. Hasegawa, M. Ishida, T. Nakajima, Y. Honda, O. Kitao, H. Nakai, M. Klene, X. Li, J. E. Knox, H. P. Hratchian, J. B. Cross, C. Adamo, J. Jaramillo, R. Gomperts, R. E. Stratmann, O. Yazyev, A. J. Austin, R. Cammi, C. Pomelli, J. W. Ochterski, P. Y. Ayala, K. Morokuma, G. A. Voth, P. Salvador, J. J. Dannenberg, V. G. Zakrzewski, S. Dapprich, A. D. Daniels, M. C. Strain, O. Farkas, D. K. Malick, A. D. Rabuck,

- K. Raghavachari, J. B. Foresman, J. V. Ortiz, Q. Cui, A. G. Baboul, S. Clifford, J. Cioslowski, B. B. Stefanov, G. Liu, A. Liashenko, P. Piskorz, I. Komaromi, R. L. Martin, D. J. Fox, T. Keith, M. A. Al-Laham, C. Y. Peng, A. Nanayakkara, M. Challacombe, P. M. W. Gill, B. Johnson, W. Chen, M. W. Wong, C. Gonzalez, and J. A. Pople, Gaussian, Inc., Pittsburgh PA, 2003.
- [97] J. Peiró-García and I. Nebot-Gil. *ChemPhysChem*, 4:843, 2003.
- [98] J. Peiró-García and I. Nebot-Gil. *J. Comput. Chem.*, 24:1657, 2003.
- [99] M. Martínez-Ávila, J. Peiró-García, V. M. Ramírez-Ramírez, and I. Nebot-Gil. *Chem. Phys. Lett.*, 370:313, 2003.
- [100] T. J. Lee, A. P. Rendell, and P. R. Taylor. *J. Phys. Chem.*, 94:5463, 1990.
- [101] J. C. Rienstra-Kiracofe, W. D. Allen, and H. F. Schaefer III. *J. Phys. Chem. A*, 104:9823, 2000.
- [102] N. Lambert, N. Kaltsoyannis, and S. D. Price. *J. Chem. Phys.*, 119:1421, 2003.
- [103] S. D. Price, S. A. Rogers, and S. R. Leone. *J. Chem. Phys.*, 98:9455, 1993.
- [104] L. Landau. *Phys. Z. Sowjetunion*, 2:26, 1932.
- [105] R. J. Le Roy. *LEVEL 7.5: A Computer Program for Solving the Radial Schrödinger Equation for Bound and Quasibound Levels*. Guelph-Waterloo Centre for Graduate Work in Chemistry, University of Waterloo, Waterloo, Ontario N2L 3G1, Canada, 2002.
- [106] E. Boleat. Personal communications, 2004.
- [107] S. D. Price. Personal communications, 2004.
- [108] M. Lange, O. Pfaff, U. Müller, and R. Brenn. *Chem. Phys.*, 230:117, 1998.
- [109] V. P. Spiridonov, N. Vogt, and J. Vogt. *Struc. Chem.*, 12:349, 2001.
- [110] K. A. Peterson and R. C. Woods. *J. Chem. Phys.*, 93:1876, 1990.
- [111] K. K. Irikura. *J. Chem. Phys.*, 102:5357, 1995.

- [112] E. R. Fisher, B. L. Kickel, and P. B. Armentrout. *J. Chem. Phys.*, 97:4859, 1992.
- [113] W. R. Jarman and R. W. Nicholls. *Can. J. Phys.*, 32:201, 1954.
- [114] R. N. Zare, E. O. Larsson, and R. A. Berg. *J. Mol. Spectrosc.*, 15:117, 1965.
- [115] T. V. Chang and M. Karplus. *J. Chem. Phys.*, 52:783, 1970.
- [116] S. Waldenstrom and K. Razi-Naqvi. *J. Chem. Phys.*, 87:3563, 1987.
- [117] A. Palma, J. R. Rivas-Silva, J. S. Durand, and L. Sandoval. *Int. J. Quant. Chem.*, 41:811, 1992.
- [118] E. Ley-Koo, S. Mateos-Cortes, and G. Villa-Torres. *Int. J. Quant. Chem.*, 56:175, 1995.
- [119] J. C. López V., A. L. Rivera, Yu. F. Smirnov, and A. Frank. arXiv:physics/0109017.
- [120] D. W. Turner, C. Baker, A. D. Baker, and C. R. Brundle. *Molecular Photoelectron Spectroscopy*. Wiley-Interscience, 1970.
- [121] J. E. Reutt, L. S. Wang, Y. T. Lee, and D. A. Shirley. *J. Chem. Phys.*, 85:6928, 1985.
- [122] W. Meyer. *Int. J. Quantum Chem. Symp.*, 5(341), 1971.
- [123] J. A. Smith, P. Jorgensen, and Y. Örn. *J. Chem. Phys.*, 62:1285, 1975.
- [124] P. C. Hariharan and J. A. Pople. *Mol. Phys.*, 27:209, 1974.
- [125] P. J. Fortune, B. J. Rosenberg, and A. C. Wahl. *J. Chem. Phys.*, 65:2201, 1976.